UNIVERZITA KARLOVA V PRAZE

Matematicko-fyzikální fakulta

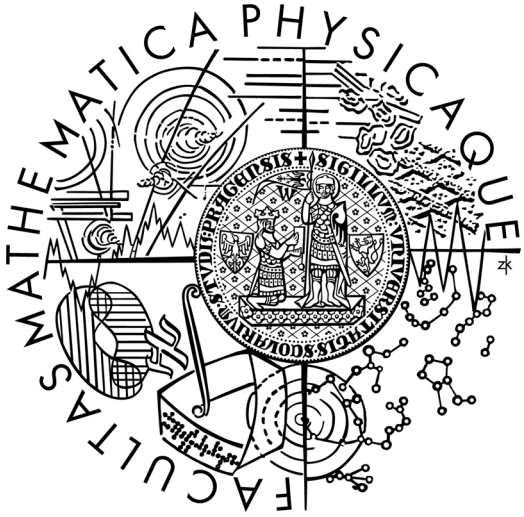

BIOLÉKAŘSKÉ APLIKACE NEROVNOVÁŽNÉHO PLAZMATU

Habilitační práce

RNDr. Ondřej Kylián, Ph.D.

Praha, 2013

Poděkování:

V posledních přibližně patnácti letech jsem měl to štěstí pracovat s mnoha lidmi, od kterých jsem se mnohému přiučil a bez nichž by žádný výsledek prezentovaný v této práci nebyl možný. V první řadě bych rád zmínil doc. V. Hrachovou, pod jejímž trpělivým vedením jsem se učil prvním vědeckým krůčkům. Mé velké poděkování směřuje i k Dr. F. Rossimu, který mne přivedl k tématu sterilizace povrchů pomocí nerovnovážného plazmatu, a prof. H. Biedermanovi, který mne zasvětil do problematiky plazmových polymerů a umožnil mi práci na KMF MFF UK. Rád bych poděkoval i všem kolegům, se kterými jsem měl možnost spolupracovat.

Obsah

1. Úvod

Slovo „plazma“ ve fyzice označuje ionizovaný kvazi-neutrální plyn vykazující kolektivní chování. Díky přítomnosti nabitých částic má plazma vysokou elektrickou vodivost a reaguje na vnější elektromagnetické pole, což je chování velmi odlišné od chování normálního plynu. Z tohoto důvodu bývá plazma často označováno jako čtvrté skupenství hmoty. Aplikačně je velmi zajímavé především takzvané nerovnovážné plazma, tj. plazma, ve kterém mají lehké elektrony výrazně vyšší teplotu (energii) než daleko těžší ionty a neutrální částice, jejichž teplota bývá blízká pokojové teplotě. Plazma je obvykle generováno pomocí elektrického průrazu v plynu za sníženého tlaku (1 – 100 Pa) vedoucího k stejnosměrnému doutnavému nebo vysokofrekvenčnímu výboji buzeného napětím o frekvenci 13.56 MHz. Většinou se používá plasma s nízkým stupněm ionizace - pro představu na 1 elektron (nebo 1 kladný iont) připadá 1 000 000 neutrálních atomů přesto jeho účinky jsou značné právě kvůli zmíněné vysoké energii elektronů (1 – 10 eV). Je potřeba zmínit, že se používají i výboje za atmosférického tlaku. Tyto však nejsou předmětem této práce.

Nerovnovážné plazma nachází v současné době využití v celé řadě aplikací, při kterých dochází k úpravě povrchů nejrůznějších materiálů. To je dáno tím, že technologie založené na plazmatu umožňují nanášet tenké funkční vrstvy, měnit morfologii a povrchové chemické složení nejrůznějších objektů, popřípadě i odstranit z povrchů nežádoucí nečistoty a to za relativně nízkých teplot při zachování objemových vlastností opracovávaných objektů. Tyto klíčové výhody stojí i v pozadí velmi rychlého rozvoje biolékařských aplikací nerovnovážného plazmatu, tj. oblasti, které se věnuje předkládaná práce. Jako příklady současného využití plazmatu je možné uvést sterilizaci povrchů nástrojů a pomůcek využívaných v lékařské praxi, modifikaci povrchů pro zvýšení jejich biokompatibility, výrobu biosenzorů a čidel, či přípravu antibakteriálních povlaků a materiálů pro řízené podávání léčiv.

V této práci budou komentovány vybrané výsledky mé práce týkající se biolékařských aplikací plazmatu, jichž jsem dosáhl během působení ve Společném výzkumném centru Evropské komise v italské Ispře a zejména na Katedře makromolekulární fyziky Matematicko-fyzikální fakulty Univerzity Karlovy v Praze. Konkrétně v kapitole 2 bude diskutována sterilizace povrchů nízkoteplotním plazmatem, v kapitole 3 budou komentovány výsledky týkající se nanášení tenkých vrstev plazmových polymerů a jejich nanočástic a v kapitole 4 budou představeny

výsledky přípravy nanoklastrů a nanočástic a jejich možného využití pro biolékařské aplikace. Z povahy těchto témat je zřejmé, že se jedná o mezní oblasti výzkumu, kde se současně využívají poznatky moderní fyziky, chemie a biologie. Vzhledem k tomuto multidisciplinárnímu charakteru je vhodné podotknout, že můj přínos a vědecký zájem se týkal zejména popisu fyzikálních procesů interakce plazmatu s biologickými systémy, nanášení tenkých vrstev plazmových polymerů, procesům vedoucím ke vzniku nanočástic a následné charakterizaci připravených materiálů.

2. Sterilizace povrchů pomocí nízkoteplotního plazmatu

Inaktivace, popřípadě i úplné odstranění různých biologických patogenů z povrchů nástrojů, přístrojů a pomůcek používaných v lékařské praxi představuje nezbytný krok pro zaručení bezpečnosti pacientů. Z tohoto důvodu byly vyvinuty nejrůznější sterilizační metody, které jsou založené na použití chemických látek (peroxid vodíku, etylenoxid atd.), energetickém záření, či na aplikaci zvýšené teploty. Nicméně všechny tyto metody mají svá omezení, která se týkají například vysoké toxicity používaných látek a s tím souvisejícími bezpečnostními a environmentálními riziky, možného ovlivnění objemových vlastností sterilizovaných objektů, anebo vysoké teploty, která neumožňuje sterilizovat většinu plastových materiálů. Mimoto se v poslední době ukazuje, že výše zmiňované sterilizační techniky jsou v případě některých biologických patogenů velmi málo účinné a v některých případech dokonce neúčinné. To platí zejména o sterilizaci bakteriálních endotoxinů, které jsou schopny vyvolat zvýšenou teplotu, a infekčních prionů, které mohou zapříčinit závažná a smrtelná neurodegenerativní onemocnění (např. Creutzfeldt-Jakobovu nemoc). Tyto obavy byly potvrzeny sérií studií prováděných v minulém desetiletí zejména ve Velké Británii, kdy se ukázalo, že takřka všechny lékařské nástroje, které prošly klasickou sterilizací, vykazovaly zbytkovou kontaminaci bílkovinami a nespecifikovanou organickou hmotou, která lokálně dosahovala hodnot až 4 $\mu g/mm^2$ (např. [1,2]). Proto je zřejmé, že vývoj nové technologie, která by zaručila úplné odstranění všech organických látek z povrchů, je prvořadým úkolem pro eliminaci možných rizik spojených s přítomností těchto látek na površích objektů, které mohou přijít přímo (například při chirurgickém zákroku) i nepřímo (například při podávání léků z kontaminovaných ampulek) do kontaktu s pacientem. Z tohoto pohledu je aplikace nerovnovážného plazmatu jednou ze slibných technologií, které se v poslední době dostává zvýšené pozornosti.

Možnost použití nerovnovážného plazmatu a shrnutí hlavních dosažených výsledků experimentů, na kterých jsem začal pracovat během působení ve Společném výzkumném centru Evropské komise italské Ispře, a které jsem následně rozpracovával na KMF MFF UK, bude podrobněji diskutována v následujících kapitolách. V kapitole 2.1 budou nejprve shrnuty výsledky dosažené při sterilizaci bakteriálních spor. Kapitola 2.2 bude věnována odstraňování organických materiálů z povrchu. V kapitole 2.3 bude představena možnost optimalizace sterilizačního procesu založená na využití ternární

výbojové směsi. V kapitole 2.4 bude prezentována možnost inaktivace bakteriálních endotoxinů. Shrnutí výsledků a nastínění dalších perspektiv možného použití plazmatu pro sterilizaci v lékařské praxi bude provedeno v kapitole 2.5.

2.1. Sterilizace bakteriálních spor

První zmínky o použití plazmatu pro sterilizaci bakteriálních spor se datují do konce šedesátých let minulého století, kdy se objevil první patent využívající koronového výboje pro sterilizaci vnitřních povrchů skleněných ampulí [3]. S pomocí takovéhoto zařízení bylo možno sterilizovat 10^6 bakterií v čase kratším než jedna sekunda. Nicméně v té době se mělo za to, že hlavním biocidálním faktorem byl velmi intenzivní ohřev bakterií v čase tak krátkém, že nedošlo k ohřevu ampulí. Ačkoliv výzkum možného použití plazmatu dále pokračoval a byly vyvinuty různé plazmové systémy pracující za sníženého tlaku v různých plynech (z počátku byly používány inertní plyny, postupně začaly být používány halogeny, vodík, kyslík a dusík), skutečný rozvoj nastal přibližně na přelomu tisíciletí. Obnovený zájem o plazmovou sterilizaci byl vyvolán několika publikacemi, které vyšly v krátké době za sebou [4-9]. Tyto přehledové články jednak shrnuly do té doby dosažené výsledky, jednak jasně prokázaly účinnost a výhody použití nízkoteplotního plazmatu zejména pro sterilizaci bakterií a bakteriálních spor. Od publikace výše zmíněných článků byla provedena celá řada studií, které se zabývaly jak identifikací hlavních procesů vedoucích k odstranění či inaktivaci bakteriálních spor, tak i optimalizací sterilizačního procesu (např. [10-20]). Na tomto místě je nutné podotknout, že ačkoliv velmi zajímavých výsledků bylo dosaženo i při použití výbojů generovaných za atmosférického tlaku (např. [21-27]), bude vzhledem k zaměření této práce pozornost v následujícím textu věnována výhradně výsledkům dosaženým při použití nízkotlakých výbojů.

Na základě srovnání sterilizační účinnosti nízkotlakých výbojů generovaných za různých podmínek (složení pracovního plynu, tlaku, dodávaného výkonu atd.) s vlastnostmi generovaného plazmatu (intenzita emitovaného záření, složení plazmatu, energie částic atd.) bylo postulováno, že hlavním sterilizačním činitelem při sterilizaci výbojovým plazmatem je UV záření emitované plazmatem (např. [14,16]). UV záření je schopno proniknout stěnou bakterií a bakteriálních spor a způsobit nevratné a letální změny jejich DNA [28]. Z tohoto důvodu byla hlavní pozornost věnována zejména maximalizaci intenzity UV záření, čehož bylo dosaženo použitím výbojových směsí

obsahujících kyslík a dusík, které produkují excitované NO molekuly emitující záření v požadovaném spektrálním rozsahu (zejména se jedná o NO-gama systém).

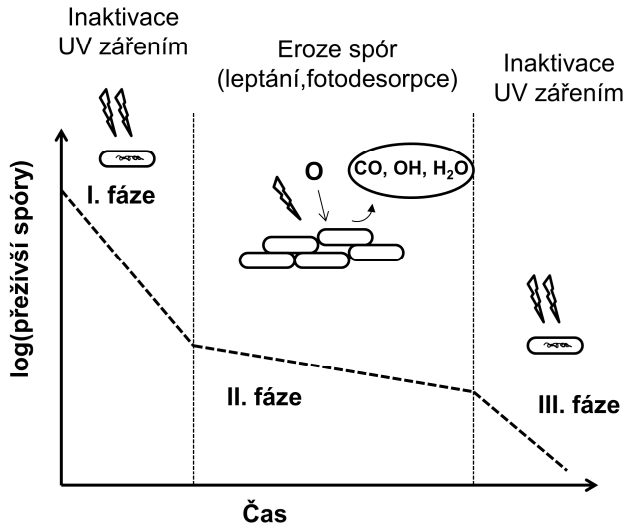

Obrázek 1. Schematické znázornění sterilizačního procesu

Výše uvedený výsledek, tedy že hlavní roli při sterilizaci hraje UV záření, byl však dosažen při použití vzorků, kde jednotlivé spory byly na povrchu víceméně izolované, a nepřekrývaly se. Nicméně bližší pohled na kinetiku poklesu životaschopných bakteriálních spor ukázal snadno odlišitelné sterilizační fáze (např. [9]), jak je schematicky znázorněno na **obrázku 1**. Přítomnost těchto fází byla interpretována následujícím způsobem:

- První fáze, kdy dochází k nejrychlejšímu poklesu životaschopných bakteriálních spor, odpovídá sterilizaci spor přímo dosažitelných UV zářením emitovaným plazmatem.
- Druhá, obvykle výrazněji pomalejší fáze, souvisí s možným stíněním některých spor jinou sporou, popřípadě další organickou nečistotou. Aby UV záření mohlo proniknout i k takovýmto sporám, je nutné nejprve stínící materiál odstranit. Rychlost sterilizace v této fázi je pak dána rychlostí odstraňování stínícího materiálu. Předpokládalo se, že k odstranění stínícího materiálu dochází buď fotodesorpcí, anebo chemickým leptáním pomocí chemicky aktivních látek produkovaných plazmatem.

- Třetí fáze, pozorovaná v některých případech, nastává v okamžiku, kdy i poslední spory jsou vystaveny působení UV záření, což se projeví opětovným nárůstem sterilizační účinnosti.

Z výše uvedeného schématu je zřejmé, že v reálné situaci, kdy bakteriální spory se vzájemně překrývají a jsou na povrchu přítomny ve formě multivrstev, je limitujícím faktorem určujícím potřebný čas pro úplnou sterilizaci rychlost eroze stínícího materiálu.

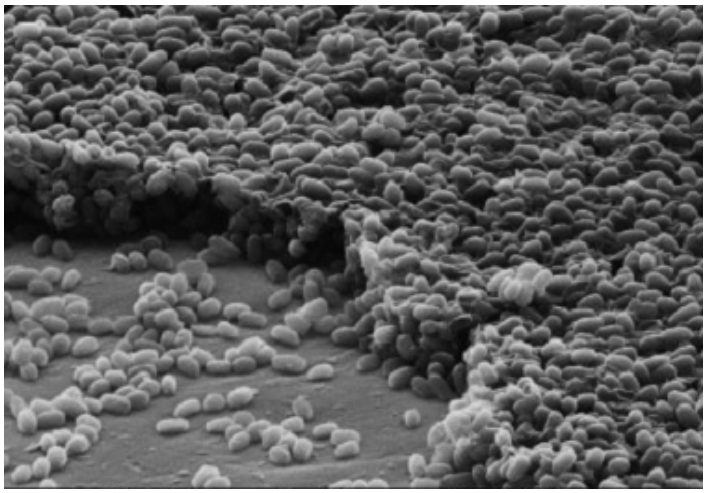

Obrázek 2. Příklad bakteriálních spor tvořících multivrstevnatou strukturu. Převzato z [**OK1**].

Pro potvrzení tohoto předpokladu jsme proto provedli experimenty [29], při kterých byly použity vzorky obsahující bakteriální spory *G. Stearothermophilus*, které tvořily multivrstevnatou strukturu (viz. **obrázek 2**). Tyto vzorky byly vystaveny induktivně vázanému nízkotlakému plazmatu generovanému ve směsích kyslík-dusík. Srovnáním naměřené intenzity UV záření, koncentrace atomárního kyslíku ve výboji určené pomocí optické emisní aktinometrie a sterilizačního účinku plazmatu bylo zjištěno, že pro použité bakteriální vzorky je čas potřebný k jejich úplné sterilizaci závislý ne na intenzitě UV záření, ale na koncentraci atomárního kyslíku produkovaného plazmatem. Následné porovnání závislosti koncentrace atomárního kyslíku na složení výbojové směsi se stupněm eroze bakteriálních spor, jež byl určen z mikrografů vzorků nasnímaných skenovacím elektronovým mikroskopem, potvrdilo, že efektivita sterilizačního procesu je v tomto případě skutečně svázána s erozí bakteriálních spor. Tento výsledek byl dále rozpracován a srovnán s teoretickým modelem, ve kterém byly předpokládány dvě různé populace spor - spory dosažitelné

UV zářením a spory stíněné jinými sporami, a dva současně působící procesy – inaktivace spor UV zářením a odleptávání stínícího materiálu. Jak je uvedeno v souhrnné práci [**OK1**] navržený teoretický model poměrně věrně odpovídá experimentálně zjištěným závislostem. Tento výsledek je velmi důležitý zejména s ohledem na optimalizaci sterilizačního procesu, kdy je nutné optimalizovat nejen intenzitu emitovaného UV záření, ale i rychlost odstraňování biologického materiálu stínícího spory. Na tomto místě je vhodné podotknout, že předpoklad o chemickém odleptávání stínícího materiálu, jak bude podrobněji diskutováno v následující kapitole, byl posléze pro případ aktivního plazmatu modifikován a jako hlavní proces vedoucí k odstranění stínícího materiálu byl identifikován proces chemického odprašování [30]. Nicméně závěry modelu, tj. závislost celkového času nutného ke kompletní sterilizaci na rychlosti odstraňování stínícího materiálu, jsou stále platné.

2.2. Odstraňování organického materiálu z povrchů pomocí nízkoteplotního plazmatu

Jak bylo zmíněno v předcházející kapitole, účinnost sterilizace je dána v reálných podmínkách nejen intenzitou UV záření emitovaného plazmatem, ale zejména rychlostí odstraňování organického materiálu, který může stínit některé spory. Z tohoto důvodu bylo nutné, především s ohledem na možnou optimalizaci sterilizačního procesu, určit hlavní mechanismus vedoucí k odstranění organického materiálu plazmatem. Mimoto, znalost mechanismu vedoucího k eliminaci organického materiálu z povrchu je zásadní i s ohledem na odstraňování dalších možných patogenních biomolekul, jako jsou infekční proteiny, či bakteriální endotoxiny. Na rozdíl od bakteriálních spor, jimž byla věnována poměrně velká pozornost v literatuře, oblast interakce plazmatu s biomolekulami byla po dlouhou dobu v pozadí zájmu. Hlavním limitujícím faktorem byla, a stále je, vysoká nebezpečnost infekčním prionů a bakteriálních endotoxinů a s ní související bezpečnostní opatření, která neumožňují provádět experimenty v běžných laboratorních podmínkách. Z tohoto důvodu byly nejprve prováděny experimenty s vybranými neinfekčními bílkovinami, konkrétně s bovin serum albuminem (BSA), lysozinem a ubiquitinem [**OK2**]. Tyto tři proteiny byly vystaveny nízkotlakému induktivně vázanému plazmatu generovanému v čistém argonu a jeho směsím s kyslíkem, dusíkem a vodíkem. Pro určení rychlosti odstraňování bílkovin z povrchu byla použita metoda založená na profilometrii. V této

metodě byly bílkoviny deponovány na substráty z vodného roztoku pomocí injekční stříkačky ve formě malých kapek. Po zaschnutí vytvářely bílkoviny na povrchu velmi dobře reprodukovatelnou strukturu s vysokým okrajem a středovou oblastí, kde byla tloušťka vrstvy výrazně nižší[1]. Účinnost plazmatu byla pak určována pomocí měření výšky okraje deponované vrstvy před a po aplikaci plazmatu jak je znázorněno na **obrázku 3**. Na základě těchto experimentů bylo zjištěno, že rychlost odstraňování použitých bílkovin z povrchu je velmi závislá na použité výbojové směsi. Z tohoto pohledu se ukázala být nejúčinnější směs argonu s kyslíkem, jejíž použití vedlo k přibližně čtyřikrát rychlejšímu odstranění všech tří bílkovin z povrchu než při použití jiných výbojových směsí [**OK2**].

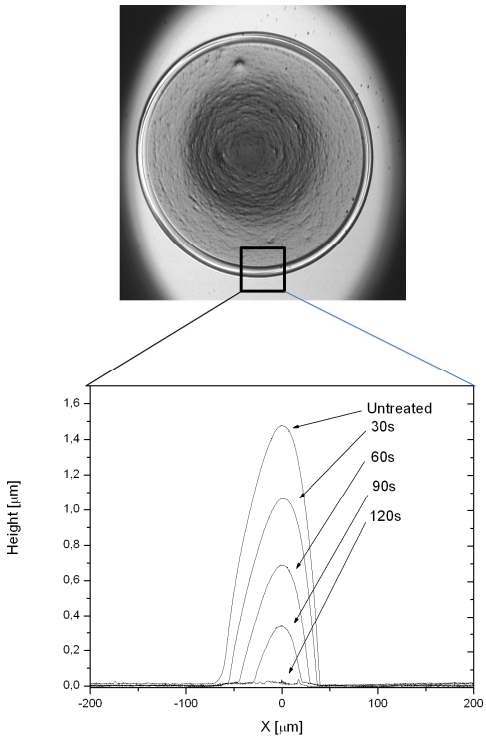

Obrázek 3. Fotografie BSA deponovaného na křemík (horní obrázek) a příklad měření poklesu výšky depozitu při vystavení vzorku výboji ve směsi Ar:O_2 20:1 při tlaku 10 Pa a příkonu 200 W (dolní obrázek)

Na základě těchto výsledků bylo předpokládáno, že hlavní mechanismus vedoucí k postupné eliminaci bílkovin z povrchu je chemické leptání bílkovin způsobené atomárním kyslíkem. Nicméně podrobnější studium ukázalo, že rychlost odstranění bílkovin z povrchu nekoresponduje s koncentrací atomárního kyslíku ve

[1] Díky podobnosti se stopou, která vznikne na podšálku po rozlití kávy, byl vzniklý tvar nazván „coffee ring effect“

výboji: zatímco s rostoucím zastoupením kyslíku ve výbojové směsi argon-kyslík, koncentrace atomárního kyslíku ve výboji monotónně roste, bílkoviny byly odstraňovány nejrychleji ve směsi Ar:O_2 95:5 [**OK3**]. Tento výsledek, tj. nejefektivnější eliminace bílkovin z povrchu ve směsi Ar:O_2 s malým množstvím kyslíku, nebylo možné vysvětlit ani působením UV záření (fotodesorpce), ani odprašováním bílkovin energetickými ionty (energie iontů měřená pomocí hmotnostní spektrometrie byla přibližně 10 eV, což není dostatečné pro odprašování organických materiálů).

Pro vysvětlení mechanismu odstraňování organického materiálu z povrchů působením nízkotlakého plazmatu proto byly provedeny experimenty s kalibrovanými zdroji argonových iontů a zdroji atomárního kyslíku [**OK4**], tj. postup, který byl použit i na studium interakce plazmatu s bakteriálními sporami a uhlovodíkovými vrstvami [30-32]. Na základě experimentů provedených v uspořádání schematicky znázorněném na **obrázku 4** bylo zjištěno, že atomární kyslík sám o sobě nemá výraznější vliv na tloušťku deponované vrstvy bílkovin: při vystavení vzorků toku atomárního kyslíku 2.4 x 10^{15}.cm^2.s^{-1} došlo po jedné hodině k poklesu tloušťky bílkovinné vrstvy pouze o 5 nm. Výrazně rychlejší pokles tloušťky deponovaných bílkovin byl pozorován při použití svazku argonových iontů (kolem 80 nm za jednu hodinu). Nicméně v tomto případě byla energie dopadajících iontů Ar^+ 100 eV, což je o řád více, než v případě induktivně vázaného výboje. Nejrychlejší odstranění bílkovin bylo pozorováno při kombinaci svazků atomárního kyslíku i argonových iontů (přes 700 nm za hodinu). Takto výrazně vyšší účinnost byla vysvětlena synergickým působením Ar^+ iontů a O atomů (popřípadě i O_2 molekul), tzv. chemickým odprašováním. Při tomto procesu argonové ionty nejprve díky své energii vytváří defekty v povrchové vrstvě bílkovin (vytvářejí otevřené vazby), které jsou následně atakovány velmi reaktivním kyslíkem. V reakcích s kyslíkem dochází k tvorbě volatilních molekul (CO_2, H_2O atd.) které jsou uvolňovány z povrchu, což má za následek postupný pokles tloušťky deponovaných bílkovinných vrstev. Na tomto místě je vhodné podotknout, že energie potřebná pro rozbití vazeb v organickém materiálu a vytvoření aktivních míst, které mohou reagovat s dopadajícím kyslíkem, je řádově několik elektronvoltů, tj. snadno dosažitelná ve výbojovém plazmatu.

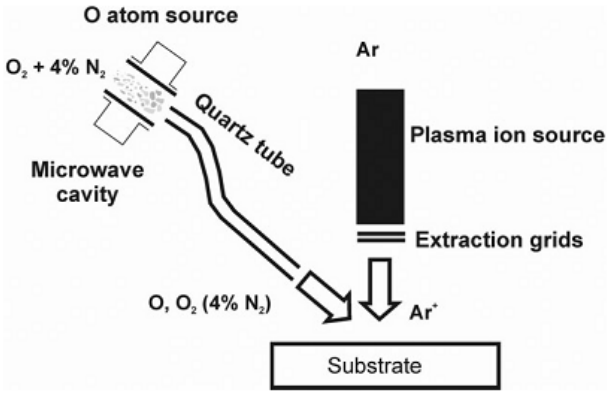

Obrázek 4. Schematické uspořádání experimentu využívajícího kalibrované zdroje atomárního kyslíku a argonových iontů. Převzato z [**OK4**].

Experimentální ověření dominance chemického odprašování v aktivním plazmatu bylo provedeno při následných cílených experimentech, kdy byly testovány postupně induktivně vázané nízkotlaké výboje generované ve směsi Ar:O_2 mající buď stejnou koncentraci iontů a různé koncentrace atomárního kyslíku, anebo výboje se stejnou koncentrací O atomů a různými koncentracemi iontů [**OK5**]. Tyto experimenty prokázaly, že rychlost odstraňování bílkovinných depozitů skutečně závisí jak na množství kyslíku produkovaného v plazmatu, tak i na koncentraci iontů. Nicméně je vhodné zdůraznit, že tyto závěry platí pouze pro zónu aktivního plazmatu, kde je dostatečně vysoká koncentrace iontů. Jak bylo prokázáno [**OK5**], v dohasínajícím plazmatu, pro které je charakteristická o několik řádů nižší koncentrace iontů, chemické odprašování ztrácí na významu a hlavním procesem vedoucím k odstranění organických látek z povrchu se stává chemické leptání spojené s přítomností chemicky aktivních částic (zejména OH radikálů a atomárním kyslíkem a vodíkem).

Důležitou vlastností chemického odprašování je nezávislost účinnosti tohoto procesu na konkrétním složení opracovávané organické látky. To je dáno tím, že na rozdíl od chemického leptání je primárním procesem vedoucím k tvorbě aktivních míst na povrchu vzorku rozbití chemické vazby energetickým iontem. To je důležité zejména s ohledem na možnost efektivně odstraňovat za stejných výbojových podmínek různé organické nečistoty z povrchů, včetně bakteriálních spor, homopolymerů aminokyselin i bakteriálních endotoxinů. Experimentální ověření bylo provedeno v následujících experimentech (například [**OK5**,**OK6**]). Tento výsledek je velmi slibný zejména s ohledem na možné odstraňování infekčních prionů, které jsou velmi odolné vůči klasickým sterilizačním procesům.

Výše zmíněná výhoda, tj. obdobná hodnota účinnosti chemického odprašování pro polymerní látky, které se liší svou chemickou strukturou, však může být v některých případech i zásadní nevýhodou, protože spolu s organickou nečistotou je s podobnou účinností chemicky odprašován i povrch jakéhokoliv plastového materiálů.

Na závěr této kapitoly bude pozornost věnována i možnosti monitorování účinnosti odstraňování biomolekul z povrchů při aplikaci nízkoteplotního plazmatu. Tato problematika je velmi důležitá zejména s ohledem na skutečné využití plazmové sterilizace, kdy je potřeba se sterilizační metodou „dodat“ i indikátor úspěšně ukončeného procesu. Na rozdíl od aplikace zvýšené teploty, záření či sterilizačních metod založených na použití chemických látek, kdy je jasně dáno sterilizační činidlo (dosažená teplota, dávka záření či množství chemické látky), v případě plazmatu, kdy efektivita procesu je dána kombinací koncentrace chemicky aktivní látky a energie a koncentrace iontů, žádný takovýto jednoznačný indikátor neexistuje. To představuje jednu z podstatných překážek, které doposud brání zavedení plazmových metod pro použití v lékařské praxi. Jednou možností ověření úspěšně proběhlého procesu je analýza vzorků obsahujících známé množství modelové biologické látky, které jsou sterilizovány spolu s lékařskými nástroji. Analýza takovýchto vzorků probíhá většinou po ukončení sterilizačního procesu a může být časově náročná. Alternativou by mohlo být monitorování sterilizačního procesu *in-situ*, které by umožnilo mimo jiné i včasnou indikaci možných problémů během sterilizace. Z tohoto důvodu byla navržena metoda založená na metodě mikrovah využívajících křemenné krystaly (quartz crystal microbalance). Při této metodě je na křemenný krystal nanesena nejprve vrstva biologické látky (v našem případě bílkoviny). Po zapálení plazmatu je pak sledován nárůst frekvence krystalu, který odpovídá postupnému odstraňování bílkoviny z jeho povrchu. Tento proces byl úspěšně testován při odstraňování bovin serum albuminu v pulzním induktivně vázaném výboji [**OK7**].

Možnost monitorování procesu odstraňování bílkovin *in-situ* během působení plazmatu přinesla i další zajímavé výsledky týkající se kinetiky tohoto procesu. Bylo zjištěno, že rychlost odstraňování bílkovin při působení plazmatu postupně klesá s časem. Jedním z možných vysvětlení tohoto efektu je přítomnost nevolatilních anorganických látek v bílkovinných vzorcích, přičemž zdrojem těchto látek mohou být jednak nečistoty při přípravě vzorků, jednak anorganické částice přítomné ve vlastní struktuře bílkovin (například síra). Na rozdíl od organických látek je efektivita chemického odprašování anorganických materiálů velmi nízká. To má za následek, že s

rostoucím časem postupně narůstá koncentrace těchto látek na povrchu opracovávaných vzorků, což vede ke vzniku velmi odolné vrstvy, která limituje další působení plazmatu. Tento efekt byl experimentálně potvrzen analýzou chemického složení povrchu bílkovin vystavených plazmatu [**OK7**].

2.3. Optimalizace sterilizačního procesu

Jak bylo uvedeno v předchozích kapitolách, pro efektivní sterilizaci bakteriálních spor a současné odstranění biologických patogenů z povrchů je nutné současně maximalizovat tři parametry:

- Intenzitu UV záření emitovaného plazmatem
- Koncentraci a energii iontů dopadajících na povrch sterilizovaných objektů
- Koncentraci atomárního kyslíku

Jednou z velmi slibných možností, jak optimalizovat všechny tyto parametry je použití ternární směsi $Ar:O_2:N_2$. Jak bylo ukázáno v [**OK8**] je možné při vhodné volbě složení této výbojové směsi (malá příměs kyslíku a dusíku v argonovém plazmatu) dosáhnout jak intenzity UV záření vyšší než v případě binární směsi $O_2:N_2$, tak rychlosti odstraňování bovin serum albuminu srovnatelné s výboji ve směsi $Ar:O_2$, která byla identifikována jako optimální pro rychlou eliminaci organického materiálu z povrchu.

Tyto výsledky je možné vysvětlit jak závislostí koncentrace nabitých částic na složení výbojové směsi, tak změnami v účinnosti produkce některých částic v plazmatu generovaném v ternární směsi.

Jak bylo ukázáno [**OK8**] koncentrace nabitých částic v ternární výbojové směsi $Ar:O_2:N_2$ narůstá s rostoucím podílem argonu, obdobně jako v případu směsi $Ar:O_2$. To je dáno zejména vyššími energetickými ztrátami elektronů v interakcích s O_2 a N_2 ve srovnání s argonovými atomy. Jinými slovy, energie dodávaná do výboje je v případě molekulárních plynů spotřebovávána nejen na jejich ionizaci, ale i na jejich rotační a vibrační excitaci, popřípadě na disociaci. Snížení podílu molekulárních plynů v ternární směsi snižuje tyto ztráty a vede k vyššímu stupni ionizace. To má několik důležitých následků.

V první řadě rostoucí koncentrace iontů zvyšuje účinnost procesu chemického odprašování organických látek. Za druhé, zvýšená produkce nabitých částic vede k

zvýšené excitaci molekul přítomných ve výboji. S ohledem na sterilizace je důležité zejména zvýšení koncentrace metastabilních molekul dusíku $N_2(A)$, které se podílejí jednak na tvorbě NO molekul (např. [33]):

$$N_2(A) + O \rightarrow NO + N(^2D) \qquad (R1)$$

jednak vedou k vybuzení NO molekul do stavu NO(A) (např.[34]) :

$$N_2(A) + NO \rightarrow NO(A) + N_2 \qquad (R2)$$

jehož deexitace je spojena s emisí záření v UV oblasti. To může vysvětlit zvýšenou intenzitu UV záření ve srovnání s binární směsí O_2:N_2.

Experimentální ověření vysoké rychlosti odstraňovaní dalších typů biologických vzorků v ternární směsi Ar:O_2:N_2 bylo představeno v publikaci [35]. Příklad srovnání účinností různých výbojových směsí pro odstraňování poly-L-histidinu je uveden na **obrázku 5**.

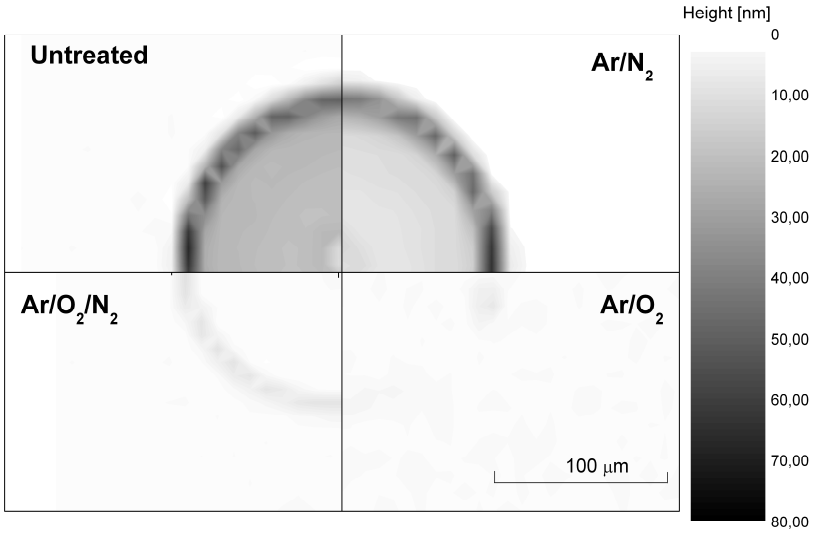

Obrázek 5. 2D mapa výšky poly-L-histidinu před a po aplikaci různých výbojových směsí (doba působení plazmatu 5s, tlak 10 Pa, příkon 200W, proud plynu 22 sccm. Převzato z [35].

2.4. Inaktivace bakteriálních endotoxinů

Posledním typem biologických patogenů, který bude stručně zmíněn, jsou bakteriální endotoxiny. Bakteriální endotoxiny jsou vysoce pyrogení látky, tj. látky schopné vyvolat zvýšenou teplotu. Přítomnost těchto látek v krvi ve vyšším množství

může mít dramatické následky – poškození tkáně či úplné selhání orgánů. Tyto látky jsou navíc velmi odolné vůči klasickým sterilizačním technikám, což představuje závažný problém. Jak bylo již zmíněno v předchozí kapitole, bakteriální endotoxiny je možné efektivně odstranit z povrchů, je-li použito nízkoteplotní plazma. Nicméně jak bylo také zmíněno v předešlé kapitole, dochází při intenzivním chemickém odprašování, tj. za situace dostatečného toku iontů a atomárního kyslíku na povrch vzorků, k postupné erozi plastových materiálů. Z tohoto důvodu se hledají šetrnější postupy, které vedou k inaktivaci patogenů (tj. ke snížení jejich biologické aktivity) bez nutnosti jejich úplného odstranění z povrchu. Pro tento postup je výhodnější použít dohasínající plazma, ve kterém je výrazně snížena koncentrace iontů, což vede k dramatickému poklesu účinnosti chemického odprašování [**OK5**], přičemž dominantním mechanizmem odstraňování organického materiálu se stává výrazněji pomalejší chemické leptání.

Pro experimenty zaměřené na možnou inaktivaci bakteriálních endotoxinů jsme proto použili dohasínající mikrovlnné plazma, jehož účinnost byla prokázána nejprve pro případ lipopolysacharidů (LPS) [36], a posléze i pro další typy endotoxinů (lipoteichoickou kyselinu, zymosan, Lipid A) [37]. Bylo zjištěno, že účinnost depyrogenizace bakteriálních endotoxinů nezávisí na intenzitě UV záření ve spektrálním rozsahu nad 200 nm ani na koncentraci nabitých částic. Jediným parametrem, který vedl k výraznému zvýšení rychlosti depyrogenizace byla přítomnost vodíku ve výbojové směsi [**OK9**]. Bylo prokázáno, že ve směsích obsahujících vodík je možné dosáhnout poklesu pyrogenicity bakteriálních endotoxinů o jeden řád v časech kratších než jedna minuta.

Následné experimenty prováděné v binárních výbojových směsích s vodíkem ukázaly, že pokles pyrogenní aktivity biologicky aktivní části LPS, takzvanému Lipidu A, je způsoben jejich chemickou modifikací, konkrétně redukcí postraních $C_xH_yO_z$ řetězců a změnám v části Lipidu A obsahující fosfor [38]. Tyto změny mohou být vyvolány buď chemickou reakcí s vodíkem, popřípadě změnami, které vyvolává vysoce energetické VUV záření. Posledně jmenovaný efekt byl potvrzen pomocí VUV lamp, kdy byly po ozařování pozorovány změny v chemické struktuře Lipidu A obdobné změnám vyvolaným dohasínajícím vodík obsahujícím plazmatem [**OK5**].

2.5. Shrnutí

Z výše uvedeného stručného přehledu dosažených výsledků je možné učinit následující závěry. V první řadě se podařilo prokázat, že nerovnovážné plazma generované za sníženého tlaku je velmi vhodným nástrojem na inaktivaci biologických patogenů, či jejich odstraňování z povrchů. Podařilo se nalézt hlavní proces vedoucí k eliminaci organických látek z povrchů v aktivním plazmatu – chemické odprašování. To umožnilo optimalizovat sterilizační proces, přičemž velmi slibné výsledky byly dosaženy při použití ternární směsi $Ar:O_2:N_2$. Tato výbojová směs v sobě kombinuje přednosti binárních směsí $O_2:N_2$, které se používají jako velmi účinný zdroj UV záření pro sterilizaci bakterií a bakteriálních spor, a směsi $Ar:O_2$, která byla identifikována jako nejvhodnější směs pro rychlé odstranění organického materiálu. Možnost současně inaktivovat bakteriální spory a odstraňovat biologickou kontaminaci povrchů snižuje čas potřebný pro úplnou sterilizaci objektů, což vede ke snížení nákladů a snižuje rizika poškození sterilizovaných materiálů.

I přes tyto výsledky je však nutné podotknout, že stále existují některé překážky, které brání využití plazmatu pro sterilizační účely. To se týká zejména možnosti sterilizovat předměty mající komplikované tvary a předměty zabalené v ochranné fólii. Mimoto se ukazuje, že účinnost odstraňování materiálů organického původu je silně redukována přítomností anorganických látek (tzv. matrix efekt).

3. Depozice plazmových polymerů

Druhou oblastí, kde nerovnovážné plazma hraje důležitou roli při biolékařských aplikacích, je příprava biomateriálů, tj. neživotaschopných materiálů, určených k interakci s biologickými systémy. V případě, že to není vyžadováno danou aplikací, biomateriál nesmí být toxický a vyvolávat záněty, či alergické reakce. Dále by biomateriál měl splňovat i další nároky, přičemž požadavky závisí na konkrétní aplikaci. Typickými příklady požadovaných vlastností je například pevnost a snadná osseointegrace kostních implantátů, průhlednost, flexibilita a dobrá smáčivost kontaktních čoček, anebo flexibilita a vysoká odolnost vůči adsorpci bílkovin u cévních náhrad. Bohužel existuje velmi málo materiálů, které by byly schopny současně splňovat všechny nároky na ně kladené. Z tohoto důvodu je často používanou strategií použití konvenčních materiálů (kovy, slitiny kovů, polymery) majících požadované objemové vlastnosti, které jsou následně povlakovány tenkou funkční vrstvou, zaručující jejich biokompatibilitu. Jednou z možností depozice tenkých funkčních vrstev je použití nerovnovážného plazmatu, které umožňuje deponovat homogenní tenké vrstvy s dobře kontrolovatelnými fyzikálními, chemickými i bioresponsivními vlastnostmi na prakticky jakýkoliv materiál, aniž by byly ovlivněny objemové vlastnosti povlakovaných materiálů.

Šíře materiálů, které je možné deponovat pomocí technologií založených na nerovnovážném plazmatu (např. magnetronovým naprašováním, depozicí z plynné fáze s aktivací plazmatem) je velmi rozsáhlá a zahrnuje jak kovy, či oxidy kovů, tak i tzv. plazmové polymery (například [39]). Termín plazmový polymer označuje materiál, který vzniká jako výsledek průchodu organických plynů nebo par doutnavým výbojem. Organické molekuly jsou nejprve ve výboji aktivovány anebo fragmentovány při srážkách s energetickými elektrony, popřípadě UV zářením emitovaným plazmatem. Takto vzniklé radikály se následně podílejí na konvenční radikálové polymerizaci, kdy dochází jednak k růstu řetězců (propagace), jednak k ukončování řetězců (terminace). Zatímco aktivace probíhá převážně v plazmatu, druhé dvě fáze mohou probíhat jak v plazmatu, tak i na povrchu substrátu vloženého do plazmatu.

Na rozdíl od klasických polymerů, které obsahují pravidelně se opakující monomerní jednotky, mají plazmové polymery velmi neuspořádanou strukturu, přičemž jednotlivé řetězce jsou velmi krátké, náhodně rozvětvené a ukončené, a vykazují vyšší

stupeň zesíťování. Tento rozdíl ve struktuře konvenčních a plazmových polymerů je demonstrován na **obrázku 6**.

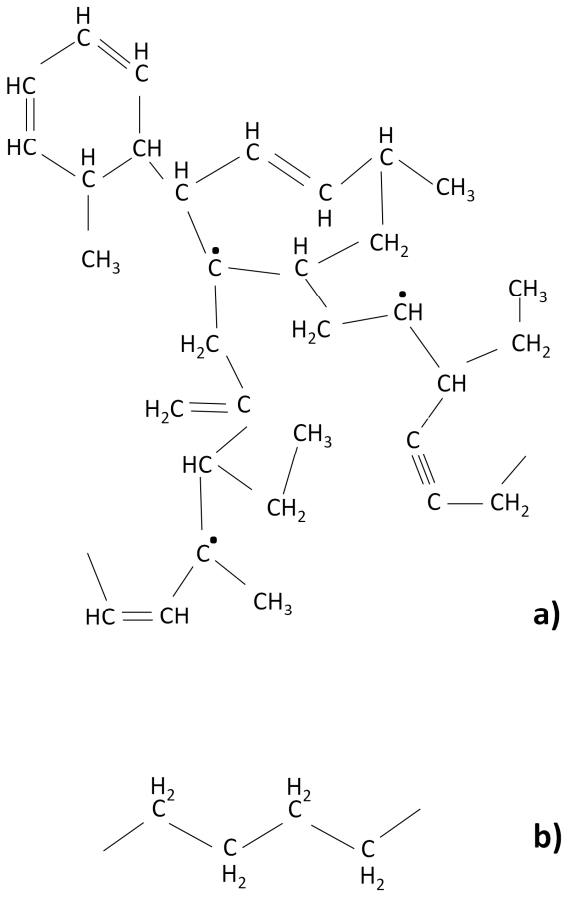

Obrázek 6. a) hypotetická struktura uhlovodíkového plazmového polymeru a b) strukturní vzorec polyethylenu

Výsledné vlastnosti deponovaných vrstev závisí na mnoha faktorech, jako je například použitý výchozí monomer, tlak, výkon a vzdálenost substrátu od aktivního plazmatu atd. Toto činí přípravu plazmových polymerů relativně složitým procesem. Na druhou stranu velká flexibilita plazmové polymerace dovoluje měnit vlastnosti deponovaných vrstev (chemické složení, morfologie, smáčivost, tvrdost atd.) v širokém rozsahu a umožňuje přípravu materiálů s vlastnostmi, které jsou velmi obtížně dosažitelné klasickými způsoby polymerace.

Pravděpodobně nejpoužívanějším způsobem přípravy plazmových polymerů je depozice z plynné fáze za aktivace plazmatem (PECVD), kdy je do plazmového reaktoru přiváděn plynný monomer, nebo jeho směs s pracovním plynem. Nevýhodou

metody PECVD je nutnost použití kapalných monomerů, popřípadě organických plynů, které jsou často toxické, popřípadě karcinogenní. Nicméně plazmové polymery je možné připravit i bez nutnosti použití těchto látek pomocí magnetronového naprašování (viz. **obrázek 7**). Při tomto způsobu přípravy je vysokofrekvenční magnetron osazen polymerním terčem, který je díky vzniklému zápornému předpětí na magnetronu odprašován dopadajícími vysokoenergetickými ionty. Terč tak slouží jako zdroj organických fragmentů pro proces plazmové polymerace, přičemž organické fragmenty jsou emitovány pouze po dobu, po kterou je zapálen výboj. Navíc tato metoda přípravy je energeticky výhodnější při případném škálování procesu.

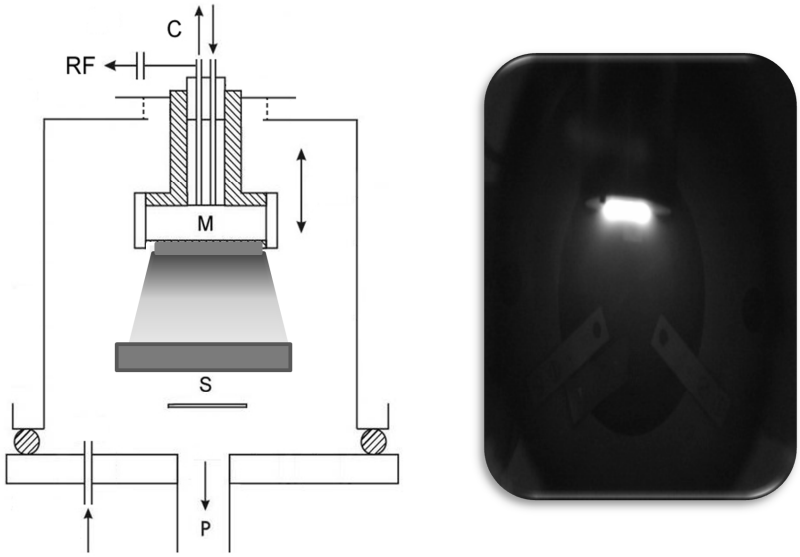

Obrázek 7. Základní uspořádání používané při vysokofrekvenčním naprašování z polymerních terčů (vlevo) a fotografie výboje při vysokofrekvenčním naprašování z nylonového terče (vpravo).

V předkládané práci bude pozornost věnována zejména plazmovým polymerům připraveným vysokofrekvenčním magnetronovým naprašováním z nylonového terče a to jak ve formě hladkých vrstev (kapitola 3.1), tak i přípravě plazmově polymerizovaných nanočástic (kapitola 3.2). Výsledky dosažené v naší skupině, na kterých jsem se částečné podílel a které se týkají dalších druhů plazmových polymerů, je možné nalézt v následujících článcích [40-43].

3.1 Příprava a aplikace tenkých vrstev plazmových polymerů obsahující aminoskupiny

3.1.1 Tenké vrstvy plazmových polymerů obsahující aminoskupiny

Jedním z nejčastěji studovaných plazmových polymerů používaných pro biolékařské aplikace jsou plazmové polymery obsahující aminy a to zejména primární aminy (NH_2). To je dáno zejména tím, že primární aminy umožňují kovalentní imobilizaci celé řady biomolekul (např. DNA, či různé typy bílkovin), usnadňují a podporují růst buněk, popřípadě se používají jako platforma pro následnou funkcionalizaci [44]. Z tohoto důvodu byla hlavní pozornost věnována optimalizaci depozičního procesu, vedoucího k vrstvám bohatým na $–NH_2$ skupiny. V těchto experimentech byly použity různé postupy využívající jak nízkotlaké výboje, tak i výboje atmosférické. Výsledky dosažené různými postupy jsou shrnuty v **tabulce 1**. Je vidět, že nejvyšších hodnot amino-efektivity, tj. poměru koncentrace primárních aminoskupin ku koncentraci uhlíku ($[NH_2]/[C]$), dosahující hodnot pod 20% bylo dosaženo plazmovou co-polymerací využívající jako pracovní směs NH_3:C_2H_4.

Metoda	**Materiál**	**NH_2/C [%]**	**Depoziční rychlost**	**Ref.**
Modifikace plazmatem	N_2:H_2 nebo NH_3/N_2	3.5	neuvedeno	[45]
Modifikace plazmatem	N_2:H_2 nebo NH_3	2	neuvedeno	[46]
Modifikace plazmatem	NH_3	2	neuvedeno	[47]
Plazmová co-polymerace	NH_3:C_2H_4	15	2.5 nm/min	[48]
Atmosférické plazma	N_2:C_2H_4	8	500 nm/min	[49]

Tabulka 1 Srovnání různých metod použitých pro přípravu vrstev bohatých na primární aminoskupiny

3.1.2 Příprava vrstev obsahujících primární aminoskupiny magnetronovým naprašováním nylonu a jejich vlastnosti

Na rozdíl od výše zmíněných studií bylo v naší laboratoři pro depozici vrstev plazmových polymerů obsahujících primární aminoskupiny využito magnetronového naprašování z nylonového terče [**OK10**]. Byly testovány různé pracovní plyny a to argon, dusík a vodík a jejich směsi. Bylo zjištěno, že depoziční rychlost roste s rostoucím zastoupením dusíku a s klesajícím zastoupením vodíku ve výbojové směsi. Tento rozdíl v depozičních rychlostech je možné vysvětlit jednak leptáním rostoucí vrstvy vysoce reaktivními vodíkovými atomy, jednak zvýšením účinnosti odprašovaní molekulárních fragmentů z nylonového terče při zvyšujícím se zastoupením dusíku ve výbojové směsi, což bylo prokázáno pomocí hmotnostní spektrometrie prováděné během depozice plazmově polymerních vrstev [**OK11**].

Složení výbojové směsi má vliv nejen na depoziční rychlost, ale i na chemické složení připravených vrstev. Bylo zjištěno, že při použití Ar jako pracovního plynu mají deponované vrstvy prvkové složení obdobné nylonu (75% C, 12.5% N, 12.5% O). Je-li použita směs Ar:N_2 dochází k nárůstu koncentrace dusíku ve vrstvách. Nicméně vrstvy připravené ve směsích Ar/N_2 mají velmi malou amino-efektivitu, jinými slovy jen malá část dusíku je v těchto vrstvách přítomna ve formě primárních aminů. Výrazné zvýšení amino-efektivity bylo pozorováno u vzorků připravených ve výbojových směsích obsahujících dusík a vodík. Bylo prokázáno, že v těchto směsích je možné připravit vrstvy mající poměr [NH_2]/[C] blížící se 20%, tj. poměr srovnatelný s maximálními hodnotami dosaženým jinými postupy, při zachování relativně vysoké depoziční rychlosti (7.5 nm/min).

Následně byly vrstvy připravené v různých výbojových směsích testovány s ohledem na kinetiku adsorpce bílkovin, konkrétně bovin serum albuminu. Bylo prokázáno, že rychlost adsorpce albuminu odpovídá zastoupení NH_2 skupin ve vrstvách: nejrychlejší adsorpce byla pozorována na vzorcích připravených v N_2:H_2 směsi, nejpomalejší pak byla adsorpce na vrstvách deponovaných při použití argonu jako pracovního plynu.

Posledním krokem bylo ověření schopnosti vrstev připravených pomocí magnetronového naprašování z nylonového terče usnadnit růst osteoblastům podobných buněk (MG-63). Tyto experimenty byly provedeny ve spolupráci s ING Greifswald. Jak je vidět na **obrázku 8**, kde jsou pro srovnání uvedeny mikrografy MG-63 buněk na

TiAlV substrátu a na TiAlV pokrytým vrstvou plazmového polymeru připraveného magnetronovým naprašováním z nylonového terče ve směsi N_2/H_2 1:1, buňky vykazují skutečně výrazněji lepší adhezi k povrchu pokrytém plazmovým polymerem [50].

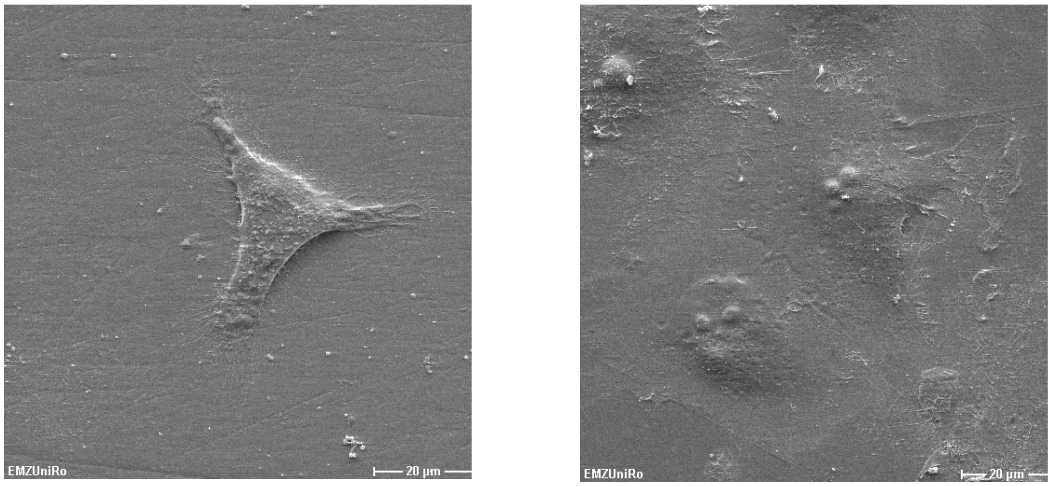

Obrázek 8. Příklady mikrografů buněk MG-63 na TiAlV disku (vlevo) a na TiAlV disku pokrytém vrstvou nylonu magnetronově naprašovaného ve směsi N_2:H_2 1:1.

3.1.3 Testování časové stálosti a odolnosti vrstev naprašovaného nylonu vůči vodnému prostředí a sterilizačním metodám

Povrchová koncentrace primárních amino skupin však není jediným parametrem ovlivňujícím použitelnost plazmových polymerů v biolékařských aplikacích. Ty díky své specifičnosti kladou i další nároky na vlastnosti deponovaných vrstev. První z vlastností, která by měla být zaručena, je časová stálost vzorků. Bohužel, plazmové polymery vystavené působení atmosféry mají tendenci měnit své vlastnosti. Jako příklad může být uvedena oxidace volných radikálu přítomných v plazmových polymerech, popřípadě nestálost některých funkčních skupin, která vede k reorganizaci povrchové vrstvy [51]. Toto je i případ plazmových polymerů obsahujících primární aminy, u kterých byl pozorován poměrně rychlý pokles amino efektivity s časem [52]. Druhou důležitou vlastností povrchů používaných v biolékařských aplikacích je jejich odolnost vůči vodnému prostředí (např. vůči tělním tekutinám, krvi nebo kultivačnímu médiu používanému pro růst buněk). Posledním aspektem důležitým pro biolékařské aplikace je odolnost plazmových polymerů vůči sterilizačnímu procesu. Tyto tři vlastnosti, tj. časová stálost, odolnost vůči vodnému prostředí a odolnost námi připravovaných vrstev magnetronově naprašovaného nylonu vůči sterilizaci byla předmětem mého systematického výzkumu na KMF MFF UK.

Na základě provedených experimentů bylo zjištěno, že již po jedné hodině na vzduchu je možné pozorovat výrazné změny v povrchovém složení připravených vrstev. Bylo zjištěno, že po vystavení vzorků atmosféře dochází k postupnému růstu zastoupení kyslíku ve vrstvách na úkor koncentrace dusíku [**OK12**]. Na základě XPS a FT-IR měření byl tento efekt vysvětlen hydrolýzou vrstev způsobenou atmosférickou vlhkostí, tj. procesem:

$$-C{=}N- + H_2O \rightarrow -C{=}O + NH_3 \qquad (R3)$$

Co se týká rozpustnosti připravených vrstev ve vodě, ukázalo se, že zatímco vrstvy připravované v čistém argonu a v binárních směsích $Ar{:}N_2$ se nerozpouští, v případě vrstev deponovaných ve směsích $N_2{:}H_2$ dochází k releativně rychlému poklesu tlouštěk vrstev (cca 40% pokles tloušky po 24 hodinách ve vodě). Tento rozdíl je konsistentní s rozdílným zastoupením primárních aminoskupin ve vrstvách; vyšší zastoupení amino skupin ve vrstvách je doprovázeno vyšším výskytem nízkomolekulárních fragmentů (oligomerů) rozpustých ve vodě [52].

Posledním požadavkem vztahujícím se k biolékařským aplikacím plazmových polymerů je jejich odolnost vůči sterilizačním procesům. Tomuto tématu se věnuje podrobně práce [**OK13**], kde byly vrstvy magnteronově naprašovaného nylonu sterilizovány třemi nejčastěji používanými sterilizačními technikami – UV zářením, suchým teplem (160^o) a autoklávem (121^o). Srovnání vlastností připravených vrstev před a po sterilizaci ukázalo, že pro zachování schopnosti vrstev naprašovaného nylonu usnadňovat adhezi buněk je nejvhodnější použití suchého tepla, po jehož aplikaci nedošlo k žádnému pozorovatelnému poklesu počtu buněk rostoucích na sterilizovaném vzrorku ve srovnání se vzorkem, který sterilizován nebyl. U dalších dvou sterilizačních metod byl naopak pozorován výrazný pokles adherujících buněk jak je vidět na **obrázku 9**, kde jsou uvedeny fotografie osteoblatům podobných buněk MG-63 po jednom dni na vrstvách naprašovaného nylonu, které byly sterilizovány různými metodami.

V práci [**OK13**] byly kromě naprašovaného nylonu studovány i vrstvy plazmově polymerizovaného poly(ethylen oxidu) (pPEO) a naprašovaného poly(tetraflour ethylenu) (pPTFE). Srovnání vlivu sterilizačních metod na bioresponsivní vlastnosti těchto plazmových polymerů vedlo k závěru, že pro každý plazmový polymer je vhodná jiná sterilizační metoda: zatímco pro naprašovaný nylon je optimální suché teplo, pro vrstvy pPEO je nejvhodnější sterilizace UV zářením a pro pPTFE je použitelné jak UV

záření tak suché teplo. Tento výsledek je velmi důležitý zejména pro použití plazmových polymerů v biolékařských aplikacích, protože jasně dokumentuje fakt, že pro každý typ plazmového polymeru je nutné najít i vhodnou sterilizační metodu.

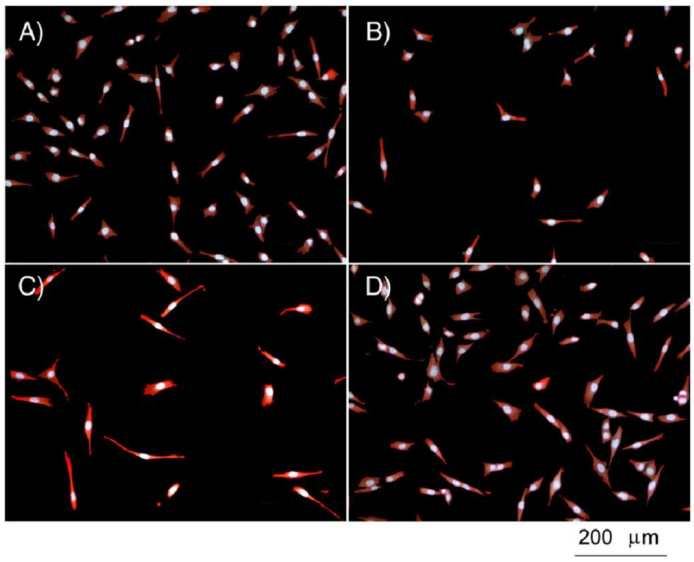

Obrázek 9. Příklady fotografií buněk MG-63 na vrstvách naprašovaného nylonu po jednom dni. A) vrstva, která nebyla sterilizována B) vrstva sterilizována UV zářením C) vrstva sterilizována autoklávem a D) vrstva sterilizována suchým teplem. Převzato z [**OK13**].

3.1.4 Použití vrstev naprašovaného nylonu pro přípravu vrstev omezujícím adsorpci bílkovin

Jak bylo uvedeno výše, vrstvy plazmových polymerů obsahující primární aminoskupiny mohou být využity i jako platforma pro další funkcionalizaci. Možnosti využití vrstev naprašovaného nylonu pro přípravu vrstev odolných vůči adsorpci bílkovin byla věnována publikace [**OK14**]. Tento typ materiálů (v literatuře označovaný jako „antifouling“) je velmi důležitý v celé řadě aplikací (například v cévních náhradách, výrobě biosenzorů či separačních membrán). V těchto aplikacích je pro správnou funkci daného materiálu nutné zajistit, aby na jeho povrchu nedocházelo k akumulaci krevních bílkovin.

Ačkoliv bylo navrženo mnoho různých postupů pro přípravu povrchů zamezujících adsorpci proteinů, jediný doposud známý typ materiálu, u kterého byl

pozorován antifouling charakter vůči krevní plazmě jsou polymerní „kartáče“ (polymer brushes) oligo(ethyleneglycol)metakrylátu a poly(karboxybetain acrylamidu). Tyto „kartáče“ se deponují na povrchy pomocí povrchově inicializované radikálové polymerace s přenosem atomu (ATRP) či metodou radikálového adičně-fragmentačního přenosu polymerního řetězce (RAFT). Při těchto metodách jsou iniciátory procesu navázány na povrch pomocí různých typů chemických reakcí (například chemisorpcí thiolů na povrch zlata) v závislosti na použitém substrátu. Toto je hlavní slabina všech těchto metod, jelikož daný proces je závislý na materiálu substrátu, což limituje šíří materiálů, které mohou být povlakovány.

Jako alternativa byl v práci [**OK14**] navržen postup schematicky znázorněný na **obrázku 10**. Při tomto postupu se nejprve nanese vrstva naprašovaného nylonu. Na ní se náváže ATRP iniciátor (α-bromoisobutyrat bromide), přičemž se využívá procesu acylace amino skupin na povrchu vrstev naprašovaného nylonu. Následně jsou na takovýchto površích vytvořeny polymerní kartáče oligo(ethyleneglycol)metakrylátu zakončeného hydroxy či metoxy skupinou, popřípadě kartáče poly(karboxybetain acrylamidu). Jak bylo ukázáno, takto připravené vrstvy mají skutečně antifouling charakter: v případě krevní plazmy byla pozorována adsorpce nižší než 35 $ng.cm^{-2}$, přičemž tento antifouling charakter byl časově stálý po dobu pěti měsíců.

Kromě dosažení velmi nízké adsorpce bílkovin na připravených površích je nutné zdůraznit i další výhody navrženého postupu. Jak bylo ukázáno chemické složení naprašovaného nylonu, tj. vrstvy, která byla použita jako platforma pro další kroky přípravy polymerních kartáčů, nezávisí na materiálu substrátu (sklo, Au, Si, TiAlV a poly(propylen)). Jinými slovy tento postup přípravy je použitelný pro takřka jakýkoliv substrát. Druhou výhodou je možnost přípravy ultratenkých vrstev naprašovaného nylonu při zachování homogenity pokrytí substrátu. Toto je velmi důležité zejména s ohledem na vývoj biosensorů (například čipů pro SPR), kdy je jedním z požadavků malá tloušťka vrstev.

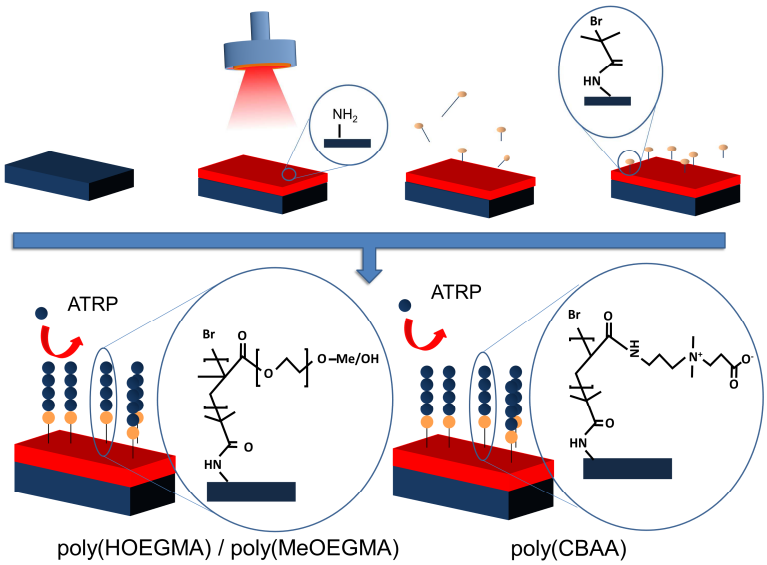

Obrázek 10. Schematické znázornění přípravy vrstev majících antifouling charakter založené na použití naprašovaného nylonu. Převzato z [**OK14**].

3.2 Příprava plazmově polymerizovaných nanočástic

Až doposud byly diskutovány pouze výsledky depozice plazmových polymerů ve formě tenkých, hladkých vrstev. Nicméně pomocí nízkoteplotního plazmatu je možné připravovat i plazmově polymerizované nanočástice. Vznik mikronových a submikronových částic plazmových polymerů byl poprvé popsán v sedmdesátých letech minulého století [53,54]. Po dlouhou dobu byla tvorba takovýchto částic velmi nežádoucím jevem, což platilo zejména pro průmyslové aplikace plazmových reaktorů používaných například při výrobě solárních článků či mikroelektronických součástek. Na druhou stranu takto vzniklé částice se staly předmětem mnoha studií a daly vzniknout oboru fyziky nazývaném fyzika prachového plazmatu (například přehledové články [55-58]). V tomto oboru byla hlavní pozornost věnována zejména studiu vzniku nanočástic a jejich vlivu na vlastnosti plazmatu. Nicméně plazmově polymerizované nanočástice je možné využít i pro přípravu nanostrukturovaných a nanoporézních materiálů, které mohou najít uplatnění i v biolékařských aplikacích (například při kontrolovaném podávání léčiv, kontrole smáčivosti povrchů). Z tohoto důvodu je patrný vzrůstající zájem o možnost kontrolované přípravy takovýchto částic.

Nejběžnějšími metodami přípravy plazmově polymerizovaných nanočástic je plazmatem aktivovaná depozice z plynné fáze či magnetronové naprašování při

zvýšeném tlaku (například [59-65]). Při těchto způsobech přípravy je možné odlišit tři fáze růstu nanočástic (například [66]):

- Vznik zárodků nanočástic. Tato fáze je řízena komplexním procesem plazmové polymerace. Na základě experimentálních výsledků bylo zjištěno, že klíčovým parametrem v této fázi je tlak: při tlaku nižším než je určitý kritický tlak (řádově desítky Pa) nedochází ke vzniku nanočástic. Tento efekt je vysvětlován nutností stabilizace vznikajících zárodků nanočástic trojsrážkami s nosným plynem.
- Koagulační fáze. S rostoucím počtem vzniklých zárodků nanočástic roste pravděpodobnost jejich vzájemných srážek, které vedou k velmi rychlému vzniku větších částic majících rozměry kolem 10 nm.
- Růstová fáze. Díky koagulaci velmi rychle klesá počet částic, které se mohou navzájem srážet. Další růst je možný připojováním neutrálních částic k již exitujícím nanočásticím.

Nicméně výše uvedené způsoby přípravy nejsou příliš vhodné pro kontrolovanou depozici nanočástic. To je dáno zejména tím, že vzniklé nanočástice v plazmatu získávají záporný náboj a jsou elektrostaticky zachyceny v plazmatu. To má za následek, že depozice je možná pouze díky gravitační síle, která překoná elektrostatické síly, a tudíž pouze relativně velké částice mohou být deponovány. Druhým možným postupem je pulzování plazmatu, nicméně v tomto případě je velmi limitovaná homogenita depozice a není možná kontinuální depozice. Alternativní postup testovaný na KMF MFF UK je využití konceptu podobnému plynně agregačním zdrojům používaným pro depozici kovových nanoklastrů [67]. Tento typ zdroje, který je schematicky představen na **obrázku 11**, se skládá z chlazené agregační komory osazené zdrojem plazmatu (v našem konkrétním případě vysokofrekvenčním magnetronem osazeným polymerním terčem), která je od depoziční komory oddělena úzkou výstupní štěrbinou. Toto uspořádání umožňuje udržovat v agregační komoře tlak dostatečně vysoký pro tvorbu nanočástic. Vzniklé nanočástice jsou pak proudem plynu unášeny skrze výstupní štěrbinu do nízkotlaké depoziční komory ve formě úzkého svazku a deponovány na substrát.

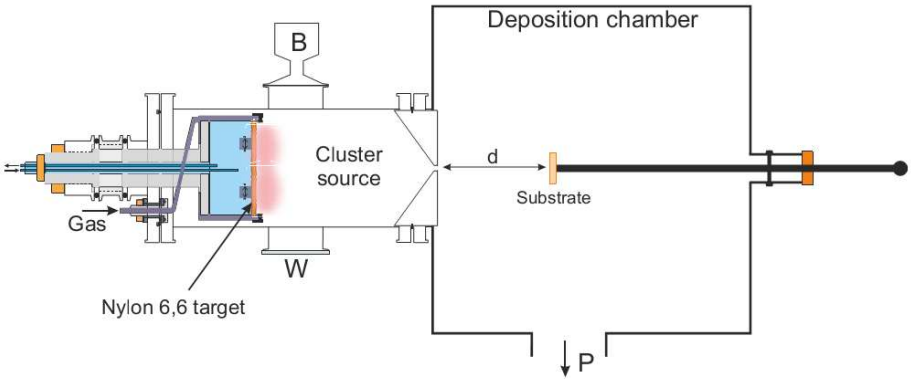

Obrázek 11. Schematické znázornění aparatury použité pro přípravy nanočástic plazmově polymerizovaného nylonu (B – tlaková měrka, W – optické okénko, P – čerpací systém, d – vzdálenost mezi substrátem a výstupní štěrbinou zdroje nanočástic). Převzato z [**OK15**].

Tento postup byl využit pro přípravu nanočástic plazmově polymerizovaného PTFE [68] i pro přípravu nanočástic plazmově polymerizovaného nylonu [**OK15**] (příklad vrstvy nanočástic plazmově polymerizovaného nylonu je uveden na **obrázku 12**).

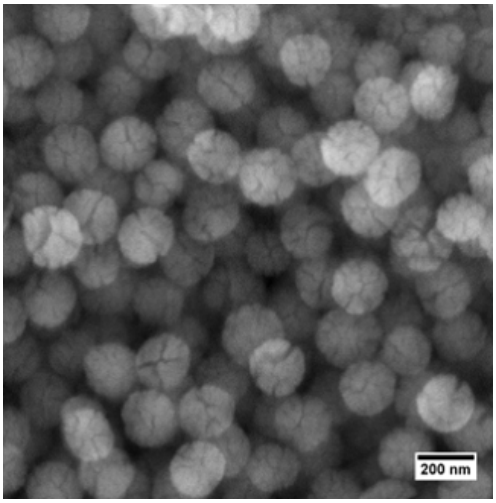

Obrázek 12. Mikrograf ze skenovacího elektronového mikroskopu vrstvy nanočástic palzmově polymerizovaného nylonu. Převzato z [**OK15**].

V práci [**OK15**] byla hlavní pozornost věnována možnosti ovlivňovat velikosti deponovaných nanočástic. Bylo zjištěno, že depoziční rychlost nanočástic i jejich průměrný poloměr mírně klesá s rostoucím příkonem přiváděným na vysokofrekvenční magnetron (20 % pokles průměru nanočástic při zvýšení příkonu z 60 na 100 W). To

pravděpodobně souvisí s vyšším zahříváním vzniklých nanočástic se zvyšujícím se příkonem. Druhým parametrem, který má zásadní vliv na výslednou velikost nanočástic je doba, kterou rostoucí nanočástice stráví v agregační komoře. Pomocí experimentů prováděných za různých průtoků nosného plynu za konstantního tlaku v agregační komoře a experimentů prováděných s různou délkou agregační komory bylo zjištěno, že objem vzniklých nanočástic roste lineárně s časem, který částice stráví v agregační komoře. Jinými slovy, změnou délky agregační komory či změnou rychlosti proudění plynu agregační komorou je možné získat nanočástice s průměrem v rozmezí 73–231 nm.

3.3. Shrnutí

V této kapitole byly představeny výsledky týkající se přípravy plazmových polymerů pomocí vysokofrekvenčního naprašování z nylonového terče. Bylo prokázáno, že tento způsob přípravy umožňuje depozici plazmových polymerů majících velmi vysoké zastoupení primárních aminoskupin, které je srovnatelné a v mnoha případech i vyšší než u vrstev připravovaných jinými plazmovými metodami. Připravené vrstvy byly navíc studovány i s ohledem na jejich časovou stálost, rozpustnost i odolnost vůči sterilizačním metodám, tj. v literatuře často přehlíženým vlastnostem plazmových polymerů. S ohledem na možné použití v biolékařských aplikacích se ukázaly jako optimální vrstvy připravené ve směsi $Ar:N_2$. Ačkoliv tyto vrstvy vykazují nižší povrchovou koncentraci primárních aminů než vrstvy deponované ve směsi $N_2:H_2$ jsou povlaky vytvořené ve směsi $Ar:N_2$ výrazně stabilnější ve vodném prostředí. To je vhodné zejména pro jejich další funkcionalizaci, čehož bylo využito při přípravě vrstev odolných vůči adhezi proteinů.

V neposlední řadě se podařilo připravit i nanočástice naprašovaného nylonu o různých velikostech, což je poměrně nový výsledek.

4. Využití nanoklastrů při přípravě vrstev s kontrolovatelnou nanodrsností a jejich možné použití v biolékařských aplikacích

Dalším typem materiálu, který nalézá čím dále častější uplatnění v biolékařských aplikacích, jsou různé typy nanoklastrů a nanočástic. Ty je možné použít samotné (například kovové klastry pro povrchově zesílenou ramanovskou spektroskopii (například [69,70]) popřípadě zabudované do matrice tvořené jiným materiálem, kdy hovoříme o nanokompozitních materiálech. Druhá zmiňovaná možnost se v současné době využívá například pro přípravu antibakteriálních povlaků, nebo jako součást senzorů (například [71-73]).

Důležitým parametrem povrchů používaných v biolékařských aplikacích je jejich drsnost na nanometrické škále. Z tohoto důvodu bylo vypracováno mnoho metod umožňujících přípravu povrchů s požadovanou nanodrsností. Tyto metody jsou založeny například na odleptávání povrchů plazmatem [74], či na dvoukrokovém procesu založeném na vytvoření zdrsněného povrchu pomocí leptání, colloidální litografie, fotolitografie či s použitím laserů, přičemž takto vytvořené povrchy jsou následně překryty materiálem mající požadované chemické složení (například [75-84]). V této kapitole bude představeno alternativní použití nanoklastrů a nanočástic pro přípravu materiálů s kontrolovatelnou povrchovou nanodrsností a možné využití takovýchto materiálů.

4.1. Příprava nanostrukturovaných vrstev s variabilní smáčivostí

Navržený postup, schematicky znázorněný na **obrázku 13**, spočívá v depozici vrstvy nanočástic, která je následovaná překrytím nadeponované nanočásticové vrstvy tenkou vrstvou jiného, popřípadě i téhož materiálu. Jako zdroj nanočástic byly použity různé druhy plynně agregačních zdrojů, s jejichž pomocí byly připraveny jak kovové nanočástice (například Ti [85,86], Pt [87], Ag [88]), tak nanočástice plazmových polymerů zmíněné již v předešlé kapitole. Jako zdroj překryvového materiálu bylo použito magnetronové naprašování z kovových či polymerních terčů, popřípadě metoda PECVD. Jak bylo ukázáno vhodnou volbou množství deponovaných nanočástic a jejich velikostí je možné dosáhnout poměrně širokého rozsahu nanodrsnoti výsledných povlaků (v rozsahu od jednotek do několika stovek nanometrů jak je vidět na **obrázku 14**). Zásadními výhodami tohoto postupu je jeho nezávislost na substrátu, možnost

depozice v jedné depoziční komoře i možnost nezávislé kontroly nanodrsnosti, která je dána jen vlastnostmi nanočásticové vrstvy, a chemického složení povrchu výsledného povlaku, která závisí jen na použitém překryvovém materiálu.

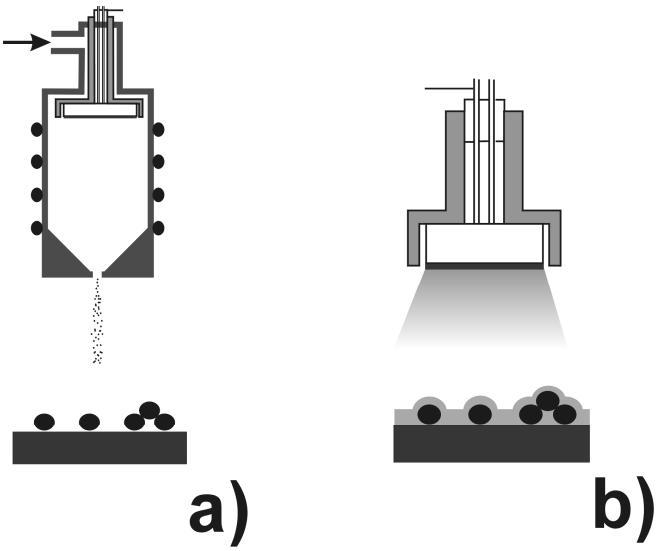

Obrázek 13. Znázornění postupu přípravy vrstev s kontrolovatelnou nanodsrností. a) depozice vrstvy nanoklastrů b) depozice překryvového materiálu.

Možnost kontrolovat drsnost povrchů nezávisle na jejich chemickém složení může být využita pro přípravu povrchů s různou smáčivostí. Tomuto tématu je věnována práce [**OK16**], kdy byly využity Ti nanoklastry, které byly překrývány vrstvou naprašovaného nylonu a vrstvou plazmově polymerizovaného n-hexanu. Bylo prokázáno, že pouhou změnou množství deponovaných Ti nanoklastrů v podkladové vrstvě je možné dosáhnout změny hodnoty kontaktního úhlu vody až o 50% (v případě hydrofilního naprašovaného nylonu byl pozorován pokles z 42^{o} až na 16^{o}, v případě hydrofobního plazmově polymerizovaného n-hexanu byl pozorován nárůst z hodnoty 90^{o} na 130^{o}). Tohoto jevu by bylo možné využít pro ovlivňování adsorpce různých bílkovin na povrch, jelikož smáčivosti povrchu výrazným způsobem ovlivňuje interakci mezi povrchem a bílkovinou.

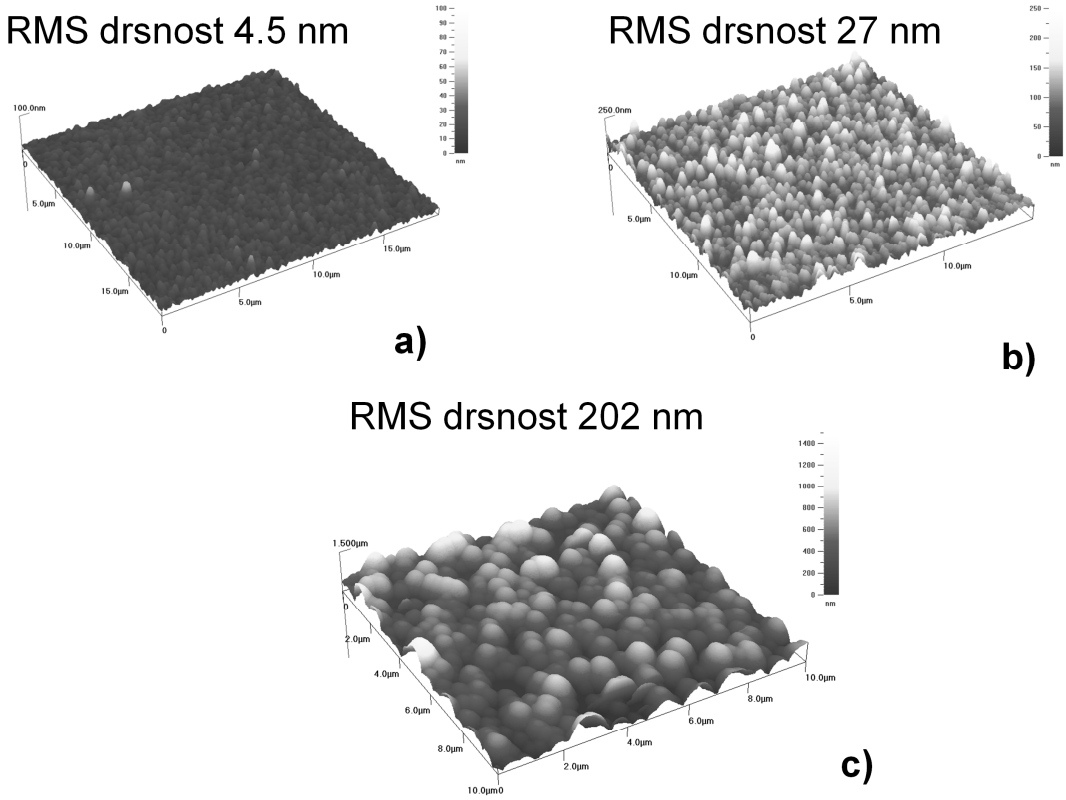

Obrázek 14. Obrázky získané pomocí mikroskopu atomárních sil. a) vrstva Pt nanoklastrů překrytých naprašovaným PTFE b) vrstva Al nanoklastrů překrytých naprašovaným PTFE c) vrstva nanočástic plazmově polymerizovaného nylonu překrytých naprašovaným PTFE. U vrstev jsou uvedeny hodnoty střední kvadratické hodnoty (RMS) drsnosti

4.2. Příprava nanostrukturovaných vrstev s variabilní nanodrsností pro studium růstu buněk

Druhou oblastí, kde je možné s výhodou použít vrstvy s kontrolovanou drsností je studium vlivu drsnosti na růst kostních buněk. Tomuto tématu se věnuje práce [**OK17**], kde byly použity plazmově polymerizované C:H nanočástice, překryté titan oxidovou vrstvou. Na základě biologických testů bylo prokázáno, že existuje optimální nanodrsnost, která usnadňuje kolonizaci povrchu osteoblastům podobnými buňkami MG-63. Následné podrobnější experimenty, které jsou v současné připravovány k publikaci, ukázaly, že z hlediska růstu MG-63 buněk je nejvýhodnější povrch mající střední kvadratickou hodnotu drsnosti kolem 30 nm. Tento závěr je zdokumentován na

obrázku 15, kde jsou uvedeny počty buněk na površích s různou nanodrsností 7 dní po nasazení buněk.

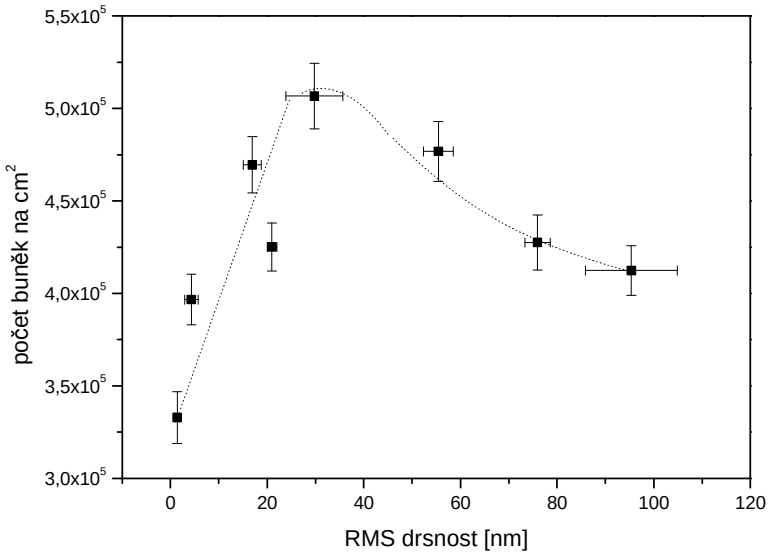

Obrázek 15. Závislost počtu buněk MG-63 na drsnosti povrchu titan oxidu po 7 dnech po nasazení buněk.

5. Závěr

V předkládané práci byly představeny a diskutovány různé možnosti využití nerovnovážného plazmatu pro biolékařské aplikace. Jako první bylo ukázáno, že nerovnovážné plazma generované za sníženého tlaku umožňuje velmi účinně sterilizovat celou řadu biologických patogenů zahrnující jak bakteriální spory, tak i různé druhy biomolekul. Byl identifikován hlavní proces vedoucí k odstraňování organického materiálu z povrchu v aktivním plazmatu – chemické odprašování. To umožnilo následně optimalizovat sterilizační proces. Mimoto byla navržena metoda pro *in-situ* monitorování sterilizačního procesu a postup pro inaktivaci bakteriálních endotoxinů.

Pomocí vysokofrekvenčního naprašování z nylonového terče se podařilo nadeponovat vrstvy mající relativně vysoké zastoupení primárních aminoskupin, které jsou vhodné pro další funkcionalizaci. Tohoto bylo využito pro přípravu povlaků odolných proti adhezi bílkovin z krevní plazmy. Mimoto byl nalezen i postup umožňující přípravu nanočástic plazmově polymerizovaného nylonu o různých velikostech.

Byla představena metoda umožňující přípravu povlaků s nezávisle kontrolovatelnou nanodrsností a chemickým složením. Tato metoda byla využita pro ovlivnění smáčivosti povrchů i pro nalezení optimální drsnosti pro růst osteoblastům podobných buněk na titan oxidu.

6. Literatura

[1] Lipscomb I P, Sihota A K, Botham M, Harris K L, Keevil C W 2006 *J. Hosp. Infections* **62** 141

[2] Lipscomb I P, Sihota A K, Keevil C W 2008 *J. Hosp. Infections* **68** 52

[3] Menashi W P, US Patent No. 3 383 163, 1968.

[4] Kelly-Wintenberg K, Hodge A, Montie T C, Deleanu L, Sherman D, Roth J R 1999 *J. Vac. Sci. Technol.* **A 17** 1539

[5] Lerouge S, Fozza A C, Wertheimer M R, Marchand R, Yahia L'H 2000 *Plasma and polymers* **5** 31

[6] Lerouge S, Wertheimer M R,Yahia L'Y 2001 *Plasmas and Polymers* **6** 175

[7] Moisan M, Barbeau J, Moreau S, Pelletier J, Tabrizian M, Yahia L'H 2001 *Int. J. of Pharmaceutics* **226** 1

[8] Lerouge S, Wertheimer M R and Yahia L'Y 2001 *Plasmas and Polymers* **6** 175

[9] Moisan M, Barbeau J, Crevier M-C, Pelletier J, Philip N, Saoudi B 2002 *Pure Appl. Chem.* **74** 349

[10] Philip N, Saoudi B, Crevier M C, Moisan M, Barbeau J, Pelletier J 2002 *IEEE Trans. Plasma Sci.* **30** 1429

[11] Mogul R, Bol'shakov A, Chan S L, Stevens R M, Khare B N, Meyyappan M, Trent J D 2003 *Biotechnol. Prog.* **19** 776

[12] Bol'shakov A A, Cruden B A, Mogul R, Rao M V V S, Sharma S P, Khare B N, Meyyapan M 2004 *AIAA Journal* **42** 823

[13] Moreau S, Moisan M, Tabrizian M, Barbeau J, Pelletier J, Ricard A, Yahia L'H 2000 *J. Appl. Phys.* **88** 1166

[14] Feichtinger J, Schulz A, Walker M, Schumacher U 2003 *Surf. Coat. Technol.* **174-175** 564

[15] Nagatsu M , Terashita F, Nonaka H, Xu L, Nagata T, Koide Y 2005 *Appl. Phys. Lett.* **86** 211502

[16] Halfmann H, Denis B, Bibinov N, Wunderlich J, Awakowicz P 2007 *J. Phys. D: Appl. Phys.* **40** 5907

[17] Cousty S, Villeger S, Sarette J P, Ricard A, Sixou M 2006 *Eur. Phys. J. Appl. Phys.* **34** 143

[18] Vujošević D, Mozetič M, Cvelbar U, Krstulović N, Milošević S 2007 *J. Appl. Phys.* **101** 103305

[19] Vicoveanu D, Popesco S, Ohtsu Y, Fujita H 2008 *Plasma Process. Polym.* **5** 350

[20] Boudam M K, Moisan M 2010 *J. Phys. D: Appl. Phys.* **43** 295202

[21] Montie T C, Kelly-Wintenberg K, Roth J R 2000 *IEEE Trans. Plasma Sci.* **28** 41

[22] Laroussi M 2002 *IEEE Trans. Plasma Sci.* **30** 1409

[23] Heise M, Neff W, Franken O, Muranyi P, Wunderlich J 2004 *Plasmas Polymers* **9** 23

[24] Laroussi M 2005 *Plasma Process. Polym.* **2** 391

[25] Akitsu T, Ohkawa H, Tsuji M, Kimura H, Kogoma M 2005 *Surf. Coat. Technol.* **193** 29

[26] Boudam M K, Moisan M, Saoudi B, Popovici C, Gherardi N, Massines F 2006 *J Phys D: Appl Phys* **39** 3494

[27] Fridman G, Brooks A D, Balasubramanian M, Fridman A, Gutsol A, Vasilets V N, Ayan H, Friedman G 2007 *Plasma Process. Polym.* **4** 370

[28] Munakata N 1974 *J. Bacteriol.* **120** 59

[29] Kylián O, Sasaki T, Rossi F 2006 *Eur. Phys. J. Appl. Phys*. **34** 139

[30] Opretzka J, Benedikt J, Awakowicz P, Wunderlich J, von Keudell A 2007 *J. Phys. D: Appl. Phys.* **40** 2826

[31] Raballand V, Benedikt J, Wunderlich J, von Keudell A 2008 *J. Phys. D: Appl. Phys* **41** 115207

[32] Benedikt J, Flötgen C, Kussel G, Raballand V, von Keudell A 2008 *J. Phys.: Conf. Ser.* **133** 012012

[33] Guerra V, Loureiro J 1997 *Plasma Sources Sci. Technol.* **6** 3

[34] Guerra V, Sá PA, Loureiro J 2001 *J. Phys. D:Appl. Phys.* **34**, 1745

[35] Kylián O, Denis B, Stapelmann K, Ruiz A, Rauscher H, Rossi F 2011 *Plasma Process. Polym.* **8** 1137

[36] Kylian O, Hasiwa M, Rossi F 2006 *Plasma Process. Polym.* **3** 272

[37] Hasiwa M, Kylián O, Hartung T, Rossi F 2008 *Innate Immunity* **14** 89.

[38] Kylián O, Hasiwa M , Gilliland D, Rossi F 2008 *Plasma Process. Polym*. **5** 26

[39] Biederman H, Osada Y 1992 *"Plasma Polymerization Processes"* Elsevier Science, Amsterdam

[40] Drábik M, Polonskyi O, Kylián O, Čechvala J, Artemenko A, Gordeev I, Choukourov A, Slavínská D, Matolínová I, Biederman H 2010 *Plasma Process. Polym*. **7** 544

[41] Kylián O, Drábik M, Polonskyi O, Čechvala J, Artemenko A, Gordeev I, Choukourov A, Matolínová I, Slavínská D, Biederman H *Thin Solid Films* **519** 6426

[42] Choukourov A, Gordeev I, Polonskyi O, Artemenko A, Hanyková L, Krakovský I, Kylián O, Slavínská D, Biederman H 2010 *Plasma Process. Polym*. **7** 445

[43] Choukourov A, Gordeev I, Arzhakov D, Artemenko A, Kousal J, Kylián O, Slavínská D, Biederman H 2012 *Plasma Process. Polym*. **9** 48

[44] Siow K S, Britcher L, Kumar S, Griesser H J 2006 *Plasma Process. Polym*. **3** 392

[45] Meyer-Plath A A, Finke B, Schroder K, Ohl A 2003 *Surf. Coat. Technol*. **174 – 175** 877

[46] Král' M, Ogino A, Nagatsu M 2008 *J. Phys. D:Appl. Phys.* **41** 105213

[47] Finke B, Schröder K, Ohl A 2008 *Plasma Process. Polym*. **5** 386

[48] Truica-Marasescu F, Wertheimer M R 2008 *Plasma Process. Polym*.**5** 44

[49] Truica-Marasescu F, Girard-Lauriault P-L, Lippitz A, Unger W E S ,Wertheimer M R 2008 *Thin Solid Films* **516** 7406

[50] Finke B, Hempel F, Testrich H, Artemenko a., Rebl H, Kylián O, Meichsner J, Biederman H, Nebe B, Weltmann K-D , Schröder K 2011 *Surf. Coat. Technol.* **205** S520

[51] Hollaender A, Thome J H 2004 „Degradation and stability of plasma polymers“ in Plasma Polymer Films Biederman (Editor), Imperial College Press, London

[52] Ruiz J-C, St-Georges-Robillard A, Thérésy C, Lerouge S, Wertheimer M R 2010 *Plasma Process. Polym.* **7** 737

[53] Kobayashi H, Bell A T, Shen M 1973 *J. Appl. Polymer Sci.* **17** 885

[54] Kobayashi H, Shen M, Bell A T 1974 *J. Macromol. Sci.* **A8** 373

[55] Northrop T G 1992 *Physica Scripta*. **45** 475

[56] Fridman A A, Boufendi L, Hbid T, Potapkin B V, Bouchoule A 1996 *J. Appl. Phys.* **79** 1303

[57] Fortov V E, Ivlev A V, Khrapak S A, Khrapak A G, Morfill G E 2005 *Phys. Reports* **421** 1

[58] Boufendi L, Jouanny M C, Kovacevic E, Berndt J, Mikikian M 2011 *J. Phys. D: Appl. Phys.***44** 174035

[59] Boufendi L, Bouchoule A 1994 *Plasma Sources Sci. Technol.* **3** 262

[60] Buss R, Hareland W 1994 *Plasma Sources Sci. Technol.* **3** 268

[61] Feng J C, Huang W, Fu G D, Kang E-T, Neoh K-G 2005 *Plasma Process. Polym.***2** 127

[62] Yang S H, Liu C-H, Hsu W-T, Chen H 2009 *Surf. Coat. Technol.* **203** 1379

[63] Takahashi K, Tachibana K 2001 *J. Vac. Sci. Technol.* **A19** 2055

[64] De Vriendt V, Maseri F, Nonet A, Lucas S 2009 *Plasma Process. Polym.* **6** S6

[65] De Vriendt V, Felten A, Blondeau J J-P, Maseri F, Pireaux J J-J, Lucas S 2011 *Surf. Coat. Technol.* **205** S582

[66] Berndt J, Kovačević E, Stefanović I, Stepanović O, Hong S H, Boufendi L, Winter J 2009 *Contrib. Plasma Phys.* **49** 107

[67] Haberland H, Karrais M, Mall M, Thurner Y 1992 *J. Vac. Sci. Technol.* **A10** 3266

[68] Drábik M, Serov A, Kylián O, Choukourov A, Artemenko A, Kousal J, Polonskyi O, Biederman H 2012 *Plasma Process. Polym*. **9** 390

[69] Baker G A, Moore D S 2005 *Anal. Bioanal Chem* **382** 1751

[70] Cialla D, März A, Böhme R, Theil F, Weber K, Schmitt M, Popp J 2012 *Anal. Bioanal Chem* **403** 27

[71] Körner E, Aguirre M H, Fortunato G, Ritter A, Rühe J, Hegemann D 2010 *Plasma Process. Polym*. **7** 619

[72] Faupel F, Zaporojtchenko V, Strunskus T, Greve H, Takele H, Hanisch C, Sai V, Chakravadhanula K, Gerber A, Quandt E, Podschun R 2008 *Polymers & polymer Composites* **16** 471

[73] Faupel F, Zaporojtchenko V, Greve H, Schürmann U, Chakravadhanula V S K, Hanisch C, Kulkarni A, Gerber A, Quandt E, Podschun R 2007 *Contrib. Plasma Phys.* **47** 537

[74] Tsougeni K, Vourdas N, Tserepi A, Gogolides E, Cardinaud C 2009. *Langmuir* **25** 11748

[75] Lejeune M, Lacroix L M, Brétagnol F, Valsesia A, Colpo P, Rossi F 2006 *Langmuir* **22** 3057

[76] Teshima K, Sugimura H, Inoue Y, Takai O, Takano A 2005 *Appl. Surf. Sci.* **244** 619

[77] Ruiz A, Valsesia A, Ceccone G, Gilliland D, Colpo P, Rossi F 2007*Langmuir* **23** 12984

[78] Weibel D E, Michels A F, Feil A F, Amaral L, Teixeira S R, Horowitz F 2010 *J. Phys. Chem. C* **114** 13219

[79] Yeh K-Y, Chen L-J, Chang J-Y 2008 *Langmuir* **24** 245

[80] Baldacchini T, Carey J E, Zhou M, Mazur E 2006 *Langmuir* **22** 4917

[81] Tsougeni K, Tserepi A, Boulousis G, Constantoudis V, Gogolides E 2007 *Plasma Process. Polym.* **4** 398

[82] Valsesia A, Colpo P, Manso Silvan M, Meziani T, Ceccone G, Rossi F 2004 *Nano Letters* **4** 1047

[83] Sardella E, Lovascio S, Favia P, d' Agostino R *Plasma Process. Polym.* **4** S887

[84] Palumbo F, Di Mundo R, Cappelluti D, d' Agostino R 2011 *Plasma Process. Polym.* **8** 118

[85] Drábik M, Choukourov A, Artemenko A, Kousal J, Polonskyi O, Solař P, Kylián O, Matoušek J, Pešička J, Matolínová I, Slavínská D, Biederman H 2011 *Plasma Process. Polym.* **8** 640

[86] Drabik M, Choukourov A, Artemenko A, Polonskyi O, Kylian O, Kousal J, Nichtova L, Cimrova V, Slavinska D, Biederman H 2011 *J. Phys. Chem. C* **115** 20937

[87] Kylián O, Valeš V, Polonskyi O, Pešička J, Čechvala J, Solař P, Choukourov A, Slavínská D, Biederman H 2012 *Materials Letters* **79** 229

[88] Polonskyi O, Solař P, Kylián O, Drábik M, Artemenko A, Kousal J, Hanuš J, Pešička J, Matolínová I, Kolíbalová E, Slavínská D, Biederman H 2012 *Thin Solid Films* **520** 4155

7. Seznam komentovaných publikací

[OK1] Rossi F, Kylián O and Hasiwa M 2006 Decontamination of Surfaces by Low Pressure Plasma Discharges *Plasma Processes and Polymers* **3** 431–42 (IF = 2,468).

[OK2] Kylián O, Rauscher H, Gilliland D, Brétagnol F and Rossi F 2008 Removal of model proteins by means of low-pressure inductively coupled plasma discharge *Journal of Physics D: Applied Physics* **41** 095201 (IF = 2,544).

[OK3] Stapelmann K, Kylián O, Denis B and Rossi F 2008 On the application of inductively coupled plasma discharges sustained in Ar/O_2 /N_2 ternary mixture for sterilization and decontamination of medical instruments *Journal of Physics D: Applied Physics* **41** 192005 (IF = 2,544).

[OK4] Kylián O, Benedikt J, Sirghi L, Reuter R, Rauscher H, von Keudell A and Rossi F 2009 Removal of Model Proteins Using Beams of Argon Ions, Oxygen Atoms and Molecules: Mimicking the Action of Low-Pressure Ar/O_2 ICP Discharges *Plasma Processes and Polymers* **6** 255–61(IF = 2,468).

[OK5] Rossi F, Kylián O, Rauscher H, Hasiwa M and Gilliland D 2009 Low pressure plasma discharges for the sterilization and decontamination of surfaces *New Journal of Physics* **11** 115017 (IF = 4,177).

[OK6] Kylián O, Rauscher H, Denis B, Ceriotti L and Rossi F 2009 Elimination of Homo-polypeptides of Amino Acids from Surfaces by means of Low Pressure Inductively Coupled Plasma Discharge *Plasma Processes and Polymers* **6** 848-854 (IF = 2,468).

[OK7] Fumagalli F, Hanuš J, Kylián O and Rossi F 2012 In situ Quartz Crystal Microbalance Measurements of Thin Protein Film Plasma Removal *Plasma Processes and Polymers* **9** 188–96 (IF = 2,468).

[OK8] Kylián O and Rossi F 2009 Sterilization and decontamination of medical instruments by low-pressure plasma discharges: application of Ar/O 2 /N 2 ternary mixture *Journal of Physics D: Applied Physics* **42** 085207 (IF = 2,544).

[OK9] Kylian O, Hasiwa M and Rossi F 2006 Effect of Low-Pressure Microwave Discharges on Pyrogen Bioactivity *IEEE Transactions on Plasma Science* **34** 2606–10 (IF = 1,174).

[OK10] Kylián O, Hanuš J, Choukourov A, Kousal J, Slavínská D and Biederman H 2009 Deposition of amino-rich thin films by RF magnetron sputtering of nylon *Journal of Physics D: Applied Physics* **42** 142001 (IF = 2,544).

[OK11] Kylián O, Kousal J, Artemenko A, Choukourov A, Petr M, Polonskyi O, Slavinska D and Biederman H 2011 Deposition of amino-rich coatings by RF magnetron sputtering of Nylon: In-situ characterization of the deposition process *Surface and Coatings Technology* **205** S558–61 (IF = 2,193).

[OK12] Artemenko A, Kylián O, Kousal J, Choukourov A, Polonskyi O, Slavinska D and Biederman H 2011 Deposition of amino-rich coatings by RF magnetron sputtering of Nylon: Investigation of their properties related to biomedical applications *Surface and Coatings Technology* **205** S529–33 (IF = 2,193).

[OK13] Artemenko A Kylián O, Choukourov A, Gordeev I, Petr M, Vandrovcová M, Polonskyi O, Bačáková L, Slavinska D and Biederman H 2012 Effect of sterilization procedures on properties of plasma polymers relevant to biomedical applications *Thin Solid Films* **520** 7115–24 (IF = 2,014).

[OK14] Rodriguez-Emmenegger C, Kylián O, Houska M, Brynda E, Artemenko A, Kousal J, Alles A B and Biederman H 2011 Substrate-independent approach for the generation of functional protein resistant surfaces *Biomacromolecules* **12** 1058–66 (IF = 5,479).

[OK15] Polonskyi O, Kylián O, Solař P, Artemenko A, Kousal J, Slavínská D, Choukourov A and Biederman 2012 Nylon-sputtered nanoparticles: fabrication and basic properties *J. Phys. D: Appl. Phys.* **45** 495301 (IF = 2,544).

[OK16]Kylián O, Polonskyi O, Kratochvíl J, Artemenko A, Choukourov A, Drábik M, Solař P, Slavínská D and Biederman H 2012 Control of Wettability of Plasma Polymers by Application of Ti Nano-Clusters *Plasma Processes and Polymers* **9** 180–7 (IF = 2,468).

[OK17] Solař P, Kylián O, Polonskyi O, Artemenko A, Arzhakov D, Drábik M, Slavínská D, Vandrovcová M, Bačáková L and Biederman H 2012 Nanocomposite coatings of Ti/C:H plasma polymer particles providing a surface with variable nanoroughness *Surface and Coatings Technology* **206** 4335-4342 (IF = 2,193).

Summary: Non-equilibrium discharges in molecular gases and their mixtures have been extensively studied due to their applicability in different areas of surface treatment, cleaning and functionalization. In this paper, the feasibility of the use of low pressure discharges for sterilization and decontamination, i.e., a topic that has attracted great attention recently, is demonstrated and discussed using examples of bacterial spore sterilization and depyrogenation of bacterial endotoxins, as well as the elimination of protein films.

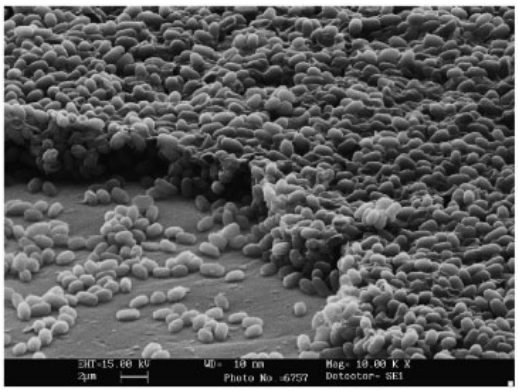

Image of spores used for sterilization, showing heavy stacking.

Decontamination of Surfaces by Low Pressure Plasma Discharges

François Rossi, Ondřej Kylián, Marina Hasiwa*

European Commission, Joint Research Centre, Institute for Health and Consumer Protection,
Via E. Fermi 1, 21020 Ispra (VA), Italy
Fax: +39 0332 785787; E-mail: francois.rossi@jrc.it

Received: February 2, 2006; Revised: May 22, 2006; Accepted: June 20, 2006; DOI: 10.1002/ppap.200600011

Keywords: bacterial spores; decontamination; endotoxins; protein films; sterilization

Introduction

The low temperature decontamination and sterilization of surfaces has received great attention in recent years, especially in the medical praxis or pharmaceutical industries, but also in the electronics industry or in space applications. Concerning medical praxis, recent statistics show that nosocomial infections are responsible for several thousand deaths each year in Europe and are responsible for a huge number of post-surgical complications every day. However, many of these infections could be avoided by the use of adequate sterilization and decontamination techniques ensuring complete inactivation or removal of all possible infectious microorganisms (e.g., bacterial spores, viruses, molds or yeasts) or other potentially harmful biological residuals (e.g., endotoxins, proteins) presented on the used instruments, in particular in invasive surgery and dental praxis.

For medical devices and instruments, the principal methods of sterilization, i.e., the inactivation of living microorganisms, are based on thermal treatment (dry or moist heat), chemical treatment (e.g., EtO, H_2O_2) or exposure to ionizing radiation (X-ray, gamma radiation, e-beams). However, these conventional processes have specific drawbacks linked to their conditions of operation, for instance to the toxicity of the active agent used (chemical treatment), the temperature conditions (thermal treatment), or the size of installation (e-Beam or gamma sterilization).

Moreover, new demands are connected with the elimination of various kinds of harmful biomolecules. These non-living organic products cannot be deactivated by DNA alterations, as in the case of living organisms such as bacteria and spores, and therefore different approaches for their destruction have to be used. This issue is particularly important in the case of bacterial endotoxin and prion elimination as will be shown in the subsequent text.

Bacterial endotoxins are an important class of fever-causing substances, called pyrogens, which are most often found on medical devices. Typical examples of endotoxins are lipopolysaccharides (LPS) which constitute a major part of the outer cell wall of Gram-negative bacteria. Their presence on surfaces in recent years has become the object of great interest, especially in biotechnology, the pharmaceutical industry and in medicinal product manufacturing. This is mainly due to the fact that LPS have been found to be one of the most potent modulators of the human immune system.[1] Their appearance in the bloodstream leads to the release of several proinflammatory mediators which initiate a complex cascade of clinically relevant events, which may span from slight inflammatory symptoms like reddening, swelling and fever to severe tissue damage.[2] Even more drastic consequences may arise including sepsis, multiple organ failure and death.[3] However, lipopolysaccharides once present on a surface are hard to remove. This is due to the fact that they are insensitive to pH changes and are extraordinarily thermostable.[4] For instance, depyrogenation of vials in pharmaceutical industry is at present performed in a heat tunnel at 200 or 250 °C for 60 and 30 min respectively.[4] The major drawback of this approach is that the heating increases proportionally to the load treated, instead of the surface, a fact which is very penalizing in energy consumption. The floor space occupied by the installation is also important due to the large heating and cooling zones necessary to avoid thermal shock. Finally, the necessity of high temperature for the depyrogenation imposes the use of glass instead of plastic vials with all the disadvantages related to this.

Even more challenging is the destruction of protein contamination, for instance prions (PrP), the transmission agent of sever diseases classified as transmissible spongiform encephalopathies (e.g., Creutzfeld-Jacob Disease or CJD). This is due to the fact that prions can successfully resist traditional cleaning techniques (e.g., autoclaving, ionizing radiation, EtO treatments[5]). The only processes validated for their inactivation at the moment are based on steam autoclaving at 134 °C for 18 min, or treatment with concentrated NaOH solution, and thus are again not applicable to many medical devices.

This brief overview indicates that new methods of sterilization and decontamination have still to be developed and validated. According to the discussion above, the optimal technique should fulfill several requirements:

- Efficiency of treatment (low treatment duration at low cost).
- Low temperature conditions enabling the treatment of thermally sensitive materials.
- Applicability to a wide range of materials and shapes.
- Avoidance of toxic reagents or by-products.

The objective of the present paper is to show that low pressure plasma can fulfill these demands and to demonstrate its applicability for the elimination of both micro-

François Rossi was born in St Etienne (France) in 1954. He received his engineering degree from Institut National Polytechnique of Grenoble in 1977, and his Ph.D. in Materials Science from Université Claude Bernard of Lyon in 1989. From 1981 to 1990, he worked at the Commissariat à l'Energie Atomique as a group leader in Materials Science and Surface Engineering. In 1991–1996, he was group leader at the Institute for Advanced Materials, Joint Research Centre of the EU in Petten (NL) in Plasma Technologies. In 1996, he moved to the JRC Ispra site where he is now head of the NanoBiotechnology laboratory.

Ondřej Kylián was born in Prague (Czech Republic) in 1975. He received his masters and Ph.D. degrees in the field of physics of plasma and ionized media from the Charles University in Prague in 1998 and 2003, respectively. He worked as a research fellow at the Institute of Atmospheric Physics of the Academy of Science of Czech Republic and as a college tutor at the Charles University in Prague. Since 2004 he has been a contractual agent of the European Commission, Joint Research Centre, Institute for Health and Consumer Protection in Italy.

Marina Hasiwa, born 1971 in Wiesensteig (Germany), received a diploma in biology in 2002 from the University of Konstanz at the chair of biochemical pharmacology. She is working on her Ph.D. in the topic of surface testing strategies by biological methods, especially in the field of immune stimulatory components on surfaces.

organisms and biomolecules. However, it should be noted that intention of this article is not only to give a summary of the results that can be found in the literature, but rather to demonstrate the possibilities of low pressure discharges and the related sterilization strategies, as well as to open questions regarding plasma-biomaterial interactions. The article is divided into two main parts. First, the principles of low pressure plasma treatment will be highlighted together with a short review of the results presented in the literature. In the second part, some important issues connected to plasma-biomaterial treatment will be presented in relation to the recent results of our studies.

Finally, it should be noted that atmospheric pressure plasma treatment has recently been the object of an excellent review,[6] and will not be presented in detail here.

Principles of the Low Pressure Plasma Based Method

Low pressure plasma sterilization has been the subject of many general studies and reviews which have indicated different potential mechanisms of its action.[7–14] The approach followed was to use non-toxic gas mixtures (for instance H_2, O_2, N_2, Ar, air etc.) producing reactive species (such as O, OH) and UV radiation at different wavelengths at relatively low temperatures. The operation is non-toxic, safe and environmentally friendly and is also suitable for the treatment of heat sensitive materials or instruments. By adjusting the process conditions (reactor geometry, pressure, power, frequency, flow and gas composition), several mechanisms can be activated and operate alone or simultaneously, which leads to sterilization or decontamination with different effects. Typically, these effects relate to the production of UV of different wavelengths which interacts with the DNA of the spores (e.g., Munakata et al.[15]), of active radicals which react with the outer layer of the spores and produce leakage and denaturation of protein and lipid components, and of ion and/or electron bombardment which sputters the contaminant material. All of these mechanisms can be operative during the surface treatment and lead to different sterilization/decontamination kinetics, which explains the apparent contradictions in the published results.

For clarity, the effect of plasma on bacterial spores, endotoxins and proteins will be presented separately below.

Bacterial Spore Sterilization

The idea to employ non-equilibrium plasmas for bacterial spores sterilization is relatively old[16] and extensive literature has been devoted to this topic (see for instance comprehensive reviews by Lerouge et al.[10] and Moisan et al.[11]). Concerning the mechanisms of sterilization, several processes have been proposed:

- Destruction of spores' induced by UV/VUV radiation which, as already mentioned, is well known to have a sporicidial effect due to its ability to alter the genetic material of spores.[15] This mechanisms of sterilization has been emphasized by several groups under several discharge configurations ranging from microwave flowing afterglow (e.g., Moisan et al.[11] and Moreau et al.[17]), direct microwave discharge (e.g., Feichtinger et al.[18]) to glow discharge (e.g., Sholoshenko et al.[19]). In contrast, UV emission was found to have little contribution to sterilization in atmospheric pressure plasma discharges, the radicals playing the major role under the different conditions tested.[6,20,21]
- Destruction of spores caused by their etching by active particles. This mechanism has been identified as the dominant one for spore destruction, for example by Lerouge et al.[8] (radio frequency and microwave direct glow discharges) and Nagatsu et al.[22] (surface-wave microwave discharge). According to these authors, the sporicidial action of the plasma is not greatly affected by UV/VUV radiation.
- The degradation of spore walls has been attributed to a synergetic effect of photo and ion assisted etching by oxygen atoms and maybe O_2* molecules in low pressure oxygen inductively coupled RF discharge by Mogul et al.[13] and Bol'shakov et al.[14] The UV contribution to the effect was however not quantified.
- Significant membrane destruction has also been evidenced in the case of atmospheric pressure plasma discharge by Montie et al.,[23] Laroussi et al.[24] and Mendis et al.[25] The 2 latter articles suggested that cell wall rupture could be caused by electrostatic forces due to accumulation of charges at the outer surface of cell membranes. Although this effect could also be operative at low pressure, it has not been clearly demonstrated and needs more investigation.

From this brief summary, it is clear that different mechanisms can lead to spore destruction and that the conditions of the process used play a major role depending on the mechanisms predominant in the conditions tested. This leads to large differences in the kinetics observed between the different groups. For instance, the time needed for a 6 Log reduction reported by the different authors varied between 1 s in the discharge[18] to typically 30 min to 1 h in the flowing afterglow.[12] The differences observed can of course be attributed to the difference of fluxes of the reactive species and the geometries of reactors.

Moreover, the survival curves of spores vary between the authors, some finding a 2 or 3 phase destruction, while others found only 2. For instance, in their study Moisan et al.[11] found that the variation of colony forming units (CFU) of *Bacillus subtilis* with time in a low pressure N_2/O_2 microwave discharge presented 3 phase kinetics. The first phase (and fastest) was related to the interaction of top layer spores

with UV radiation. The second phase was the slowest and was attributed to the erosion by atomic oxygen of dead spores and debris remaining after the 1st phase. The 3rd phase, which had kinetics similar to phase 1, was attributed to the interaction of the buried spores with UV after the removal of the masking material in phase 2. It is important to stress that the 2nd phase, the duration of which is related to the time needed for the removal of material shielding spore genetic material from the direct UV/VUV action, is dependent on the quantity and the nature of the shielding material. This point illustrates the role of the spores' distribution in the interpretation of results, the kinetics observed for complete sterilization being different depending on the contamination layer (monolayer or stacked spores). This will be further illustrated in the Experimental Part of this work.

Depyrogenation

Compared to the case of bacterial spore sterilization, endotoxin depyrogenation by means of gas discharges is a relatively new topic. Although the possibility of employing non-equilibrium plasmas for pyrogens elimination had been proposed by Peeples et al.[26] and Lerouge et al.,[9] there was, until recently, very little work published on this subject and the only paper demonstrating the experimental feasibility of plasma technology for LPS depyrogenation was published recently by our group.[27] According to the obtained results, the following conclusions were stated:

- Low pressure microwave discharge is capable of decreasing significantly the pyrogenicity of LPS within several minutes of plasma treatment.
- The efficiency of LPS deactivation depends on the gas mixture used. From this point of view, the most potent mixtures are hydrogen containing ones (H_2/O_2, H_2/Ar and H_2/N_2).
- The observed decrease in LPS bioactivity is predominately caused by plasma-LPS interaction. In other words, it has been demonstrated that under the conditions tested, LPS bioactivity was not greatly affected by other possible mechanisms such as increased temperature, microwave radiation or low pressure conditions, at least within the treatment time.

Although the results obtained are promising, important issues still remain that have to be investigated, such as the possibility of removing LPS derived from different bacterial strains or the identification of the mechanism of plasma LPS deactivation. In order to obtain a better idea of the answer to these questions, new sets of experiments have been performed. The results obtained will be presented and discussed in the Experimental Part of this paper.

Protein and Prion Removal

The removal of protein residues from surgical instruments has been studied by Whittaker et al.[28] Those results showed that the surgical instruments were still contaminated by protein residues after the typical decontamination and sterilization procedure applied in hospitals. Those residues identified by EDX and SEM were strongly adherent on metallic surfaces but could be removed by an RF Ar/O_2 plasma discharge. More specifically, Baxter et al.[29] have shown that elimination of PrP was possible with a capacitively coupled Ar/O_2 RF plasma. In that particular case, ion bombardment was excluded due to the electrode configuration which did not create a bias. The interaction of plasma with Bovine Serum Albumin (BSA) and Soybean Lipoxygenase (SLO) was also studied by Mogul et al.,[13] with an O_2 inductive RF plasma. It was found that an increase in the discharge power resulted in a non-linear decrease of BSA and the enzymatic activity of SLO.

However, no systematic study of plasma-protein interactions is available in the literature. In order to find out which gas mixture is the most efficient, a systematic study of protein removal rate was done for collagen films and brain homogenate as model proteins. The results will be presented in the subsequent text.

Experimental Part

Sterilization of Bacterial Spores

Experimental Setup

The experimental setup for the sterilization studies was a self-made double inductively coupled plasma source.[30] This ICP plasma source consisted of two oppositely faced RF coils placed against the 2 dielectric windows of the processing chamber. The coils were connected in parallel to the power supply, and the connection was made to generate a magnetic flux perpendicular to the substrate in the entire space between the coils. This results in the creation of an electric field in the whole substrate volume and enables a uniform plasma treatment, even in small diameter tubes or cavities.

The discharge chamber was evacuated by a primary pump and was connected to an inlet system composed of four mass flow controllers (maximum flow 10 sccm) connected to the gas lines (O_2, H_2, N_2 and Ar). The background pressure that could be reached in this configuration was 0.5 Pa. Bacterial samples to be sterilized were inserted into the discharge chamber by means of the load lock mounted on the chamber. In all the experiments described below, the treatment was done in pulsed mode to ensure that the temperature of the samples did not increase beyond 60 °C.

Optical Emission Spectroscopy (OES) was performed with an Avantes AVS-PC2000 monochromator equipped with a 2 048 element linear CCD array to identify the different species present in the discharge and to evaluate the UV emission. In that case, UV intensity was measured by calculating the integral of the OES peaks between 200 and 300 nm.

Biological Tests

The sterilization tests were performed using stainless steel coupons covered with *G. stearothermophilus* spores, a sterility

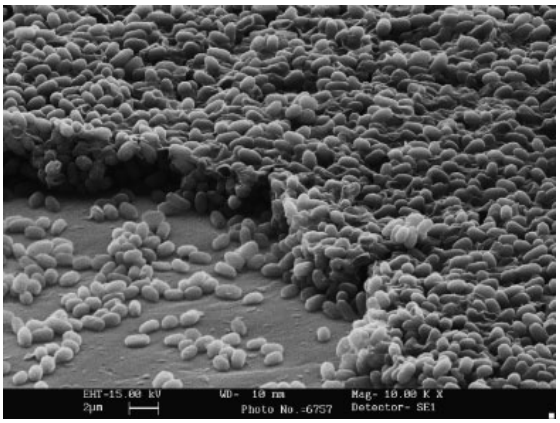

Figure 1. Image of spores used for sterilization, showing heavy stacking.

indicator produced by Raven Biological, USA, with a declared number of spores of 2.5×10^6. The spores were not dispersed in a monolayer but were stacked, in order to be representative of a real contamination situation (see Figure 1). The samples were treated at different plasma conditions and for different treatment times. Afterwards, the treated coupons were placed into the culture media and incubated for 7 d at 60 °C, i.e., a temperature allowing the growth of the tested spores on the one hand and high enough to reduce the likelihood of any other contaminant growing on the other. The samples were thereafter declared sterile if no positive growth of spore colonies was observed. For each experiment, 5 to 10 samples were treated and cultured, giving a sterilization probability in the tested conditions.

It must be stressed that this procedure did not give the kinetics of the decrease of colony forming units as a function of time but a probability that the initial spore population was completely inactivated. It thus gives an idea of the global efficiency of the process, but does not allow detailed investigation of the different processes contributing to the sterilization mechanisms. However, it is more relevant to a real application situation requiring complete sterility only.

Besides biological tests, the morphology of the treated spores was examined by scanning electron microscopy (SEM) using a LEO 435VP microscope. Microscopic observations were preceded by the deposition of a thin gold layer on the samples.

Depyrogenation and Protein Removal Studies

Experimental Setup

A different experimental setup was used for the depyrogenation, as well as for the protein removal studies. It was based on a microwave discharge and consisted of a stainless steel chamber (a cylinder 200 mm in diameter and 380 mm in length) with several windows for in situ diagnostics. The plasma was excited in the 13.3 to 133 Pa pressure range by a microwave power supply working at 2.45 GHz. Microwaves were introduced into the chamber through a silica window placed at the extremity of a circular 100 mm waveguide. The microwave circuit included the microwave supply (2 kW), a circulator, a three-stub impedance matching system and a rectangular-circular wave-guide transition. The chamber was pumped by a primary pump and a roots blower allowing a base vacuum of 0.3 Pa. The gas flows were controlled by mass flow controllers connected to gas lines (O_2, H_2, N_2 and Ar). More details are given in our previous article.[31] It should be noted that in all reported experiments, the temperature inside the processing chamber measured by means of IR pyrometry never went beyond 60 °C, and thus was much lower than the temperature necessary for a thermal decrease of pyrogen bioactivity.[4]

Endotoxin Detection

The routinely performed test for the estimation of the LPS content on a solid surface consists of extensive washing of the surface with pyrogen-free water and measuring the pyrogenic content of the solution using the rabbit pyrogen test (detection of the body temperature increase of the animal after injection) or with the Limulus Amebocyte Lysate Assay (LAL test). We instead used the human whole blood incubation developed at JRC and the University of Konstanz.[32,33] The test uses immune defense mechanisms based on cytokine release (e.g., IL-1β, TNF-α), from monocytes and macrophages from human blood in contact with the foreign surface to be tested. By adding LPS or their biological active part (Lipid A) to human whole blood and measuring the cytokines released by an enzyme-linked immuno-sorbent assay (ELISA), we were able to simulate the human fever reaction to immune-stimulating principles in vitro. The detection limit is much lower than the rabbit or LAL test and can be performed directly on the surface detecting the whole pyrogen amount,[33] i.e., the soluble and sticky parts, in contrast to the classical methods which work by the elution of the soluble part and therefore do not taking into account the whole immune stimulating capacity of the contaminated surface.

In the experiments reported below, the bioactivity of both LPS and Lipid A after treatment was detected by a specific IL-1β ELISA (antibodies obtained from R&D, Wiesbaden, Germany). The use of Lipid A was dictated by the fact that its structure is well known and allows analysis of the chemical modification of the surface in relation to its biological activity.

Sample Preparation

The samples to be depyrogenated were plastic 24 well cell culture plates (Greiner Bio-One, Frickenhausen, Germany) covered with 100 µl of LPS from *Escherichia coli* 0111:B4 and K-235, LPS from *Salmonella abortus equi* (Sigma Aldrich, Deisendorf, Germany) as well as Lipid A (Sigma Aldrich, Deisendorf, Germany) diluted in pyrogen-free water having different initial LPS or Lipid A concentrations ranging from 0.01 ng · ml^{-1} to 10 ng · ml^{-1}. The well plates were allowed to dry overnight and then introduced into the plasma chamber and exposed to different gas mixture plasmas.

In a different set of experiments, the mass loss of Lipid A during its plasma treatment was studied. In this case, 10 µl of Lipid A water solution (0.1 mg · ml^{-1}) were deposited on a gold coated quartz crystal and dried. The quartz crystal was placed in a quartz crystal microbalance (Leybold, Germany) in the

microwave chamber described above and treated in different gas mixtures in the near post discharge.

Protein Removal Tests

Brain homogenate was obtained by placing the cerebral cortex of 7 d old rats (OFA/SPF strain) in PBS (phosphate buffered saline, pH 7.2, Gibco, Milano Italy), homogenating them in a mechanical mixer and storing them until use in 1 ml aliquots at −80 °C. Protein films from collagen (Sigma Aldrich, Germany) and brain homogenate prepared as indicated above were deposited from a distilled water solution on a quartz crystal covered with a gold film. 5 µl of solution (1 mg · ml^{-1}) were pipetted onto each of the coupons and allowed to dry in air. Afterwards the etching of protein films was monitored as in the case of Lipid A.

Results

Sterilization of Bacterial Spores

According to the introduction, two principal sterilization agents have been proposed for low pressure conditions – UV/VUV radiation and etching of the treated spores by active particles. In order to determine the factual importance of both of them, sterilization tests were performed in different O_2/N_2 mixtures ranging from the discharge in pure nitrogen to a pure oxygen one.[34] This mixture was selected since, by varying the O_2/N_2 ratio, it is easily possible to adjust both the UV radiation intensity in the spectral range found to be the most effective for killing spores (200–300 nm[10]) and the density of atomic oxygen responsible for the etching of spores. This allows the evaluation of their contributions during the sterilization process.

Comparing the sterilization results obtained with the UV radiation intensity and O atom density, it was found that the best sterilization results were achieved in mixtures with higher amounts of atomic oxygen, (complete sterilization was obtained in the mixture 95% O_2:5% N_2 within 5 min), as is shown in Figure 2. In contrast, under our experimental conditions, the mixtures producing the highest UV emission gave a low sterilization probability for the treatment duration. This indicates the significance of etching for reaching complete sterility.

In order to verify the role of etching during the sterilization tests, systematic SEM analysis of treated spores was performed. It was found, as demonstrated in Figure 3, that significant changes in the dimensions of spores were observed after the plasma treatment in discharges with higher amounts of atomic oxygen. In contrast, almost no variation in spore size was observed in mixtures with a low O atom concentration and a high intensity of UV radiation for the same treatment time.

Concerning the time evolution of spore erosion, it was found that a significant spore size reduction occurred after 5 min of plasma treatment in O_2 containing discharges, as is demonstrated in Figure 4. This time corresponded to the time when complete sterility of samples has been achieved according to the biological tests. In contrast, almost no size reduction was observed within 10 min in an N_2 discharge.

The comparison between SEM observations and biological results confirms that, under the experimental conditions used in this study, the process determining the time to reach complete spore inactivation was etching rather than UV action on the genetic material of spores, i.e., results in contradiction with a large part of the results published in the literature (e.g., ref.,[7] ref.[11]).

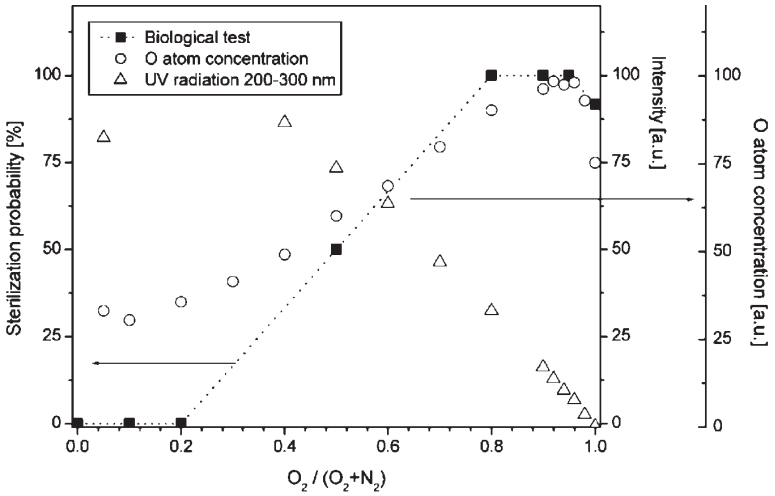

Figure 2. Comparison of UV radiation intensity, O atom density and sterilization tests in O_2/N_2 mixtures (treatment time 10 min, power 500 W, 20% DC, 5 ms time on, 13.3 Pa, 10 sccm).[34]

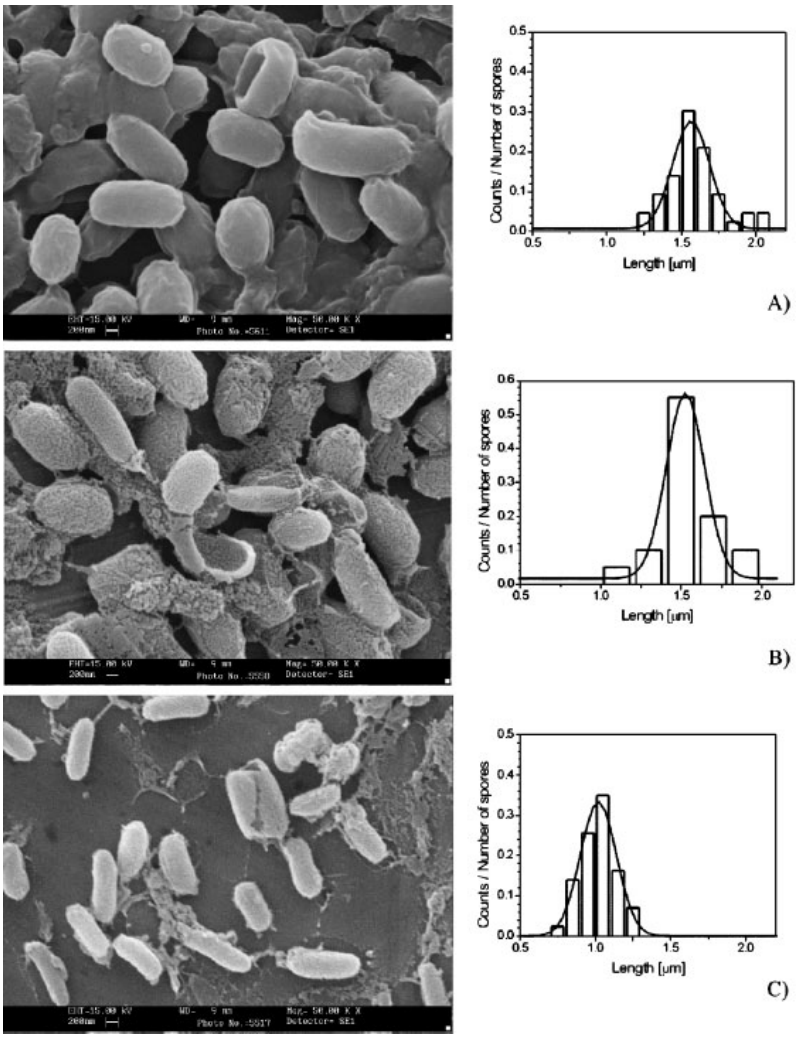

Figure 3. SEM pictures of treated spores in different gas mixtures and estimation of their lengths: (A) pure N_2; (B) O_2/N_2 20:80; (C) pure O_2 (treatment time 10 min, power 500 W, 20% DC, 5 ms time on, 13.3 Pa, 10 sccm).

Depyrogenation

As mentioned above, the depyrogenation of bacterial endotoxins by means of plasma is a new topic. Therefore it is first essential to demonstrate its applicability, as well as to estimate the time scale of plasma treatment necessary for LPS elimination. Taking in to account the conclusions of our previous work,[27] we focused on the hydrogen containing mixtures that were found to produce the most potent conditions for depyrogenation.

Firstly, the results of experiments performed in the microwave plasma reactor with an O_2/H_2 (50:50) mixture are reported in Figure 5, which shows the reduction of the biological activity expressed in terms of IL-1β release as a function of the treatment duration. According to these results, it can be concluded that a significant reduction of the LPS bioactivity, around 2 orders of magnitude, can be reached within 5 min of plasma treatment.

Other important results are related to the comparison of the plasma treatment effect on bioactivities of different LPS and Lipid A. The results are depicted in Figure 6 and demonstrate that plasma is able to sufficiently decrease the biological activity of all of them. Nevertheless, it can be seen that the rates of LPS depyrogenation vary depending on the LPS type, which can probably be attributed to differences in their composition and structure. Moreover, the same depyrogenation effect was qualitatively observed for Lipid A samples.

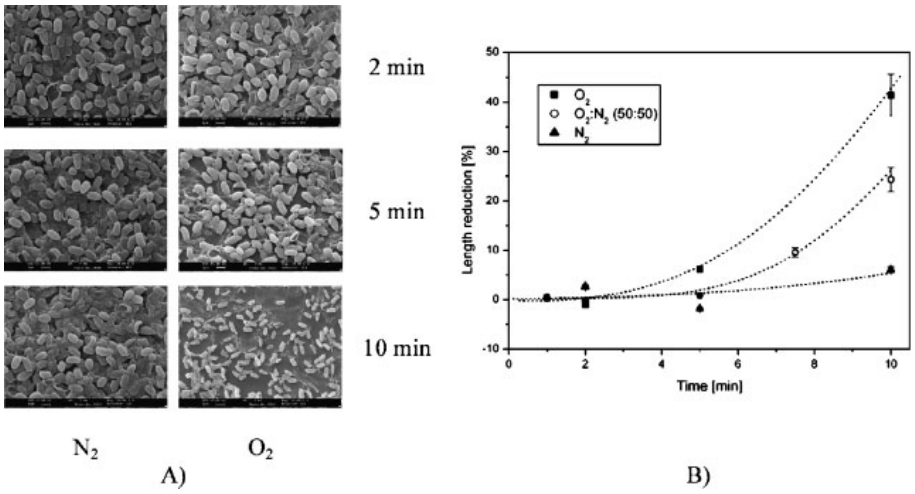

Figure 4. (A) SEM images of spores treated for different times; (B) Time evolution of spore length reduction after plasma treatment (power 500 W, 20% DC, 5 ms time on, 13.3 Pa, 10 sccm).

Furthermore, it was found that the efficiency of depyrogenation of LPS and Lipid A was significantly accelerated by the enhancement of hydrogen content in the plasma gas mixture, as shown in Figure 7 and 8 for mixtures of Ar/H_2 and O_2/H_2.

In order to have a better insight in the mechanisms responsible for depyrogenation, further experiments were done focusing on Lipid A etching in Ar/H_2 and O_2/H_2, i.e., in the mixtures that gave almost the same depyrogenation efficiencies (Figure 8). Surprisingly, completely different etching results were observed for these two mixtures, as can be seen in Figure 9. It has been found that the etching rate of the O_2/H_2 mixtures increased strongly beyond 30% of H_2 in the discharge whereas the etching rate stayed low in all the tested Ar/H_2 mixtures. Theses tendencies and their comparison with the bioactivity of the surface are particularly interesting since they demonstrate that depyrogenation by plasma can be explained either by etching (in the case of the O_2/H_2 mixture) or by deactivation of the chemical groups responsible for the pyrogenic effect (in the case of Ar/H_2) without the need to physically remove the deposit. According to preliminary results obtained by FT-IR spectroscopy on the treated samples, this latter effect can possibly be attributed to the reduction of long carbon chains in the Lipid A structure, namely pentaacyl, tetraacyl and hexaacyl chains. These chains all have a particular contribution to the biological effect, as demonstrated by Erridge et al.[35] Verification of this hypothesis is a subject of ongoing studies.

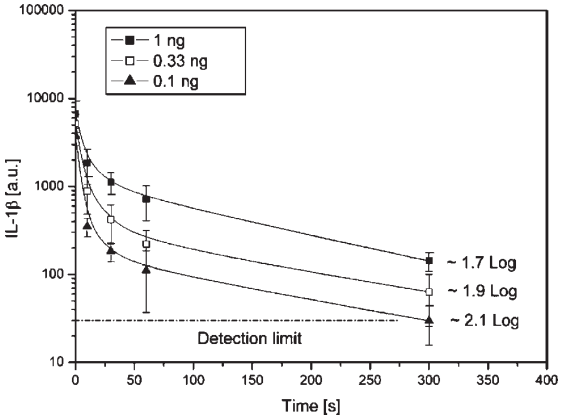

Figure 5. Time evolution of bioactivity of LPS after plasma treatment (*E. Coli* O111:B4, applied power 1 000 W, 13.3 Pa, 100 sccm, O_2/H_2 50:50).

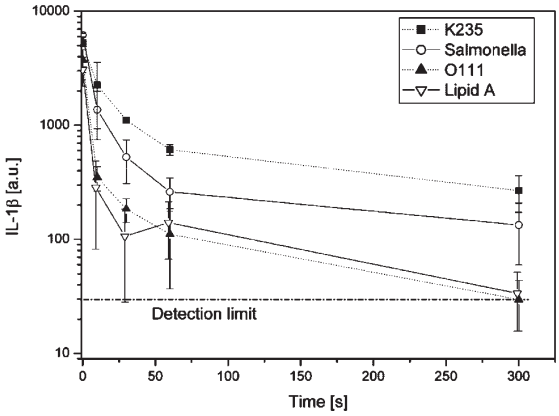

Figure 6. Time evolution of bioactivity reduction of different kinds of LPS and Lipid A (deposited 0.1 ng, applied power 1 000 W, 13.3 Pa, 100 sccm, O_2/H_2 50:50).

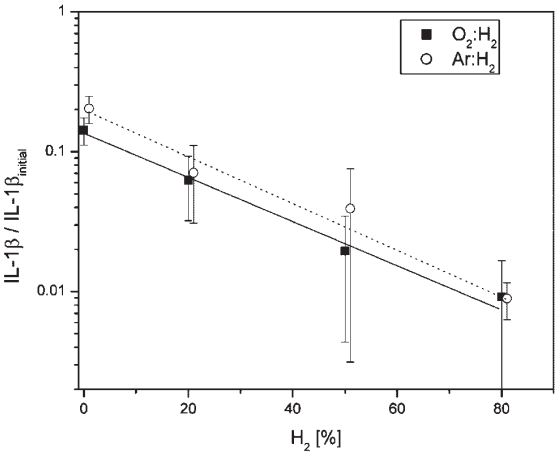

Figure 7. LPS deactivation in Ar/H_2 and O_2/H_2 gas mixtures (deposited 0.1 ng of *E. Coli* O111:B4 LPS, applied power 1 000 W, 13.3 Pa, 100 sccm).

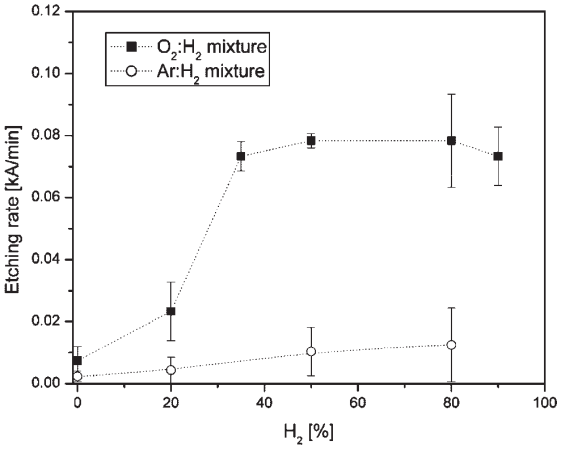

Figure 9. Etching rate of Lipid A in O_2/H_2 and Ar/H_2 discharges (applied power 1 000 W, 13.3 Pa, 100 sccm).

Protein Removal

The efficiency of protein removal by plasma discharge was studied using the same gas mixtures found to be effective for depyrogenation.

Figure 10 shows the time evolution of a collagen films thickness (normalized to its initial value) treated in different plasma gas mixtures under the same operational conditions. It can be seen that initially the thickness of treated films decreased linearly with time, and that the etching rate observed varied strongly with the gas used, the highest values being obtained for O_2/H_2 (50:50) mixture. For these conditions, the removal rate was nearly 5 times higher than the one obtained with the other discharges tested. It can also be seen that the removal rate of the collagen for O_2/H_2 initially varied linearly with time, followed by a slowing of the removal rate, probably owing to the consumption of the treated films leading to a change of surface composition related to the removal of volatile compounds.

Similar results have been obtained also for brain homogenate films, as demonstrated in Figure 11. Also in this case, significantly faster removal was observed with an O_2/H_2 mixture compared to other discharges.

Discussion

Plasma Sterilization

Comparison of the sterilization results with analysis of the gas phase by optical emission spectroscopy (Figure 2) and

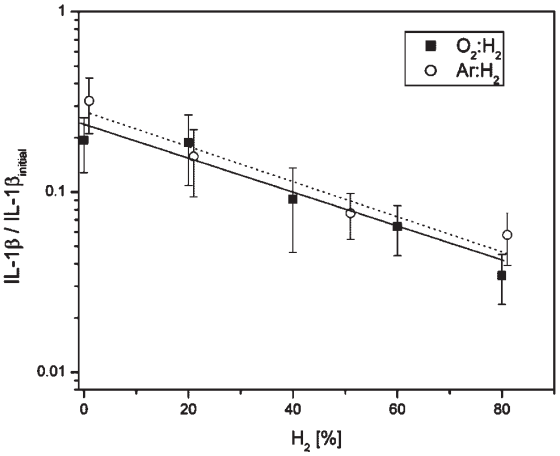

Figure 8. Lipid A deactivation in Ar/H_2 and O_2/H_2 gas mixtures (deposited 0.1 ng Lipid A, applied power 1 000 W, 13.3 Pa, 100 sccm).

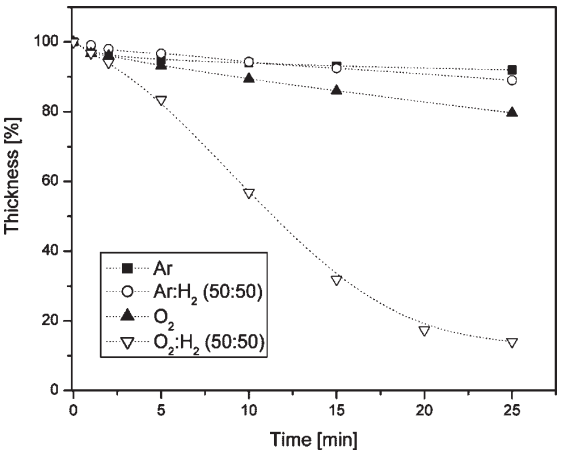

Figure 10. Collagen film etching (16 Pa, 100 sccm, applied power 500 W; 1 000 W in the case of treatment in pure Ar).

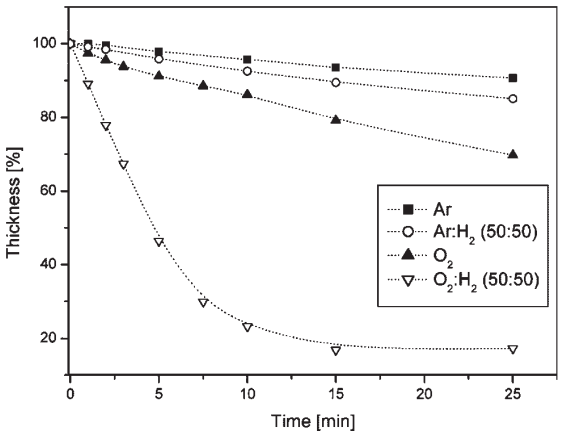

Figure 11. Etching of brain homogenate (16 Pa, 100 sccm, applied power 500 W; 1 000 W in the case of treatment in pure Ar).

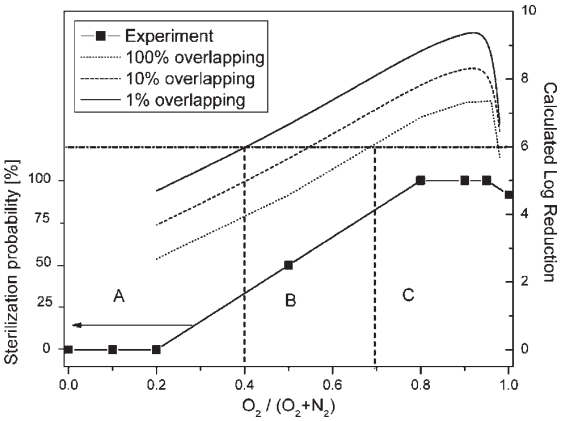

Figure 12. Comparison of the predicted log reduction and experimental probability to obtain complete sterilization after 10 min of plasma treatment in O_2/N_2 mixtures (ICP plasma source, 500 W, 20% DC, time-on 5 ms, 10 sccm, 13.3 Pa, 10 min).

with the SEM study of treated and untreated samples (Figure 3 and Figure 4) led to the conclusion that, under the experimental conditions employed, the total sterilization efficiency was controlled by the etching and erosion of the spores and not by UV radiation. As underlined above, this is in contradiction with several recent studies.[7,11]

To explain these contrasting findings, we propose a simplified kinetics model, where it is assumed that there are two kinds of spores with given initial quantities, which are subjected to two different actions from the plasma discharge. The first group of spores has genetic material that can be directly reached and destroyed by the UV radiation. The second type of spores represent spores shielded from UV radiation either by other spores or by some residuals (e.g., cell debris). In order to enable UV radiation to destroy DNA of these buried spores, it is necessary to remove the shielding material by etching, in other words to transform shielded spores into unshielded ones. If the first group of spores are denoted as S_1 and the second group as S_2 the following equations governing sterilization kinetics can be written:

$$\frac{d[S_1]}{dt} = -k_1 \cdot UV \cdot [S_1] + k_2 \cdot [X] \cdot [S_2] \quad (1)$$

$$\frac{d[S_2]}{dt} = -k_2 \cdot [X] \cdot [S_2] \quad (2)$$

where UV is the intensity of UV radiation emitted by the plasma, $[X]$ is the amount of etching agent and k_1 and k_2 are the rate constants of UV radiation killing of spores and the removal of shielding material, respectively.

Although the proposed schema is very simplified, for example, it is considered that shielded material can be completely removed which need not always be true, it qualitatively describes the trend of the experimental results. As can be seen in Figure 12, the sterilization probability estimated on the basis of experiments (left scale) as well as the log reduction of the spore population predicted by the model after 10 min (right scale) of plasma treatment follows the same trend, i.e., faster sterilization is achieved with a higher amount of oxygen in the initial discharge mixture. Moreover, depending on the mixture composition, three regions can be distinguished:

- The region between pure nitrogen discharge and discharge with 40% of oxygen, in which complete sterilization is never reached after 10 min of the treatment.
- The region between 40% and 70% of oxygen, where complete sterilization is only reached for the lowest level of spores overlapping, (i.e., some samples are completely sterile after 10 min of treatment and some are not, depending on the initial spore distribution). This corresponds to the experimental results, since for 50% of oxygen, a 50% probability of obtaining full sterility was estimated.
- More than 70% of the oxygen in the mixture finally assured complete sterility after 10 min for all of the samples, as was observed experimentally, due to the fast etching of the spores, as illustrated by the SEM pictures.

To conclude, although the UV/VUV radiation is the only mechanism in the proposed model leading directly to the spores' death (in agreement with the conclusions of several authors[11,12,19]), the sterilization efficiency depends essentially on the stacking of the spores and is governed mainly by the efficiency of the shielding material removal. On the other hand, in the case of a monolayer, the etching is not needed and therefore the time to reach complete sterility is given by the UV radiation intensity. The suggested schema, although very simplified, allows resolution of the apparent contradiction between the results reported in the literature.

Depyrogenation

Our results clearly show that reduction of the biological response via cytokine release (i.e., depyrogenation) can be obtained at temperatures lower than 60 °C for durations which depend on the type of pyrogen and the level of contamination. These results must be compared to the thermal treatment commonly used for depyrogenation. For instance, a similar decontamination using dry heat would be obtained at 170 °C after 100 min[36] or at 200 °C after 20 min,[4] which must be compared to the maximum temperature of 60 °C and a plasma treatment duration of 5 min. This clearly demonstrates why plasma discharge for the treatment of temperature sensitive materials is of interest.

However, we observed depyrogenation kinetics with 2 phases, a fast one in the first minutes, followed by a slower one. Preliminary sets of experiments focused on the surface analysis of the deposit at different treatment times showed that this effect is most likely related to the heterogeneous reaction rates of different components of Lipid A.

We also showed that 2 mechanisms can be operating for depyrogenation: etching or deactivation. An interesting perspective thus exists where the 2 mechanisms are applied simultaneously or sequentially to reduce the quantity of contamination material without having an adverse effect on the substrate structure.

Another important point refers to the legislation which imposes a 3 Log reduction for validation of a depyrogenation process. We have not tested the process under conditions which allow a 3 Log reduction of the initial surface activity, mostly due to the fact that after 5 min, we almost reached the detection limit of the test for the lowest initial LPS content, but we do not see any reason not to reach such a value. Extrapolation of our results led to a 3 Log reduction being obtained after 30 to 50 min depending on the nature of the pyrogen tested, which is still much lower than the results obtained from a thermal treatment. This is related of course to the slowing of the removal kinetics, as mentioned above.

Protein Removal

Both collagen and brain homogenate films followed a linear decrease of their thickness as a function of time for the different plasma compositions tested, apart from longer treatment times in the O_2/H_2 mixture, for which slowing of etching kinetics occurred. As in the case of Lipid A removal, the O_2/H_2 gas mixture led to a major removal efficiency of the tested protein films, almost 5 times larger than in pure Ar and O_2 plasma respectively. The appearance of the observed 1 or 2 phase behavior was not completely understood until now. One possible explanation is that the high removal rate is connected with the fast removal of reactive compounds in the first phase, e.g., by its oxidation and volatilization, followed by much slower kinetics as the residues are enriched in the non-volatile compounds such as Na.[37] Further investigations are being carried out to examine this point. Our results demonstrate that plasma can be used efficiently to decontaminate surfaces of protein residues, opening new perspectives in the field of prion decontamination.

Conclusion

The applicability of low pressure plasma treatment for the sterilization of bacterial spores, for the reduction of the biological activity of bacterial endotoxins and the removal of proteins has been demonstrated.

For sterilization, the apparent discrepancy between our results and some results in the literature has been explained by the role of spore stacking. To demonstrate this effect, a simple theoretical model of sterilization has been proposed. According to the performed calculations, it was found that the main feature that governed sterilization efficiency was the presence of material shielding spores from direct UV/VUV radiation and the efficiency of its removal. The practical consequences of our results could be particularly important since, in a real situation, the spores are stacked and so an efficient process must rely on etching and not only on UV sterilization. Moreover these findings reveal the need for further investigation of the mechanisms of spore erosion and etching, e.g., in the O_2/H_2 mixture that was found to be most potent in etching both Lipid A and protein films.

In the case of depyrogenation, it was demonstrated that low temperature discharge can significantly inactivate different kinds of LPS as well as Lipid A within several minutes of plasma treatment. It was found that 2 mechanisms can possibly be used, either for the removal of the pyrogenic contamination by etching, the O_2/H_2 plasma being the most efficient in this case, or by a chemical reaction of the Lipid A with hydrogen radicals in the case of H_2 containing discharges. This kind of mechanism might be particularly interesting for a deactivation process without damaging the underlying substrate. However, the application of surface analysis methods is crucial in order to find out the mechanism behind the deactivation of pyrogens, as well as to check the possible influence of plasma on the substrates during their treatment. This topic is the subject of ongoing studies.

Finally, we demonstrated the removal of protein films, namely collagen and brain homogenate, at low temperature in typical durations of a few tens of minutes. The most efficient gas mixture for protein film removal was O_2/H_2, as in the case of Lipid A. A 1 or 2 phase mechanism was observed depending on the case, and this phenomenon has still to be confirmed. Further experiments are ongoing for the analysis of the chemical mechanisms operating during etching and/or de-activation.

Nevertheless, these results also give us good reason to think that the removal and/or deactivation of PrP on sur-

faces is possible without damaging the substrates treated. The initial results that have been obtained with brain homogenate are encouraging and demonstrate that the etching kinetics can be quite high with O_2 containing plasma. This has to be compared to the positive results obtained by Baxter et al.[29] on the removal of infectivity from PrP contaminated samples observed with Ar/O_2 plasma. It must be point out that O_2/H_2 plasma gives significantly higher removal kinetics that O_2 plasma for our model proteins.

The results presented confirm that a plasma discharge can be operated efficiently to sterilize and decontaminate surfaces from biological products. This must be emphasized, though a trade-off still has to be found during the plasma decontamination or sterilization treatment between the etching/removal of biological contamination and damaging the substrate (polymers). For this, a multi-step process could be necessary to find selectivity between biological material and substrate composition, and since more generally the optimum conditions are different for sterilization and decontamination.

Acknowledgements: This work has been supported by the *EU Growth project Steriplas* (GRD1-1999-10584), and the *FP6 2005 NEST project* "*Biodecon*". Support from *CSMA Ltd* (UK) and *Manchester Metropolitan University* as well as the contribution of *T. Sasaki* with scanning electron microscopy and *E. Parnisari* for technical help are gratefully acknowledged.

[1] B. Beutler, E. T. Rietschel, *Nat. Rev. Immunol.* **2003**, *3*, 169.
[2] C. A. Dinarello, *Chest* **2000**, *118*, 503.
[3] M. T. Abreu, M. Arditi, *J. Pediatr.* **2004**, *144*, 421.
[4] W. Hecker, D. Witthauer, A. Staerk, *PDA J. Pharm. Sci. Technol.* **1994**, *48*, 197.
[5] J. C. Darbord, *Biomed. Pharmacother.* **1999**, *53*, 34.
[6] M. Laroussi, *Plasma Process. Polym.* **2005**, *2*, 391.
[7] N. Philip, B. Saoudi, M. A. Crevier, M. Moisan, J. Barbeau, J. Pelletier, *IEEE Transactions on Plasma Science* **2002**, *30*, 1429.
[8] S. Lerouge, M. R. Wertheimer, R. Marchand, M. Tabrizian, L. H. Yahia, *J. Biomed. Mater. Res.* **2000**, *51*, 128.
[9] S. Lerouge, M. R. Wertheimer, L. H. Yahia, *Plasma Polym.* **2001**, *6*, 175.
[10] S. Lerouge, A. C. Fozza, M. R. Wertheimer, R. Marchand, L. H. Yahia, *Plasma Polym.* **2000**, *5*, 31.
[11] M. Moisan, J. Barbeau, S. Moreau, J. Pelletier, M. Tabrizian, L. H. Yahia, *Inter. J. Pharm.* **2001**, *226*, 1.
[12] M. Moisan, B. Saoudi, M. C. Crevier, N. Philip, E. Fafard, J. Barbeau, J. Pelletier, "*5th Int. Workshop Microwave Discharges*", Greifswald, Germany 2003, p. 210.
[13] R. Mogul, A. Bol'shakov, S. L. Chan, R. M. Stevens, B. N. Khare, M. Meyyappan, J. D. Trent, *Biotechnol. Prog.* **2003**, *19*, 776.
[14] A. A. Bol'shakov, B. A. Cruden, R. Mogul, M. V. V. S. Rao, S. P. Sharma, B. N. Khare, M. Meyyapan, *AIAA J.* **2004**, *42*, 823.
[15] N. Munakata, M. Saito, K. Hieda, *Photochem. Photobiol.* **1991**, *54*, 761.
[16] US 3 383 163 (1968), inv.: W. P. Menashi.
[17] S. Moreau, M. Moisan, M. Tabrizian, J. Barbeau, J. Pelletier, A. Ricard, L. H. Yahia, *J. Appl. Phys.* **2000**, *88*, 1166.
[18] J. Feichtinger, A. Schulz, M. Walker, U. Schumacher, *Surf. Coat. Technol.* **2003**, *174–175*, 564.
[19] I. A. Soloshenko, V. V. Tsiolko, V. A. Khomich, A. I. Schedrin, A. V. Ryabtsev, V. Yu. Bazhenov, I. L. Mikhno, *Plasma Phys. Rep.* **2000**, *26*, 845.
[20] K. Kelly-Wintenberg, A. Hodge, T. C. Montie, L. Deleanu, D. Sherman, J. R. Roth, *J. Vac. Sci. Technol.* **1999**, *A 17*, 1539.
[21] M. Laroussi, F. Leipold, *Int. J. Mass Spectrom.* **2004**, *233*, 81.
[22] M. Nagatsu, F. Terashita, H. Nonaka, L. Xu, T. Nagata, Y. Koide, *Appl. Phys. Lett.* **2005**, *8*, 128.
[23] T. C. Montie, K. Kelly-Wintenberg, J. C. Roth, *IEEE Trans. Plasma Sci.* **2000**, *28*, 41.
[24] [24a] M. Laroussi, D. A. Mendis, M. Rosenberg, *New J. Phys.* **2003**, *5*, 41.1–41.10; [24b] M. Laroussi, F. Leipold, *Int. J. Mass Spectrom.* **2004**, *233*, 81.
[25] D. A. Mendis, M. Rosenberg, F. Azam, *IEEE Transaction on Plasma Science* **2000**, *28*, 1304.
[26] R. E. Peeples, N. R. Anderson, *J. Parenter. Sci. Technol.* **1985**, *39*, 9.
[27] O. Kylián, M. Hasiwa, F. Rossi, *Plasma Processes Polym.* **2006**, *3*, 272.
[28] A. G. Whittaker, E. M. Graham, R. L. Baxter, A. C. Jones, P. R. Richardson, G. Meek, G. A. Campbell, A. Aitken, H. C. Baxter, *J. Hosp. Infect.* **2004**, *56*, 37.
[29] H. C. Baxter, G. A. Campbell, A. G. Whittaker, A. C. Jones, A. Aitken, A. H. Simpson, M. Casey, L. Bountiff, L. Gibbard, R. L. Baxter, *J. Gen. Virol.* **2005**, *86*, 2393.
[30] [30a] EP 00100445.3, invs.: P. Colpo, F. Rossi; "Method and apparatus for inductively coupled plasma treatments"; [30b] EP 1253216, invs.: P. Colpo, F. Rossi; "Method and apparatus for sequential plasma treatments".
[31] F. Rossi, "Plasma sterilisation: Mechanisms overview and influence of discharge parameters" in: *Plasma Processes and Polymers*, R. d'Agostino, P. Favia, M. R. Wertheimer, C. Oehr, Eds., Wiley-VCH, Weinheim 2004.
[32] S. Hoffmann, A. Peterbauer, S. Schindler, S. Fennrich, S. Poole, Y. Mistry, T. Montag-Lessing, I. Spreitzer, B. Löschner, M. van Aalderen, R. Bos, M. Gommer, R. Nibbeling, G. Werner-Felmayer, P. Loitzl, T. Jungi, M. Brcic, P. Brügger, E. Frey, G. Bowe, J. Casado, S. Coecke, J. de Lange, B. Mogster, L. M. Næss, I. S. Aaberge, A. Wendel, T. Hartung, *J. Immunol. Methods* **2005**, *298*, 161.
[33] M. Hasiwa, K. Kullmann, S. von Aulock, T. Hartung, submitted.
[34] O. Kylián, T. Sasaki, F. Rossi, *Eur. Phys. J. Appl. Phys.* **2006**, *34*, 139.
[35] C. Erridge, E. Bennett-Guerrero, I. R. Poxton, *Microbes Infect.* **2002**, *4*, 837.
[36] K. Tsuji, S. J. Harrison, *Appl. Environ. Microbiology* **1978**, *36*, 710.
[37] G. Ceccone, D. Gilliland, O. Kylián, M. Westermeier, F. Rossi, *Czech. J. Phys.* **2006**, *56*, B672.

IOP PUBLISHING JOURNAL OF PHYSICS D: APPLIED PHYSICS
J. Phys. D: Appl. Phys. **41** (2008) 095201 (8pp) doi:10.1088/0022-3727/41/9/095201

Removal of model proteins by means of low-pressure inductively coupled plasma discharge

O Kylián, H Rauscher, D Gilliland, F Brétagnol and F Rossi[1]

European Commission, Joint Research Centre, Institute for Health and Consumer Protection, Via E Fermi 2749, 21027 Ispra (VA), Italy

E-mail: francois.rossi@jrc.it

Received 23 November 2007, in final form 3 February 2008
Published 27 March 2008
Online at stacks.iop.org/JPhysD/41/095201

Abstract
Surgical instruments are intended to come into direct contact with the patients' tissues and thus interact with their first immune defence system. Therefore they have to be cleaned, sterilized and decontaminated, in order to prevent any kind of infections and inflammations or to exclude the possibility of transmission of diseases. From this perspective, the removal of protein residues from their surfaces constitutes new challenges, since certain proteins exhibit high resistance to commonly used sterilization and decontamination techniques and hence are difficult to remove without inducing major damages to the object treated. Therefore new approaches must be developed for that purpose and the application of non-equilibrium plasma discharges represents an interesting option. The possibility to effectively remove model proteins (bovine serum albumin, lysozyme and ubiquitin) from surfaces of different materials (Si wafer, glass, polystyrene and gold) by means of inductively coupled plasma discharges sustained in different argon containing mixtures is demonstrated and discussed in this paper.

1. Introduction

The idea to utilize non-equilibrium discharges for sterilization of surfaces of medical instruments was first reported in 1968 [1]. Since then, the popularity of this method substantially increased because of its advantageous and unique features. Compared with the traditionally employed sterilization techniques, such as thermal treatment, chemical treatment or application of ionizing radiation, the non-equilibrium plasma discharges can be operated at low temperatures, using non-toxic substances and having no or modest influence on the integrity and properties of the sterilized objects themselves, while maintaining a high treatment efficiency. According to the extensive studies published in the literature, the high sterilization potency of plasma discharges is connected to the emission of energetic UV photons (e.g. [2–7]) that are capable of causing lesions on the spores' genetic material, or by chemically active species produced in the plasma phase that damage spore walls by etching (e.g. [8–13]) or by chemical sputtering [14].

Moreover, plasma discharges have recently been found to act not only as potent microbiocidal agents but also as an effective tool for the depyrogenation of bacterial endotoxins [12, 15, 16] or for the destruction of prions (the infectious proteins capable of causing severe neurodegenerative diseases classified as transmissible spongiform encephalopathies) [17]. In particular, the latter is of significant interest since prions are exceptionally resistant to both physical and chemical treatment [18]. As a consequence of this, a large number of surgical instruments were found to exhibit a high degree of protein soiling after their routine decontamination in sterile services (e.g. [19, 20]). High risks associated with the presence of infectious proteins together with the impossibility of removing them by currently used hospital decontamination techniques lead to disposal of many surgical instruments after single use, which in turn represents an enormous burden for the public health budget. Thus the possibility of applying plasma discharges for the removal of proteins from the surfaces of surgical instruments gained increased attention in the past years, since these processes have the potential of answering the needs of health services analogously to the cases of bacterial spores or endotoxins.

[1] Author to whom any correspondence should be addressed.

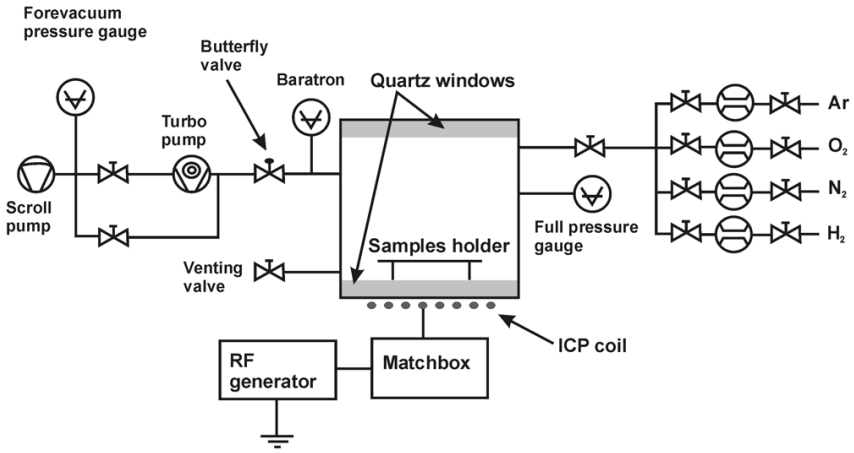

Figure 1. Experimental set-up.

Indeed, the possibility of removing various model proteins from surfaces by means of plasma discharges sustained either at reduced pressures or at atmospheric pressure has been recently demonstrated by several groups employing different methods for the evaluation of treatment efficiency. They range from biological assays [21,22], electrophoresis [21,23], application of fluorescently labelled proteins [24], imaging ellipsometry [25], surface diagnostic methods [26–28] to applications of surface plasmon resonance (SPR) [22] or quartz crystal microbalance (QCM) [12] used for on-line monitoring of protein removal. Nevertheless, the applicability of these methods is limited, particularly for the determination of etching rates of proteins under different experimental conditions; this determination, however, represents a crucial step both for the identification of the main processes leading to protein elimination and for optimization of the treatment. For example, in the case of fluorescently labelled proteins, the intense radiation emitted by plasma discharges can destroy the fluorescent dye, leading to an overestimation of the protein removal rates. Surface analytical methods, such as x-ray photoelectron spectroscopy (XPS) or time-of-flight secondary ion mass spectroscopy (ToF-SIMS), can give an important insight into the nature of the changes of the chemical structure of proteins induced by an applied plasma discharge, but due to their relative high surface sensitivity, which is typically in the range of 10 nm and 2 nm, respectively, they are not suitable for the monitoring of protein removal when the height of the initial protein coating is in the order of micrometres. Biological assays are on one hand a direct method for the evaluation of the decrease in biological activity of treated proteins, but this method is highly protein specific and thus lacks universality. Electrophoresis is a useful method for the demonstration of fragmentation of proteins exposed to the plasma discharges, but it is difficult to obtain quantitative results. Finally, SPR and QCM can be used for on-line observation of the kinetics of protein removal, but the applicability of these methods is limited to a narrow spectrum of substrate materials; typically gold is used for that purpose.

In order to overcome these limitations, a new approach based on stylus profilometry is employed in this study. It allows direct evaluation of etching rates of different proteins independently on the substrate material as discussed in this paper.

2. Experimental

The samples were prepared by spotting an aqueous solution (ranging from 10 to 0.1 mg ml^{-1} of protein content) of different model proteins (bovine serum albumin, lysozyme and ubiquitin) on polished Si wafers, microscopic glass slides, gold and polystyrene plates. After the deposition, the samples were dried overnight in a common flow hood in order to mimic the most difficult situation for the removal of proteins [29]. Subsequently, the samples were plasma treated using a planar double coil inductively coupled plasma source (ICP) schematically depicted in figure 1. This plasma reactor allows igniting plasma discharges with a power between 100 and 500 W, in a pressure range from 0.1 to 20 Pa and gas flows from 1 to 50 sccm. The processing chamber has a volume of approximately 5 L and is evacuated by a primary and turbomolecular pump. It is fed by a gas mixture controlled by MKS mass flow controllers.

In order to enable the comparison with the previously reported results regarding sterilization of bacterial spores [30] the experiments were performed employing pure argon and its mixtures (20 sccm : 1 sccm) with hydrogen, nitrogen and oxygen at a pressure of 10 Pa and an applied RF power of 200 W. To keep the treatment conditions (i.e. power density and gas residence time) as close as possible to the ones given by Halfmann *et al* [30] the applied power and mass flows were lowered by a factor of 5 as compared to the values given in [30], corresponding to the volume ratios of the two employed discharge chambers.

3. Results and discussion

3.1. Characterization of untreated samples

The protocol of protein deposition chosen for this study leads to the formation of a reproducible and well-organized structure of

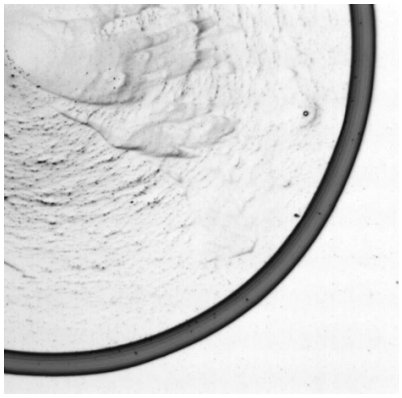

Figure 2. Part of BSA sample visualized by the optical microscope.

proteins on the surface as seen in figure 2, where a section of the BSA sample imaged by an optical microscope is presented, and in figure 3 where examples of ellispometric images of bovine serum albumin (BSA), lysozyme and ubiquitin obtained by an EP^3 imaging ellipsometer are shown (Nanofilm Surface Analysis GmbH, angle of incidence of 42°, field of view of 2000 μm × 2000μm, $\lambda = 554.3$ nm). The images show a 'coffee ring effect' and two distinctly different regions can be easily observed. At the border of the dried droplet a relatively thick ring is formed, whereas in the central region the coating is much thinner, i.e. a situation similar to the one mentioned already by Deng *et al* [24].

Stylus profilometry (Alpha-step® profilometer produced by KLA-Tencor, scan speed 20 μm min^{-1}, sampling rate of 50 Hz, equivalent force exerted by the stylus tip on the surface corresponded to 27.4 mg) showed that the ring height typically exceeds 1 μm and is more than ten times higher than the maximal height of the deposit in the central part of the droplet. Naturally the profile of the deposit depends on the protein used, the dilution of the solution and the properties of the substrate used (e.g. on its hydrophilicity). Concretely, increasing the hydrophilicity of the substrate leads, for the same volume of deposited protein solution, to the formation of larger spots and thus to a lowering of the ring border as demonstrated in figure 4. Regarding differences between proteins, it was found that the ring height is maximal, at the same dilution, in the case of ubiquitin followed by BSA and lysozyme (see figure 5). For the latter two, the typical heights have been found to be very close. Nevertheless, the dilution of the proteins can be easily adjusted in order to obtain similar ring heights for all tested protein-substrate material combinations. Moreover, the formation of a well-defined, relatively high protein ring, which can be considered as a kind of protein self-patterning, allows us to measure its height decrease after the different treatment steps from which the protein etching rate can be directly estimated.

To assure that the observed pattern reflects the protein distribution over the surface and is not caused, e.g. by the accumulation of salts or airborne impurities at the border of the drying drop, additional tests have been performed using fluorescently labelled BSA (fluorescein isothiocyanate, Sigma Aldrich), which allows direct visualization of the protein

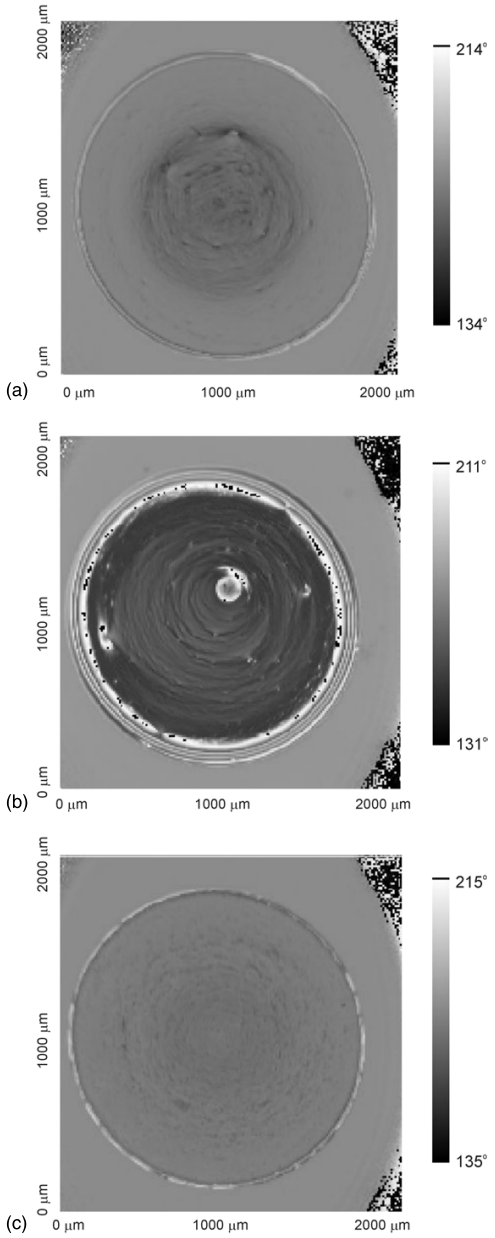

Figure 3. Ellipsometric maps of Δ angles of different proteins. (*a*) BSA (0.5 mg ml^{-1}), (*b*) lysozyme (1 mg ml^{-1}) and (*c*) ubiquitin (0.1 mg ml^{-1}).

distribution, and with ToF-SIMS (TOF SIMS IV by IONTOF equipped with a bismuth cluster primary ion source operating at 25 keV, acquisition area 500 μm × 500 μm, total primary ion flux below 10^{13} ions cm^{-2}) that allows us to monitor the surface distribution of fragments characteristic for the native structure of the protein.

The images obtained by fluorescent optical microscopy (see figure 6(*a*) and ToF-SIMS (figure 6(*b*) showed a similar distribution as those observed by optical microscopy, ellipsometry and profilometry measurements. Hence, the

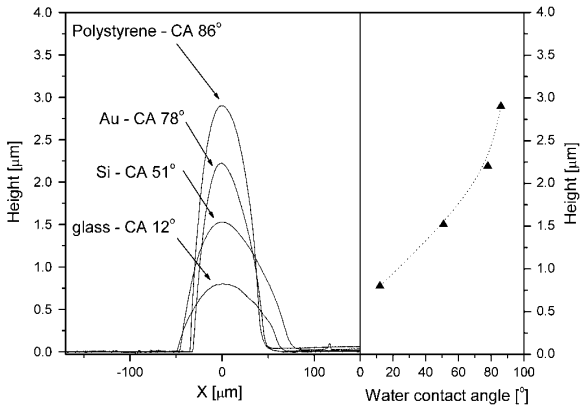

Figure 4. Ring profiles of BSA deposited on different substrates (left panel) and dependence of the ring height on the substrate water contact angle (right panel); BSA dilution 1 mg ml^{-1}.

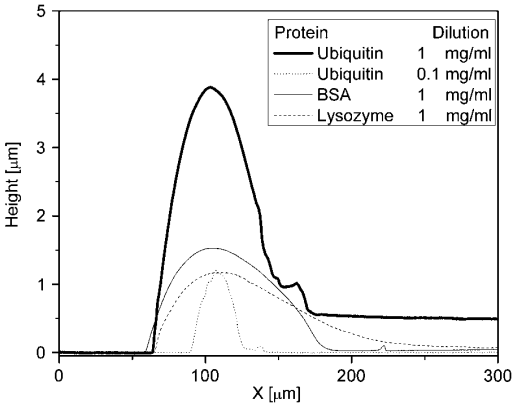

Figure 5. Ring profiles of different proteins deposited on Si wafer.

topography of the observed structure is indeed determined qualitatively by the distribution of protein.

3.2. Effect of plasma treatment

After the plasma treatment, visible modifications of the protein samples were observed indicating gradual removal of the protein coating. An example of this behaviour is given in figure 7, where the ellipsometric 2D maps of the Δ angles of an ubiquitin sample before and after plasma treatment in the Ar/O_2 plasma discharge for 60 s are depicted.

The rate of these modifications was however found to be strongly dependent on the gas mixture used. In order to quantify this rate, profilometric measurements of the height of the droplet ring before and after the treatment were performed. In all the experiments, a linear decrease of the border height was observed with increasing treatment time as demonstrated in figure 8 for Argon and Ar/O_2 treatment.

The slope of the protein ring decrease can be furthermore used as a direct measure of the protein etching rate. According to the experimental results (based on 40 measurements for each experimental condition), it was found that the BSA etching

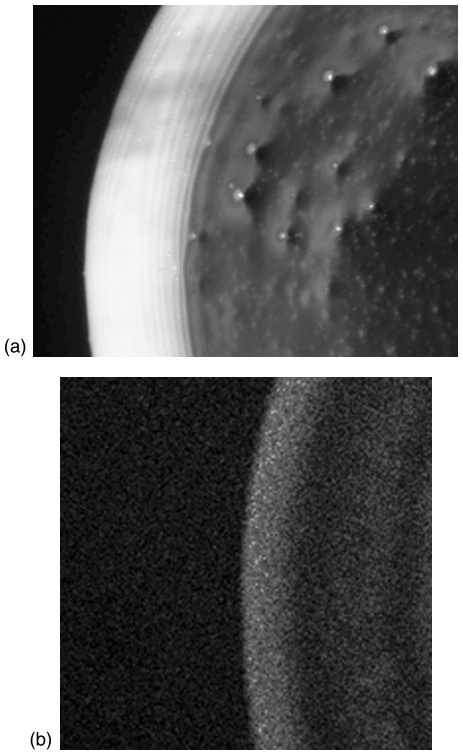

Figure 6. Images of (*a*) fluorescently labelled BSA obtained by a fluorescent microscope and (*b*) the 2D map of the lysine peak ($C_5H_{10}N^+$, atomic mass 84.085 [31]) of a BSA sample obtained by ToF-SIMS.

rate is markedly higher in the case of the Ar/O_2 discharge ($0.77 \pm 0.02\,\mu$m min^{-1}) compared with the values obtained for argon, Ar/N_2 and Ar/H_2 plasma discharges (see figure 9) that were found to be at least three times lower.

Regarding the plasma etching efficiency on different proteins, we observed systematic variations depending on the applied plasma discharge, as seen in figure 10. For example the etching rate of ubiquitin in Ar/O_2 plasma discharge was found to be markedly lower than that observed for BSA and lysozyme, whereas the Ar/N_2 plasma seems to etch ubiquitin faster than the other two proteins. Nevertheless, in spite of these differences, it can be concluded that the Ar/O_2 plasma discharge removes all tested proteins substantially faster as compared with the other discharges employed in this study. This is however an important difference with respect to the results on sterilization of bacterial spores, where under similar experimental conditions as those employed here only a slight dependence on the used gas mixture was found (complete sterility was reached in between 40 and 60 s for all tested gas mixtures [30]). In this case sterilization itself was attributed solely to the action of UV radiation emitted in the 200–275 nm spectral range [7]. However, although the photons emitted in this spectral range carry enough energy to break C–C and C–H bonds they do not seem to have a significant influence on the proteins removal under the experimental conditions we have used. First, the intensity of UV emission in the spectral

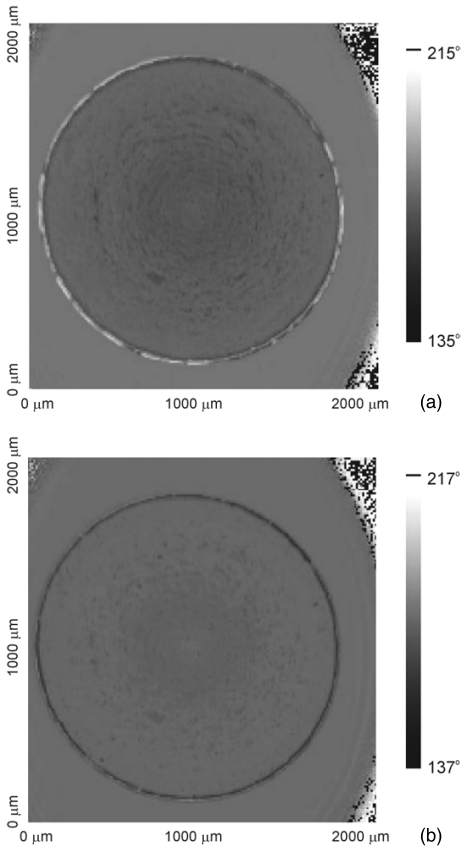

Figure 7. The 2D maps of the Δ angles of ubiquitin before treatment (*a*) and after 60 s treatment in Ar/O_2 20 : 1 mixture (*b*); protein dilution 0.1 mg ml^{-1}, Si wafer.

range of interest is fairly weak and is linked almost solely to the presence of impurities leading to the formation of NO or OH molecules. Moreover, as seen in figure 11 the integral intensity of UV radiation between 200 and 275 nm was found to be highest in the Ar/N_2 mixture, followed by Ar/H_2, Ar/O_2 and finally by the argon discharge, which does not correspond to the sequence of protein removal efficiency. Therefore it seems that only the presence of oxygen in the discharge is the determining factor for high protein removal efficiency. This is above all due to the high capability of O atoms to abstract hydrogen from the polymer backbone, thus creating radical sites which initiate subsequent processes that lead to the cleavage of the polymer chain as well as the formation of volatile compounds by subsequent reaction with oxygen atoms or molecules (e.g. [32, 33]).

However, it is to be noted that the reasons for the relatively similar etching rates observed for the treatment performed in Ar, Ar/N_2 and Ar/H_2 plasma discharges are not clear. One possible explanation for these results is the presence of unavoidable traces of oxygen (originating either from the reactor walls, residual moisture or directly from the samples) reported also in other studies using discharges in pure argon (e.g. [34, 35]). Indeed, optical emission spectroscopy showed the presence of spectral lines of atomic oxygen in all the

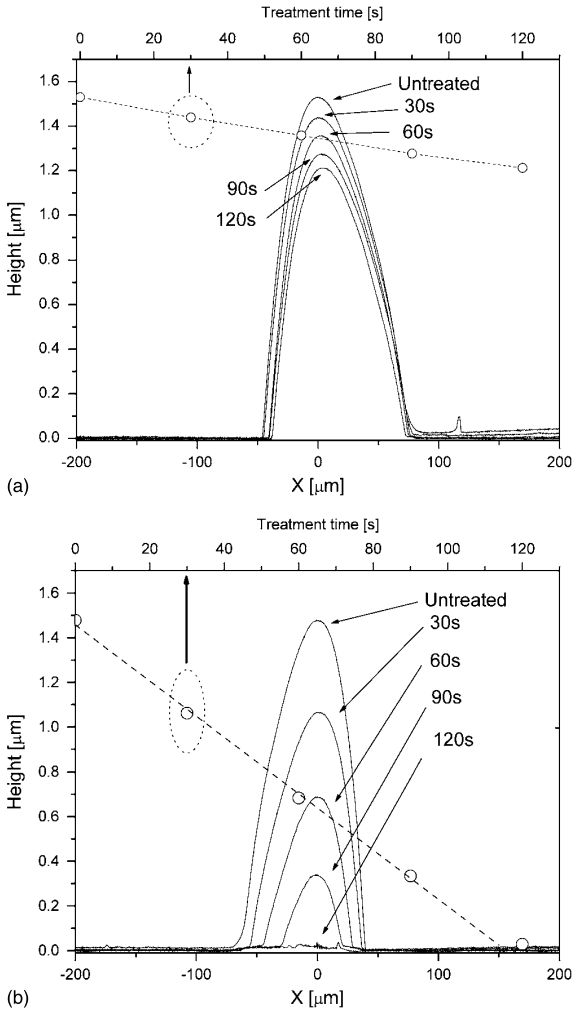

Figure 8. Temporal evolution of the ring profile of BSA samples treated in argon (*a*) and Ar/O_2 20 : 1 mixture (*b*); protein dilution 1 mg ml^{-1}, substrate Si wafer. The full lines represent the measured ring profile, open symbols and the dashed line indicate the temporal evolution of the maximal height of the ring.

mixtures (see figure 12). Nevertheless, according to the actinometric evaluation of O atom densities, the number of oxygen atoms in Ar/O_2 discharge is almost 20 times higher than the one observed in the discharge in pure argon, which does not correspond to the differences in the etching rates. Therefore this hypothesis does not seem to be plausible and other mechanisms of protein removal have to be considered. These mechanisms may be based either on chemical sputtering [14] or on the effect of VUV radiation. In particular, the latter is known to be capable of significantly affecting polymeric materials by the creation of radical sites by hydrogen abstraction, induction of backbone scission or formation of volatile compounds (e.g. [36]).

Since the highest etching rate was achieved in the Ar/O_2 mixture independently of the protein, an evaluation of the role of the substrate material on the etching rate was performed

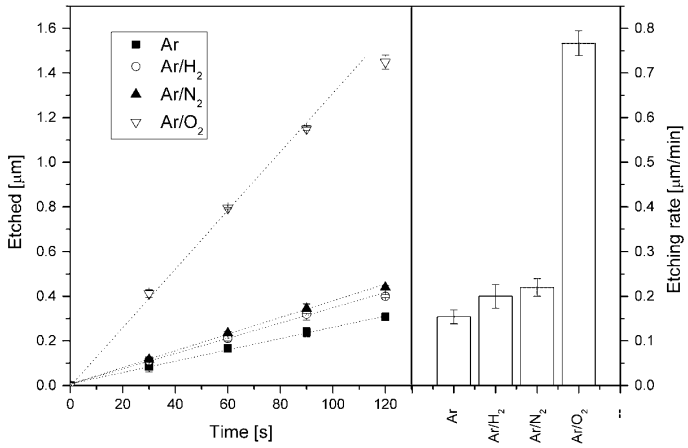

Figure 9. Temporal evolution of the thickness of BSA measured on the protein ring (left panel) and corresponding etching rates (right panel); protein dilution 1 mg ml^{-1} Si wafer.

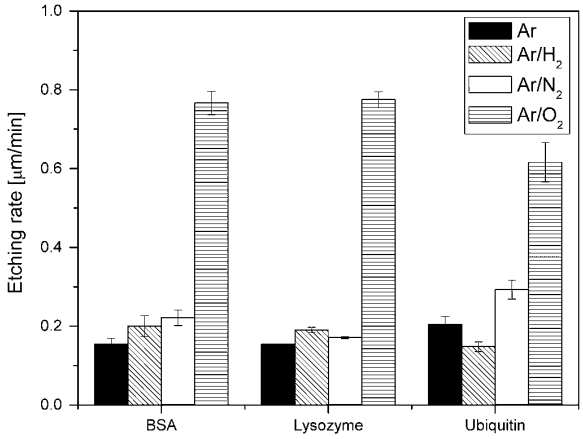

Figure 10. Etching rates of different proteins deposited on Si wafer (BSA and lysozyme dilution 1 mg ml^{-1}, ubiquitin 0.1 mg ml^{-1}).

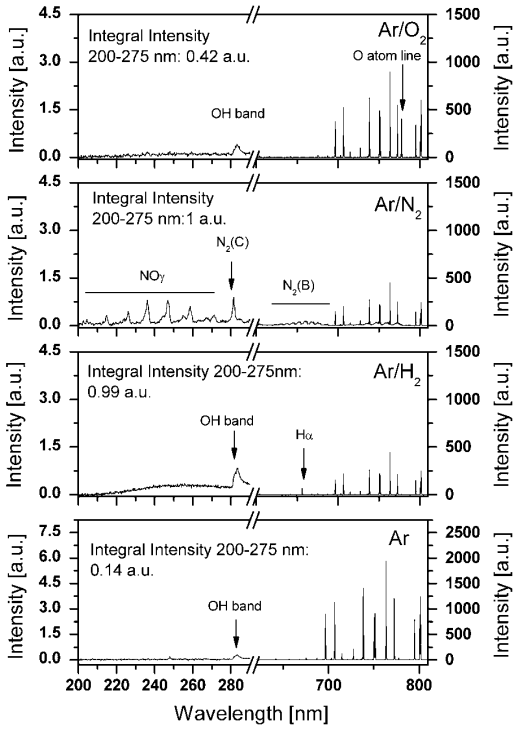

Figure 11. Optical emission spectra of gas mixtures used for protein removal experiments (left axis: intensities measured in the spectral range 200–300 nm; right axis: intensities in the spectral range 650–810 nm).

using only BSA treated in this discharge mixture. As seen in figure 13, the etching rates were found to be almost equal for BSA deposited on gold and Si, the etching was slightly slower for protein on glass and markedly slower when polystyrene was used as a substrate. However, additional examination showed that in the case of polystyrene the Ar/O_2 plasma treatment causes a significant etching of the substrate, around 0.3 μm min^{-1}, as shown in figure 14. If we take this effect into account, i.e. if we consider that the base from which the ring height is measured decreases itself with plasma treatment by 0.3 μm min^{-1}, we can conclude that the real etching rate of BSA is similar to that when BSA was deposited on the other materials. This excludes the influence of local heating due to recombination of radicals on the surface.

4. Conclusions

In this study protein etching by means of a low-pressure ICP discharge was investigated. For this purpose a new method based on stylus profilometry was introduced. This method allows us to quantitatively determine the protein etching rates independently of the proteins, which was demonstrated for bovine serum albumin, lysozyme and ubiquitin, i.e. proteins differing significantly in their physical (e.g. molecular weight) and chemical properties (e.g. in the primary and the secondary structure), as well as for different substrate materials

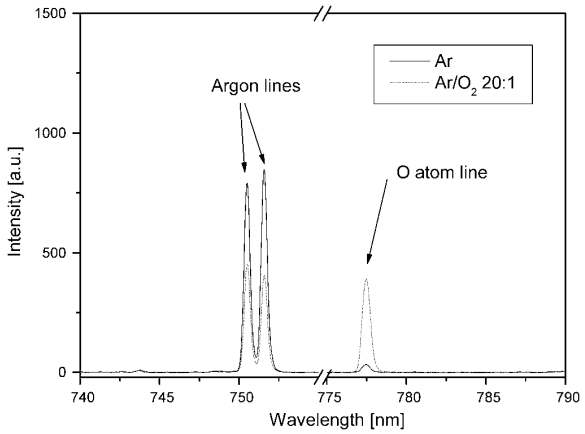

Figure 12. Parts of optical emission spectra acquired during the plasma treatment of BSA samples in Ar and Ar/O_2 discharges.

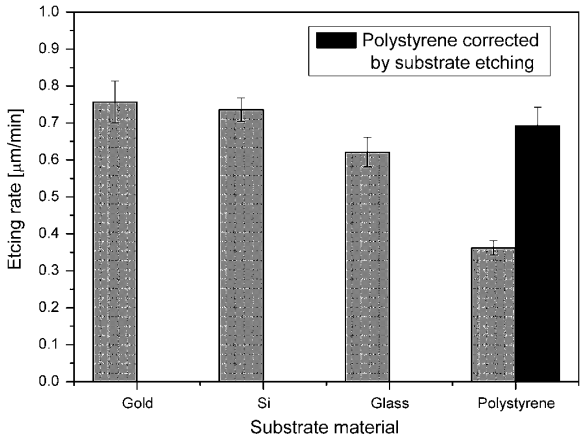

Figure 13. BSA etching rates depending on the substrate material (Ar/O_2 20 : 1 plasma discharge, 10 Pa, 200 W).

ranging from metallic surfaces to polymeric materials. The results show that the highest etching rates can be reached by employing an Ar/O_2 mixture. Comparing this result with previously published experiments aiming at the killing of bacterial spores under similar experimental conditions, it clearly highlights the dissimilarity between the sterilization process and the removal of biomolecules. This is, however, an important point that has to be considered in the optimization of the treatment process in realistic applications (i.e. at hospital central sterilization services), when not only sterility but also complete removal of other possibly pathogenic substances of biological origin is desired. From this perspective, basing the process on Ar/O_2 mixture represents a favourable option compared with discharges sustained in other gases or gas mixture, since it allows fast elimination of proteins and killing of bacterial spores. Moreover, application of this mixture overcomes drawbacks of fluorine containing mixtures, found to be capable of sterilising and etching organic materials (e.g. [9]), which are related to the environmental (greenhouse effect) and safety aspects (possible formation of toxic by-products).

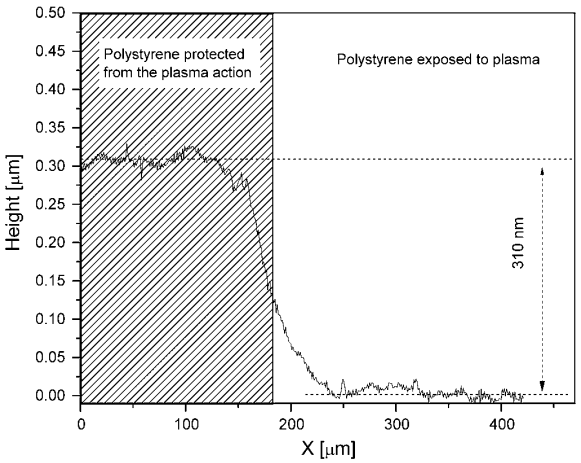

Figure 14. Profile of a polystyrene plate treated for 60 s in Ar/O_2 20 : 1 plasma discharge. The shaded part of the figure corresponds to the part of polystyrene protected from the plasma action by a Si mask.

Our results moreover show that plasma discharges which remove protein deposits with high efficiency can also substantially affect polymeric materials. Consequently, there is now the challenge to develop a treatment which is selective enough to affect the biological residues, without modifying too much the polymers of the substrates.

Acknowledgments

This work has been supported by the FP6 2005 NEST project 'Biodecon' and the JRC Action 15008: NanoBiotechnology for Health.

References

[1] Menashi W P 1968 *US Patent* 3383163
[2] Soloshenko I A, Tsiolko V V, Khomich V A, Shchedrin A I, Ryabtsev A V, Bazhenov V Yu and Mikhno I L 2000 Sterilization of medical products in low-pressure glow discharges *Plasma Phys. Rep.* **26** 792–800
[3] Moisan M, Barbeau J, Moreau S, Pelletier J, Tabrizian M and Yahia L'H 2001 Low-temperature sterilization using gas plasmas: a review of the experiments and an analysis of the inactivation mechanisms *Int. J. Pharmaceutics* **226** 1–21
[4] Philip N, Saoudi B, Crevier M-C, Moisan M, Barbeau J and Pelletier J 2002 The respective roles of UV photons and oxygen atoms in plasma sterilization at reduced gas pressure: the case of N_2-O_2 mixtures *IEEE Trans. Plasma Sci.* **30** 1429–36
[5] Feichtinger J, Schulz A, Walker M and Schumacher U 2003 Sterilisation with low-pressure microwave plasmas *Surf. Coat. Technol.* **174–175** 564–9
[6] Boudam M K, Moisan M, Saoudi B, Popovici C, Gherardi N and Massines F 2006 Bacterial spore inactivation by atmospheric-pressure plasmas in the presence or absence of UV photons as obtained with the same gas mixture *J. Phys. D: Appl. Phys.* **39** 3494–507
[7] Halfmann H, Denis B, Bibinov N, Wunderlich J and Awakowicz P 2007 Identification of the most efficient

VUV/UV radiation for plasma based inactivation of Bacillus atrophaeus spores *J. Phys. D: Appl. Phys.* **40** 5907–11
[8] Nagatsu M , Terashita F, Nonaka H, Xu L, Nagata T and Koide Y 2005 Effects of oxygen radicals in low-pressure surface-wave plasma on sterilization *Appl. Phys. Lett.* **86** 211502
[9] Lerouge S, Wertheimer M R, Marchand R and Yahia L'H 2000 Effect of gas composition on spore mortality and etching during low-pressure plasma sterilization *J. Biomed. Mater. Res.* **51** 128–35
[10] Kylián O, Sasaki T and Rossi F 2006 Plasma sterilization of *Geobacillus Stearothermophilus* by $O_2 : N_2$ RF inductively coupled plasma *Eur. Phys. J. Appl. Phys.* **34** 139–42
[11] Cousty S, Villeger S, Sarette J P, Ricard A and Sixou M 2006 Inactivation of *Escheria coli* in the flowing afterglow of N_2 discharge at reduced pressure: study of destruction mechanism of bacteria and hydrodynamics of the afterglow flow *Eur. Phys. J. Appl. Phys.* **34** 143–6
[12] Rossi F, Kylián O and Hasiwa M 2006 Decontamination of surfaces by low pressure plasma discharges *Plasma Process. Polym.* **3** 431–42
[13] Rossi F, Kylián O and Hasiwa M 2007 Mechanisms of sterilization and decontamination of surfaces by low pressure plasma *Advanced Plasma Technology* ed R d'Agostino *et al* (New York: Wiley)
[14] Opretzka J, Benedikt J, Awakowicz P, Wunderlich J and von Keudell A 2007 The role of chemical sputtering during plasma sterilization of Bacillus atrophaeus *J. Phys. D: Appl. Phys.* **40** 2826–30
[15] Kylián O, Hasiwa M and Rossi F 2006 Effect of low-pressure microwave discharges on pyrogen bioactivity *IEEE Trans. Plasma Sci.* **34** 2606–10
[16] Kylián O, Hasiwa M, Gilliland D and Rossi F 2008 Experimental study of the influence of Ar/H_2 microwave discharges on Lipid A *Plasma Process. Polym.* **5** 26–32
[17] Baxter H C, Campbell G A, Whittaker A G, Jones A C, Aitken A, Simpson A H, Casey M, Bountiff L, Gibbard L and Baxter R L 2005 Elimination of transmissible spongiform encephalopathy infectivity and decontamination of surgical instruments by using radio-frequency gas-plasma treatment *J. Gen. Virol.* **86** 2393–9
[18] Taylor D M 1999 Inactivation of prions by physical and chemical means *J. Hosp. Infec.* **43** S69–76
[19] Lipscomb I P, Sihota A K and Keevil C W 2006 Comparative study of surgical instruments from sterile-service departments for presence of residual gram-negative endotoxin and proteinaceous deposits *J. Clin. Microbiol.* **44** 3728–33
[20] Murdoch H, Taylor D, Dickinson J, Walker J T, Perrett D, Raven N D H and Sutton J M 2006 Surface decontamination of surgical instruments: an ongoing dilemma *J. Hosp. Infec.* **63** 432–8
[21] Mogul R, Bol'shakov A A, Chan S L, Stevens R M, Khare B N, Meyyappan M and Trent J D 2003 Impact of low-temperature plasmas on Deinococcus radiodurans and biomolecules *Biotechnol. Prog.* **19** 776–83
[22] Bernard C, Leduc A, Bardeau J, Saoudi B, Yahia L'Y and De Crescenzo G 2006 Validation of cold plasma treatment for protein inactivation: a surface plasmon resonance-based biosensor study *J. Phys. D: Appl. Phys.* **39** 3470–8
[23] Deng X T, Shi J J, Chen H L and Kong M G 2007 Protein destruction by atmospheric pressure glow discharge *Appl. Phys. Lett.* **90** 013903
[24] Deng X T, Shi J J and Kong M G 2007 Protein destruction by a helium atmospheric pressure glow discharge: capability and mechanisms *J. Appl. Phys.* **101** 074701
[25] Kylián O, Rauscher H, Sirghi L and Rossi F 2008 Protein film removal by means of low-pressure microwave plasma—an imaging ellipsometry study *J. Phys.: Conf. Ser.* at press
[26] Whittaker A G, Graham E M, Baxter R L, Jones A C, Richardson P R, Meek G, Campbell G A, Aitken A and Baxter H C 2004 Plasma cleaning of dental instruments *J. Hosp. Infec.* **56** 37–41
[27] Baxter H C, Campbell G A, Richardson P R, Jones A C, Whittle I R, Casey M, Whittaker A G and Baxter R L 2006 Surgical instrument decontamination: efficacy of introducing an argon: oxygen RF gas-plasma cleaning step as part of the cleaning cycle for stainless steel instruments *IEEE Trans. Plasma Sci.* **34** 1337–44
[28] Ceccone G, Gilliland D, Kylián O and Rossi F 2006 Experimental study of effect of low-pressure $O_2 : H_2$ microwave discharge on protein films *Czech. J. Phys.* **56** B672–5
[29] Lipscomb I P, Pinchin H, Collin R and Keevil C W 2007 Effect of drying time, ambient temperature and pre-soaks on prion-infected tissue contamination level on surgical stainless steel: concerns over prolonged transportation of instruments from theatre to central sterile service departments *J. Hosp. Infec.* **65** 72–7
[30] Halfmann H, Bibinov N, Wunderlich J and Awakowicz P 2007 A double inductively coupled plasma for sterilization of medical devices *J. Phys. D: Appl. Phys.* **40** 4145–54
[31] Brűning C, Hellweg S, Dambach S, Lipinsky D and Arlinghaus H F 2006 Improving the interpretation of ToF-SIMS measurements on adsorbed proteins using PCA *Surf. Interface Anal.* **38** 191–3
[32] Moss S J, Jolly A M and Tighe B J 1986 Plasma oxidation of polymers *Plasma Chem. Plasma Process.* **6** 401–16
[33] Egitto F D 1990 Plasma etching and modification of organic polymers *Pure Appl. Chem.* **62** 1699–708
[34] Masoud N, Martus K and Becker K 2005 VUV emission from a cylindrical dieletric barrier discharge in Ar and in Ar/N_2 and Ar/air mixtures *J. Phys. D: Appl. Phys.* **38** 1674–83
[35] Pollak J, Moisan M, Kéroack D, Séguin J and Barbeau J 2008 Plasma sterilisation within long and narrow bore dielectric tubes contaminated with stacked bacterial spores *Plasma Process. Polym.* **5** 14–25
[36] Fozza A C, Klemberg-Sapieha J E and Wertheimer M R 1999 Vacuum ultraviolet irradiation of polymers *Plasma Polym.* **4** 183–206

IOP PUBLISHING
IOP FTC
JOURNAL OF PHYSICS D: APPLIED PHYSICS
J. Phys. D: Appl. Phys. **41** (2008) 192005 (6pp)
doi:10.1088/0022-3727/41/19/192005

FAST TRACK COMMUNICATION

On the application of inductively coupled plasma discharges sustained in $Ar/O_2/N_2$ ternary mixture for sterilization and decontamination of medical instruments

K Stapelmann[1,2], O Kylián[1], B Denis[1,2] and F Rossi[1]

[1] European Commission, Joint Research Centre, Institute for Health and Consumer Protection, Via E Fermi 1, 21020 Ispra (VA), Italy
[2] Institute for Electrical Engineering and Plasma Technology, Ruhr–Universität Bochum, Universitätsstrasse 150, 44780 Bochum, Germany

E-mail: francois.rossi@jrc.it

Received 9 June 2008, in final form 7 August 2008
Published 12 September 2008
Online at stacks.iop.org/JPhysD/41/192005

Abstract
Non-equilibrium low pressure-plasma discharges are extensively studied for their high potential in the field of sterilization and decontamination of medical devices. This increased interest in plasma discharges arises from, among other reasons, their capability not only to inactivate bacterial spores but also to eliminate, destroy or remove pathogenic biomolecules and thus to provide a one-step process assuring safety of treated instruments. However, recent studies have shown that optimal conditions leading to inactivation of spores and physical removal of pathogens differ significantly—the efficiency of spores sterilization is above all dependent on the UV radiation intensity, whereas high etching rates are connected with the presence of the etching agent, typically atomic oxygen. The aim of this contribution is to discuss and demonstrate the feasibility of $Ar/N_2/O_2$ low-pressure inductively coupled plasma discharges as an option to provide intense UV radiation while maintaining the high etching rates of biomolecules.

1. Introduction

Elimination of potentially harmful micro-organisms and biomolecules presented on surfaces is a major concern in many different areas ranging from the food and packaging industry, the textile industry, and the preservation of ancient manuscripts to space missions. However, the prominent field where sterilization and decontamination are of paramount importance is the medical praxis, where these processes represent a crucial step in guaranteeing the safety of patients. Sterilization is traditionally accomplished by techniques employing heat, ionizing radiation or chemicals. Nevertheless, the necessity of treatment of heat sensitive materials, which makes the routinely used thermal treatment impossible, as well as the toxicity of substances used for chemical treatment, has triggered the development of new sterilization methods. In this perspective, the application of non-equilibrium plasma discharges (e.g. review papers [1–4]), and in particular low-pressure inductively coupled plasma (ICP) discharges (e.g. [5–11]), represents an interesting alternative to the conventionally used sterilization techniques. This is mainly due to the fact that this kind of discharges is a potent source of chemically active particles, ions as well as energetic photons interacting with the treated surfaces and thus leading to the fast suppression of the contaminants' bioactivity or eventually to their complete removal from surfaces. The used gases (typically oxygen, nitrogen, argon or hydrogen) are usually non-toxic, i.e. environment friendly, therefore reducing

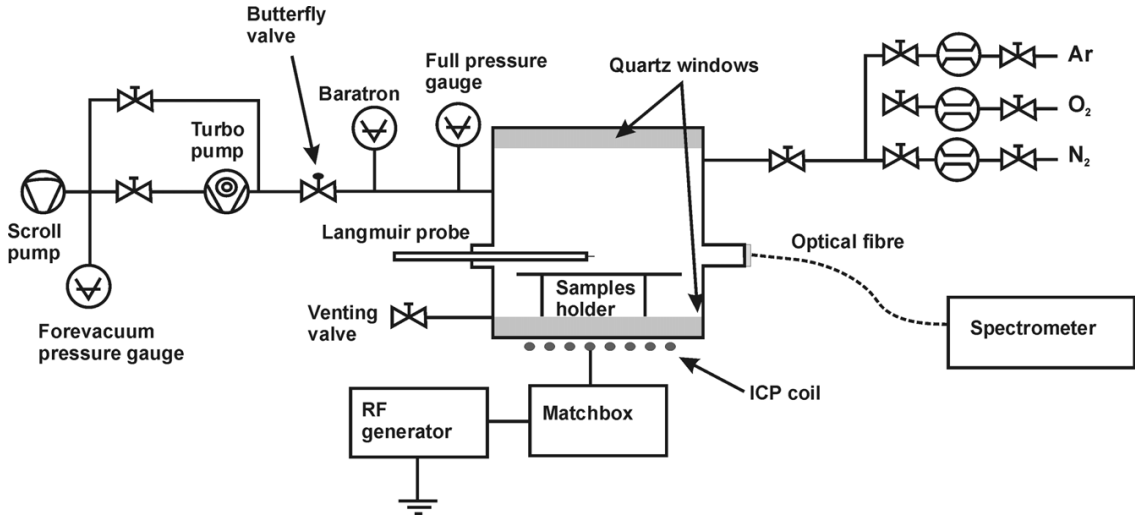

Figure 1. Experimental set-up.

additional costs related to the disposal of chemicals. The ICP discharges can be furthermore operated at relatively low temperatures compatible with the treatment of heat sensitive objects. Moreover, the ICP plasma discharges seem to be capable of not only inactivating bacterial spores but also of removing effectively pathogenic biomolecules that exhibit high resistance towards common decontamination techniques (e.g. bacterial endotoxins or protein residuals [12, 13]), and thus offer the possibility to be a universal tool for the elimination of a full spectrum of biological pathogens.

Nevertheless, the operational conditions favourable for the sterilization of bacterial spores are not automatically the best for the elimination of biomolecules. This is primarily due to the different pathways leading to the desired effects. Regarding this point, it has been found that the potency of plasma discharges to inactivate bacterial spores is determined mainly by the intensity of UV radiation emitted by plasma (e.g. [2, 10, 14]), at least in the initial stage of the treatment [11]. However, operational conditions providing intense UV radiation in the spectral range suitable for spores inactivation do not typically represent favourable conditions for physical removal of biological materials: these conditions are required for the elimination of pathogenic biomolecules as well as for removal of biological materials shielding spores from the direct action of UV radiation and thus limiting UV sterilization efficiency (e.g. [3, 15]). Although the exact mechanism leading to removal of biomolecules or erosion of bacterial spores is not clear up to now, it has been observed that within the discharges sustained in common gases (air, oxygen, nitrogen, argon, hydrogen) these processes are fastest under conditions providing high densities of atomic oxygen [13].

The difference between optimized conditions for sterilization of bacterial spores and for removal of biomolecules has an important implication for the optimization of the treatment in a real situation when both sterility and elimination of pathogenic molecules has to be assured. This can be demonstrated, for instance, in the case of the O_2/N_2 discharge mixture, i.e. the most common one used for plasma based sterilization at low pressures. Using this discharge mixture, the highest UV radiation intensity is typically achieved for $O_2 : N_2$ ratio around $1 : 4$, while this particular mixture has only limited capability for etching biomolecules or bacterial spores. In contrast, high etching rates can be achieved when only a small amount of nitrogen is added into the oxygen discharge, but this is at the expense of UV radiation that is rather slight [6]. The impossibility of assuring simultaneously high UV light intensity and high etching rate using binary discharge mixtures leads to the necessity of prolonging plasma treatment, which consequently represents an enhanced risk for the treated objects (e.g. due to the elevated thermal load). This problem can, in principle, be overcome by a two-step process (one optimized for sterilization of spores, the second one tuned for effective removal of biomolecules) or, as it will be discussed in this paper, by utilization of a discharge sustained in a ternary mixture composed of argon, oxygen and nitrogen. To demonstrate this possibility, the ICP plasma discharge sustained in $Ar/N_2/O_2$ mixtures having different ratios of pure gases was characterized by means of optical emission spectroscopy in order to evaluate conditions providing high UV radiation intensity. Subsequently, the capability of etching biomolecules by the studied plasma discharges was estimated with stylus profilometry using bovine serum albumin as a model biomolecule. The results of these experiments are summarized in this paper.

2. Experimental

An ICP source schematically depicted in figure 1 was used in this study. The plasma discharges sustained in $Ar/N_2/O_2$ mixtures (pressure 10 Pa, RF power 200 W and total gas flow 22 sccm) were characterized by optical emission spectroscopy (OES) in order to evaluate the intensity of UV radiation. In addition, the density of ground state oxygen atoms was estimated by actinometry, using the O atom spectral line

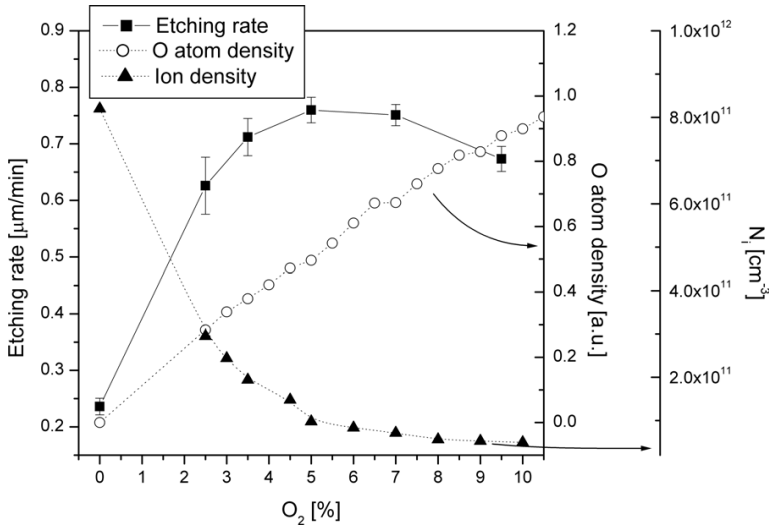

Figure 2. BSA etching rate, O atom density and ion density in dependence on Ar/O_2 mixture composition (200 W, 10 Pa).

844.6 nm (transition $^3P \rightarrow {}^3S$) and argon line 750.4 nm transition $2p_1 \rightarrow 1s_2$) [16]. The emission spectra of the plasma discharge were collected through a silica optical window and analysed by an Avantes AVS-PC2000 monochromator equipped with a 2048-element linear CCD array. Furthermore, the densities of positive ions were determined by means of Langmuir probe (Smart probe™; Scientific Systems Ltd) from the ion saturation current. It should be noted that especially in the case of discharge mixtures, where different ions having distinct masses are present in the discharge plasma, this method cannot be used for the exact evaluation of total ion density. However, since the most abundant positive ions in the studied discharge plasmas (namely N_2^+, O_2^+ and NO^+) differ relatively slightly in their masses (from 28 to 40 mass units) the maximal uncertainty in the total positive ion density is lower than 20% and thus this approach still remains plausible for the determination of the behaviour of charged particle densities in the studied discharge mixtures.

Besides emission spectroscopy and Langmuir probe measurements, the substrate temperature was monitored during plasma treatment by means of IR pyrometry. Regarding these measurements the temperature increase under the experimental conditions used in this study was lower than 50 °C within the treatment duration, i.e. the temperature load is still well acceptable for the treatment of a wide variety of materials.

The samples used for the evaluation of the etching rate of biomolecules were prepared by spotting an aqueous solution (0.5 mg ml^{-1}) of bovine serum albumin (BSA, Sigma Aldrich) on polished Si wafers. After the deposition, the samples were dried overnight in a common flow hood, to mimic the worst situation for protein removal during a typical sterilization process [17]. Subsequently, the samples were plasma treated and the removal rate was determined by stylus profilometry. Details regarding samples preparation and evaluation of etching rates can be found in the literature [13].

3. Results and discussion

As mentioned above, the net efficiency of sterilization of a multilayer of bacterial spores as well as the rate of elimination of biomolecules are dependent on several factors, primarily the intensity of UV radiation crucial for sterilization of bacterial spores [2, 10, 14] and on the etching rate providing physical removal of pathogens [12, 13] or contributing to the sterilization process itself [11, 18]. Regarding etching, it has been shown that significant erosion of spores or biomolecules can, in principle, be achieved by employing discharges sustained in hydrogen or nitrogen containing mixtures (e.g. [13, 19]). However, the process is substantially faster in the oxygen-rich plasmas, which was demonstrated by direct comparison of the removal rates of model proteins using argon, Ar/N_2, Ar/H_2 and Ar/O_2 plasma discharges operated at otherwise identical conditions (i.e. RF power, pressure and total gas flow) [13].

Naturally, the etching rate of Ar/O_2 discharge plasma depends on the ratio of Ar and oxygen in the initial mixture. In order to find out the optimal conditions in terms of the biomolecules' removal, the etching rate was measured as a function of the oxygen concentration and these values were compared with the density of ground state oxygen atoms as measured by actinometry and ion density as measured with a Langmuir probe.

As can be seen in figure 2, the etching rate is not a monotonic function of O_2 content in the discharge mixture: it exhibits a clear maximum for about 5% of oxygen in Ar/O_2. Furthermore, this behaviour cannot be ascribed solely to the variations in O atom density, i.e. density of particles supposed to be capable of etching chemically organic materials, which increases monotonically with increased portion of O_2 in the initial discharge mixture. Although the exact mechanism of protein removal still needs to be clarified, the observed dependence of etching rate on gas mixture composition can be explained by the dominant role of chemical sputtering as

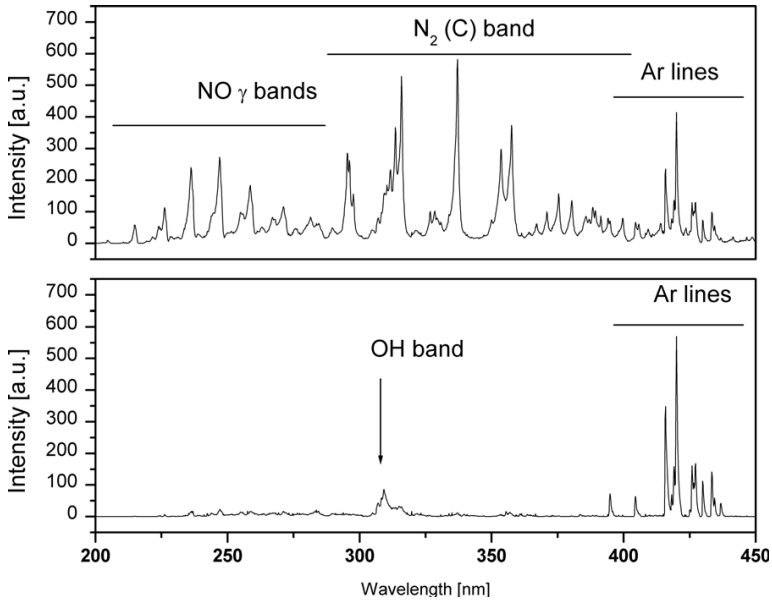

Figure 3. Part of emission spectra of discharge sustained in $Ar/O_2/N_2$ 20 : 1 : 1 plasma discharge (upper panel) and in Ar/O_2 20 : 2 discharge (lower panel) (200 W, 10 Pa, total gas flow 22 sccm).

proposed recently for the erosion of bacterial spores based on experiments employing individually controlled and absolutely calibrated particle beams [20, 21]. This mechanism combines the impact of energetic ions, which are able to break bonds in the protein layers within the collision cascade, and the subsequent reaction of the created sites with highly chemically active oxygen species (e.g. O atoms or O_2 molecules), leading to the formation of volatile products. Obviously the efficiency of this process is governed by fluxes of both ionic species and oxygen species to the protein surface. Whereas densities of O atoms and molecules increase with increasing O_2 content in the discharge mixture, leading to an enhancement of the removal of proteins, the density of charged particles steeply decreases at the same time (figure 2). This reduces the creation of defects in the protein film and consequently reduces the number of reaction sites, thereby limiting the etching rate of the film. These two opposing effects can explain the appearance of a well-defined maximum of the etching rate at the conditions representing an optimal trade-off between the fluxes of oxygen species and energetic ions.

However, neither argon nor oxygen has intense spectral peaks in the spectral range 230–275 nm, i.e. in the range recently proposed to be crucial for the fast sterilization of bacterial spores. This wavelength range corresponds to photons with energies high enough to break C–C or C–H bonds of DNA strands [10]. The only peaks that can be observed between 230 and 275 nm originate from impurities (desorbing from the reactor walls or from samples to be sterilized) whose amount is typically unknown and can vary significantly from treatment to treatment. Difficulty in controlling the amount of impurities and consequently the intensity of UV radiation in turn limits the applicability and reliability of Ar/O_2 discharges for sterilization purposes.

Nevertheless, the UV intensity in the desired spectral range can be significantly enhanced (more than 1 order of magnitude) by the addition of nitrogen to the Ar/O_2 binary mixture, which leads to the production of excited NO molecules, whose radiative de-excitation results in emission of the NO γ system predominantly in the spectral range 200–300 nm as demonstrated in figure 3.

The integral intensity of radiation emitted by an $Ar/O_2/N_2$ plasma discharge in the spectral window 230–275 nm is obviously strongly linked with the composition of the gas discharge. Regarding this, it has been found that at fixed pressure, total gas flow, RF power and O_2/N_2 ratio, increasing the amount of argon in the mixture initially leads to an enhancement of UV intensity, reaches its maximal value for around 60% of argon and afterwards starts to decrease (see figure 4). In other words, the presence of argon increases the production of excited NO molecules as compared with the discharges sustained in O_2/N_2 binary mixture. This has important implications for optimization of the sterilization and decontamination process, since even if the total number of O_2 and N_2 molecules in the $Ar/O_2/N_2$ ternary mixture decreases to 10%, the UV emission intensity of such a discharge is still comparable to the maximal one measured in the O_2/N_2 binary mixture and thus has the same potency to inactivate bacterial spores.

Naturally, the partial substitution of O_2 in the discharge mixture by nitrogen, which leads to a significant increase in UV emission intensity desirable for sterilization of bacterial spores, influences the etching rates of biomolecules. Nevertheless, as can be seen in figure 5, the etching rate of BSA does not linearly follow the decrease in the number of O_2 molecules in the initial discharge mixture, but decreases much more slightly. For example, the substitution of 50% of O_2 by N_2 results in

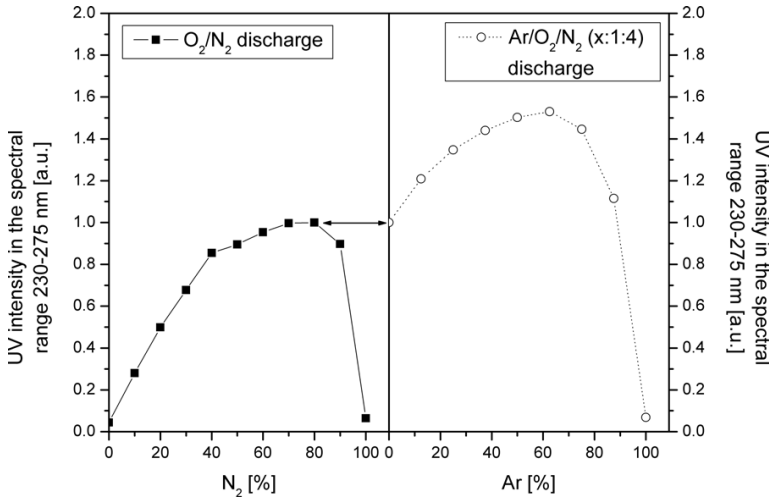

Figure 4. Integral intensity of UV radiation in the spectral range 230–275 nm as a function of discharge mixture measured in O_2/N_2 discharge (left panel) and in $Ar/O_2/N_2$ discharge with fixed O_2 over N_2 ratio 1 : 4 (right panel).

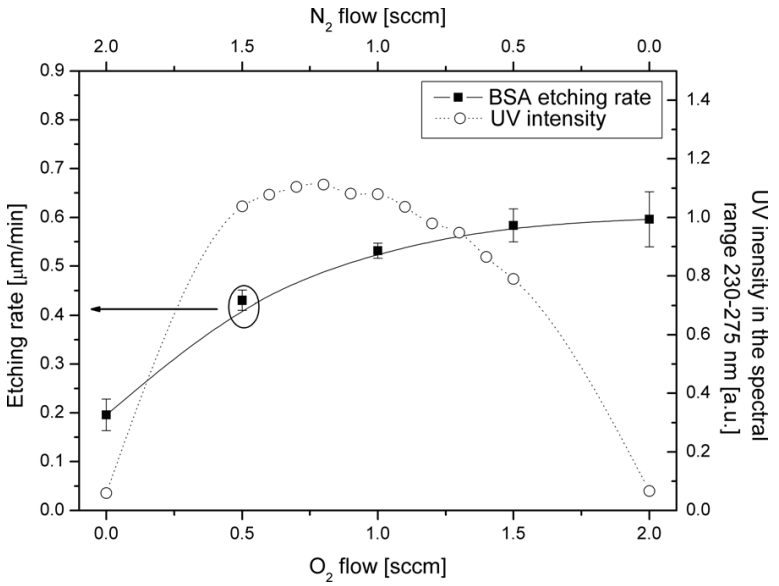

Figure 5. Integral intensity of UV radiation in the spectral range 230–275 nm and BSA etching rate as a function of O_2/N_2 ratio in $Ar/O_2/N_2$ discharge mixture with constant Ar flow 20 sccm (total gas flow 22 sccm, 200 W, 10 Pa).

only 10% decrease in the etching rate. Analogously to the case of the argon–oxygen binary mixture, this trend does not correspond exclusively to the variations of O atom density that decreases linearly with decreasing O_2 content in the discharge mixture (figure 6), but also reflects the density and energy distribution of charged particles that were found to be almost insensitive to the oxygen/nitrogen ratio in the ternary mixture having fixed argon content, as demonstrated in figure 6.

4. Conclusions

In summary, it can be concluded that the results presented here clearly demonstrate that the application of a ternary $Ar/O_2/N_2$ discharge mixture has advantageous properties in terms of sterilization and decontamination of surfaces, especially compared with the discharges sustained in Ar/O_2 and O_2/N_2 mixtures, i.e. the most common binary mixtures used for inactivation of micro-organisms and elimination of pathogenic biomolecules.

First, it has been revealed that low-pressure ICP discharge sustained in the studied ternary mixture leads to the higher emission of UV radiation desired for sterilization of bacterial spores as compared with discharges operated in binary mixtures. This confirms previous observations of high efficiency of bacterial spore inactivation using a similar discharge mixture ($Ar : N_2 : O_2$ 100 : 4 : 1 [10]). Moreover,

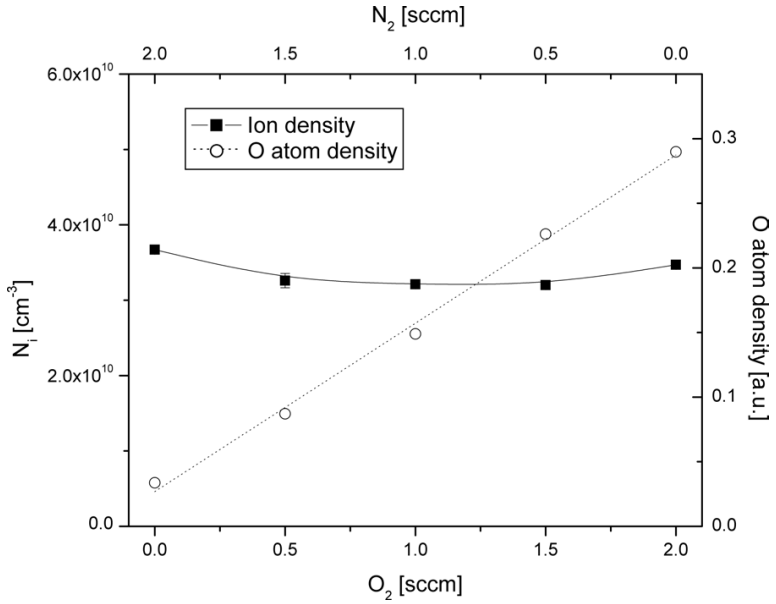

Figure 6. O atom and ions densities as a function of O_2/N_2 ratio in $Ar/O_2/N_2$ discharge mixture with constant Ar flow 20 sccm (total gas flow 22 sccm, 200 W, 10 Pa).

besides increased emission of UV radiation intensity, which alone is an important finding with respect to inactivation of bacterial spores, the $Ar/O_2/N_2$ ternary mixture also provides a high etching rate of biomolecules (demonstrated in the example of bovine serum albumin that has been used as a representative model of biomolecules present on the surfaces of medical instruments), which has been found to be only slightly lower compared with that reached employing an argon–oxygen binary mixture.

These results have important consequences since they allow the presumption that the use of an $Ar/O_2/N_2$ discharge mixture can assure fast inactivation of bacterial spores combining both the effect of UV radiation and high etching rate and the effective elimination of pathogenic molecules (e.g. bacterial endotoxins or infectious proteins—prions) in one treatment step, i.e. to fulfil the requirements of sterile services.

Acknowledgments

This work has been supported by the FP6 2005 NEST project 'Biodecon' and the JRC Action 15008: NanoBiotechnology for Health.

References

[1] Lerouge S, Wertheimer M R and Yahia L'H 2001 *Plasma Polym.* **6** 175
[2] Moisan M, Barbeau J, Crevier M C, Pelletier J, Philip N and Saoudi B 2002 *Pure Appl. Chem.* **74** 349
[3] Moisan M, Barbeau J, Moreau S, Pellettier J, Tabrizian M and Yahia L'H 2001 *Int. J. Pharm.* **226** 1
[4] Laroussi M 2005 *Plasma Process. Polym.* **2** 391
[5] Bol'shakov A A, Cruden B A, Mogul R, Rao M V V S, Sharma S P, Khare B N and Meyyappan M 2004 *AIAA J.* **42** 823
[6] Kylián O, Sasaki T and Rossi F 2006 *Eur. Phys. J. Appl. Phys.* **34** 139
[7] Cvelbar U, Vujosevic D Vratnica Z and Mozetic M 2006 *J. Phys. D: Appl. Phys.* **39** 3487
[8] Hayashi N, Guan W, Tsutsui S, Tomari T and Hanada Y 2006 *Japan. J. Appl. Phys.* **45** 8358
[9] Halfmann H, Bibinov N, Wunderlich J and Awakowicz P 2007 *J. Phys. D: Appl. Phys.* **40** 4145
[10] Halfmann H, Denis B, Bibinov N, Wunderlich J and Awakowicz P 2007 *J. Phys. D: Appl. Phys.* **40** 5907
[11] Vicoveanu D, Popesco S, Ohtsu Y and Fujita H 2008 *Plasma Process. Polym.* **5** 350
[12] Rossi F, Kylián O, Rauscher H, Gilliland D and Sirghi L 2008 *Pure Appl. Chem.* at press
[13] Kylián O, Rauscher H, Gilliland D, Brétagnol F and Rossi F 2008 *J. Phys. D: Appl. Phys.* **41** 095201
[14] Philip N, Saoudi B, Crevier M C, Moisan M, Barbeau J and Pelletier J 2002 *IEEE Trans. Plasma Sci.* **30** 1429
[15] Rossi F, Kylián O and Hasiwa M 2006 *Plasma Process. Polym.* **3** 431
[16] Coburn J W and Chen M 1980 *J. Appl. Phys.* **51** 3134
[17] Lipscomb I, Sihota A and Keevil C 2006 *J. Clin. Microbiol.* **44** 3728
[18] Xu L, Nonaka H, Zhou H Y, Ogino A, Nagata T, Koide Y, Nanko S, Kurawaki I and Nagatsu M 2007 *J. Phys. D: Appl. Phys.* **40** 803
[19] Cousty S, Villeger S, Sarette J P, Ricard A and Sixou M 2006 *Eur. Phys. J. Appl. Phys.* **34** 143
[20] Opretzka J, Benedikt J, Awakowicz P, Wunderlich J and von Keudell A 2007 *J. Phys. D: Appl. Phys.* **40** 2826
[21] Raballand V, Benedikt J, Wunderlich J and von Keudell A 2008 *J. Phys. D: Appl. Phys* **41** 115207

Removal of Model Proteins Using Beams of Argon Ions, Oxygen Atoms and Molecules: Mimicking the Action of Low-Pressure Ar/O_2 ICP Discharges

Ondřej Kylián,* Jan Benedikt, Lucel Sirghi, Rüdiger Reuter, Hubert Rauscher, Achim von Keudell, François Rossi

The action of Ar/O_2 plasmas with proteins is mimicked by employing a particle beam experiment with individually controllable and absolutely calibrated sources of O atoms/O_2 molecules and of argon ions. It is demonstrated that beams of thermal O atoms and of O_2 molecules with fluences up to $j_O = 8.6 \times 10^{18}$ cm^{-2} and $j_{O2} = 5.4 \times 10^{20}$ cm^{-2} have no measurable effect on the proteins at room temperature, whereas the combination of an O/O_2 beam and of an 100 eV Ar^+ ion beam induces very efficient protein removal, which is accompanied by a significant increase of their surface roughness. These observations are attributed to the process of chemical sputtering caused by the simultaneous impact of incident radicals and energetic ions.

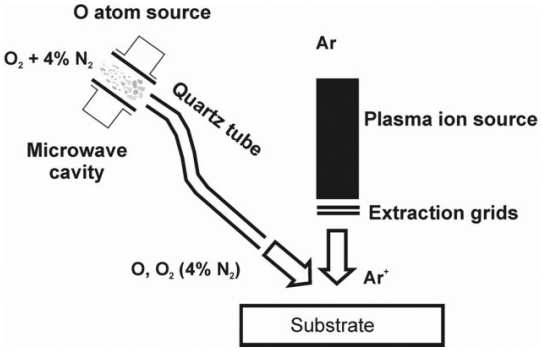

Introduction

Decontamination and sterilization of medical equipment are crucial demands in present day health care facilities. The main objective of these processes is to guarantee a safe, repetitive utilization of various medical tools, instruments or accessories. This is achieved by killing, removing or biologically deactivating any kind of potentially harmful micro-organisms or substances of biological origin that can be present on surfaces of medical instruments. In this context, the elimination of specific proteins, namely prions, which are capable to cause severe neurodegenerative diseases (e.g. the Creutzfeld-Jakob disease), poses a particularly new challenge. This is mainly due to the extraordinarily high resistance of various proteins to common sterilization procedures based on thermal treatment, ionizing radiation or chemical treatment,[1] which in turn leads to high levels of proteins soiling of the medical instruments after their routine sterilization and decontamination performed in sterile services.[2,3] Consequently, there is a clear demand for the development of new, effective decontamination approaches assuring complete elimination of protein contamination from surfaces. From this perspective, non-equilibrium plasma discharges are believed to be well suited for fulfilling this demand, as they are already

O. Kylián, L. Sirghi, H. Rauscher, F. Rossi
European Commission, Joint Research Centre, Institute for Health and Consumer Protection, Via E. Fermi 1, 21027 Ispra (VA), Italy
O. Kylián
Charles University, Faculty of Mathematics and Physics, V Holešovičkách 2, Prague 8, 180 00, Czech Republic
Fax: +420 22191 2350; E-mail: ondrej.kylian@gmail.com
J. Benedikt, R. Reuter, A. von Keudell
Research Group Reactive Plasmas, Ruhr-Universität Bochum, 44780 Bochum, Germany

Plasma Process. Polym. **2009**, *6*, 255–261

DOI: 10.1002/ppap.200800199

known to be very efficient in inactivating bacterial spores (e.g. review articles[4–8]) and pyrogenic compounds.[8–10] However, experimental studies focussed on the destruction of infectious prions by plasma discharges are rather problematic. This is due to stringent safety precautions that are necessary because of the extreme biohazard associated with those molecules, which naturally limits the number of possible experiments. Therefore, in order to overcome this restriction, non-pathogenic proteins are usually used as representatives of proteic contamination of surfaces to facilitate the investigation of the mechanisms of plasma-protein interactions, as well as to evaluate favourable conditions for their destruction, i.e. knowledge that constitutes a necessary starting base for successful application and validation of this technique towards infectious proteins. Indeed, the possibility to remove various proteins from surfaces was already proven using different discharge plasmas operated at ambient,[11,12] or at low pressures.[8,13–17] Regarding the results using low-pressure plasma discharges, it was found that high removal rates of proteins can be achieved in Ar/O_2 plasmas,[16,17] which provide removal rates that are at least three times higher as compared to those observed in pure Ar plasmas or Ar/N_2 and Ar/H_2 mixtures operated at otherwise identical experimental conditions such as applied power, pressure and gas flow.[16] However, the mechanisms leading to protein elimination remain still unclear. This is foremost due to the inherent complexity of the processes occurring at the plasma-protein interfaces, which involve various chemically active species, ions or UV/VUV radiation. The distinction and quantification of the individual contributions to the overall treatment efficiency is therefore very challenging. Moreover, the uncertainty of identifying the principal mechanisms of protein removal represents a serious limitation for any optimisation of the treatment. A possible solution for identifying principal mechanisms contributing to proteins elimination is the use of calibrated sources of radiation covering a wide spectral range, and/or particle beams comprising sources of neutral, as well as charged species. This allows to isolate individual processes and to identify possible synergisms among several reactants as recently demonstrated for the case of bacterial spores.[18–20] The same approach is used in this study: the interaction of an Ar/O_2 plasma with model proteins is mimicked by employing a particle beam experiment with individually controllable and absolutely calibrated sources of O atoms/O_2 molecules and of energetic argon ions. However, in contrary to the previous studies, where the action of ions and atomic species was estimated only qualitatively by comparing SEM images of treated spores, the effects of the employed beams on the treated proteins are evaluated quantitatively in this study.

Experimental Part

Samples Preparation and Analysis

The protein samples were prepared by dropping 0.1% aqueous solution of Bovine Serum Albumin (BSA) and Lysozyme (both provided by Sigma Aldrich) on the surface of polished Si wafers. The samples were then allowed to dry in a common flow leading to a ring shaped deposit on the substrate. The dried samples were then exposed to the particle beams and the resulting modifications were evaluated by the following diagnostic methods. First, the overall modifications of the protein films were visualised by an EP^3 imaging ellipsometer (Nanofilm Surface Analysis GmbH, angle of incidence of 42°, field of view of $2\,000 \times 2\,000$ μm^2, $\lambda = 554.3$ nm). The removal rates of the proteins were obtained using stylus profilometry (Alpha-step® profilometer produced by KLA-Tencor, scan speed 20 $\mu m \cdot min^{-1}$, sampling rate of 50 Hz, equivalent force exerted from the stylus tip on the surface corresponded to 27.4 mg), as described in detail previously.[16] Finally, the morphological changes of the protein deposits at the nanometre scale were determined by atomic force microscopy (AFM type Solver P47H, NT-MDT Co. operated in the tapping mode). The AFM measurements were made using silicon AFM probes (NSG11 from NTMDT) with sharp conical tips (nominal tip radius 10 nm and cone angle of 22°) and stiff cantilevers (elasticity constant of 5 $N \cdot m^{-1}$). The topography images were corrected to compensate for the tilting of the sample surfaces.

Beam Experiments

A sketch of the beam experiment is shown in Figure 1. It consists of an exposition chamber containing the particle sources and a load lock system. The base pressure is about 10^{-4} Pa in the exposition chamber and 10^{-3} Pa in the load lock chamber, and the pressure during the processing of the samples is 10^{-2} Pa. The temperature of the samples during treatment can be varied and is monitored by a thermocouple mounted on the sample holder. The oxygen source is based on a microwave plasma excited in an Evenson cavity,[21] which is connected to the processing chamber via an S-bend quartz tube with a length of 30 cm. The microwave

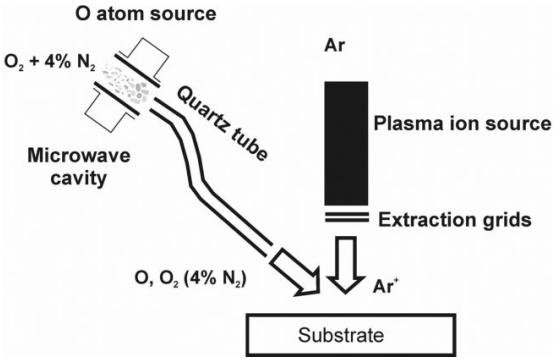

Figure 1. Schematic of the experimental set-up consisting of an exposition chamber equipped with Ar^+ ion beam and O and O_2 sources.

Plasma Process. Polym. **2009**, *6*, 255–261

DOI: 10.1002/ppap.200800199

power is held at 40 W and an oxygen flow of 5 sccm is used in this study. Moreover, in order to increase the O atom flux reaching treated samples, an admixture of 0.2 sccm nitrogen is used, which drastically enhances the dissociation degree of oxygen due to a decrease in a wall diffusion loss of O atoms.[22,23] Moreover, it has to be noted that S-bend shape of the connecting tube avoids direct line-of-sight from the microwave plasma to the sample eliminating the exposure of the sample to possible UV and VUV radiation, which is connected with production of excited NO molecules and which can contribute to the proteins removal. The negligible flux of UV radiation on treated samples has been confirmed in previous studies that revealed no observable inactivation of spores of *Bacillus Atrophaeus*, which are spores highly sensitive to UV radiation bellow 300 nm, within of 4 h of beam operation.[19] The shape and the length of the quartz tube leads also to an effective quenching of oxygen or nitrogen metastables produced in the MW cavity due to wall collisions. This, together with the operational pressure 10^{-2} Pa, which excludes effective production of O_3 that are created predominately via three-body interactions, assures that the dominant active particle produced in the MW cavity and reaching samples is atomic oxygen. Based on the calibration using comparison of etch rates of a-CH films performed in the previous study,[19] the arrangement used yields an O atom flux of 2.4×10^{15} cm^{-2} s^{-1} on the sample. However, it has to be noted that the microwave source remains also a source of O_2 molecules (background O_2 flux of $j_{O2} = 1.5 \times 10^{17}$ cm$^{-2} \cdot$ s^{-1} at the sample surface). This is important, because it was shown that the exposure of hydrocarbon films or of bacterial spores to the combined impact of argon ions and of O_2 molecules induces significant etching.[19,24,25] Consequently, the exposure of the samples needs to be regarded as exposure to an O/O_2 beam. In order to separate the effect of O_2 molecules from the effect of O atoms, additional tests were performed using only a flux of non-dissociated neutral O_2 molecules instead of the O/O_2 beam. The Ar^+ ion beam is produced using a commercial plasma ion source (type Gen2 by Tectra GmbH) based on a magnetically enhanced microwave plasma. Ions are extracted from the plasma discharge and are accelerated to energies of 100 eV using a two grid system. Under the experimental conditions used in this study, the Ar^+ ion flux density at the sample is $j_{Ar+} = 1.8 \times 10^{14}$ cm^{-2} s^{-1}, as calibrated by measuring the physical sputtering yield of an amorphous hydrogenated carbon film (a-C:H) with known properties.

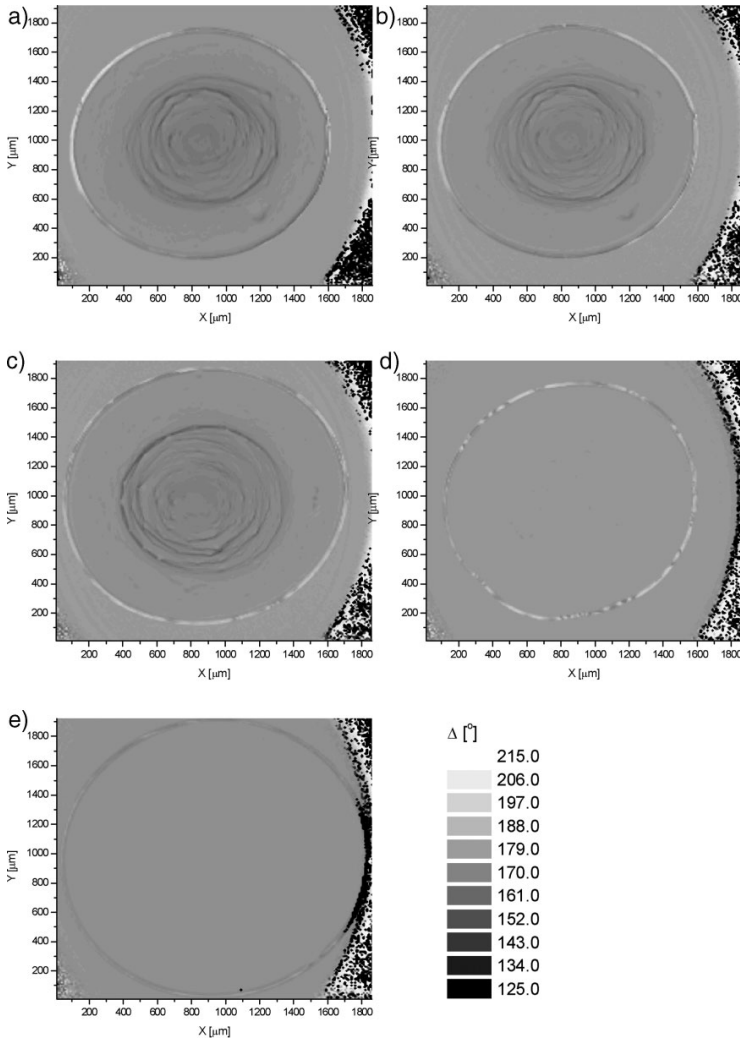

Figure 2. 2D ellipsometric maps of Δ angles of a) untreated BSA sample and BSA samples exposed for 60 min to b) O_2 flow, c) O/O_2 beam, d) Ar^+ beam only, and e) O/O_2 beam combined with Ar^+ beam.

Results and Discussion

Effect of the O/O_2 Beam

The treatment by the O_2 or O/O_2 beams was found to have only a negligible influence on the protein films as can be seen in Figure 2 showing 2D maps of the ellipsometric angles Δ of untreated BSA sample (Figure 2a) and samples exposed for 60 min to these two beams (Figure 2b and c). According to stylus profilometry, the removal rates are in both cases lower than 0.1 nm $\cdot$ min^{-1} (Figure 3) and the protein surface remains unaffected by the treatment (see Figure 4). Whereas O_2 molecules alone are not expected to significantly affect proteins at room

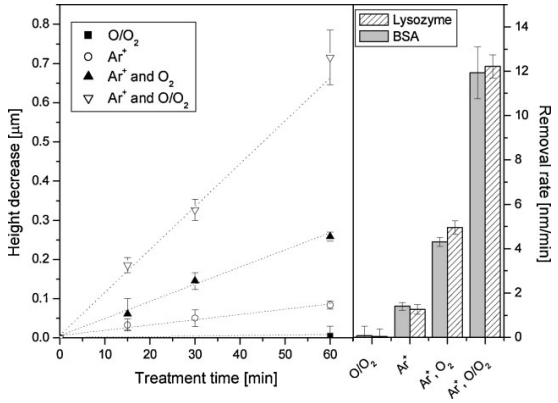

Figure 3. Temporal evolution of BSA height decrease (left panel) and corresponding removal rates (right panel).

temperature,[25] O atoms or O_2 metastables produced in the O/O_2 beam source are expected to be capable to induce a removal of biological material by its chemical etching. However, the absence of any significant etching demonstrates that an O fluence of $j_O = 8.6 \times 10^{18}$ cm^{-2} is unable to contribute significantly to the process of protein removal at substrate temperatures of 30 °C. Additional experiments have shown that the protein removal rate can be enhanced by rising the substrate temperature indicating that O etching is a temperature activated process.[25] However, even if the substrate temperature was elevated to 120 °C, i.e. the substrate temperature exceeding the one observed during the plasma treatment of proteins,[17] the removal rate using the O/O_2 beam was only 0.56 nm · min^{-1}.

Effect of Energetic Ar^+ Ions

Bombardment of proteins by Ar^+ ions leads to markedly faster removal and erosion of proteins as compared to the O/O_2 beam (see Figure 2 and 3); the removal rate is slightly higher than 1 nm · min^{-1}, and it also causes an increase of the surface roughness, which is more than 4 times larger after 15 min treatment as compared to the untreated samples (Figure 4). Since no chemically active species were present in the processing chamber during the treatment, the observed effects can be attributed solely to the physical sputtering process of proteins by energetic (100 eV) Ar^+ ions.

Simultaneous Exposure to Ar^+, O/O_2 and O_2 Beams

Simultaneous exposure to Ar^+ and O/O_2 beams resulted in markedly faster removal of both model proteins (reaching values of around 12 nm · min^{-1}) and a higher roughness of the protein surfaces compared to the previous two cases as it is demonstrated in Figure 3 and 4. It is, however, clear that the observed removal rates and the enhancement of the surface roughness in this experiment cannot be explained by simply adding the net actions of chemical etching as observed in the experiment employing only the O/O_2 beam and of physical sputtering from the experiment using solely argon ions. Instead, the process of chemical sputtering, as being induced by the *simultaneous* impact of reactive neutrals and energetic ions on treated surface is able to explain the enhancement in removal rate: impinging ions break bonds in the protein layers within their corresponding collision cascade via nuclear stopping. Such broken bonds created on or close to the surface of the deposit subsequently react with the additional flux of oxygen atoms or molecular oxygen, which can lead either to their passivation or to the formation of volatile products, presumably H_2O, OH, CO, and CO_2, induced by chemical interaction of oxygen with surface active sites. Whereas, the second process leads to the gradual removal of proteins, fast passivation of broken bonds disables their relaxation or cross-linking. This in turn facilities any further erosion by incident oxygen species due to preferred material removal from once affected sites, leading to formation of deep etch channels as observed by AFM (Figure 4e).

Since it is not possible to disregard O_2 molecules impinging on the samples in the experiments using an O/O_2 beam, additional experiments were performed using the Ar^+ ion beam in combination with an O_2 flow only. These experiments showed, in agreement with previous experiments using bacterial spores or hard a-C:H films,[19,25] that addition of molecular oxygen to the energetic argon ion beam leads to pronounced removal of proteins as compared to the effect of Ar^+ bombardment only. The measured removal rate is slightly higher than 4 nm · min^{-1} for both proteins employed in this study, i.e. it is more than three times higher as compared to the protein removal rate measured using solely the argon ion beam (see Figure 3). This is explained by the fact that O_2 with its triplet ground state is a bi-radical and can directly react with broken bonds at the surface.[26] Nevertheless, it should be stressed that the presence of even a small fraction of O atoms in the O/O_2 beam (around 1% in our experiments) leads to a dramatic increase of the protein removal rate, reaching values up to 12 nm · min^{-1}. This indicates that O is much more reactive compared to O_2.

Relevance for the Plasma Treatment of Protein Samples

The results presented here constitute an important step in the understanding of processes taking part during plasma treatment of proteins. Although the results are difficult to

Plasma Process. Polym. **2009**, *6*, 255–261

DOI: 10.1002/ppap.200800199

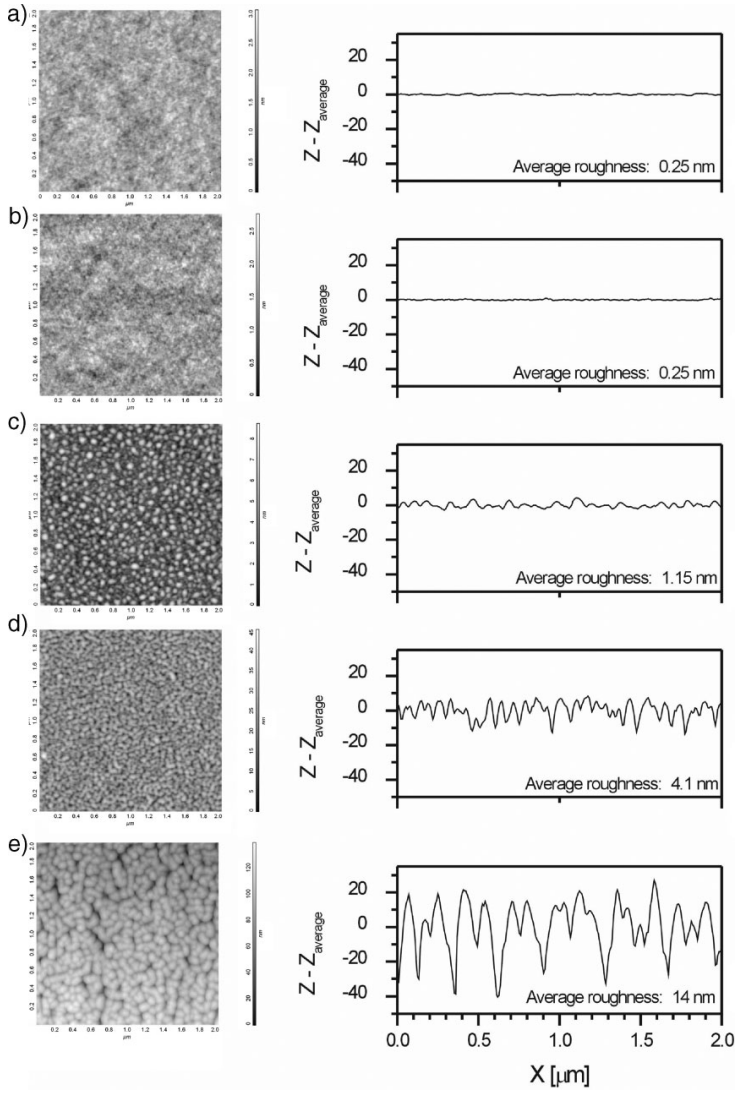

Figure 4. Typical surface profiles (right panel) and AFM topographic images of 2 × 2 µm² area (left panel) of a) untreated BSA sample and BSA samples exposed for 15 min to b) O/O_2 beam, c) Ar^+ beam only, d) Ar^+ beam combined with O_2 flow, and e) and O/O_2 beam combined with Ar^+ beam.

compare directly with the results obtained with active plasma discharges, which is mainly due to the differences of particle fluxes, as well as to the higher ion energy used in the beam experiments, the following conclusions can be drawn:

(i) It is demonstrated that chemical etching involving oxygen atoms should not be considered as the only or the most dominant process leading to the elimination of proteins from surfaces in plasma discharges. This finding is consistent with observations from previous studies, which showed that the rate of protein removal in Ar/O_2 plasma discharge does not follow solely the density of O atoms.[17,20]

(ii) Analogously to the erosion of bacterial spores,[19,20] the high removal rates of proteins observed in Ar/O_2 plasma discharges can be explained by the process of chemical sputtering involving both ions and impinging oxygen species (both atomic and molecular oxygen). This can also explain the occurrence of a well defined maximum of the protein removal rate, as observed for a 20:1 Ar/O_2 discharge mixture.[17] As previously reported,[17,20] the density of positive ions drastically decreases with an increasing fraction of oxygen in the oxygen-argon discharge mixture in a plasma kept at constant power. This consequently limits the creation of defects on the protein structure that can be subsequently attacked by oxygen species, although the density of oxygen species monotonously increases with increasing oxygen fraction in the discharge mixture.[17,20] In this reaction scheme the 20:1 argon-oxygen mixture therefore represents an optimum balance between the fluxes of ions, which are needed for the initiation of the process of chemical sputtering by creation of dangling bonds near the protein surface, and the flux of chemically active oxygen particles interacting with such created active sites.

In this context, it has to be noted that, although the energy of ions used in this study is much higher than the one observed in low-pressure ICP discharges (typically tens of eV), the mechanism of chemical sputtering is still plausible for ions having lower energies as already demonstrated for treatment of hydrocarbons.[25]

(iii) It has been demonstrated that for chemical sputtering of proteins, the presence of atomic oxygen is not crucial, since also ground state oxygen molecules are capable to induce volatilisation of proteins. However,

the present results clearly show that 1% dissociation degree of oxygen molecules leads to 3 times faster protein elimination as compared to the flow of undissociated O_2 molecules. Taking into account this finding together with a typical dissociation degree of O_2 molecules in low-pressure ICP discharges, reaching commonly values higher than 1%, allows us to presume that in plasma discharges the fast elimination of proteins is connected predominantly with the action of O atoms.

(iv) Finally, it is interesting to note that the removal rates of BSA and Lysozyme are almost identical, which is in agreement with the results reached during plasma treatment of proteins.[16] This finding is, as discussed bellow, also consistent with the postulated process of chemical sputtering:

The protein elimination from surfaces occurs due to their gradual volatilization, which is caused by interaction with oxygen atoms or molecules. Although the exact chemical structure of proteins treated is significantly different, they can be in the first approximation considered as a polymeric substances composed from carbon, hydrogen, nitrogen and oxygen mainly, i.e. species that can all easily form volatile products in chemical interactions with oxygen (e.g. O_2, CO, OH, NO). Nevertheless, for the initiation of the process of volatilization, active sites have to be formed on the surface. This can be achieved either by hydrogen abstraction from the polymeric structure, which is a major mechanism in the case of pure chemical etching in oxygen containing atmosphere, or by bonds cleavage caused by impact of energetic ions in the case of chemical sputtering. However, it is clear that, whereas the first mechanism is highly dependent on the exact chemical structure of treated deposits, which would consequently lead to different etch rates for different polymeric materials, the second mechanism is due to the high energies of impinging ions rather insensitive to the chemical composition of treated substances, which renders their exact chemical structure irrelevant for the resulting etch rate as observed in our experiments. The insensitivity of chemical sputtering to the chemical structure of proteins (together with recent results reached with bacterial spores showing similar trends[19]) is of paramount importance, since it allows to presume that all the biomolecules and biological systems comprising pathogenic ones will be eliminated at rather similar rates in plasma discharges. Verification of this hypothesis is a subject of on-going studies.

Conclusion

Deposits of Bovine Serum Albumin and Lysozyme, selected as model proteins with distinctly different chemical and physical properties, were exposed to beams of Ar^+ ions, oxygen molecules and oxygen atoms. It is demonstrated, that at room temperature only the simultaneous impact of O atoms or O_2 molecules and of argon ions leads to effective removal of proteins from surfaces and to significant roughening of their surfaces. This is explained by the process of chemical sputtering, i.e. process where the oxygen species interact with ion-induced defects at the protein surface leading to the formation of volatile compounds. This reaction scheme can moreover explain observed variations of protein removal rates with variation of composition of Ar/O_2 low-pressure inductively coupled plasma discharges reported in previous studies. From this perspective, maximal protein removal rates observed for about 5% of oxygen in argon discharges can be seen as a result of optimal compromise between the ion and the O atom fluxes to the substrate in such discharges.

Identification of the significant contribution of chemical sputtering to the elimination of proteins from surfaces is of great importance, since it allows effective development and optimisation of plasma based decontamination processes.

Acknowledgements: This work has been supported by the FP6 2005 NEST project *"Biodecon"*.

Received: October 16, 2008; Revised: January 16, 2009; Accepted: January 20, 2009; DOI: 10.1002/ppap.200800199

Keywords: beam experiments; ICP discharges; plasma treatments; proteins; sterilisation

[1] D. M. Taylor, *J. Hosp. Infection* **1999**, *43*, S69.
[2] D. M. Miller, I. Youkhana, W. U. Karunaratne, P. Pearce, *Anaesthesia* **2001**, *56*, 1069.
[3] I. P. Lipscomb, A. K. Sihota, C. W. Keevil, *J. Clin. Microbiol.* **2006**, *44*, 3728.
[4] M. Moisan, J. Barbeau, S. Moreau, J. Pelletier, M. Tabrizian, L'. H. Yahia, *Int. J. Pharm.* **2001**, *226*, 1.
[5] S. Lerouge, M. Wertheimer, L'. H. Yahia, *Plasmas Polym.* **2001**, *6*, 175.
[6] M. Laroussi, *IEEE Trans. Plasma Sci.* **2002**, *30*, 1409.
[7] M. Laroussi, *Plasma Process. Polym.* **2005**, *2*, 391.
[8] F. Rossi, O. Kylián, M. Hasiwa, *Plasma Process. Polym.* **2006**, *3*, 431.
[9] O. Kylián, M. Hasiwa, F. Rossi, *IEEE Trans. Plasma Sci.* **2006**, *34*, 2606.
[10] M. Hasiwa, O. Kylián, T. Hartung, F. Rossi, *Innate Immunity* **2008**, *14*, 89.
[11] X. T. Deng, J. J. Shi, H. L. Chen, M. G. Kong, *Appl. Phys. Lett.* **2007**, *90*, 3904.
[12] X. T. Deng, J. J. Shi, M. G. Kong, *J. Appl. Phys.* **2007**, *101*, 4701.
[13] H. C. Baxter, G. A. Campbell, A. G. Whittaker, A. C. Jones, A. Aitken, A. H. Simpson, M. Casey, L. Bountiff, L. Gibbard, R. L. Baxter, *J. Gen. Virol.* **2005**, *86*, 2393.
[14] H. C. Baxter, G. A. Campbell, P. R. Richardson, A. C. Jones, I. R. Whittle, M. Casey, A. G. Whittaker, R. L. Baxter, *IEEE Trans. Plasma Sci.* **2006**, *34*, 1337.

DOI: 10.1002/ppap.200800199

[15] C. Bernard, A. Leduc, J. Bardeau, B. Saoudi, L'Y., Yahia, G. De Crescenzo, *J. Phys. D: Appl. Phys.* **2006**, *39*, 3470.
[16] O. Kylián, H. Rauscher, D. Gilliland, F. Brétagnol, F. Rossi, *J. Phys. D: Appl. Phys.* **2008**, *41*, 5201.
[17] K. Stapelmann, O. Kylián, B. Denis, F. Rossi, *J. Phys. D: Appl. Phys.* **2008**, *41*, 2005.
[18] J. Opretzka, J. Benedikt, P. Awakowicz, J. Wunderlich, A. von Keudell, *J. Phys. D: Appl. Phys.* **2007**, *40*, 2826.
[19] V. Raballand, J. Benedikt, J. Wunderlich, A. von Keudell, *J. Phys. D: Appl. Phys.* **2008**, *41*, 5207.
[20] J. Benedikt, C. Flötgen, G. Kussel, V. Raballand, A. von Keudell, *J. Phys. : Conf. Series* **2008**, *133*, 012012.
[21] F. C. Fehsenfeld, K. M. Evenson, H. P. Broida, *Rev. Sci. Instrum.* **1965**, *36*, 294.
[22] A. R. de Souza, C. M. Mahlmann, J. J. Muzart, C. V. Speller, *J. Phys. D: Appl. Phys.* **1993**, *26*, 2164.
[23] L. S. Yu-Jahnes, W. T. Brogan, A. C. Anderson, M. J. Cima, *Rev. Sci. Instrum.* **1992**, *63*, 4149.
[24] C. Hopf, M. Schlüter, W. Jacob, *Appl. Phys. Lett.* **2007**, *90*, 224106.
[25] C. Hopf, M. Schlüter, T. Schwarz-Selinger, U. von Toussaint, W. Jacob, *New J. Phys.* **2008**, *10*, 3022.
[26] J. F. Friedrich, G. Kühn, J. Gähde, *Acta Polym.* **1979**, *30*, 470.

New Journal of Physics
The open-access journal for physics

Low pressure plasma discharges for the sterilization and decontamination of surfaces

F Rossi[1,3], O Kylián[2], H Rauscher[1], M Hasiwa[1] and D Gilliland[1]

[1] European Commission, Joint Research Centre, Institute for Health and Consumer Protection, Via E. Fermi 2749, 21027 Ispra (VA), Italy

[2] Faculty of Mathematics and Physics, Charles University, V Holešovičkách 2, Prague 8, 180 00, Czech Republic

E-mail: francois.rossi@jrc.ec.europa.eu

New Journal of Physics **11** (2009) 115017 (33pp)
Received 20 March 2009
Published 26 November 2009
Online at http://www.njp.org/
doi:10.1088/1367-2630/11/11/115017

Abstract. The mechanisms of sterilization and decontamination of surfaces are compared in direct and post discharge plasma treatments in two low-pressure reactors, microwave and inductively coupled plasma. It is shown that the removal of various biomolecules, such as proteins, pyrogens or peptides, can be obtained at high rates and low temperatures in the inductively coupled plasma (ICP) by using Ar/O_2 mixtures. Similar efficiency is obtained for bacterial spores. Analysis of the discharge conditions illustrates the role of ion bombardment associated with O radicals, leading to a fast etching of organic matter. By contrast, the conditions obtained in the post discharge lead to much lower etching rates but also to a chemical modification of pyrogens, leading to their de-activation. The advantages of the two processes are discussed for the application to the practical case of decontamination of medical devices and reduction of hospital infections, illustrating the advantages and drawbacks of the two approaches.

[3] Author to whom any correspondence should be addressed.

Contents

1. Introduction

In the US, approximately 46.5 million surgical procedures and even more invasive medical procedures—including approximately 5 million gastrointestinal endoscopies—are performed each year. Each procedure involves contact between a surgical instrument and a patient's sterile tissue or mucous membranes. These procedures present a major risk of contamination by the introduction of pathogens during the operation. Failure to properly disinfect or sterilize equipment not only carries a risk associated with the breach of host barriers but also a risk of person-to-person transmission (e.g. hepatitis B virus) and transmission of environmental pathogens (e.g. *Pseudomonas aeruginosa*).

Multiple studies in different countries have documented a lack of compliance with established guidelines for disinfection and sterilization. Failure to comply with scientifically based guidelines has led to numerous outbreaks. In 2002, the estimated number of Hospital Acquired Infections (HAI) in the US, was approximately 1.7 million. The estimated deaths associated with HAIs in US hospitals were about 10 000 [1] at a cost of the order of 5–7 billion dollars. Similar figures were also reported for the UK, France and Italy, with 100 000 HAI leading to about 5000 deaths in 2000 for the UK [2], 4000 for France [3] and 5000–7000 in Italy [4].

Although these cases cannot all be directly attributed to contamination present on surgical instruments, it is generally recognized that disinfection and sterilization are essential

for ensuring that medical and surgical instruments do not transmit infectious pathogens to patients. These operations are normally realized by placing the instrument in a mechanical washer/disinfector and subjecting them to a pre-wash at room temperature to prevent blood coagulation and adhesion of proteins. The instruments are then cleaned and sonicated with an alkaline enzymatic detergent, and finally, at high temperature, washed and rinsed. They are then visually inspected after drying and packaged for sterilization (in most cases by autoclaving, but also by use of chemical reagents such as hydrogen peroxide or EtO). These operations normally have to follow strict rules such as the ones described in the norm ISO EN 15883.

However, recent studies made in the UK have shown that visual inspection is not enough to prevent significant quantities of residues to be left on surgical instruments after complete cleaning operations [5]–[8]. In these studies made on real instruments decontaminated in a Sterile Service Unit, all items tested were showing residual contamination, sometimes severe with levels larger than 4 μg mm^{-2} locally. These residues were composed of salts, proteins and undefined organic matter. This observation raises serious concerns since it has been shown that prion protein can accumulate in peripheral and skeletal tissues of patients having the different forms of Creutzfeld Jacob Disease (CJD) and could be potentially transmitted iatrogenically by contaminated medical devices.

Another concern linked to these residues is related to pyrogens coming from both gram-negative (lipopolysaccharides (LPS)) and gram-positive (peptidoglycans or lipoteichoic acids) bacteria. These pyrogens can cause sepsis when in contact with the patient bloodstream and provoke septic shock, which is a major cause of death among hospitalized patients. They are, however, extremely resistant to temperature (e.g. [9, 10]) and difficult to remove by conventional sterilization procedures (e.g. [11]).

Therefore new methods of decontamination and sterilization, which could ensure complete removal of bacteria, pyrogens and proteins, are urgently desired. As we will see, the application of non-equilibrium plasma discharges currently appears as an interesting option. This is mainly due to the capacity of plasma processes to remove organic material with high efficiency, while working at low temperature and using non-toxic gases, thus reducing both environmental impacts and safety risks. These key advantages naturally result in increased interest in the investigations of the plasma interactions with substances of biological origin and micro-organisms.

Indeed, it has been shown that many pathogens can be destroyed by employing non-equilibrium plasma discharges (e.g. [12]–[14]) and the nature of plasma interactions with micro-organisms or biomolecules has been extensively studied in the past few years, with aim (i) to identify the dominant processes leading to the desired effect, (ii) for treatment optimization and (iii) validation of the process. However, it has to be noted that this is a rather challenging objective: plasma discharges are capable of producing high fluxes of various neutral or ionized active species as well as energetic photons, which all interact with treated biological systems via different mechanisms that contribute to the overall efficiency of the treatment. The exact role of each of these processes naturally depends on many parameters such as e.g. process conditions (pressure, applied power, gas flow and excitation frequency), geometry of the system as well as on the kind of target to be inactivated; this considerably complicates the comparison of the results obtained in different experimental configurations and leads to controversy concerning the mechanisms at play during the process. However, as will be outlined in the following section, recent results allow us to draw certain general conclusions regarding possible strategies of plasma-based sterilization and decontamination of surfaces. Subsequently, some of the aspects

related to the proposed approaches will be discussed on the basis of experiments employing low-pressure plasma discharges and involving various kinds of biological systems, with the objective to demonstrate their advantages as well as limitations and drawbacks.

2. Principles of low-pressure plasma-based sterilization and decontamination

2.1. Bacterial spore sterilization

The main mechanisms of spore destruction or deactivation by plasma discharge have been the object of several reviews (e.g. [14]–[19]) that the reader should refer to for more details. In brief, two main mechanisms can be invoked for spore inactivation or destruction employing low-pressure plasma discharges[4]:

- The first one is related to the inactivation of spores by interaction of the UV photons emitted by the discharge with the DNA (e.g. [20]–[22]). It was found that the maximum efficiency of the UV photons is typically in the wavelength range 200–300 nm [22, 23], and that there exists a minimum dose necessary for preventing DNA repair [24] that leads to sterilization.
- The second mechanism is linked to spore etching and erosion by the radicals and active species produced by the plasma discharge (e.g. atomic oxygen, atomic nitrogen and OH radicals or fluorine atoms [25]–[32]). The etching leads to the direct killing of spores by destruction of their membrane and to the removal of the material that shields the spores from exposure to UV radiation. Both effects result in an acceleration of the sterilization rate.

Nevertheless, it is clear that in common situations, both processes may act simultaneously during the treatment and thus contribute to the killing/deactivation of spores. The rates of the two mechanisms are often markedly different, which leads to the two phases of kinetics reported in the literature (e.g. [12, 15]). Moreover, the significance of these two processes is strongly dependent on the local plasma conditions, and as a consequence, on the position of treated object with respect to the plasma discharge: whereas position in the active plasma favors spore etching promoted by ion bombardment, placing samples in the discharge afterglow increases the relative role of UV radiation since ions are normally absent in these conditions.

However, it must also be emphasized that basing sterilization on the action of UV only has two serious drawbacks: the first one is connected to the distribution of the spores on the surface: in practical cases, the spores might be stacked and mixed with protein residues or biological film. With the UV photons flux decreasing exponentially with the thickness of the film they go through, the time needed for reaching the minimum dose necessary for spore inactivation increases exponentially. This makes sterilization difficult to achieve in practical cases with this approach and therefore some etching that uncovers shielded spores is normally necessary for acceptable treatment durations [14]. The second limitation is that UV photons have little or no effect on other contamination sources such as pyrogens or proteins, which results in a treatment that addresses only a part of the problem.

This is why we deliberately favor the approach where etching contributes significantly to the decontamination treatment. We will see that this approach has the advantage of sterilizing

[4] It has to be noted that also other mechanisms have been suggested as for instance electrostatic disruption of the outer cells walls [18] or their killing by ozone [19]. However, the significance of these processes is more important for discharges operated at higher pressures than the ones reported here.

the surface even when significant soiling is present, and it also removes the other contaminants such as pyrogens or proteins at low temperatures and with limited treatment durations.

2.2. Destruction of pyrogens

As mentioned before, another surface contamination, overlooked most of the time, is represented by pyrogens. The outer coats of spores and bacteria contain endotoxins (e.g. LPS, peptidoglycans or lipoteichoic acids, etc), which are pyrogenic substances. They act as potent modulators of the human immune system, and their presence in the blood stream leads to physiological events such as fever, swelling or sepsis and, at higher doses, to death [33]. UV radiation in the 200–300 nm range has little effect on such substances, as we have already demonstrated [34]. Moreover, after a plasma treatment based on UV radiation only, the surface treated can have an increased pyrogenic activity due to the endotoxins liberated by the spores, and can consequently provoke an unexpected immunological response [35]. Nevertheless, it has been recently demonstrated that distinct kinds of pyrogenic substances can be inactivated readily by plasma treatment (e.g. [14, 34, 36, 37]).

2.3. Elimination of proteins

Another group of possible contaminants is constituted by protein residues, which might contain pathogens, such as the infectious prions associated with the transmission of the CJD. Unlike the case of bacterial spores, prions do not contain genetic material and UV radiation is ineffective for their destruction. Moreover, prions have been found to be extremely resistant toward the conventional sterilization and decontamination techniques (e.g. [38, 39]) because of their unique and stable secondary and ternary structure that cannot be easily altered.

Although the possibility to remove prions by means of non-equilibrium plasma discharges has already been demonstrated by Baxter *et al* [40], the studies focusing on their removal mechanisms are rather limited. This is primarily because of the necessity of high containment laboratories due to the biohazard connected with such proteins. Therefore, in order to understand the mechanisms of plasma–prions interactions, the effects of non-equilibrium plasma discharges on non-pathogenic models of proteins were studied (e.g. [14], [41]–[48]) using different methods for monitoring their elimination. The results of these studies reveal general important facts regarding the action of low-pressure plasma discharges on proteins, and show the possibility to remove them by oxygen-containing discharges, which induce their fragmentation and volatilization after oxidation. Nevertheless, there is still a lack of systematic analysis related to the protein removal efficiency under different experimental conditions as well as to the identification of the principal mechanism of their elimination.

The results published in the literature lead us to the conclusion that low pressure plasma processes, operated in conditions leading to high etching rates of organic matter, are the route to pursue for the development of a treatment able to both sterilize and decontaminate surface of medical devices, with a number of caveats that will be discussed at the end of this paper.

In order to get a better insight into the possibilities and limitations of low pressure plasma discharges, two types of processes (direct and post discharge) will be presented and their effect on different types of contaminations will be discussed.

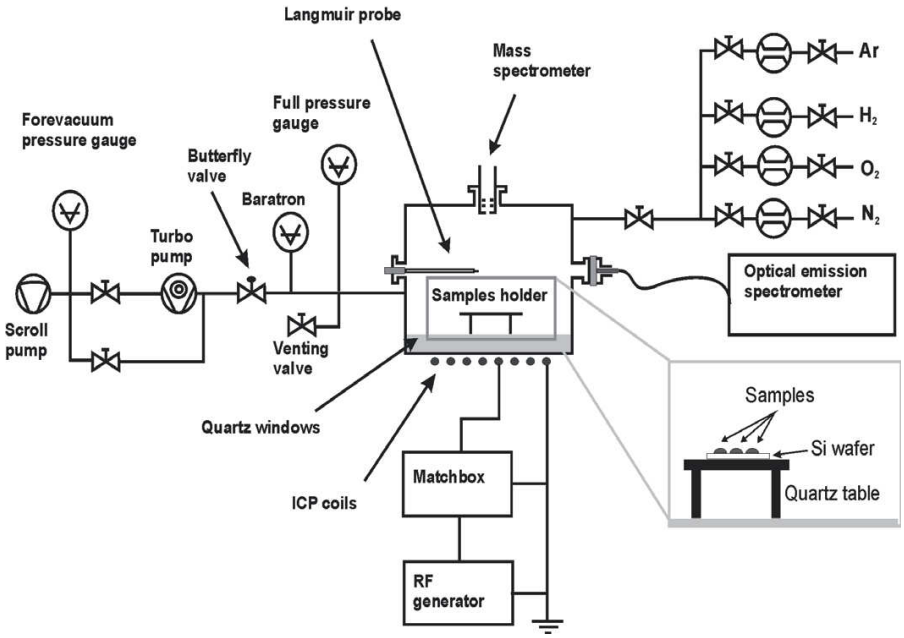

Figure 1. Schematics of the ICP reactor.

3. Experimental

3.1. Plasma treatments

Two different types of plasma reactors have been used in the present work.

The first type of discharge used is a planar double coil inductively coupled plasma (ICP) source schematically depicted in figure 1. This plasma reactor allows igniting plasma discharges with a power between 100 and 500 W, in a pressure range from 0.1 to 20 Pa and gas flows from 1 to 20 sccm.

The processing chamber has a volume of approximately 5 liters and is evacuated by primary and turbomolecular pumps. The gas mixture used for the discharge is controlled by MKS mass flow controllers. The biological samples were placed 20 mm from the bottom quartz window.

The second experimental set-up used is a microwave plasma reactor schematically depicted in figure 2. It consists of a cylindrical stainless steel vacuum chamber having a volume of approximately 12 liters, equipped with several diagnostics windows and one port for sample introduction. The processing chamber is fed from a gas handling system composed of mass flow controllers attached to the process gas lines and is evacuated by a primary pump and a roots blower. The pressure in the chamber during plasma operation is regulated by an MKS butterfly valve. The plasma discharge is generated at a total gas flow of 100 sccm at a pressure of 16 Pa by a microwave source (excitation frequency 2.45 GHz, applied power 1000 W) introduced into the plasma chamber through a silica window placed at the end of a circular 100 mm waveguide. In contrast to the ICP set-up, the samples to be treated were placed outside the active plasma zone at a distance of 300 mm from the quartz window, i.e. in the near post discharge, where plasma densities are low, as indicated in table 1.

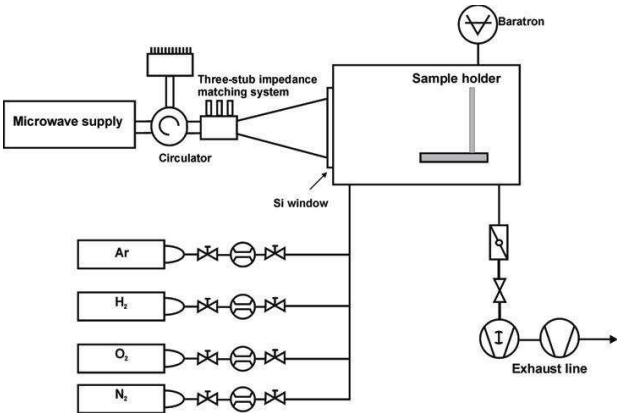

Figure 2. Schematics of the microwave plasma reactor.

Table 1. Electron density and electron temperature at samples position in used reactors (MW: 1000 W, 100 sccm, 16 Pa; ICP: 350 W, 20 sccm, 10 Pa).

Gas mixture	Ne (cm^{-3})		Te (eV)	
Reactor	ICP	MW	ICP	MW
Ar	$(8.3 \pm 0.1) \times 10^{11}$	$(2 \pm 0.1) \times 10^{9}$	1.7 ± 0.1	1.03 ± 0.03
O_2	$(2.0 \pm 0.3) \times 10^{10}$	$(2.5 \pm 0.4) \times 10^{9}$	2.7 ± 0.2	1.1 ± 0.2
N_2	$(1.8 \pm 0.2) \times 10^{10}$	$(1.2 \pm 0.1) \times 10^{9}$	2.6 ± 0.2	0.55 ± 0.04
O_2/N_2 (50 : 50)	$(1.8 \pm 0.1) \times 10^{10}$	$(1.5 \pm 0.3) \times 10^{9}$	2.6 ± 0.1	0.8 ± 0.2

In order to characterize the plasma discharges produced in both reactors, different diagnostics methods were used, namely a Langmuir probe (SmartProbe™; Scientific Systems Ltd) placed at the samples positions, optical emission spectroscopy (Avantes AVS-PC2000 monochromator equipped with a 2048-element linear CCD array) and mass spectrometry (HAL4, Hiden Analytical). Moreover, the substrate temperature during plasma treatment has been determined by IR pyrometry (Raynger MX4, Raytek).

The two reactors differ strongly by the conditions produced and the processes applied. In the microwave (MW) reactor, the samples are placed outside of the active plasma zone and submitted mostly to a flux of neutrals and radicals, while in the discharge in the ICP reactor, they are also subjected to a significant ion bombardment. In other words, although in both reactors comparable fluxes of active species reach the samples, which can be demonstrated for instance by actinometric measurements of O atom density (see figure 3), the fluxes of charged particles to the sample differ enormously, as can be seen from figure 4 and table 1, where the plasma characteristics measured at the samples' position are given for both reactors.

Moreover, the two reactors cause markedly different heating of the treated samples. For instance, whereas temperature of Si wafer after 1 min of plasma duration in Ar was found to be 180 °C in the ICP reactor, only a slight increase of the substrate temperature was observed in the MW reactor even after 10 min of plasma duration (see figure 5). Such a difference in the heating of the samples could affect significantly the kinetics of the etching of biological

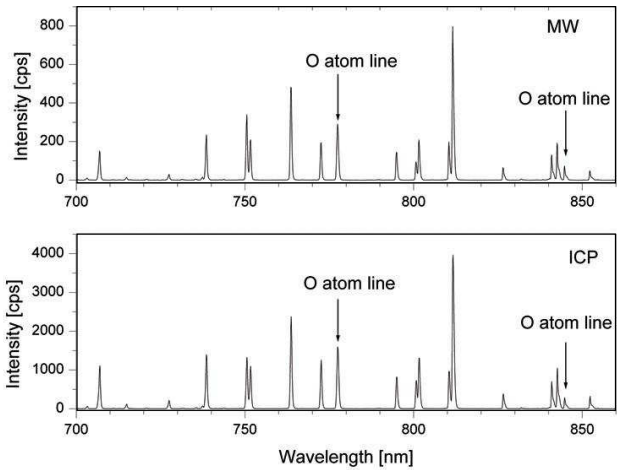

Figure 3. Emission spectra of Ar/O_2 9 : 1 discharges (MW: 1000 W, 100 sccm, 16 Pa; ICP: 300 W, 20 sccm, 10 Pa).

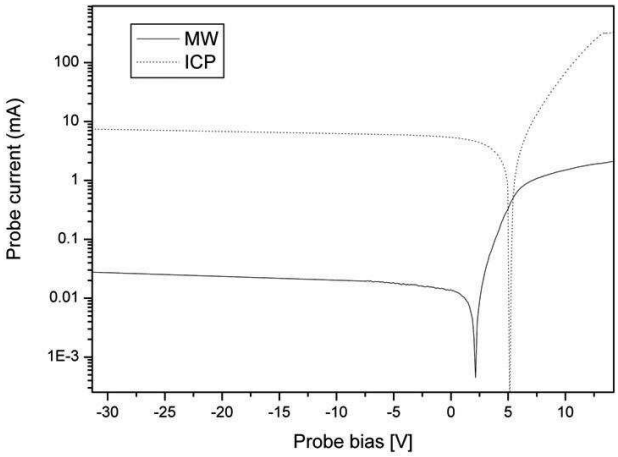

Figure 4. Langmuir probe characteristic measured in Ar discharges at the samples' position (MW: 1000 W, 100 sccm, 16 Pa; ICP: 300 W, 20 sccm, 10 Pa).

samples or the sterilization process in general (e.g. [49]–[51]). Therefore, in order to limit this side effect, preliminarily tests were undertaken to find out a treatment time allowing us to neglect the heating influence. Based on these experiments performed at a variable treatment duration, it has been found that the onset of the nonlinearity of the etching rate with treatment time, which can be attributed to the temperature effect, starts when the substrate is heated to the temperature of approximately 100 °C, that corresponds to the treatment duration around 30 s for ICP discharge operated at 300 W (see figure 6). Therefore, for all the etching tests performed in the ICP reactor the treatment duration was kept below 30 s (i.e. in the case of longer treatment times, the plasma treatment was performed in several consecutive steps).

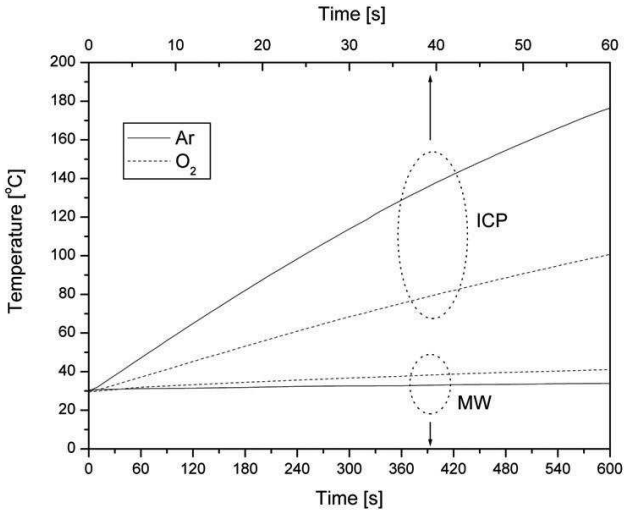

Figure 5. Temporal evolution of substrate temperature in Ar and O_2 plasma (MW: 1000 W, 100 sccm, 16 Pa; ICP: 300 W, 20 sccm, 10 Pa).

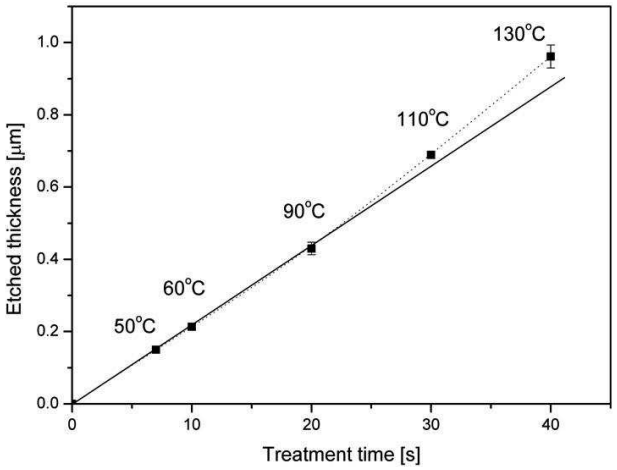

Figure 6. Etching of BSA for plasma treatment having variable duration (ICP reactor, Ar/O_2 20 : 1 mixture, 10 Pa, 300 W). The numbers indicate substrate temperature reached after end of each of the treatment steps.

3.2. Coating of proteins and amino acids

The samples were prepared by spotting an aqueous solutions (0.1% wt) of different selected substances, namely bovine serum albumin (BSA), lysozyme, ubiquitin as representatives of proteins and poly-L-histidine, on one-side polished, cleaned Si wafers. This substrate has been chosen to allow a precise analysis of the decontamination mechanisms, but represents an ideal case as compared with stainless steel substrates that present many surface defects

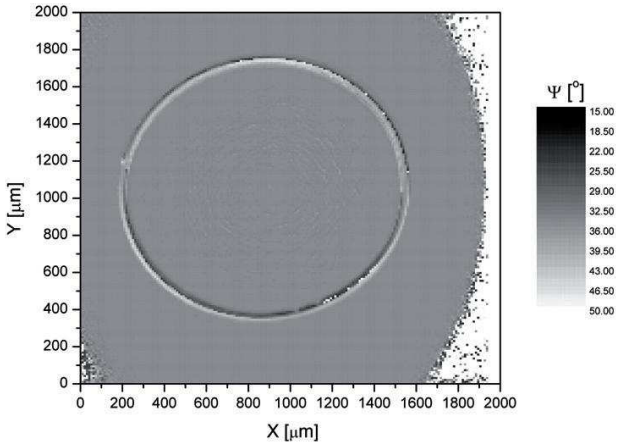

Figure 7. 2D map of ellipsometric angle Ψ of the BSA sample.

after repeated usage. After deposition, the samples were dried overnight in a common flow hood. During the drying of the droplet, the deposit forms a thin central part with a thickness of about 100 nm, surrounded by a thicker ring (coffee ring effect) as can be seen in figure 7 for the BSA sample. Both treated and untreated samples were subsequently examined by various surface diagnostic methods: stylus profilometry (Alpha-step IQ, KLA-Tencor), atomic force microscopy (AFM type Solver P47H, NT-MDT Co.) and ToF-SIM spectroscopy (TOF-SIMS IV, IONTOF). Finally, the samples were visualized by imaging ellipsometry, which is a diagnostic method based on the determination of changes in polarized light upon its reflection from a scanned surface and allowing us to detect deposited material having thickness as low as a few nanometers. Ellipsometry measurements were performed using a variable angle multi-wavelength imaging ellipsometer (EP3, Nanofilm Surface Analysis GmbH) in air at room temperature at a wavelength of 554.3 nm at an angle of incidence of 42° and a field of view of 2000 μm × 2000 μm. A conventional PCSA (Polarizer–Compensator–Sample–Analyzer) null-ellipsometric procedure is used to obtain two-dimensional (2D) maps of ellipsometric Δ and Ψ angles [52]. In the following, the evolution of the Δ and Ψ angles are used as a semi-quantitative indication of the organic layer removal.

3.3. Coatings of bacterial endotoxins

The efficiency of the plasma treatment in terms of etching of pyrogenic biomolecules was studied with LPS, peptidoglycan (PGN) and lipid A, the latter constituting the major pyrogenic component of LPS. The samples were prepared following the same protocol used for deposition of proteins and poly-L-histidine, i.e. by spotting small droplets of 0.1% wt aqueous solution of these substances on polished Si wafers. The untreated samples as well as samples exposed to plasma discharges were examined by the same surface diagnostic methods used for proteins and poly-L-histidine. However, it has to be noted that in contrast to the protein samples, the deposits of bacterial endotoxins were rather spatially inhomogeneous (see figure 8), which made profilometric removal measurements unreliable.

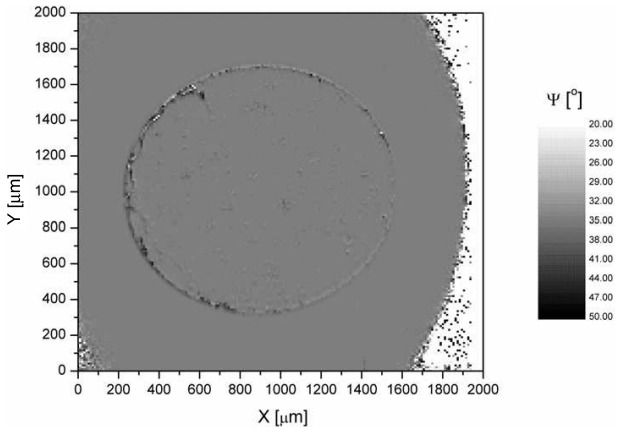

Figure 8. 2D map of ellipsometric angle Ψ of the lipid A sample.

In addition, the biological activity of the surface (i.e. its pyrogenicity) was evaluated by the 'whole blood test', which measures the production of interleukin IL-1β, induced by the contact between the contaminated surface and blood cells [53, 54]. To create a controlled surface contamination by pyrogens, 24 well plates were incubated with 100 μl of pyrogen solution (LPS, lipid A and PGN diluted in a range of 0.01–10 ng ml^{-1} for LPS and lipid A, and 0.1–10 μg ml^{-1} for PGN). The plates were dried overnight in a flow hood, exposed to the plasma discharge and afterwards tested by the whole blood incubation the next day in order to estimate remaining biological activity of the deposit. The surface biological activity was then evaluated before and after treatment by measuring the IL-1β cytokine release from human whole blood sample placed in contact with the surface treated. An enzyme-linked immunosorbent assay (ELISA) is used to measure the release of IL-1β, which is detected with commercially available antibody pairs (RD systems, Space Import-Export srl.). Detection of the biotinylated antibody is quantified by streptavidin-peroxidase (Biosource, Prodotti Gianni SpA) and its substrate TMB (3,3′,5,5′-tetramethylbenzidine; Sigma). Recombinant cytokines were used as standards (National Institute of Biological Standard and Control (NIBSC), South Mimms). Full details on the procedure can be found in [54].

3.4. Bacterial spores

The effect of plasma discharges on bacterial spores was studied using stainless steel coupons covered with a known number (about 2.5×10^6) of *Geobacillus stearothermophilus* spores (Raven Biological). As can be seen in figure 9, the spores on coupons are not disposed in a monolayer but are stacked and shielded by organic matter, which has a major impact on the treatment efficiency and kinetics.

Moreover, it has to be stressed that since the main aim of the present paper is to evaluate the capability of different discharges to erode or etch biological contamination, the treatment efficiency reported here refers solely to the degree of morphological changes of spores exposed to plasma, which was determined by scanning electron microscopy (SEM LEO 435VP). To the reader interested in further details concerning biological tests, we can recommend extensive literature devoted to this topic [12, 13, 15, 16, 24].

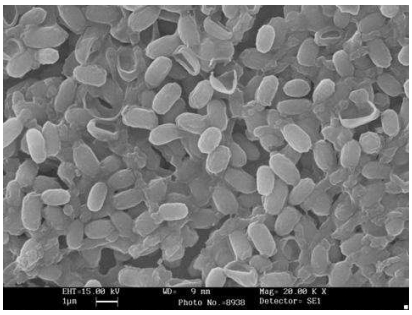

Figure 9. SEM image of untreated *G. stearothermophilus*.

4. Results obtained with the ICP discharge

The main objective of this section is to present a comprehensive study of plasma interaction with biological systems with emphasis to their etching processes. In order to meet this objective, the section is subdivided.

First, the experiments focused on the conditions leading to the fastest reduction of deposited biological matter as well as on the identification of possible mechanisms contributing to this process are presented. In these experiments, the etching rates of BSA selected as a model substance are measured under different operational conditions (discharge mixture composition, power and pressure). These results are then compared with the properties of the discharges determined by *in situ* plasma diagnostics, which enables estimation of roles of different agents leading to BSA removal.

Subsequently, the operational conditions identified to be the optimal for BSA elimination are used for the plasma processing of other biological samples to test the universality of such treatment on a wider set of different biological materials.

4.1. Model case of BSA

4.1.1. Screening tests. After the plasma treatment with an Ar/O_2 ICP discharge, visible modifications of the protein samples were observed indicating gradual removal of the protein deposit. An example of this behavior is given in figure 10, where the ellipsometric 2D maps of the Δ angles of a BSA sample before and after plasma treatment are presented.

Moreover, the etching rate of the deposit, evaluated by surface profilometry performed on the rings of the BSA spot, was found to be strongly dependent on the gas mixture used. This is demonstrated in figure 11, where the results of screening tests performed in pure argon, and its binary and ternary discharge mixtures with hydrogen, nitrogen and oxygen are summarized. It can be clearly seen that Ar, Ar/H_2 and Ar/N_2 discharges lead to approximately the same rate of BSA elimination (around 200 nm min^{-1}), whereas BSA is removed markedly faster in Ar/O_2 plasma at otherwise identical operational conditions (i.e. pressure, power and gas flow). The removal rates obtained in this last case were higher than 600 nm min^{-1}, showing importance of oxygen for fast volatilization of proteins. Moreover, it can be seen as well that etching efficiency of Ar/O_2 discharge is not enhanced either by nitrogen or by hydrogen addition. This also indicates that other molecular radicals produced in such plasmas, like OH or NO, whose presence has been confirmed by OES (figure 12), do not contribute significantly to the process of BSA elimination.

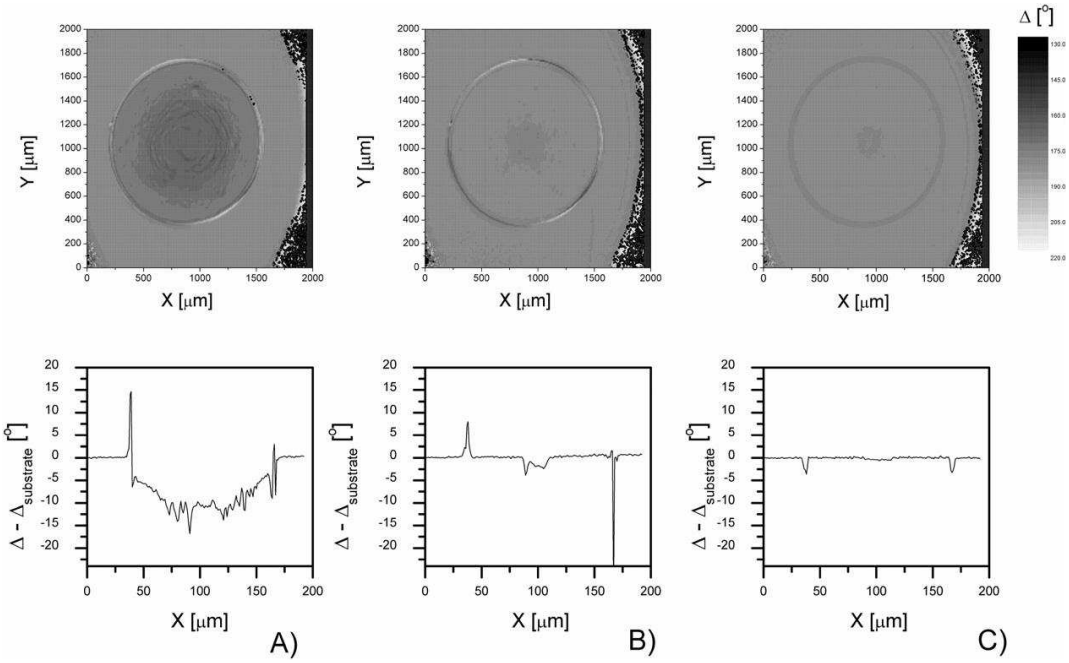

Figure 10. 2D maps of the Δ angles of BSA (upper row) and corresponding cross-sections (lower row) before treatment (a) and after 15 s (b) and 120 s (c) of treatment in Ar/O_2 20 : 1 mixture—protein dilution 1 mg ml^{-1}, Si wafer.

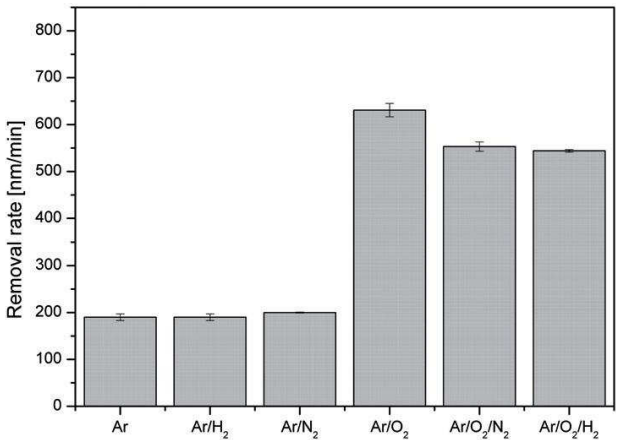

Figure 11. BSA etching rates—protein dilution 1 mg ml^{-1}, Si wafer, plasma treatment 10 Pa, 200 W, 22 sccm.

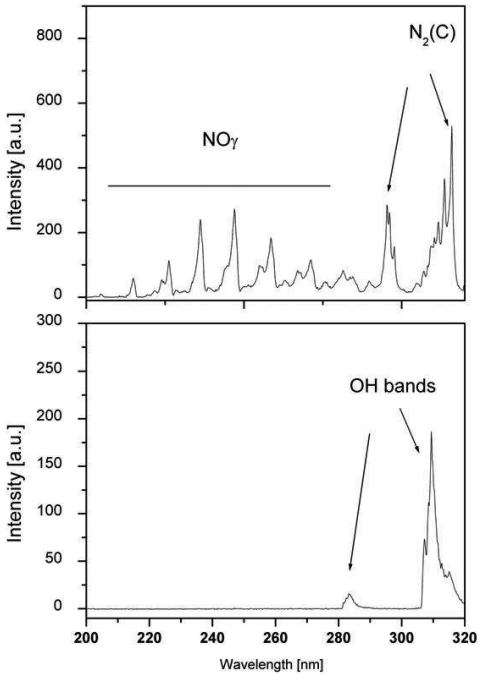

Figure 12. Optical emission spectra of $Ar/O_2/N_2$ 20 : 0.5 : 0.5 (upper) and $Ar/O_2/H_2$ 20 : 0.5 : 0.5 (lower) plasma discharges (10 Pa, 200 W, 22 sccm).

4.1.2. Ar/O_2 plasma discharge—process optimization. As demonstrated above, the BSA removal rate has been found to be the highest in Ar/O_2 mixture as compared with the discharges sustained in other gas mixtures. In order to identify the optimal treatment conditions, the etching rate was measured as a function of argon/oxygen ratio, pressure and applied RF power.

Regarding the dependence of removal rate on discharge mixture composition, it has been found that the addition of oxygen into argon leads initially to a strong enhancement of the BSA removal rate. Nevertheless, further increase of oxygen fraction in the Ar/O_2 mixture above approximately 10–15% results in a gradual decrease of removal efficiency as depicted in figure 13. Moreover, it can be seen that the pressure dependence of BSA etching rate changes with discharge mixture composition: whereas in argon-dominated mixtures increase of pressure causes increase of etching rate, the opposite trend has been observed in oxygen-rich mixtures.

Finally, the etching rate has been found to rise substantially with the applied RF power. For instance, a power increase from 200 to 300 W resulted in almost double the BSA removal rate in Ar/O_2 20 : 1.

4.1.3. Ar/O_2 ICP plasma discharge—study of etching mechanism

4.1.3.1. Influence of O atoms. As mentioned above, the capability of ICP discharges to eliminate BSA protein is strongly dependent on the presence of oxygen in the discharge mixture. Therefore, the main mechanism leading to the protein removal could be chemical etching. In order to test this hypothesis, O atom density in Ar/O_2 discharges has been measured by mass

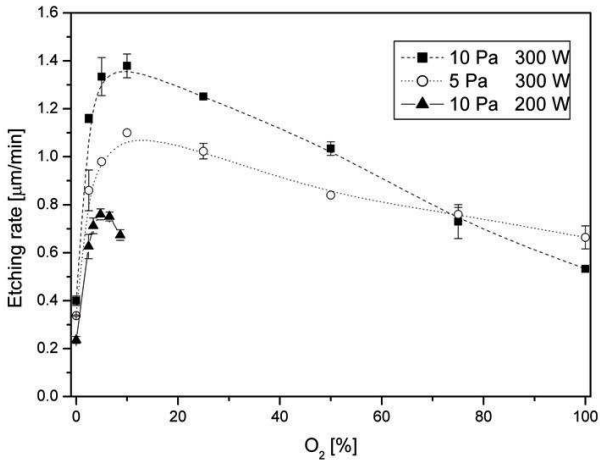

Figure 13. Etching rate of BSA as a function of Ar/O_2 discharge mixture composition (total gas flow 20 sccm).

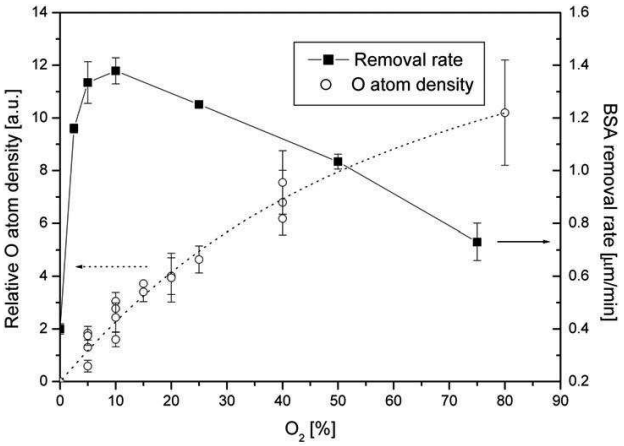

Figure 14. O atom density and BSA removal rate in Ar/O_2 (300 W, 10 Pa, 20 sccm).

spectroscopy and the obtained results were compared with BSA etching rates. It can be seen in figure 14 that the density of O atoms increases monotonically with rising O_2 content in the discharge mixture in contrast to the etching rate, which shows a well-defined maximum for Ar/O_2 ratio around 9 : 1. This finding therefore suggests that pure chemical etching is not dominant, or at least is not the only mechanism that causes BSA removal.

However, changing the composition of Ar/O_2 discharge mixture not only causes changes in the O atom density, but also in the density of positive ions as will be discussed later in the text. Therefore, to exclude the possible effect of ions, additional experiments were performed at fixed plasma density and variable O atom density, i.e. conditions achieved by simultaneously decreasing the argon over oxygen ratio and increasing the applied RF power. The results of

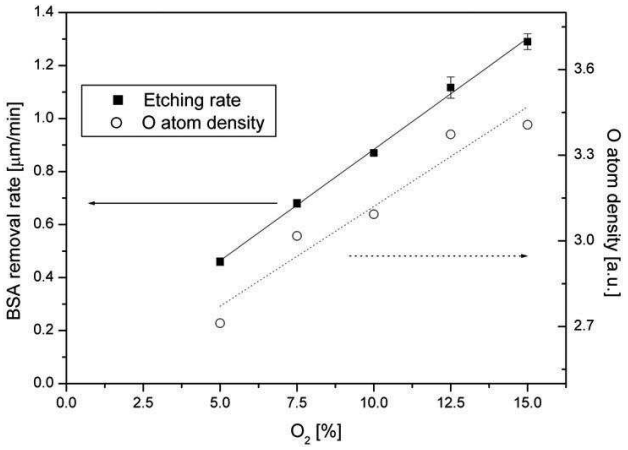

Figure 15. O atom density and etching rate at constant N_i (10 Pa, total gas flow 20 sccm).

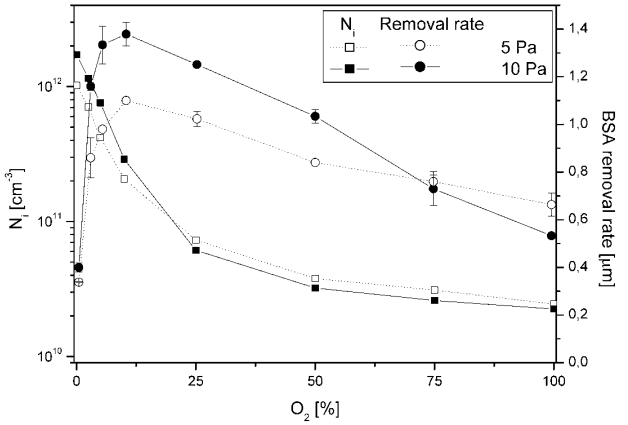

Figure 16. Ion density and BSA removal rate in the Ar/O_2 discharge (300 W, total gas flow 20 sccm).

these experiments revealed that the rate of BSA removal follows concentration of O atoms in the discharge (figure 15), which clearly shows that there exists a correlation between these two quantities.

4.1.3.2. Influence of charged particles. The removal of biological material from surfaces could be attributed to sputtering of the deposit by charged particles. However, this mechanism does not seem to be the major cause of the observed effects: the density of charged particles dramatically decreases with increasing O_2 fraction in the discharge mixture (see figure 16), which is in contrast to the evolution of the etching results. Furthermore, the energies of ions, measured by ion mass spectrometry, are too low to enable effective sputtering of BSA protein (figure 17): based on the preliminary experiments using ion beams with variable ions energy, effective organic material sputtering requires ion energy beyond 150–200 eV [55, 59].

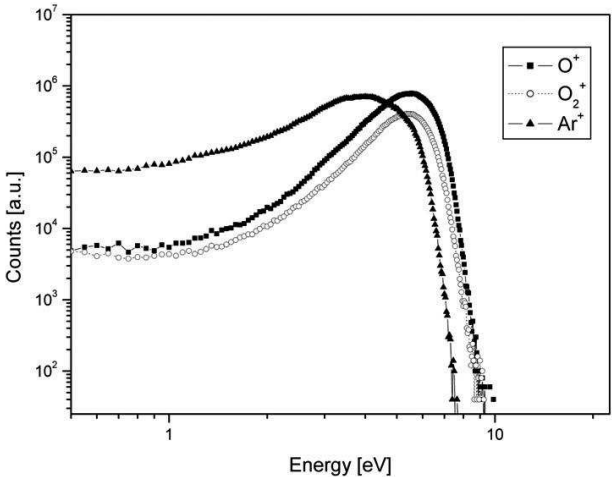

Figure 17. Energy distribution of positive ions (Ar/O_2 20 : 1, 10 Pa, 200 W).

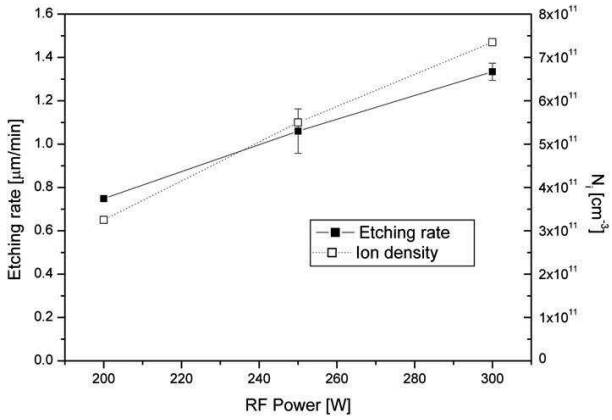

Figure 18. Comparison of ion density and the rate of BSA removal at constant O atom density (10 Pa, total gas flow 20 sccm).

Analogous to the case of evaluating the effect of O atoms, further experiments were performed at constant O atom density and variable plasma density. Such conditions were achieved by increasing applied RF power at fixed Ar/O_2 mixture composition and pressure, as verified both by mass spectrometry and OES. The results obtained in this set of experiments are summarized in figure 18, which shows that the rate of BSA removal follows plasma density. Since O atom density variations in these experiments are negligible, this result indicates the important contribution of charged particles to the process of protein elimination.

4.1.3.3. Combined effect of O atoms and ions. As demonstrated in the previous sections, the variation of the BSA removal rate with composition of the Ar/O_2 discharge mixture cannot be fully explained either by pure chemical etching connected with atomic oxygen or by sputtering

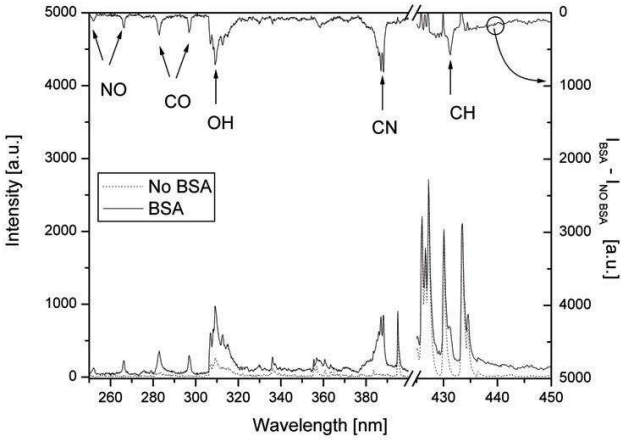

Figure 19. Optical emission spectra of Ar/O_2 20 : 1 plasma discharge with and without BSA sample in the ICP reactor acquired after 10 s of plasma duration together with their difference.

of the protein by energetic ions: it has been found that atomic oxygen alone does not contribute significantly to the etching of the films, while Ar sputtering is observed only at energies much higher than those measured in our experiments. Nevertheless, it was found that O atoms and ions together contribute to the process and therefore it can be assumed that their synergetic action is behind the observed behavior of the BSA removal rate. One possible reaction scheme combining the effects of O etching and impact of ions is the process of chemical sputtering. In this reaction scheme, the role of ions is a cleavage of bonds in the protein structure. This occurs by the displacement of atoms caused by impact of energetic ions, which leads to the creation of dangling bonds and thus to the rise of radical sites close to the protein surface. Such created sites react with impinging oxygen atoms leading to the formation of volatile products (such as CO, NO and OH) that are indeed observed in the emission spectra in the initial stage of plasma treatment (figure 19). These two sequences have to occur simultaneously because the passivation of an open bond by O species needs to happen faster than recombination in the cascade volume. In other words, cleavage of bonds in the protein structure by ions facilitate surface reaction of O atoms and enhance their natural capability to volatilize organic substances.

Obviously, the efficiency of this process is governed by fluxes of both ionic species and oxygen atoms to the protein surface, and the ratio of ion/atom fluxes need to be high to observe this effect. Whereas O atom density, and thus the flux of O atoms, increases with increasing O_2 in the discharge mixture (figure 14), leading to an enhancement of the removal of proteins, the density of charged particles steeply decreases at the same time (figure 16). The latter reduces the creation of defects in the protein film and consequently lowers the number of active reaction sites, thereby limiting the etching rate of the film. These two opposing effects can explain the appearance of a well-defined maximum of the etching rate at the conditions representing an optimal trade-off between the radicals' production and ion density.

This reaction scheme has also been observed in experiments performed on bacterial spores [56]–[58] and proteins [59] with Ar ions and O neutral beams applied for mimicking plasma effects. These experiments demonstrated the synergetic effect of O radicals and ions on

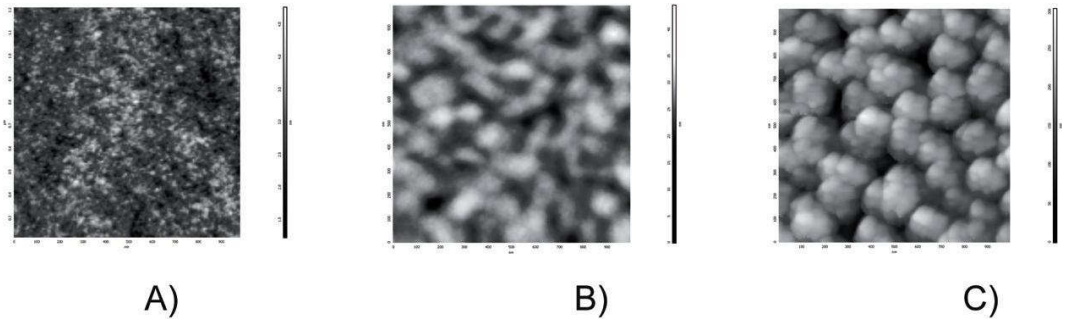

Figure 20. AFM images of $1 \times 1\,\mu$m section of BSA surfaces (a) before treatment and after 1 min treatment in (b) argon and (c) Ar/O_2 20 : 1 mixture (plasma treatment 10 Pa, 200 W).

decontamination of surfaces, further supporting the role of chemical sputtering in the removal of biological films by low pressure plasma discharges.

4.1.4. Detailed characterization of treated samples. In order to better characterize changes of chemical composition and morphology of protein samples, further experiments were performed using atomic force microscopy (AFM) and time-of-flight secondary ion mass spectroscopy (ToF-SIMS) on protein films before and after treatment.

It has been found that the etching of the protein films is not homogenous but accompanied by a strong increase of their roughness (see figure 20) indicating a spatial inhomogeneity of the etching process.

Moreover, a detailed investigation of temporal evolution of root mean square (rms) roughness of BSA samples exposed to plasma discharges revealed three distinct phases (see figure 21):

- Initially the rms roughness increases relatively slightly with the amount of removed material (denoted as phase I).
- After removal of a sufficient quantity of the protein film, a second phase starts, which is characterized by an enhanced increase of the rms roughness with increasing amount of removed BSA.
- Finally, as soon as the amount of removed material reaches a value close to the initial thickness of protein deposit, the surface roughness starts to decrease with further protein removal.

Whereas the transition between phases II and III, observed also in previous study [60], can be easily identified as the point at which underlying Si substrate is locally reached by plasma treatment, the transition between phases I and II remains unclear. This phenomenon has already been observed in other studies, for instance, during the plasma etching of polymer resist, where it was attributed to an amplification of initially random defects created at the surface, related to a local preferential sputtering due to the change of angle of incidence of ions impinging the defects' surface when the surface topography evolves.

Another possibility can be related to the presence of inorganic compounds or impurities in the protein native structure or preparation (sulphur, sodium, calcium, etc). Plasma discharge in the first phase volatilizes carbon-containing species, but due to the presence of inorganic

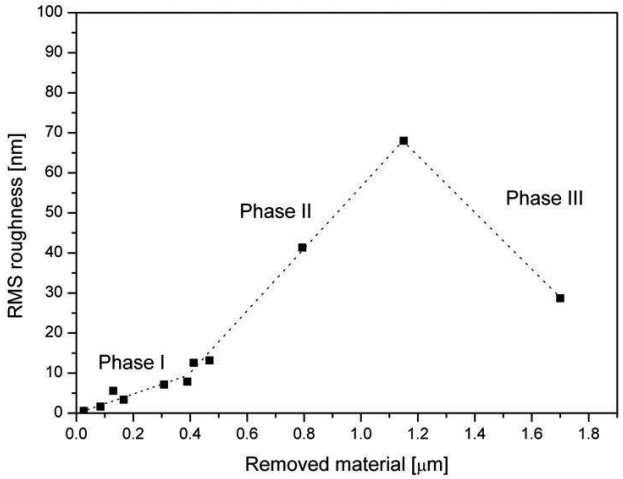

Figure 21. Variation of rms roughness with the total amount of etched material.

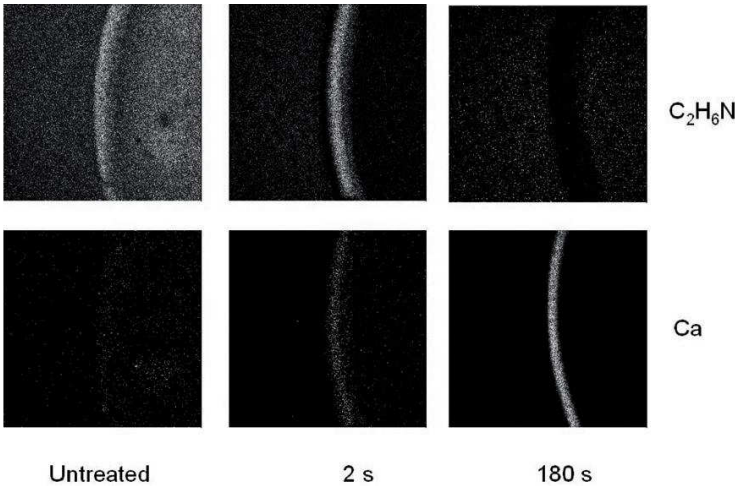

Figure 22. ToF-SIMS 2D maps of distribution of C_2H_6N and Ca on samples treated in Ar/O_2 20 : 1 mixture (10 Pa, 200 W).

compounds that are distributed in the deposit, certain parts of protein surface will be enriched in such compounds, which are much more difficult to remove. Subsequent plasma action will therefore remove preferably the parts not covered by these inorganic residuals. The delayed onset of the phase II can be—under this hypothesis—caused by time needed for the formation of local sites with high density of non-volatile residuals.

Although another series of dedicated experiments are still necessary for identification of process leading to the observed time evolution of surface roughens of treated samples, the presence and densification of non-organic compounds with treatment time has been confirmed by means of ToF-SIMS analysis. As is demonstrated in figure 22, the organic compounds

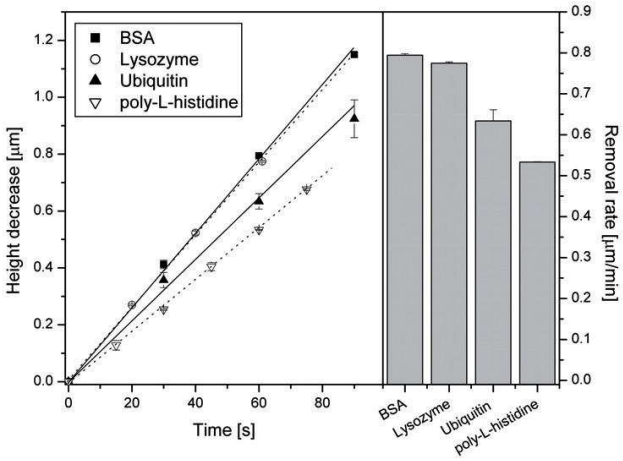

Figure 23. Temporal variation of height decrease of BSA, lysozyme, ubiquitin and poly-L-histidine (left panel) and corresponding removal rates (right panel) (Ar/O_2 20 : 1, 10 Pa, 200 W).

characteristic for proteins (C, H, O and N containing compounds) gradually disappeared from mass spectra with plasma treatment, the fraction of inorganic compounds increases and finally such compounds represent the only remaining material.

4.2. Application of Ar/O_2 plasma for elimination of other biological species

In order to demonstrate the capability of Ar/O_2 ICP plasma discharge optimized for BSA to remove other biological deposits, further experiments were performed using different proteins, as well as poly-L-histidine, lipid A and bacterial spores. To limit the heating of the samples during their plasma treatment, the applied RF power was decreased to 200 W.

Regarding the plasma etching efficiency of different proteins and poly-L-histidine, i.e. one elemental building blocks of proteins, we observe only relatively small differences in terms of their etching rates as depicted in figure 23. However, these differences can be caused by variable presence of inorganic compounds—for instance poly-L-histidine solution was prepared from HCl-containing powders—whose presence could influence the removal efficiency. Moreover, it should be noted that a recent study performed on different homopolymers of amino acids revealed that their etching rates are very similar in spite of their distinct chemical properties [61]. This finding, i.e. similarity of the etching rates of various biomolecules, supports the proposed mechanism of chemical sputtering. For the initiation of the destruction of biomolecules, active sites have to be formed on their surfaces. In the case of pure chemical etching in oxygen containing mixtures, this is achieved by hydrogen abstraction from the polymeric structure, which is a process highly dependent on the exact chemical structure of treated substance. In contrast, in the case of chemical sputtering, the active sites are generated by bond cleavage caused by impact of energetic ions, which is rather insensitive to the chemical composition of treated biomolecules in this energy range. This in turn makes the exact chemical structure of treated substance irrelevant for resulting etch rate as observed in our experiments.

As mentioned above, the samples of bacterial endotoxins were highly spatially inhomogeneous and therefore it was not possible to estimate their removal rate directly.

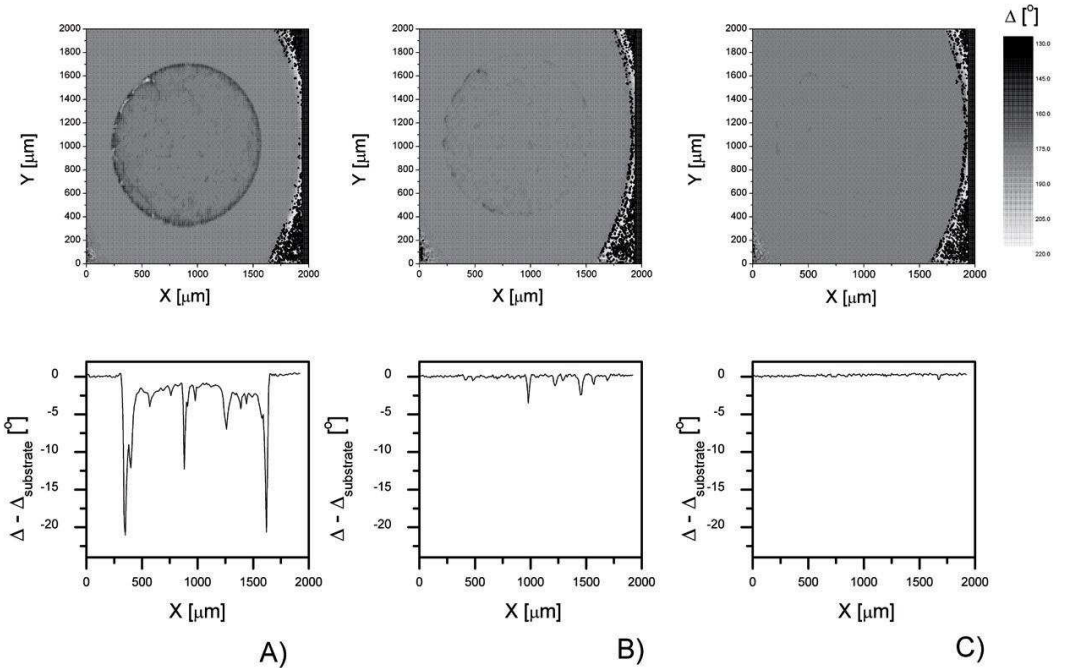

Figure 24. 2D maps of ellipsometric angle Δ and corresponding cross-sections of lipid A sample (a) untreated (b) treated 10 s and (c) sample treated 270 s in Ar/O_2 20 : 1 plasma (10 Pa, 200 W).

However, imaging ellipsometry showed that similarly to the previous cases, lipid A and PGN can be readily removed from the surface by Ar/O_2 plasma as can be seen in figures 24 and 25, which show 2D maps of ellipsometric angles Δ of untreated and plasma treated samples together with their typical cross-sections.

Finally, it has been found that bacterial spores can also be significantly eroded by Ar/O_2 plasma discharge as demonstrated in figure 26. This finding clearly demonstrates, contrary to the statements made previously [62], that etching can significantly contribute to the sterilization process; etching can explain fast inactivation of bacterial spores in those plasma discharges where only limited intensity of UV radiation is produced.

Nevertheless, our results also revealed a significant difference between plasma treatment of biomolecules and spores: namely temporal nonlinearity of the etching rate and the much lower values obtained in the case of spores (see figure 27). This is most likely due to much higher fraction of inorganic compounds in the spores' outer walls than in the protein samples, which reduces the efficiency of the process.

4.3. Concluding remarks

It has been demonstrated that the ICP plasma discharge is capable of effectively removing or eroding a wide range of biomolecules having distinctly different chemical structures as well as bacterial spores representing highly resistant types of micro-organisms. Regarding the rates of

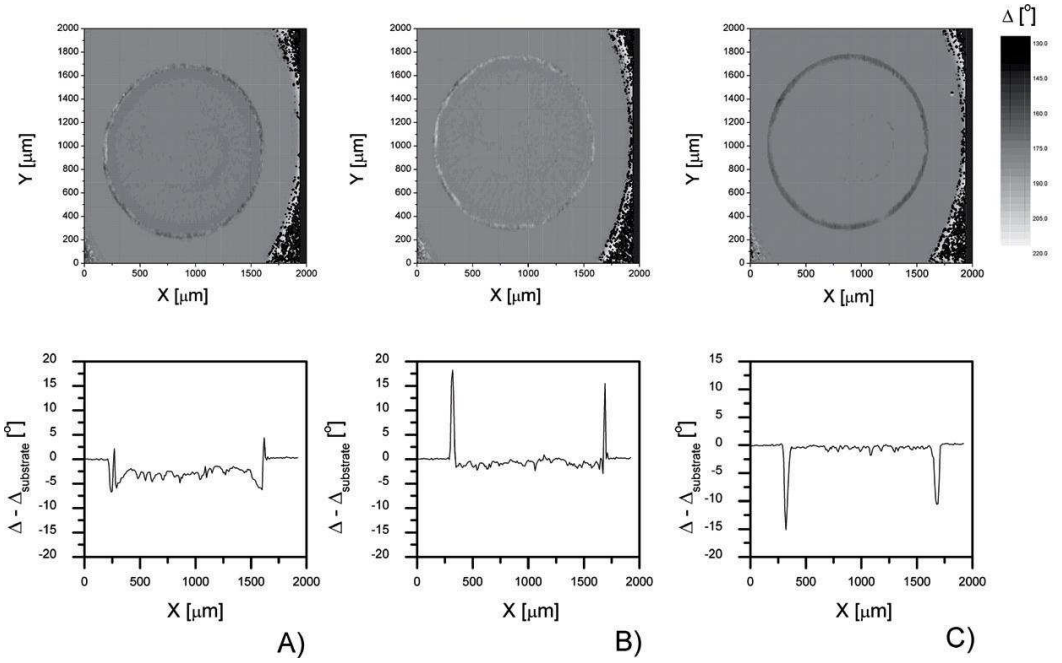

Figure 25. 2D maps of ellipsometric angle Δ and corresponding cross-sections of PGN sample (a) untreated (b) treated 10 s and (c) sample treated 270 s in Ar/O_2 20 : 1 plasma (10 Pa, 200 W).

these processes, their highest values can be achieved in an Ar/O_2 discharge mixture. It has been shown that this is a result of not only high fluxes of O atoms reaching the treated samples but also by the action of ions bombarding their surfaces and thus promoting creation of surface active sites. Moreover, it should be noted that this discharge mixture was already found to inactivate effectively bacterial spores (e.g. 6 log reduction of surviving spores was reported to be achieved within 40 s of plasma treatment under similar operational conditions [61]). Therefore, the plasma treatment based on the Ar/O_2 discharge mixture has all the pre-conditions to be a highly universal sterilization and decontamination method.

In spite of these highly encouraging results, certain drawbacks of the process based solely on extensive etching of pathogens have to be mentioned.

Firstly, it has been demonstrated that Ar/O_2 plasma is not well suited for volatilization of inorganic compounds. This results in severe implications for application of this approach in a real situation, when the pathogens are for instance mixed with salts originating from body fluids or contain such compounds *per se*, as in the case for bacterial spores. The markedly lower etching rates connected with presence of inorganic compounds implies the necessity of longer treatment duration that consequently represents risk of degradation of treated objects by their extensive heating. The effect of heating can be significantly reduced either by pulsing the discharge, or—as suggested recently for the case of bacterial spores—by application of ternary $Ar/O_2/N_2$ [63, 64], or Ar/NO [65] mixtures providing not only high etching rates but also intense UV radiation capable of inactivating spores effectively. However, the persistence of

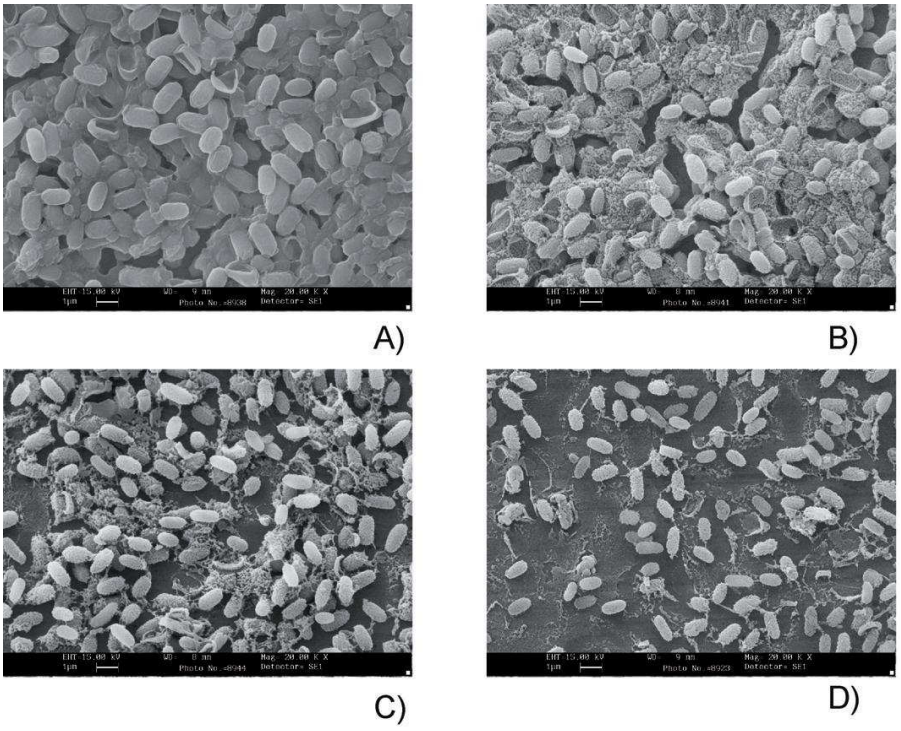

Figure 26. SEM images of (a) untreated *G. stearothermophilus* spores and spores treated for (b) 30 s (c) 60 s and (d) 120 s (Ar/O_2 20 : 1, 10 Pa, 200 W).

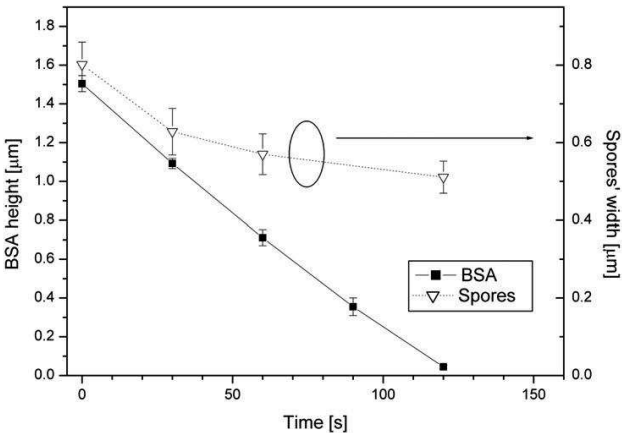

Figure 27. Comparison of etching of BSA and *G. stearothermophilus* spores (Ar/O_2 20 : 1, 10 Pa, 200 W).

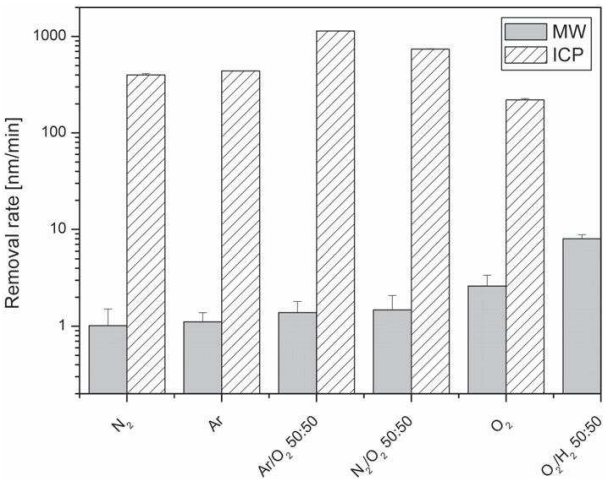

Figure 28. Comparison of BSA removal rates in ICP and MW reactors (ICP: 300 W, 10 Pa, 20 sccm; MW: 1000 W, 13 Pa, 100 sccm).

remaining inorganic material, whose relevance for the safety of medical instruments still needs to be investigated, seems to be the limiting factor of the process based on oxygen-containing mixtures.

Secondly, the conditions suitable for effective etching of biological samples can cause etching also of surfaces of polymer-based instruments, or at least could induce significant alterations of their chemical and physical properties. For instance, recent comparison of the effect of different sterilization methods on polyethylene glycol coatings revealed that their exposure to plasma leads to a much faster decrease of their non-fouling character as compared with traditional sterilization techniques [66]. Therefore, other approaches have to be developed to limit these undesirable effects.

5. Results obtained with the MW discharge

As mentioned above, basing sterilization and decontamination of surfaces solely of etching has certain drawbacks, connected mainly with undesirable etching of polymeric substrates. Moreover, it has been demonstrated that for fast etching of biomolecules, high flux of ions on their surfaces is necessary. Therefore in order to reduce the possible impact of plasma processes on the treated objects, further experiments were performed using a MW plasma reactor with samples placed downstream of the active discharge.

5.1. Etching of proteins

As expected, placing samples outside the active plasma zone has a strong impact on the etching of biomolecules: whereas in the case of the ICP reactor the BSA etching rates were typically higher than 200 nm min^{-1}, the values obtained in the case of a post discharge were not greater than several nanometers per minute as can be seen in figure 28, which compares BSA etching rates in different gas mixtures.

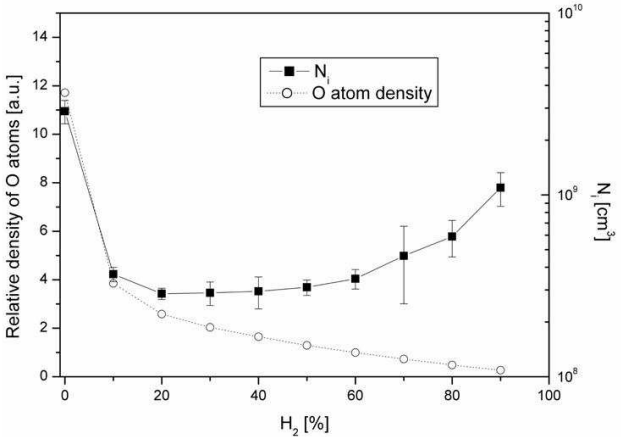

Figure 29. O atom density and ion density in O_2/H_2 MW discharge (1000 W, 13 Pa, 100 sccm).

Moreover, the optimal discharge mixture in terms of BSA removal differs for the two employed plasma discharges: whereas in the case of ICP discharge, the fastest BSA removal was achieved in Ar/O_2 mixture having low fraction of oxygen, the discharge offering highest efficiency of removal of BSA in the MW reactor is the one sustained in an O_2/H_2 mixture. However, unlike the case of ICP discharge, the increased etching rate after hydrogen addition into oxygen discharge cannot be explained by chemical sputtering, since both O atom density and ion density decrease with increasing amounts of hydrogen as can be seen in figure 29. Therefore, the observed tendency has to be explained purely by action of chemically active radicals produced under such conditions. In order to volatilize organic compounds, active sites have to be created on the deposit surface first, which can be done either by impact of ions as described in the previous section, or by abstraction of hydrogen from the polymeric structure of treated material. This can proceed by chemical reaction with atomic oxygen, but also by reaction with H atoms or highly reactive OH radicals, both effectively produced in O_2/H_2 plasma discharge (see figure 30), which can in turn explain the observed results.

5.2. Bacterial endotoxins

Similarly to BSA protein, the fastest removal rate of bacterial endotoxins can be achieved in the MW reactor in O_2/H_2 mixture as reported previously [14]. However, the rate of this process is again markedly lower than that obtained in the ICP reactor. Nevertheless, biological tests performed on untreated and treated samples showed significant decrease of their bio-activity after their exposure to the plasma discharge. Concretely, as can be seen in figure 31, the bioactivity of 1 ng of coated LPS decreased after 5 min of the treatment to the value lower than that corresponding to the pyrogenicity of 0.001 ng of the initially deposited material. In other words, 5 min of plasma treatment is sufficient to cause decrease of LPS bioactivity corresponding to more than 3 log lower than initial contamination.

Similar depyrogenation efficiency was observed for other hydrogen containing discharge mixtures (see figure 32) that offers even markedly lower etching rates of pyrogens than that

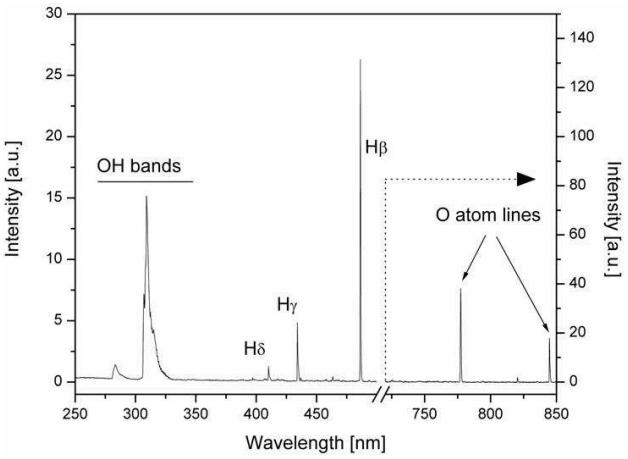

Figure 30. Optical emission spectra of O_2/H_2 50 : 50 MW discharge (1000 W, 13 Pa, 100 sccm).

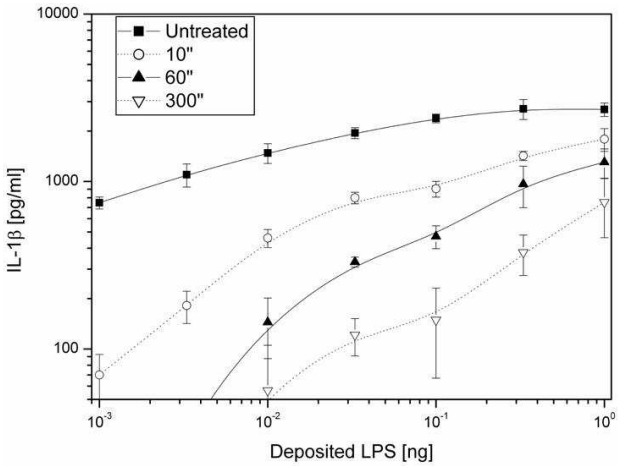

Figure 31. LPS pyrogenicity before and after its treatment in O_2/H_2 50 : 50 MW discharge (1000 W, 13 Pa, 100 sccm).

obtained in O_2/H_2 mixture [14]. This is a finding of high importance, since it clearly shows that depyrogenation of surfaces can be reached not only by physico-chemical elimination of pyrogenic substances from surfaces as in the case of ICP discharge but also by alteration of their chemical structure.

In order to evaluate the chemical changes leading to the suppression of the pyrogens' bioactivity, ToF-SIMS analysis was performed on treated and untreated Lipid A, i.e. pyrogenic center of LPS. As can be seen in figure 33 and in detail in figure 34, treatment in hydrogen containing mixtures cause significant changes in the ToF-SIMS spectra, namely rapid decrease

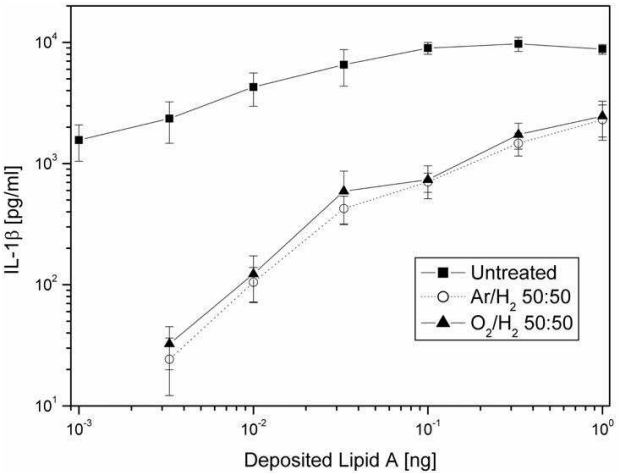

Figure 32. Lipid A pyrogenicity before and after 60 s of its treatment in O_2/H_2 50 : 50 MW discharge (1000 W, 13 Pa, 100 sccm).

of the peaks originating from the fatty acid chains (e.g. $C_{12}H_{23}O_2$ and $C_{14}H_{27}O_2$) as well as substantial alterations of phosphoryl groups (PO, PO_2, PO_3 and PH_2O_4), i.e. two parts of lipid A structure suggested to govern its bioactivity.

However, the mechanism leading to such modification is still not clear, and it should be noted that a similar effect has been observed after irradiation of lipid A samples by intense VUV radiation emitted by a deuterium lamp having the peak of radiation intensity at 162 nm (see figure 35), which shows that VUV radiation removes peaks corresponding to the whole lipid A molecule as well as its major fragments. Therefore, one possible explanation refers to the degradation of lipid A induced by intense VUV radiation emitted by hydrogen-containing plasma discharges.

5.3. Concluding remarks

As was demonstrated on the example of the MW reactor, placing samples to the plasma afterglow reduces drastically the removal rate of the biomolecules. This effect is produced predominantly by the significant decrease of ion flux reaching surface of the samples, which in turn leads to the lowering of the importance of chemical sputtering that plays a major role in the active discharge. However, this effect can be seen from two different points of view, depending on the particular application. It is obvious that lowering etching rates of organic materials slows down the efficiency of the sterilization and decontamination process and thus represents a clear disadvantage as compared with the treatment done in the active plasma zone. In contrast, this approach lowers adverse impact of the treatment on the integrity and properties of processed instruments. Moreover, it has been demonstrated as well that even under conditions leading to almost negligible physico-chemical removal of biomolecules from surfaces, it is possible to find out conditions leading to the fast decrease of their bioactivity. Nevertheless, concerning this issue, it is important to stress that optimal conditions for inactivation of biological pathogens are strongly dependent on their nature. As an example of the selectivity of plasma post-discharge,

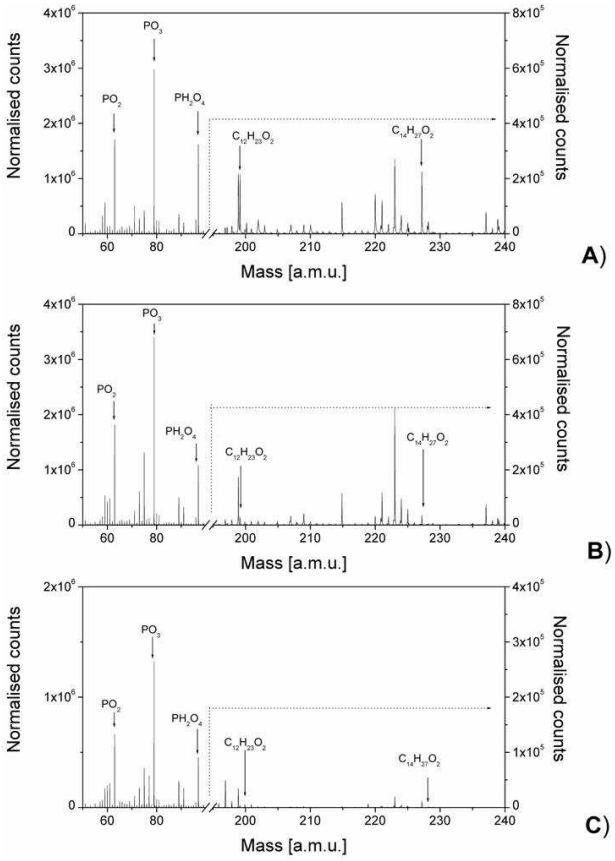

Figure 33. ToF-SIMS spectra of untreated lipid A (a) and lipid A treated 10 s in (b) Ar/H_2 50 : 50 and (c) O_2/H_2 50 : 50 MW discharges (1000 W, 13 Pa, 100 sccm).

the inactivation of bacterial spores requires high intensity of UV radiation that cannot be achieved in hydrogen-based mixtures found to be advantageous for depyrogenation of bacterial endotoxins. Therefore, the process based on the inactivation lacks universality of the process based on the extensive etching of biological systems. Moreover, it is still not clear whether chemical inactivation is possible for all types of pathogens.

6. Conclusions

While the use of plasma discharges for the sterilization of bacterial spores has been studied in detail in the past few years, relatively fewer results have been published concerning the removal of proteins and pyrogens from surgical instruments. Recent studies revealed, however, that the limited effect of the present decontamination and sterilization procedures pose a real public health problem. Therefore, the possibility to eliminate such biomolecules by two types of low-pressure plasma treatment was addressed in this study.

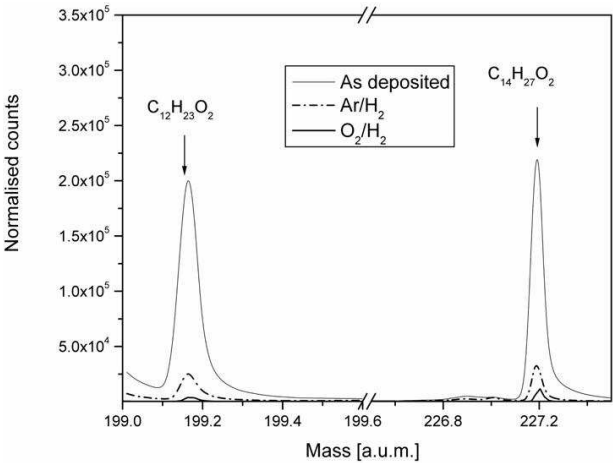

Figure 34. Part of ToF-SIMS spectra of untreated lipid A and lipid A treated 10 s in different MW discharges (1000 W, 13 Pa, 100 sccm).

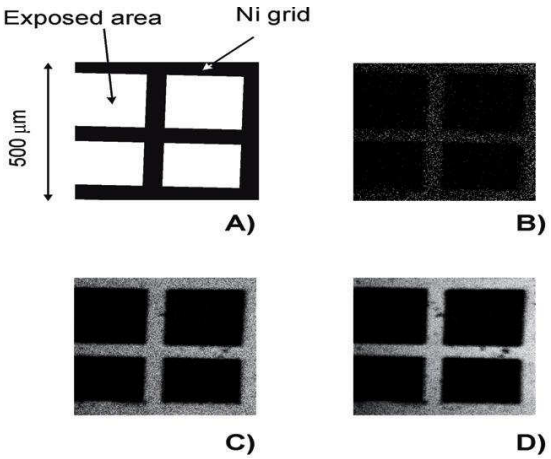

Figure 35. (a) Geometry of grid placed on the lipid A sample and corresponding 2D chemical maps of samples irradiated by VUV lamp, (b) whole lipid A image, (c) $C_{12}H_{23}O_2$ peaks and (d) $C_{14}H_{27}O_2$ peak (the squares correspond to lipid A exposed to VUV and destroyed by the radiation).

It was demonstrated, using model proteins and peptides, that biomolecules having distinctly different properties can be efficiently removed by directly exposing the surface to be treated to low pressure ICP discharges. Analysis of various discharges shows that Ar/O_2 mixtures are the most efficient for a fast removal of these residues by a mechanism related to chemical sputtering involving both radicals and ions. This mechanism also intervenes for bacterial spores that are inactivated and destroyed by etching as well, which is advantageous

mainly with respect to the universality of this approach. Nevertheless, the etching of biomolecules could be accompanied by etching of substrate materials.

Different conclusions can be drawn concerning treatment performed in a post discharge. Although in this case it is still possible to sterilize bacterial spores laying on a surface by the UV radiation emitted in post-discharge or inactivate pyrogens by the chemical reaction of radicals with their surfaces, the protein removal rates observed in a post discharge are much lower as compared with a direct plasma treatment. This result illustrates the problem related to the treatment of real surgical instrument surfaces: since the practical experience obtained from hospitals shows that protein residues can be found on a significant proportion of surgical tools after the decontamination, the strategy relying on a post discharge treatment can be questioned, since no assurance can be given that these residues will be harmless after treatment. These findings have a serious implication on the type of material that can be treated without serious deleterious effects.

However, our results have to be confirmed by experiments on more relevant types of contamination (involving inorganic compounds, lipids, blood, etc), since complex matrices can significantly reduce the etching rates obtained on pure proteins.

Acknowledgments

This work has been supported by the FP6 2005 NEST project 'Biodecon'. We thank K Stapelmann and B Denis for technical help during experiments.

References

[1] Klevens R M, Edwards R, Richards C L, Horan T C, Gaynes R P, Pollock D A and Cardo D M 2007 *Public Health Rep.* **122** 160–6
[2] Kmietowicz Z 2000 *Br. Med. J.* **320** 534
[3] Anonymous. Délégation Générale de la Santé. http://www.sante.gouv.fr/htm/pointsur/nosoco
[4] Anonymous. Dipartimento di Sanita Pubblica, Università degli Studi di Firenze. http://www.anio.it/file/15_infezioni_ospedaliere.pdf
[5] Lipscomb I P, Sihota A K, Botham M, Harris K L and Keevil C W 2006 *J. Hosp. Infect.* **62** 141–8
[6] Lipscomb I P, Sihota A K and Keevil C W 2008 *J. Hosp. Infect.* **68** 52–8
[7] Baxter L, Baxter H C, Campbell G A, Grant K, Jones A, Richardson P and Whittaker G 2006 *J. Hosp. Infect.* **63** 439–44
[8] Murdoch H, Taylor D, Dickinson J, Walker J T, Perrett D, Raven N D H and Sutton J M 2006 *J. Hosp. Infect.* **63** 432–8
[9] Tsuji K and Harrison S J 1978 *Appl. Environ. Microbiol.* **36** 710–4
[10] Ludwig J D and Avis K E 1990 *J. Parenter. Sci. Technol.* **44** 4–12
[11] Moesby L, Hansen E W, Christensen J D, Hoyer C H, Juhl G L and Olsen H B 2005 *Eur. J. Pharm. Sci.* **26** 318–23
[12] Moisan M, Barbeau J, Moreau S, Pelletier J, Tabrizian M and Yahia L'H 2001 *Int. J. Pharm.* **226** 1–21
[13] Lerouge S, Wertheimer M R and Yahia L'Y 2001 *Plasmas Polym.* **6** 175–88
[14] Rossi F, Kylián O and Hasiwa M 2006 *Plasma Process. Polym.* **3** 431–42
[15] Moisan M, Barbeau J, Crevier M-C, Pelletier J, Philip N and Saoudi B 2002 *Pure Appl. Chem.* **74** 349–58
[16] Laroussi M 2002 *IEEE Trans. Plasma Sci.* **30** 1409–15
[17] Laroussi M 2005 *Plasma Process. Polym.* **2** 391–400

[18] Laroussi M, Mendis D A and Rosenberg M 2003 *New J. Phys.* **5** 41
[19] Eto H, Ono Y, Ogino A and Nagatsu M 2008 *Appl. Phys. Lett.* **93** 221502
[20] Feichtinger J, Schulz A, Walker M and Schumacher U 2003 *Surf. Coat. Technol.* **174–175** 564–9
[21] Boudam M K, Moisan M, Saoudi B, Popovici C, Gherardi N and Massines F 2006 *J. Phys. D: Appl. Phys.* **39** 3494–507
[22] Halfmann H, Denis B, Bibinov N, Wunderlich J and Awakowicz P 2007 *J. Phys. D: Appl. Phys.* **40** 5907–11
[23] Lerouge S, Fozza A C, Wertheimer M R, Marchand R and Yahia L'H 2000 *Plasma Polym.* **5** 31–46
[24] Philip N, Saoudi B, Crevier M-C, Moisan M, Barbeau J and Pelletier J 2002 *IEEE Trans. Plasma Sci.* **30** 1429–36
[25] Nagatsu M, Terashita F, Nonaka H, Xu L, Nagata T and Koide Y 2005 *Appl. Phys. Lett.* **86** 211502
[26] Lerouge S, Wertheimer M R, Marchand R and Yahia L'H 2000 *J. Biomed. Mater. Res.* **51** 128–35
[27] Kylián O, Sasaki T and Rossi F 2006 *Eur. Phys. J. Appl. Phys.* **34** 139–42
[28] Cousty S, Villeger S, Sarette J P, Ricard A and Sixou M 2006 *Eur. Phys. J. Appl. Phys.* **34** 143–6
[29] Hayashi N, Guan W, Tsutsui S, Tomari T and Hanada Y 2006 *Japan. J. Appl. Phys.* **45** 8358–63
[30] Vujošević D, Mozetič M, Cvelbar U, Krstulović N and Milošević S 2007 *J. Appl. Phys.* **101** 103305
[31] Vratnica Z, Vujošević D, Cvelbar U and Mozetič M 2008 *IEEE Trans. Plasma Sci.* **36** 1300–1
[32] Vicoveanu D, Popesco S, Ohtsu Y and Fujita H 2008 *Plasma Process. Polym.* **5** 350–8
[33] Beutler B, Hoebe K, Du X and Ulevitch R J 2003 *J. Leukoc. Biol.* **74** 479–85
[34] Kylián O, Hasiwa M and Rossi F 2006 *IEEE Trans. Plasma Sci.* **34** 2606–10
[35] Williams D 2003 *Med. Device Technol.* **14** 8–11
[36] Kylián O, Hasiwa M and Rossi F 2006 *Plasma Process. Polym.* **3** 272–5
[37] Hasiwa M, Kylián O, Hartung T and Rossi F 2008 *Innate Immun.* **14** 89–97
[38] Taylor D M 1999 *J. Hosp. Infect.* **43** S69–76
[39] Lipscomb I P, Sihota A K and Keevil C W 2006 *J. Clin. Microbiol.* **44** 3728–33
[40] Baxter H C, Campbell G A, Whittaker A G, Jones A C, Aitken A, Simpson A H, Casey M, Bountiff L, Gibbard L and Baxter R L 2005 *J. Gen. Virol.* **86** 2393–9
[41] Mogul R, Bol'shakov A A, Chan S L, Stevens R M, Khare B N, Meyyappan M and Trent J D 2003 *Biotechnol. Prog.* **19** 776–83
[42] Ceccone G, Gilliland D, Kylián O and Rossi F 2006 *Czech. J. Phys.* **56** B672–7
[43] Baxter H C, Campbell G A, Richardson P R, Jones A C, Whittle I R, Casey M, Whittaker A G and Baxter R L 2006 *IEEE Trans. Plasma Sci.* **34** 1337
[44] Bernard C, Leduc A, Barbeau J, Saoudi B, Yahia L'H and De Crescenzo G 2006 *J. Phys. D: Appl. Phys.* **39** 3470–8
[45] Deng X T, Shi J J, Chen H L and Kong M G 2007 *Appl. Phys. Lett.* **90** 013903
[46] Deng X T, Shi J J and Kong M G 2007 *J. Appl. Phys.* **101** 074701
[47] Kylián O, Rauscher H, Gilliland D, Brétagnol F and Rossi F 2008 *J. Phys. D: Appl. Phys.* **41** 095201
[48] Kylián O, Rauscher H, Sirghi L and Rossi F 2008 *J. Phys.: Conf. Ser.* **100** 062017
[49] Moreau S, Moisan M, Tabrizian M, Barbeau J, Pelletier J, Ricard A and Yahia L'H 2000 *J. Appl. Phys.* **88** 1166–74
[50] Villeger S, Ricard A and Sixou M 2004 *Eur. Phys. J. Appl. Phys.* **26** 203–8
[51] Cvelbar U, Vujošević, Vratnica Z, and and Mozetič M 2006 *J. Phys. D: Appl. Phys.* **39** 3487–93
[52] Tompkins H G and Irene E A (ed) 2005 *Handbook of Ellipsometry* (Berlin: Springer)
[53] Mazotti F, Hartung T and von Aulock S 2007 *J. Biomed. Mater. Res.* A **80** 276–82
[54] Hasiwa M, Kullmann K, von Aulock S, Klein C L and Hartung T 2007 *Biomaterials* **3** 1367–75
[55] Eckstein W 1991 *Computer Simulation of Ion Solid Interactions* 1st edn (*Springer Series in Materials Science*) (Berlin: Springer)
[56] Opretzka J, Benedikt J, Awakowicz P, Wunderlich J and von Keudell A 2007 *J. Phys. D: Appl. Phys.* **40** 2826–30

[57] Raballand V, Benedikt J, Wunderlich J and von Keudell A 2008 *J. Phys. D: Appl. Phys.* **41** 115207
[58] Benedikt J, Flötgen C, Kussel G, Raballand V and von Keudell A 2008 *J. Phys.: Conf. Ser.* **133** 012012
[59] Kylián O, Benedikt J, Sirghi L, Reuter R, Rauscher H, von Keudell A and Rossi F 2009 *Plasma Process. Polym.* **6** 255
[60] Rossi F, Kylián O, Rauscher H, Gilliland D and Sirghi L 2008 *Pure Appl. Chem.* **80** 1939–51
[61] Kylián O, Rauscher H, Denis B, Ceriotti L and Rossi F 2009 submitted
[62] Halfmann H, Bibinov N, Wunderlich J and Awakowicz P 2007 *J. Phys. D: Appl. Phys.* **40** 4145–54
[63] Stapelmann K, Kylián O, Denis B and Rossi F 2008 *J. Phys. D: Appl. Phys.* **41** 192005
[64] Kylián O and Rossi F 2009 *J. Phys. D: Appl. Phys.* **42** 085207
[65] Hueso J L, Rico V J, Frías J E, Cotrino J and Gonzáles-Elipe A R 2008 *J. Phys. D: Appl. Phys.* **41** 2002
[66] Bretagnol F, Rauscher H, Hasiwa M, Kylián O, Ceccone G, Hazell L, Paul A J, Lefranc O and Rossi F 2008 *Acta Biomater.* **4** 1745–51

Elimination of Homo-Polypeptides of Amino Acids from Surfaces by Means of Low Pressure Inductively Coupled Plasma Discharge

Ondřej Kylián, Hubert Rauscher, Benjamin Denis, Laura Ceriotti, François Rossi*

The action of low-pressure inductively coupled plasma discharge on selected homo-polypeptides of amino acids, i.e., fundamental building blocks of proteins, has been investigated in order to evaluate their removal rates under different treatment conditions. It has been found that the removal rates of the homo-polypeptides studied are strongly linked to the composition of the plasma discharges, but they are almost insensitive to their chemical composition. This provides an indication that all proteins could be removed at similar rates by a given plasma discharge, which is a finding of paramount importance mainly with respect to decontamination of surfaces and elimination of infectious proteins like prions.

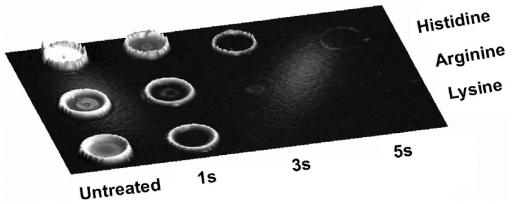

Introduction

Inactivation of living micro-organisms as well as elimination of diverse pathogenic biomolecules, which can be present on surfaces of medical instruments, is of paramount importance in health care facilities. However, according to recent studies pointed on the evaluation of the level of biological contamination of reprocessed medical equipment, it appeared that the currently used sterilization and decontamination methods are in many cases inadequate to assure complete inactivation or elimination of biological pathogens, which is especially true in the case of proteins.[1–3] As a result, a large number of medical instruments exhibits a high degree of protein soiling after their routine sterilization and decontamination, which imposes a risk for the patients' health connected with possible transmission of severe diseases classified as transmissible spongiform encephalopathies (e.g., Creutzfeld–Jacob Disease).[4] Therefore, there is an urgent demand from the side of hospital sterilization services for the development of improved sterilization and decontamination methods.

One of the intensively discussed options to overcome limitations of the traditional decontamination techniques consists in the application of non-equilibrium plasma discharges. This is in the first place due to the capability of such plasma discharges not only to inactivate bacterial spores (e.g., review articles[5–9]), but also to eliminate a wide range of biological pathogens, comprising bacterial endotoxins,[9–12] and infectious prions.[13] Furthermore, the non-toxicity of commonly used gases and gas mixtures is also an advantage because it reduces environmental risks. Last but not least, plasma discharges operate, under appropriate conditions, at low temperatures, and allow the treatment of thermo-degradable objects.

However, it should be noted that the knowledge regarding the possibility of prions removal by means of

O. Kylián, H. Rauscher, B. Denis, L. Ceriotti, F. Rossi
European Commission, Joint Research Centre, Institute for Health and Consumer Protection, Via E. Fermi, 21027 Ispra (VA), Italy
Fax: +39 0332 785787; E-mail: francois.rossi@jrc.ec.europa.eu
O. Kylián
Charles University in Prague, Faculty of Mathematics and Physics, V Holešovičkách 2, Prague 8, 180 00, Czech Republic
B. Denis
Institute for Electrical Engineering and Plasma Technology, Ruhr–Universität Bochum, Universitätsstrasse 150, 44780 Bochum, Germany

Plasma Process. Polym. **2009**, *6*, 848–854

DOI: 10.1002/ppap.200900027

plasma discharges is rather limited. This is mainly due to the extremely high level of biohazard connected with these biomolecules that in turn represents a serious restriction for routine testing and optimization of the plasma treatment. In order to overcome this principal obstacle, non-pathogenic proteins were used as model systems to study the mechanisms of plasma–protein interactions as well as for identification of favourable conditions for their elimination.[14–21] Although it has been shown recently that different proteins (namely bovine serum albumin, lysozyme and ubiquitine) can be removed from surfaces at the same treatment conditions with similar rates,[20] the generalization of this finding to other proteins, including infectious prions, is rather questionable because of the limited set of proteins used so far and the large variety of chemical and structural properties of proteins. Although it is in principle possible to repeat experiments using more non-pathogenic proteins as sample substances, the generalization of the results is going to remain still of relevance.

Therefore, instead of evaluating the removal rates of a larger number of proteins, a different strategy is proposed in this study. It is based on the evaluation of the removal efficiency of plasma discharges for different amino acids, which constitute from the biological point of view the fundamental building blocks of *all* proteins. Determination of removal rates of different amino acids and their variations with the discharge mixture composition can subsequently improve understanding of plasma interaction with the whole protein.

The main intention of this article is therefore (i) to determine the removal rates of different homo-polypeptides of amino acids treated in low-pressure inductively coupled (ICP) plasma discharges and (ii) to identify the conditions leading to their fastest elimination from surfaces. To meet this general aim, three homo-polypeptides of amino acids that differ significantly in their chemical composition, namely poly(L-histidine), poly(L-lysine) and poly(L-arginine), have been exposed to ICP discharges sustained in argon and its mixtures with nitrogen and oxygen and their removal efficiency has been evaluated by imaging ellipsometry.

Experimental Part

Sample Preparation and Evaluation of the Effect of a Plasma Treatment

Aqueous solution (0.1 wt.-%) of poly(L-histidine), poly(L-lysine) and poly(L-arginine) (Sigma Aldrich), whose chemical structures are given in Table 1, were spotted by a programmable automatic piezoelectric spotter S3 sciFLEXARRAYER (Scienion AG, Germany) on one side polished Si wafers, and allowed to dry in common flow hood. For the preparation of the samples, four droplets with a volume of 0.4 nl each were deposited from a glass nozzle of 80 μm diameter to create spots with a pitch of 500 μm.

For the analysis of the samples before and after plasma treatment, imaging ellipsometry was employed. This non-contact optical method is based on the measurement of variations of the polarization state of light reflected from a surface and allows determination of the thickness of the deposit from measured ellipsometric Δ and ψ angles by solving Fresnel's equations, using a suitable optical multilayer model. All measurements reported in this article were performed using a variable angle multi-wavelength imaging ellipsometer (EP3, Nanofilm Surface Analysis GmbH) in air at room temperature at an angle of incidence of 42° and a field of view of 2 000 μm × 2 000 μm. A monochromatized Xe-arc lamp tuned to a wavelength of 554.3 nm was used as a light source. A conventional PCSA (polarizer–compensator– sample-analyzer) null-ellipsometric procedure is used to obtain 2D maps of ellipsometric Δ and ψ angles.[22] The optical modelling needed for the determination of the thickness of the deposits was carried out with a commercial program provided with the ellipsometer (EP3View), using a three layer structure (Si/SiO_2/homopolymer of amino acid).

Plasma Treatment

The samples were treated using a low-pressure, double coil, ICP plasma source schematically depicted in Figure 1. The plasma reactor, already used and described in previous studies,[20,21] consists

Table 1. Structures and molecular weights of the three used homo-polypeptides of amino acids.

Poly(L-histidine) hydrochloride	**Poly(L-arginine) hydrochloride**	**Poly(L-lysine) hydrochloride**
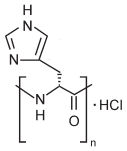	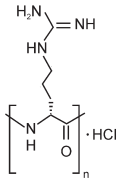	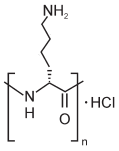
Molecular weight ≥5 000	Molecular weight 15 000–70 000	Molecular weight 15 000–30 000

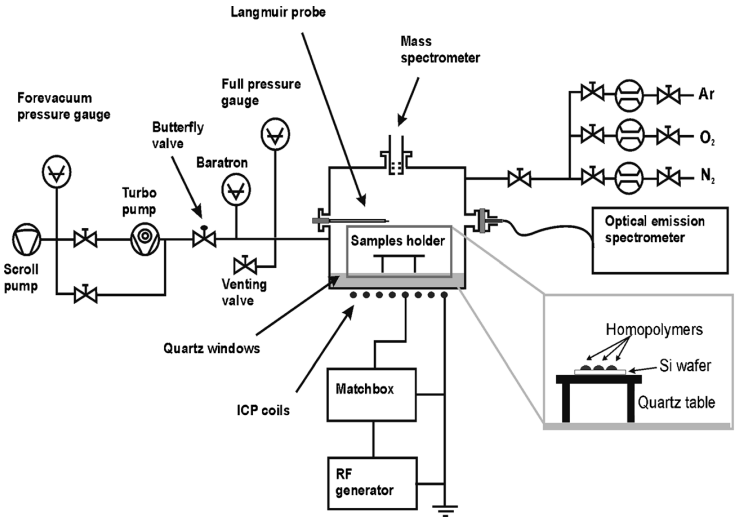

Figure 1. Schematic of the plasma reactor.

of a cylindrical stainless-steel vacuum chamber (diameter 200 mm, height 100 mm) connected to a pumping stage, which is composed of a primary pump and a turbomolecular pump and to a gas inlet system made from mass-flow controllers with operational ranges of 0.5–50 sccm. Below the quartz window at the bottom of the discharge chamber, two spiral RF coils are placed. The two coils are connected to the RF generator working at 13.56 MHz by a tuneable matching network that adapts the total discharge impedance (plasma plus antennas) to the output impedance of the power supply. In the study reported here, the plasma treatment was performed in discharges sustained in pure Ar as well as its 20:1 mixtures with nitrogen and oxygen at a pressure of 10 Pa and an applied RF power of 200 W. In all the experiments, the reflected RF power was kept below 3 W and before each treatment the discharge chamber was evacuated to a base pressure below 0.01 Pa.

The plasma discharges were characterized by Langmuir probe (SmartProbe, Scientific Systems Ltd.), mass spectroscopy (PSM probe, Hiden Analytical Ltd.), optical emission spectroscopy (Avantes AVS-PC2000 monochromator equipped with a 2048-element linear CCD array). In addition, the substrate temperature was measured by infrared pyrometry (Raynger MX4, Raytek) through an IR transparent window temporarily mounted on the upper diagnostics flange instead of the mass spectrometer.

The samples to be treated were placed on a quartz support serving as a sample holder. The distance between the bottom quartz window and the samples was 20 mm and the samples' position was as indicated in the detail of Figure 1.

Results and Discussion

Characterization of Untreated Samples

As can be seen in Figure 2, which shows 2D maps of the ellipsometric angles Δ and ψ of untreated samples together with a calculated thickness map and typical height profiles

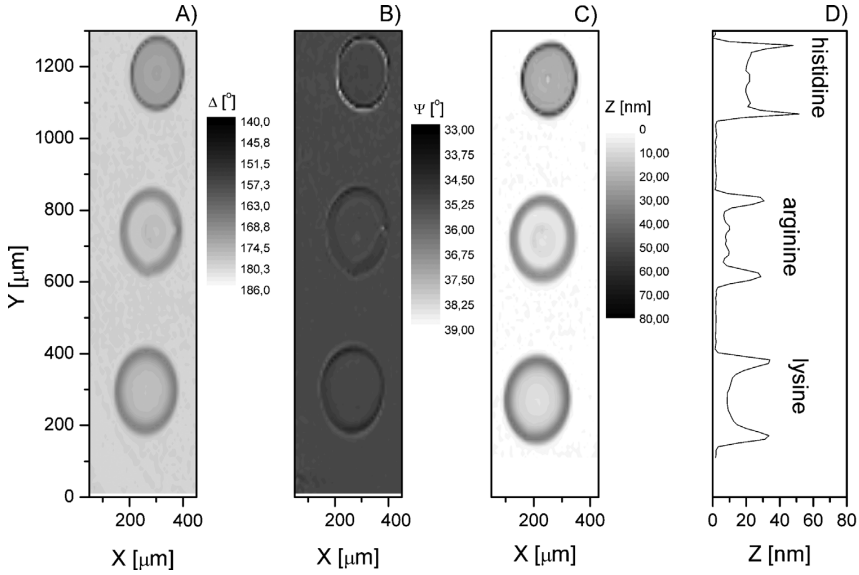

Figure 2. 2D maps of the ellipsometric angles A) Δ B) ψ. C) calculated 2D thickness map together with a D) typical height profile of the deposits. (poly(L-histidine) (top), poly(L-arginine) (middle) and poly(L-lysine) (bottom)).

Plasma Process. Polym. **2009**, *6*, 848–854

DOI: 10.1002/ppap.200900027

of the deposited homo-polypeptides, all three substances used in this study form after drying a well-defined ring structure similar to the one observed for protein samples prepared in similar conditions:[20] at the border of the dried droplets, a relatively thick ring is formed, whereas in the central region, the coating is considerably thinner. Moreover, slight differences in the height profiles of the employed homo-polypeptides can be observed. The deposits were found to be the highest in the case of poly(L-histidine), followed by poly(L-lysine) and poly(L-arginine), which might be related to the difference in molecular weight of the different molecules (see Table 1).

Characterization of Plasma Discharges

The investigation of the processes occurring at the interfaces between plasma and biological systems is a highly challenging issue, which is mainly due to the complexity of plasma discharges that act as a source of energetic radiation and neutral or charged particles. All of these interact with the biological samples and could thus contribute to the overall process of biomolecule elimination. Therefore, the determination of the properties of plasma discharges is very important, since it gives a fundamental knowledge needed for the correct assessment of the various processes occurring during plasma treatment. Therefore, the plasma properties, i.e., plasma density, energy distribution of ions impinging the sample surface, heating of the samples and the presence of highly reactive atomic species, were first determined by means of various diagnostics methods. The results obtained are given below.

First, the initial discharge mixture composition has a strong effect on the overall density of charged particles. It was found that the plasma density is highest in the case of an Ar discharge and rapidly decreases with addition of N_2 or O_2, as can be seen in Figure 3, which summarizes the Langmuir probe measurement of corresponding electron densities. This effect can be ascribed to higher electron energy losses in molecular gases than argon discharges:[23] the energy supplied to the discharge is consumed in molecular gases not only for ionization, but also for vibrational and rotational excitations. Addition of molecular gases consequently leads to enhancement of such losses and less energy is available for ionization, which results in a lower plasma density.

The decrease of the plasma density with addition of a molecular gas to an Ar plasma is accompanied by the appearance of various positive atomic and molecular ions (O^+ and O_2^+ in the case of Ar/O_2 plasma and N^+ and N_2^+ in the case of a discharge sustained in an Ar/N_2 mixture) as measured by mass spectrometry. Furthermore, admixing molecular gases to an Ar plasma slightly modifies the ions' energy distribution function as demonstrated in Figure 4. Nevertheless, it has to be noted that the ion energy does not, under the experimental conditions used in this study, exceed 10 eV, i.e., the ions energy is too low for significant physical sputtering of biomolecules.

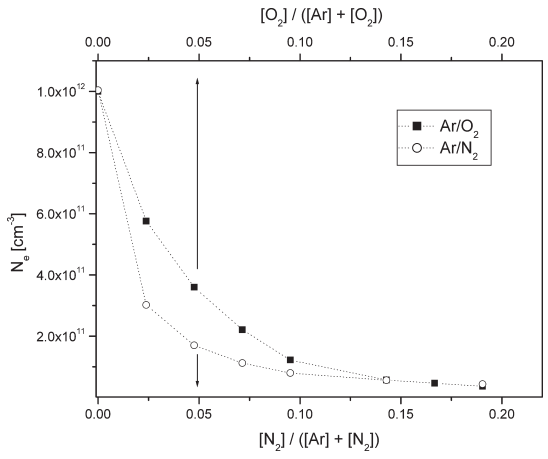

Figure 3. Electron densities determined by Langmuir probe for different gas mixtures (200 W, 10 Pa).

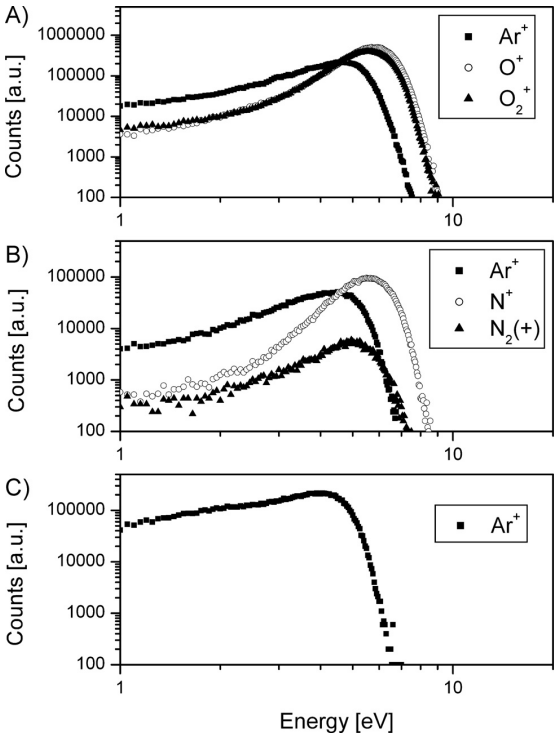

Figure 4. Ion energy distribution function in A) Ar/O_2 (20:1) B) Ar/N_2 (20:1) and C) argon plasma discharges. (200 W, 10 Pa).

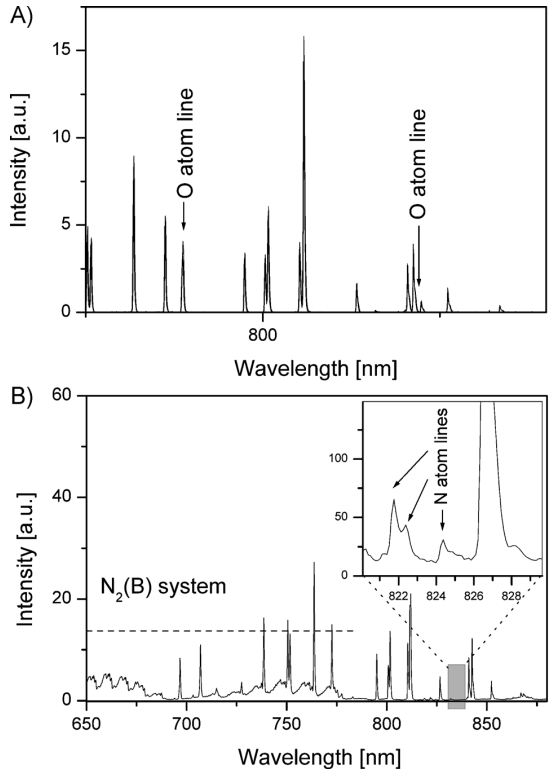

Figure 5. Optical emission spectra of A) Ar/O_2 (20:1) and B) Ar/N_2 (20:1) plasma discharges. (200 W, 10 Pa).

In the emission spectra of the two discharge mixtures that contain molecular gases, it was possible to detect spectral lines of atomic species. More precisely, in the case of a discharge sustained in Ar/O_2 mixture, intense spectral lines of atomic oxygen were observed at wavelengths of 777.4 and 844.6 nm, whereas weak spectral lines of atomic nitrogen (e.g., lines at wavelengths of 821.6, 822.3 and 824.2 nm) were detected in the case of Ar/N_2 plasma, as depicted in Figure 5. Although the intensities of the N and O atom lines differ significantly, their presence in the emission spectra is an indication that, in both discharge mixtures, a considerable fraction of the molecular gas is dissociated, which gives rise to the density of atomic species, i.e., the species reported to play a dominant role in the interactions of plasma with biological materials because of their high reactivity.

Finally, the composition of the discharge also affects the heating of the treated substrate. Regarding this aspect, the highest rise of the substrate temperature was found in discharge sustained in pure argon, whereas the lowest temperature increase was observed in Ar/N_2 plasma discharge as demonstrated in Figure 6.

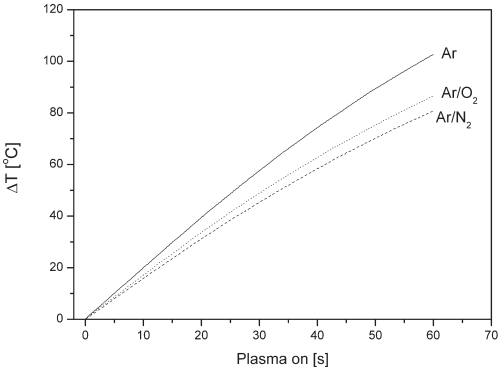

Figure 6. Time evolution of substrate temperature for different discharge compositions (pure Ar, Ar/N_2 (20:1) and Ar/O_2 (20:1), 200 W, 10 Pa).

Plasma Treatment of the Deposits

Plasma treatment considerably modifies the appearance of the samples, which indicates that the deposited homo-polypeptides are gradually removed from the surface (see Figure 7). Moreover, it can be seen that the removal rate is strongly linked to the gas composition: whereas Ar and Ar/N_2 treatments result in only a slight and almost identical decrease of thickness of the deposits — reaching values in the range 200–250 $nm \cdot min^{-1}$ — an oxygen containing discharge eliminates all three homo-polypeptides considerably faster (the observed removal rates lie in the range 500–600 $nm \cdot min^{-1}$), in good agreement with previously reported results obtained with protein samples.[20,21]

Taking into account the results presented in the previous section as well as previously reported evaluation of the intensity of UV radiation emitted by the employed plasma discharges, the following conclusions can be made:

i) The effect of homo-polypeptides elimination is not due to physical sputtering by ions. The evidence supporting this conclusion is twofold. First, the plasma density rapidly decreases after addition of the two molecular gases in to the Ar plasma (Figure 3), which does not conform the observed rates of homo-polypeptides elimination. Second, although a slight increase of the ion energy was observed when O_2 or N_2 was added to the Ar plasma (Figure 4), the energy of ions remains too low for effective sputtering of biological materials.

ii) Although it has been already demonstrated that etching of biological substances can be significantly enhanced by rising the sample temperature (e.g., the etching rate of proteins induced by O atoms was reported to increase more than five times when increasing the temperature from 30 to 120 °C [26]), the heating of the substrates is negligible for the treatment times as employed in this study (Figure 6) and therefore the temperature effect can be neglected in our case.

Plasma Process. Polym. **2009**, *6*, 848–854

DOI: 10.1002/ppap.200900027

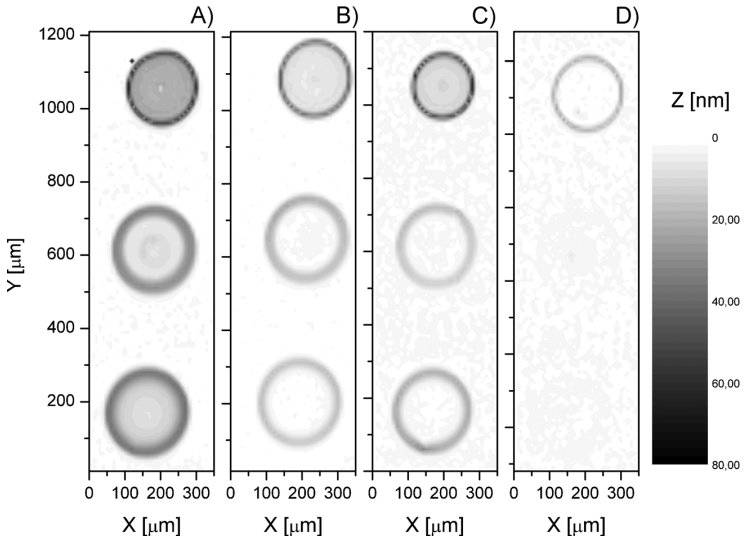

Figure 7. 2D thickness maps of poly(L-histidine) (top), poly(L-arginine) (middle) and poly(L-lysine) (bottom) A) untreated sample and samples treated for 3s in B) Argon C) Ar/N_2 (20:1) and D) Ar/O_2 (20:1) plasma discharges. Sample compositions as in figure 2 (200 W, 10 Pa).

iii) Even if UV radiation could induce chemical modifications of the treated homo-polypeptides due to its relatively high energy, it does not seem to play an important role in the process under our experimental conditions. This is reasonable, since none of the discharges used in this study emits the UV spectral range identified to induce such changes, as demonstrated previously.[21]

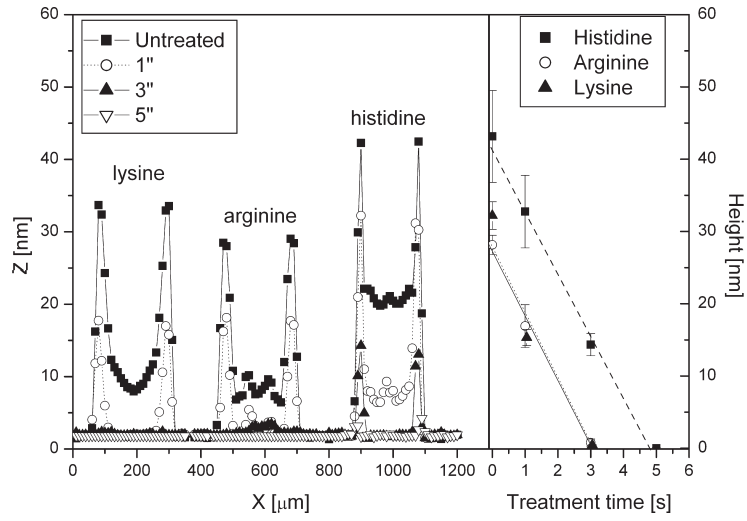

Figure 8. Typical height profiles of homo-polypeptides before treatment and after exposure to Ar/O_2 plasma discharge (left) and the temporal evolution of maximal heights of deposits (right). Conditions: Ar/O_2 20:1, 10 Pa, 200 W.

iv) The variations of the observed removal rates can be related to different reactivity of species produced in the plasma discharges. Our results clearly demonstrate the importance of oxygen for the erosion process of organic substances, due to its capability to form volatile species.

Moreover, another important fact revealed by the experiments is the similarity of the removal rates of the three treated homo-polypeptides, in spite of their different chemical structure. This is highlighted in Figure 8, which shows typical height profiles of the three homo-polypeptides exposed to Ar/O_2 plasma together with the resulting temporal evolution of their maximal heights.

The observed similarity of the removal rates for all three homo-polypeptides having distinct chemical composition can be related to the process of ion-enhanced etching, also called chemical sputtering, in analogy to the recent results reached with hydrocarbon films,[24] bacterial spores[24,25] or model proteins.[26] This process is initiated by the physical impact of energetic ions having sufficient energies to disrupt the chemical structure of a target material and to create dangling bonds near its surface. Such active surface sites are attacked by active species, in our case by oxygen atoms, whose presence was confirmed by optical emission spectroscopy (Figure 5), and in some extend also by oxygen molecules,[25,26] which can lead to the formation of volatile components and in turn to the gradual erosion and removal of the deposit. However, since this process is governed by physical impact of energetic ions, the exact chemical structure of the treated biomolecules is relatively irrelevant for the overall removal rate, on the contrary to pure chemical etching. This has important consequences for optimization of the treatment of infectious protein residues (e.g., prions). The overall efficiency of proteins removal from the surfaces will be linked in first approximation to the removal rate of their different molecular domains, which are, on the chemical and biological level, represented by different amino acids. Therefore, the finding that different amino acids are eliminated at similar rates leads to the conclusion that various proteins would be removed at similar rates, a

finding that corresponds to the observations reported in a previous study.[20]

Conclusion

In this study, the removal efficiency of different homopolypeptides of amino acids by low-pressure ICP discharges was investigated. Based on the results obtained, it seems that although plasma capability to eliminate distinct amino acids from a surface depends strongly on the plasma discharge composition, and in particular in the presence of oxygen in the discharge mixture, the process is rather insensitive to the chemical composition of the treated amino acids. This finding allows to presume that also different proteins composed of distinct sequences of amino acids will be removed with similar rates, which agrees well with recent results obtained with protein deposits, and which is in agreement with recently suggested mechanism of chemical sputtering playing a dominant role in the process of elimination of biological systems from surfaces. The similarity of the elimination rates independently on the amino acid chemical structure has moreover important consequences for the optimization of the treatment of infectious proteic residues (e.g., prions), since it allows comparing results obtained from non-pathogenic proteins to those of their pathogenic forms. Finally, it is important to stress that these conclusions are of validity for substances that can be easily volatilized by oxygen, i.e., substance without inorganic components. Nevertheless, in the real conditions, the composition of the surface can be far from this simplified situation. In particular, the content in salts and elements (such as K, Ca, Na), which cannot be volatilized by the plasma discharge, will have a strong influence on the practical validity of these results. More studies using complex mixtures close to the real cases reported in the literature have to be carried out to confirm these conclusions.

Acknowledgements: This work has been supported by the *FP6 2005 NEST project "Biodecon"* and the *JRC Action 15008: NanoBiotechnology for Health and the IHCP Exploratory Research Programme.*

Received: February 16, 2009; Revised: July 1, 2009; Accepted: July 11, 2009; DOI: 10.1002/ppap.200900027

Keywords: amino acids; decontamination; prions; proteins; radiation; RF discharges; sterilization

[1] I. P. Lipscomb, A. K. Sihota, C. W. Keevil, *J. Clin. Microbiol.* **2006**, *44*, 3728.
[2] H. Murdoch, D. Taylor, J. Dickinson, J. T. Walker, D. Perrett, N. D. H. Raven, J. M. Sutton, *J. Hosp. Infect* **2006**, *63*, 432.
[3] R. L. Baxter, H. C. Baxter, G. A. Campbell, K. Grant, A. Jones, P. Richardson, G. Wittaker, *J. Hosp. Infect* **2006**, *63*, 439.
[4] D. M. Taylor, J. R. Fraser, *J. Hosp. Infect* **2000**, *44*, 318.
[5] S. Lerouge, M. Wertheimer, L'H. Yahia, *Plasmas Polym.* **2001**, *6*, 175.
[6] M. Moisan, J. Barbeau, S. Moreau, J. Pelletier, M. Tabrizian, L'H. Yahia, *Int. J. Pharm.* **2001**, *226*, 1.
[7] M. Laroussi, *IEEE Trans. Plasma Sci.* **2002**, *30*, 1409.
[8] M. Laroussi, *Plasma Process. Polym.* **2005**, *2*, 391.
[9] F. Rossi, O. Kylián, M. Hasiwa, *Plasma Process. Polym.* **2006**, *3*, 431.
[10] O. Kylián, M. Hasiwa, F. Rossi, *Plasma Process. Polym.* **2006**, *3*, 272.
[11] O. Kylián, M. Hasiwa, F. Rossi, *IEEE Trans. Plasma Sci.* **2006**, *34*, 2606.
[12] M. Hasiwa, O. Kylián, T. Hartung, F. Rossi, *Innate Immun.* **2008**, *14*, 89.
[13] H. C. Baxter, G. A. Campbell, A. G. Whittaker, A. C. Jones, A. Aitken, A. H. Simpson, M. Casey, L. Bountiff, L. Gibbard, R. L. Baxter, *J. General Virol.* **2005**, *86*, 2393.
[14] X. T. Deng, J. J. Shi, H. L. Chen, M. G. Kong, *Appl. Phys. Lett.* **2007**, *90*, 013903.
[15] X. T. Deng, J. J. Shi, M. G. Kong, *J. Appl. Phys.* **2007**, *101*, 074701.
[16] R. Mogul, A. A. Bol'shakov, S. L. Chan, R. M. Stevens, B. N. Khare, M. Meyyappan, J. D. Trent, *Biotechnol. Prog.* **2003**, *19*, 776.
[17] G. Ceccone, D. Gilliland, O. Kylián, F. Rossi, *Czech. J. Phys.* **2006**, *56*, B672.
[18] C. Bernard, A. Leduc, J. Bardeau, B. Saoudi, L'Y. Yahia, G. De Crescenzo, *J. Phys. D: Appl. Phys.* **2006**, *39*, 3470.
[19] H. C. Baxter, G. A. Campbell, P. R. Richardson, A. C. Jones, I. R. Whittle, M. Casey, A. G. Whittaker, R. L. Baxter, *IEEE Trans. Plasma Sci.* **2006**, *34*, 1337.
[20] O. Kylián, H. Rauscher, D. Gilliland, F. Brétagnol, F. Rossi, *J. Phys. D: Appl. Phys.* **2008**, *41*, 095201.
[21] K. Stapelmann, O. Kylián, B. Denis, F. Rossi, *J. Phys. D: Appl. Phys.* **2008**, *41*, 192005.
[22] H. G. Tompkins, E. A. Irene, Eds., Handbook of Ellipsometry Springer, Berlin 2005.
[23] J. T. Gudmundsson, T. Kimura, M. A. Lieberman, *Plasma Sources Sci. Technol.* **1999**, *8*, 22.
[24] J. Benedikt, C. Flötgen, G. Kussel, V. Raballand, A. von Keudell, *J. Phys. D: Conference Series* **2008**, *133*, 012012.
[25] V. Raballand, J. Benedikt, J. Wunderlich, A. von Keudell, *J. Phys. D: Appl. Phys.* **2008**, *41*, 115207.
[26] O. Kylián, J. Benedikt, L. Sirghi, R. Reuter, H. Rauscher, A. von Keudell, F. Rossi, *Plasma Process. Polym.* **2009**, *6*, 255.

In situ Quartz Crystal Microbalance Measurements of Thin Protein Film Plasma Removal

Francesco Fumagalli, Jan Hanuš, Ondřej Kylián, François Rossi*

Surgical instruments are intended to come into direct contact with the patients' tissue and thus need to be sterilized and decontaminated in order to prevent infections, inflammations or transmission of diseases. In this study, plasma interactions with low contamination levels (typically less than $3\,\mu g \cdot mm^{-2}$) of BSA proteins were investigated in situ by means of quartz crystal microbalance. Mass removal rates were found to depend on treatment time showing a self-limiting behavior. Removal rates kinetics were characterized by descriptive parameters and correlated with plasma induced chemical composition changes and morphological modification of the protein film.

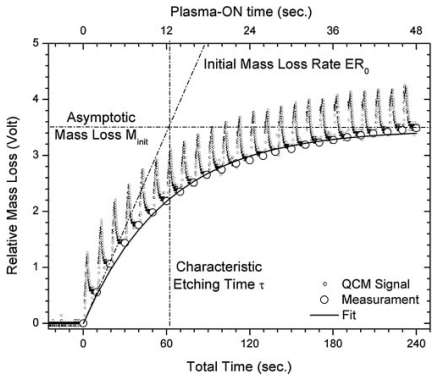

1. Introduction

Elimination of potentially harmful microorganisms and biomolecules present on surfaces is a major concern in many different technological areas ranging from food and packaging industry, textile industry, to aerospace industry. However, the field where sterilization and decontamination are of paramount importance is the medical praxis, where these processes represent a crucial step in guaranteeing the safety of the patients. This is especially true for the cases of reused instruments, such us endoscopes, dental drills, or surgical tools whose insufficient cleanness in terms of presence of biological contamination has been reported to be a potential cause of post-intervention infections or disease transmission.[1,2]

However, in most of the cases mentioned above, surface sterilization and decontamination cannot be achieved in practical terms with the currently available technologies. Drawbacks in actual sterilization techniques refer in particular to the high resistance of certain biomolecules, prions in particular, toward routine chemical and physical cleaning processes[3] or incompatibilies between materials used in biomedical applications and sterilization process parameters.[4–6] Infectious proteins, i.e., prions, are pathogens composed of proteins in a misfolded form responsible of transmissible spongiform encephalopathies for a variety of mammals, including humans.[7] All known prions-related diseases affect the function of the brain and other neural tissue and all are currently untreatable and universally fatal.[8] A recent study from Hervé et al. shows that currently marketed cleaning chemistries and recent decontamination protocols do not completely suppress the threat from iatrogenic Creutzfeldt-Jakob Disease (CJD) transmission connected with re-usable surgical instruments; it was also found that self-aggregating

F. Fumagalli, J. Hanuš, F. Rossi
European Commission, Joint Research Centre, Institute for Health and Consumer Protection, Via E. Fermi 2749, 21027 Ispra (VA), Italy
E-mail: francois.rossi@jrc.ec.europa.eu
O. Kylián
Faculty of Mathematics and Physics, Charles University, V Holešovičkách 2, 18000 Prague 8, Czech Republic

DOI: 10.1002/ppap.201100098

protease resistant prions proteins constituted the main component of the biological residuals left on the sterilized surfaces.[9]

High risks associated with the presence of potentially infectious proteins, together with the impossibility of removing them by currently used hospital decontamination techniques, lead to disposal of many surgical instruments after single use, which in turn represents an enormous burden for the public health budget. Thus the possibility of applying plasma discharges for the removal of proteins from the surfaces gained increased attention in the past years, since these processes have the potential of answering the needs of health services analogously to the cases of bacterial spores or endotoxins.[10–14]

However, in most of the works published until now, only ex situ techniques (such as profilometer and ellipsometry) were used to measure plasma induced biomaterials removal.[15,16] Linear etching rates (i.e., decrease of a contamination residue height profile) were the standard figure used to characterize decontamination processes. In this work, we propose a quartz crystal microbalance (QCM) method for in situ measurement of protein mass removal during operation of a pulsed plasma discharge. The proposed technique allows detailed investigation of etching dynamics during plasma treatment. Moreover, quantification of the etching process by mass removal allows direct comparison of plasma process data with biological results on vCJD iatrogenic transmission (number of molecules per ID_{50} unit)[17] and state-of-the-art detection techniques of prions protein residual contamination on surgical instruments.[18] Contamination levels used for experiments in this work where chosen to mimic a realistic biological residual after standard hospital sterilization procedures. Lipscomb[19] in a study on contaminated surgical instruments taken from U.K. hospitals, define a contamination indicator according to residual biological mass density after sterilization. Simulated contaminations corresponding to level 2 ($0.042–0.42\ \mu g \cdot mm^{-2}$) and 3 ($0.42–4.2\ \mu g \cdot mm^{-2}$) were used in this work (from 0.2 to $3\ \mu g \cdot mm^{-2}$). According to Lipscomb, levels 2 and 3 define situations of low or moderate contamination and were found on the 44% of analyzed surgical instruments (while the rest was found in level 4, more than $4.2\ \mu g \cdot mm^{-2}$, categorized as heavily contaminated).

2. Experimental Section

The experimental apparatus used in this work consists of double coil planar inductive plasma reactor designed for basic studies in plasma processing and already described in detail elsewhere.[14,16]

Plasma conditions for all the experiments were: operating pressure 10 Pa, base pressure 2×10^{-2} Pa, radio frequency (RF) delivered power 350 W, total gas flow 22 sccm, O_2/Ar flow ratio 0.27, pulsing frequency 100 mHz, and duty cycle 20% unless stated otherwise in the discussion.

Protein film mass removal was monitored by a QCM (Inficon). All experiments were performed at a substrate temperature of 303 ± 7 K pulsing the plasma discharge and with water-cooling of the QCM crystal. The QCM crystal signal was monitored on line with an USB oscilloscope (Picoscope), by means of the external output voltage signal, proportional to the crystal frequency shift. The conversion factor between the measured voltage V and the mass of the protein deposit M used in this study was $M/V = 4.36\ \mu g \cdot V^{-1}$, all the mass data are indicated as mass per unit area of the crystal.

X-ray photoelectron spectroscopy (XPS) measurements for protein film surface analysis have been performed with an AXIS ULTRA Spectrometer (KRATOS Analytical, UK). For each sample, a survey spectrum (0–1 150 eV), from which the surface chemical compositions without hydrogen were determined, was recorded. In addition one set of high-resolution spectra was also recorded on each sample. The morphological changes of the protein deposits were determined by atomic force microscopy (AFM type Solver P47H, NT-MDT Co. operated in the tapping mode).

Model biological contaminations used in this work consist of bovine serum albumin (BSA) protein films deposited on QCM gold coated crystals with a calibrated pipette. BSA protein was diluted at different concentrations in 2,2,2 trifluoroethanol (TFE, Fluka, 99%), which is commonly used as a solvent in biochemistry,[20] and spotted on the QCM crystals. TFE was chosen also for its low boiling point (351 K) that results in its fast evaporation. A low evaporation time is desired to reduce the coffee ring effect in the protein films deposited on QCM crystals.[21]

3. Results and Discussion

3.1. Mass Loss Curves

Examples of the QCM signal as recorded by an oscilloscope during the plasma process are shown in Figure 1 and Figure 2. The strategy for QCM measurements during the plasma discharge is derived from the work of Heil et al.[22] and consists in pulsing the plasma discharge and measuring the crystal frequency shift during the plasma-off phase after each treatment cycle. The effect of plasma discharge on a blank QCM crystal is shown in Figure 1. In the top panel the QCM response to a series of plasma pulses is plotted: a sharp increase in the monitor output voltage signal is observed when the discharge is ignited, while during the off phase, the signal relaxes at the initial voltage offset level V_0. The black circles in Figure 1 indicate the relaxation voltage measurement points after each plasma cycle. The spike during the plasma-on phase can be considered as an artifact due to AT-cut crystal response to pressure and temperature variation as well as to parasitic voltages developing during the active phase of the discharge. The lower panel of Figure 1 shows the histogram of the final relaxation voltages measured after each plasma cycle. The statistics has been calculated using a voltage measurements dataset from a

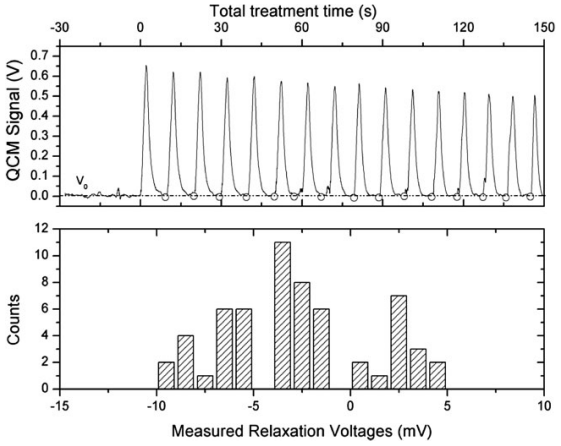

Figure 1. Top panel: apparent mass change due to plasma–crystal interaction during QCM measurements on a clean crystal exposed to several cycles of plasma treatment, $O_2/Ar = 0.27$, $P = 350$ W, $p = 10$ Pa, $\Phi_{tot} = 20$ sccm, 20% DC, and $f = 100$ mHz, the black circles indicate the measured relaxation voltages. Lower panel: distribution of the measured relaxation voltages.

60 plasma cycles experiment. The mean value of the recorded voltages is -2 ± 4 mV, with the lowest and highest recorded voltages of -9.7 mV and $+4.5$ mV, respectively. Experimental errors due to fluctuations in the offset voltage became comparable to measured etching rates only for values below $0.1\ ng \cdot s^{-1} \cdot mm^{-2}$. It can be seen that the mean of the histogram is not precisely zero. This is because of the numerical algorithm used for automatic identification of the voltage measurement points based on the identification of the minima in the smoothed QCM output signal, which results in a clean crystal voltage measurements distribution slightly unbalanced toward negative values. An example of QCM measurements on protein-covered crystals is shown in Figure 2. Three series of plasma pulses at different repetition frequencies are shown for a total plasma-on time of 4 s for each series. After each run, the frequency is changed and the QCM monitor is reset to zero voltage. When the discharge is ignited on a protein covered crystal a sharp increase in the monitor output voltage signal is again observed but now, during the off phase, the signal relaxes to a new voltage level, V_1, slightly higher than the starting voltage V_0. Moreover, it is observed that the same final relaxation voltage is reached using different treatment time steps, but keeping the total plasma on time fixed. According to these observations, the difference between the offset voltage and the relaxation voltage is interpreted as a quantity proportional to the mass loss occurred during a plasma treatment and the difference between two consecutive relaxation voltages is interpreted as the mass loss occurred during a plasma-on cycle.

If the same procedure is applied during a pulsed plasma treatment (see Figure 3), mass loss curves describing the evolution of the material removal from the surface exposed to plasma are obtained by measuring the QCM voltage signal at consecutive relaxation points. The open circles in Figure 3 identify the measurement points after signal relaxation.

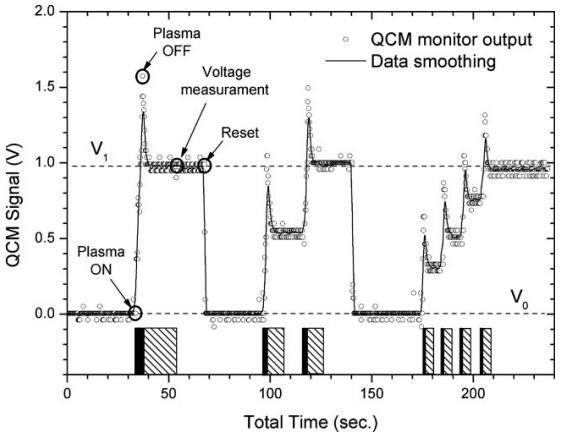

Figure 2. QCM measurements, apparent mass change due to plasma–crystal interaction for different pulsing frequencies but identical total treatment time ($t_{tot} = 4$ s). Black columns indicate the plasma ON time, shaded columns indicate the standard plasma OFF time at 20% DC used in the decontamination experiments. Plasma parameters are $O_2/Ar = 0.27$, $P = 350$ W, $p = 10$ Pa, $\Phi_{tot} = 20$ sccm, and BSA solution concentration $= 10\ mg \cdot ml^{-1}$.

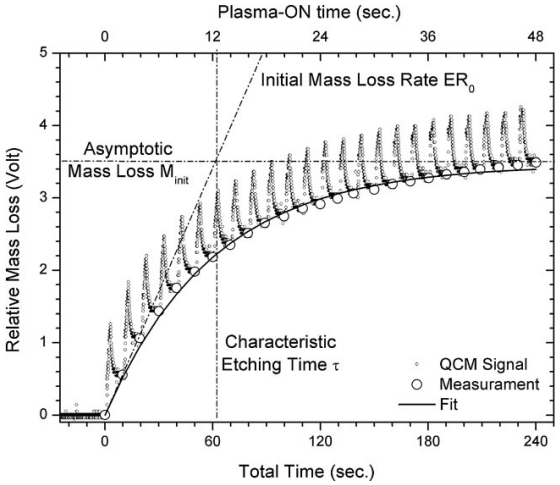

Figure 3. In situ QCM measurements during protein film removal by pulsed plasma treatment. Plasma treatment parameters are $O_2/Ar = 0.27$, $P = 350$ W, $p = 10$ Pa, $\Phi_{tot} = 20$ sccm, BSA solution concentration $= 1.5\ mg \cdot ml^{-1}$. Bottom x-axis display total treatment at 20% DC and $f = 100$ mHz, top x-axis display effective plasma-ON time.

Plasma Process. Polym. **2012**, *9*, 188–196

DOI: 10.1002/ppap.201100098

The mass loss curves can be described by an exponential function of the form:

$$M_{\text{loss}} = M_{\text{init}} \cdot \left(1 - e^{-\frac{t}{\tau}}\right) \quad (1)$$

In the above equation, M_{init}, is the mass initially deposited on the crystal, t is the effective plasma treatment time, and τ is the characteristic etching time. In this work, the end point is defined as the moment when the etch rate, i.e., the voltage difference between the measurement points of two successive plasma cycles, does not change anymore or drops below the sensitivity of the monitoring oscilloscope. The self-limiting nature of the process is described by the term $(1-e^{-t/\tau})$, which may be related to two factors: the raising concentration of non-volatile compounds on the film surface and the reduction of the effective interaction area due to substrate exposure, as shown later in the text. In the example of Figure 3, the values of M_{init} and τ, as determined from least square fit of the data, are respectively 0.19 $\mu g \cdot mm^{-2}$ and 12.07 s.

The time dependent protein mass removal rate ER(t) can be expressed by the time derivative of Equation (1):

$$\text{ER}(t) = \frac{dM_{\text{loss}}}{dt} = \left(\frac{M_{\text{init}}}{\tau}\right) \cdot e^{-\frac{t}{\tau}} = \text{ER}_0 \cdot e^{-\frac{t}{\tau}} \quad (2)$$

The constant multiplicative term (M_{init}/τ), or ER_0, represents the initial mass removal rate, and is plotted in Figure 3 as the slope of the ER(t) curve at $t = 0$ s. This specific functional form was chosen as an empirical model for the following two reasons: (i) it is the simplest model that both fits the data (see Figure 3) and exhibits the proper asymptotic behavior (finite etching rate at $t = 0$ and zero etching rate at $t = \infty$); (ii) under the assumption that the etching rate ER(t) is limited by the number of non-etchable sites on the surface θ, and proportional to the number of etchable sites on the surface $1-\theta$, the non-etchable film formation can be compared to a simple model which assumes a constant exposure rate for non-etchable compounds:

$$\frac{d\theta}{dt} = k \cdot (1 - \theta) \quad (3)$$

where $k \sim \tau^{-1}$ is the rate constant. This leads to an integrated expression for the etching rate of the form:

$$\text{ER}(t) \propto 1 - \theta = \exp(-k \cdot t) \quad (4)$$

Additional blocking mechanisms (e.g., substrate exposure) under similar hypothesis might contribute to the lowering of the etching rate by introducing additional time constants. Time dependent mass removal rates for protein films have already been reported in plasma decontamination experiments, when low levels of biological contamination were present.[23] Equation (1 and 2) in their simple forms are a parameterization of the experimental data and serve to determine the principal features of the mass loss curves time dependency, allowing thus a direct and quantitative comparison between the different experimental conditions.

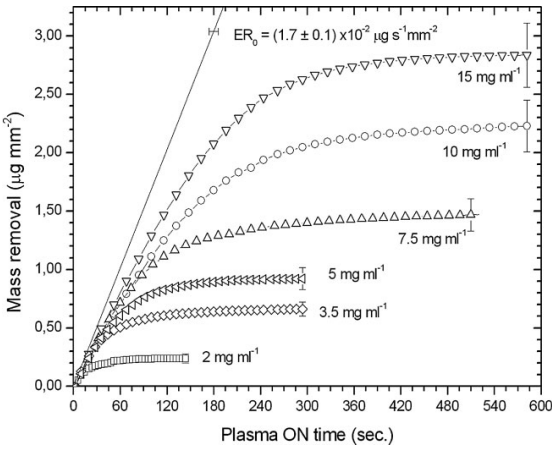

Figure 4. Mass loss curves as a function of initial concentration of BSA protein solution used for protein deposition on the QCM crystal. Plasma treatment parameters are $O_2/Ar = 0.27$, $P = 350$ W, $p = 10$ Pa, $\Phi_{\text{tot}} = 20$ sccm.

The effect of Ar/O_2 plasma treatment on protein films is shown in Figure 4 for different concentrations of used protein solution, which determines amount of deposited protein. All the discharge parameters (i.e., applied RF power, processing pressure, and gas flow) were kept constant for all the treatments and every data series are the average of at least three independent experiments. The mass loss curves show a saturation behavior for long treatment times indicating that the etching process of the protein layer approaches its endpoint, the position of M_{init} is concentration-dependent and shifts to higher values as the amount of deposited material increases. Since also the characteristic etching time τ shifts to higher values following the same trend as M_{init}, the ratio of these two quantities, ER_0, remains almost constant (with the possible exception of the curve at 2 $mg \cdot ml^{-1}$). As a consequence of this, all the curves show in the initial phase the same removal kinetics indicating that the same plasma–biomaterial interaction mechanism is operating. A summary of the descriptive parameters for this set of curves is given in Table 1.

From the analysis of the mass loss curves presented, it results that the simple forms of Equation (1) and (2) describe the main features of the mass loss kinetics, but poorly describe the details of the QCM signal evolution. This is evident, e.g., from the mass loss rates (plotted in Figure 5 in

Table 1. Summary of calculated mass loss curves descriptive parameters for different initial protein concentrations.

Concentration [mg · ml^{-1}]	M_{init} [μg · mm^{-2}]	τ [s]	ER_0 [ng · s^{-1} · mm^{-2}]	t_{trans} [s]
2.0	0.23 ± 0.04	20.0 ± 0.5	11.7 ± 2.2	n.m.[a)]
3.5	0.66 ± 0.06	40.3 ± 2.5	16.5 ± 2.4	n.m.[a)]
5.0	0.97 ± 0.04	60.2 ± 0.8	16.2 ± 0.8	43 ± 8
7.5	1.54 ± 0.14	92.2 ± 1.5	16.7 ± 1.8	75 ± 5
10.0	2.63 ± 0.22	152.0 ± 1.6	17.3 ± 1.6	155 ± 13
15.0	3.06 ± 0.28	181.0 ± 1.7	19.3 ± 1.9	205 ± 14

[a)]Not measurable.

a log scale) calculated from the mass loss curves already presented in Figure 4. If Equation (2) strictly holds, a linear trend for ER(t) would be expected in semi-logarithmic plot against the treatment time. Data in Figure 5 show instead that the data trends in the range 0.97–3.06 μg · mm^{-2} are closely described by Equation (2) when a two-valued characteristic etching time is considered, i.e., the process is described using two different time constants. In the curves in Figure 5, the kinetic of the mass loss rate at short treatment times is described by a time constant value higher than the average characteristic etching time calculated on the complete dataset, while after a certain transition, the time constant describing the exponential decay changes suddenly to a lower value. In other words, the decay of the mass loss rates is slower at short treatment times and is faster at long treatments times. Since the mass loss rate curves [Equation (2)] are described by the same set of parameters of the mass loss curves [Equation (1)] it is possible to derive from the observations described above

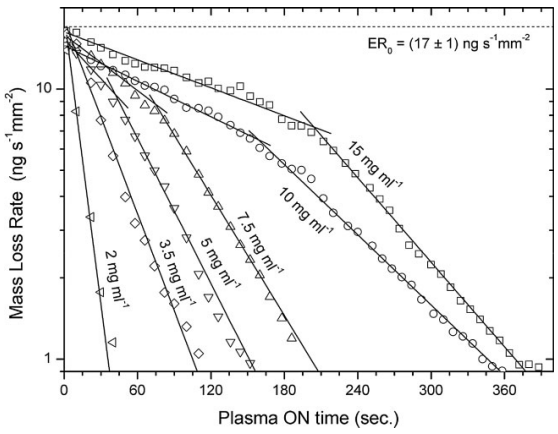

Figure 5. Kinetics of the time dependent mass loss rate for different initial solution concentrations. Rates are calculated from mass loss curve shown in Figure 4.

that at the beginning of the treatment, the protein mass loss due to plasma exposure proceeds with a slower kinetic i.e., the material removal rate deviates slowly from ER_0, while after the transition point a new regime with a faster kinetics is observed, i.e., the instantaneous ER(t) drops rapidly to zero.

This sudden jump in the value of the parameter τ at the time t_{trans} is the indication of a modification in the conditions of the removal process. Some indications about the surface processes related to this phenomenon can be derived from XPS and AFM surface analysis.

Data points for the low contamination experiments (0.23 – 0.66 μg mm^{-2}) are well approximated by Equation (1) and (2) using a single valued time constant.

3.2. Plasma Induced Chemical and Morphological Changes

Bovine serum albumin (BSA) survey XPS spectra (not shown) recorded for different plasma treatment times generally shows peaks corresponding to oxygen (O, 1s at 532 eV), nitrogen (N, 1s at 400 eV), carbon (C, 1s at about 285 eV), sulfur (S, 2p at about 164 eV) and, for long treatment times, Au (Au, 4f at 84 eV), i.e., the substrate. Oxygen carbon and nitrogen are the main components of the protein molecular structure while sulfur is attributed to the cysteine present in the BSA.[24] Traces of sodium and calcium together with a substantial peak from fluorine (F 1s, 684 eV) are also detected, probably originated from the protein solution preparation, crystal cleaning protocol or from contamination of the vacuum chamber. XPS data presented in this section are summarized in Table 2.

Figure 6 shows the elemental composition of the protein film at different plasma treatment times. The three most important elements present in our samples that do not form volatile compounds after oxygen driven plasma reactions (gold, fluorine, and sulfur) are shown. As the treatment time increases, the signals corresponding to gold and fluorine increases: this is due to the plasma etching process which

Plasma Process. Polym. **2012**, *9*, 188–196

DOI: 10.1002/ppap.201100098

Table 2. Elemental composition time evolution of BSA thin films during O_2/Ar plasma treatment. Data refers to principal XPS peak relative intensities as a function of the treatment time. Plasma parameters are O_2/Ar = 0.27, P = 350 W, p = 10 Pa, Φ_{tot} = 20 sccm.

Treat. time [s]	Au [%]	F [%]	S [%]	C [%]	N [%]	O [%]
0	0.0	0.3	0.6	64.3	15.8	19.0
2	0.0	4.3	1.2	57.5	13.3	23.7
6	0.0	4.7	1.8	52.7	13.8	27.0
20	0.1	7.2	2.5	48.5	11.6	28.7
40	1.6	9.3	2.5	45.1	9.9	30.1
60	2.9	9.8	1.9	44.5	7.4	30.5
80	3.1	12.0	2.4	42.8	5.7	31.1
100	4.2	9.7	3.2	41.0	0.9	32.6
150	15.3	14.7	2.2	38.1	0.0	29.3
200	22.7	13.2	1.7	35.6	0.0	26.8

removes the protein layer exposing the substrate (therefore the increase of the Au signal) and increasing the concentration of non-removable species (increase of F, from 5 to 12% after one characteristic etching time). Sulfur signal rises immediately at about three times its initial concentration, and then accounts for about 2% of the total composition, showing no further kinetics. Moreover, strong oxidation of sulfur was observed during the treatment and consequent shift of the XPS peak was found. The BSA as deposited shows the S2p doublet around 164 eV, which is typical of C−S bonding.[25] On the other hand, after exposure to the plasma a second peak around 168 eV binding energy that can be attributed to oxidized sulfur starts appearing.[26]

The total concentration of these three elements rises to (31 ± 5%) in one characteristic etching time (152.0 ± 1.6 s) for the specific plasma treatment under investigation, indicating substantial build up of inorganic non-volatile compounds at the surface. This implies the progressive and fast depletion of potential reaction sites for excited atoms and molecules from the surface. This in turn explains the reduction of the mass loss rates as the treatment time progresses. It must be underlined that as soon as the gold substrate signal is observed at a significant concentration (above 3–5%), the BSA protein film has becomes most likely thinner than 10–12 nm, which is the typical analysis depth of XPS at 90° take off angle (TOA).[27]

Figure 7 shows, as a function of the plasma treatment time, the elemental composition concentration ratios of gold over the sum of nitrogen and carbon, for the three different initial deposit situations. The transition time for the corresponding process is indicated as the shaded area below the data and the width corresponds to the experimental error. The Au/(N + C) ratio is zero at the beginning of the treatment, when the crystal surface is still fully covered with the protein layer, and it remains very low for the early stages of the treatment. At treatment times comparable with the transition times points derived from data plotted in Figure 5, the Au/(N + C) ratio shows a fast increase and reaches plateau values around 0.5. This behavior indicates that in the initial stages the plasma

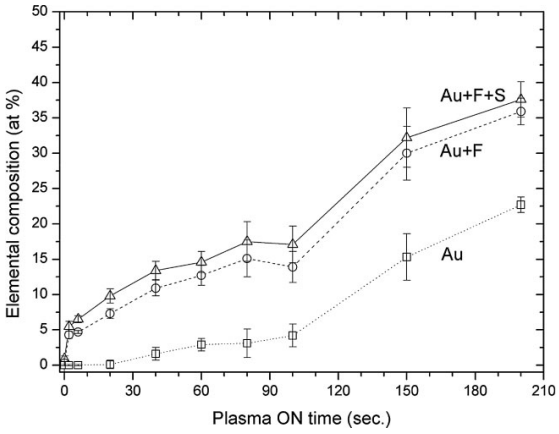

Figure 6. Surface elemental composition (at.-%) of Au, Au + F and Au + F + S as a function of plasma treatment time. Data refer to deposits obtained from 7.5 mg · ml^{-1} BSA solution, plasma treatment parameters are O_2/Ar = 0.27, P = 350 W, p = 10 Pa, Φ_{tot} = 20 sccm. Typical elemental composition measurement error is around ±10%. XPS data are summarized in Table 2.

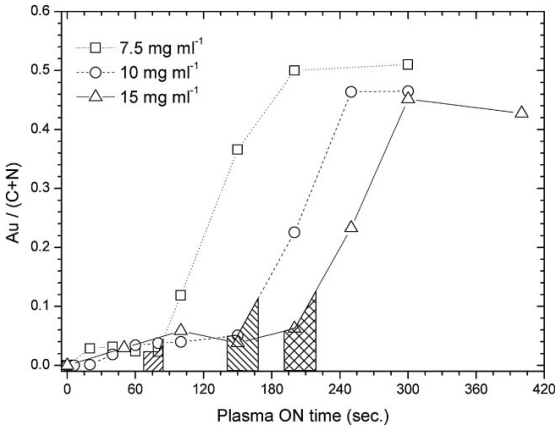

Figure 7. Elemental composition (at.-%) ratio of gold over the sum of carbon and nitrogen as a function of the plasma treatment time obtained from XPS analysis recorded at 90° TOA (mean of three independent measurements). The transition time for the corresponding plasma process is indicated as the shaded area below data. Plasma treatment parameters are O_2/Ar = 0.27, P = 350 W, p = 10 Pa, Φ_{tot} = 20 sccm. Typical elemental composition measurement error ±10%.

interaction happens with a bulk biological material while later, as soon as this material is removed, the substrate is exposed and the surface covered with proteins is reduced to about half the initial value.

Evidence of substrate exposure for long treatment times is supported also by AFM measurements of protein layers microscopic root-mean-square (RMS) roughness (calculated over an area of 1 μm^2) as a function of the treatment time (see Figure 8). Deposits obtained from three different initial solution concentrations were investigated. It can be seen that just few seconds of plasma treatment are enough to induce morphological changes on initially smooth surface of BSA. Further plasma treatment leads to the increase of the maximum peak-to-valley height difference, which reaches its maximal value. After reaching this point, the peak flattening effect is observed. The transition between these two phases happens around the transition time derived from the etching rates curves, which is consistent with interpretation of the XPS data shown in Figure 7. Measured roughness evolution as shown in Figure 8 is representative of the different stages of the material removal process,[23] for short treatment times the increasing roughness is related to inhomogeneous etching, where the surface reactions happens at preferential sites; for long treatment times, the average roughness decreases indicating exposure of the flat substrate layer.

To further explain the slower kinetic of the mass removal rates after the transition time C1s XPS high resolution spectra recorded at 90° TOA at different plasma treatment times have been analyzed. In Figure 9 are shown spectra of as-deposited protein, 2 and 20 s plasma treated protein (before transition time) and 200 s plasma treated protein (after transition time). It is known that BSA C1s peak is the envelope of five components (C0–C4) which can be attributed respectively to C−C/C−H (E_{bind} = 285 eV), C−N (E_{bind} = 285.8 eV), C−O, N−C−O (E_{bind} = 286.8 eV), C=O, N−C=O (E_{bind} = 288.4 eV), and COOH/R (E_{bind} = 289.5 eV).[25] Comparing the as deposited protein spectrum with the spectra recorded at 2 and 20 s treatment time, a general reduction of the intensity in all the components is observed, with the exception of the high energy contribution of peak C4, which is increasing. This is an indication that the percentage of carbon bonded to oxygen is increasing and supports the idea of oxidation processes at the surface. The spectrum recorded at 200 s plasma treatment time, well after the transition time for the corresponding mass loss curves (t_{trans} = 155 ± 13 s), appears to be dominated by the C0 peak with probably some minor contribution by C−O, C2 peak. Eventual contribution from the C1 (C−N) peak is ruled out by the elemental analysis displayed in Figure 10 showing that at 200 s the nitrogen concentration is zero. These results (Figure 7–10) show that in the second phase, the residual protein film is localized and composed mainly of amorphous carbon-based deposit, the protein chemical structure being destroyed by the plasma interaction. Films of amorphous carbon show in general slower etch rates under exposure to oxygen–argon plasma. Benedikt et al.,[28] using a plasma setup very similar to the one used in this study, measured amorphous hydrogenated carbon film etching rate around 0.3 nm · s^{-1}. On the other hand, Kylián and coworkers,[13] always in very similar conditions, measured for bulk BSA etching rates around 20 nm · s^{-1}. The substantial modification of the chemical identity of the material and the corresponding reduction in the mass removal rates after the transition point, together with the reduction of the effective area available for plasma interaction (substrate exposure and residuals build up) can explain the slower kinetics of the mass loss curve second regime after the transition.

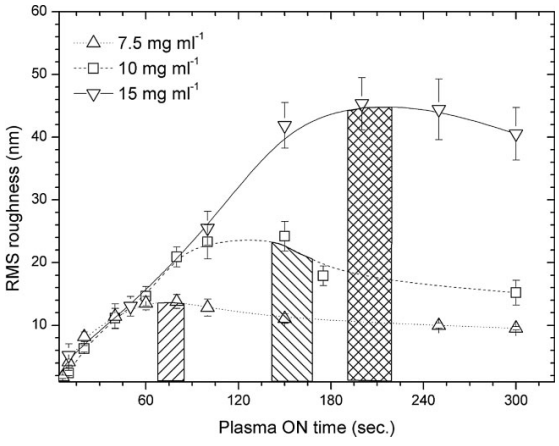

Figure 8. Microscopic RMS roughness of the protein surface layer (1 μm × 1 μm) as a function of the plasma treatment time as measured by means of AFM. The transition time for the corresponding plasma process is indicated as the shaded area below data. Plasma treatment parameters are O_2/Ar = 0.27, P = 350 W, p = 10 Pa, Φ_{tot} = 20 sccm.

The ratio N/C shown in Figure 10 is an indicator of the presence of the protein backbone structure. The N/C ratio exhibits for short treatment times values around 0.25 compatible with the macromolecular elemental composition of the undamaged BSA protein (2 932C and 780N per protein, ratio N/C is 0.266). This considerably changes at long treatment times, namely beyond the transition time, when this ratio falls almost to zero in both cases. This indicates the destruction in the surface layer of the basic building blocks of the proteins primary structure.

Comparison of the data for N/C and Au/(N + C) ratios shows that the destruction of the last protein units and the substrate exposure are simultaneous events and both happens just around the transition time.

From the overall picture derived from the data shown in Figure 6–10, it is possible to define the general mechanisms related to the two mass loss curves regimes observed in

Plasma Process. Polym. **2012**, *9*, 188–196

DOI: 10.1002/ppap.201100098

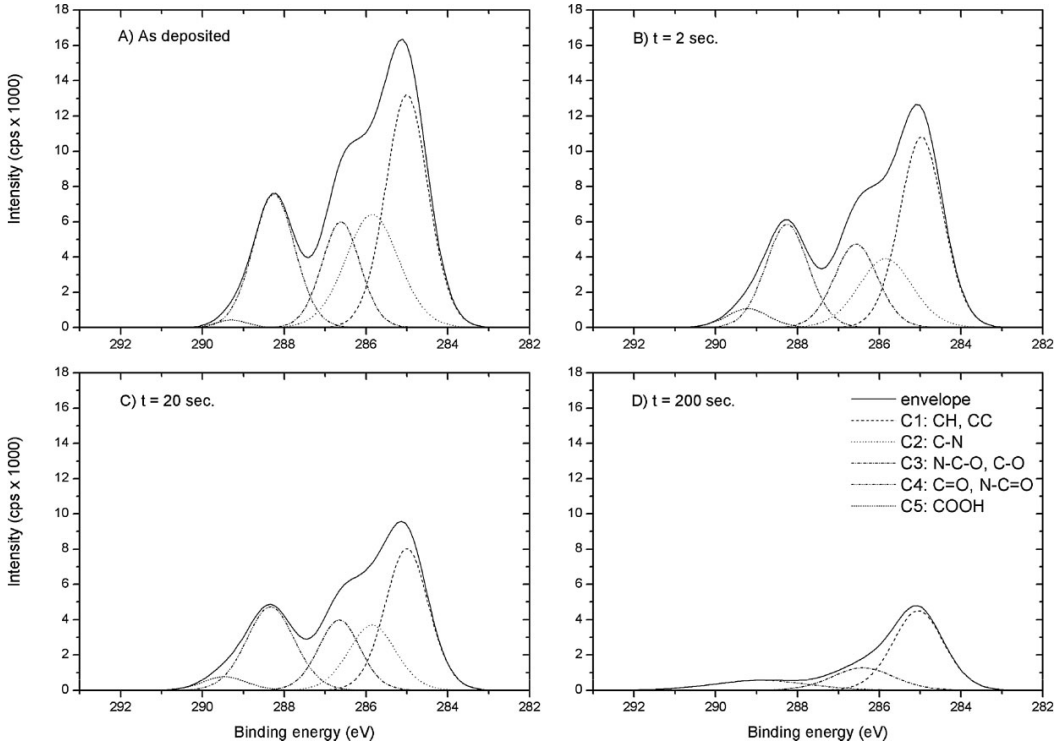

Figure 9. C1s high resolution XPS spectra recorded at 90° TOA on plasma treated BSA protein films before (A), after 2" (B), after 20" (C) and after 200" (D) Ar/O_2 plasma exposure. Data refer to deposits obtained from 10 mg · ml^{-1} BSA solution, plasma treatment parameters are $O_2/Ar = 0.27$, $P = 350$ W, $p = 10$ Pa, $\Phi_{tot} = 20$ sccm.

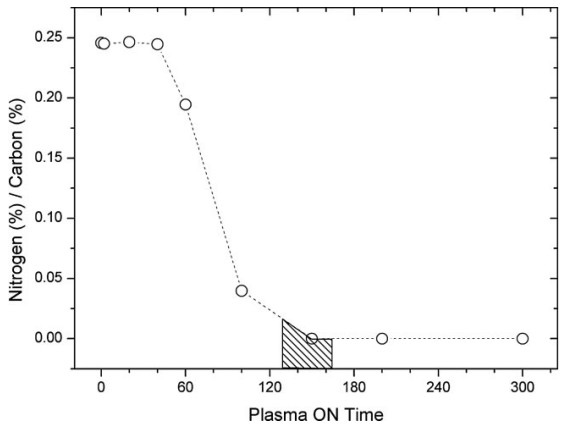

Figure 10. Elemental composition (at.-%) ratio of nitrogen over carbon as a function of the plasma treatment time obtained from XPS survey spectra recorded at 90° TOA (mean of three independent measurements). The transition time for the corresponding plasma process is indicated as the shaded area below data. Plasma treatment parameters are $O_2/Ar = 0.27$, $P = 350$ W, $p = 10$ Pa, $\Phi_{tot} = 20$ sccm. Typical elemental composition measurement error ±10%.

Figure 5. The first regime, when the plasma mass removal is faster (higher ER(t) values), corresponds to the ion-enhanced plasma etching of the bulk protein film.[14,29] Hydrogen, oxygen, carbon, and nitrogen in the protein are consumed by surface reactions with oxygen and removed from the surface as volatile by-products. This process initiates at a rate described by the characteristic etching rate ER_0, and slows down because of the increasing surface concentration of inorganic compounds, that corresponds to superficial non-reactive site. When the process approaches the transition time, it is found that most of the biological material has been removed and the non reactive sites on the surface (either due to exposed substrate or presence of non-etchable inorganic compounds) determine a slower kinetic of the mass removal, being the plasma etching mechanism less efficient in attacking the residuals left at the end of the processes.

4. Conclusion

In this study proteins etching by means of a low pressure inductively coupled plasma discharge was investigated. For

this purpose an in situ diagnostic method based on QCM was introduced. This method allows quantitative measurements in terms of plasma removed protein mass and detailed investigation of etching rate kinetics. Mass loss curves have been measured and characterized for different model contaminations reproducing the same areal mass density of realistic contamination situations and using substrates (Au coated QCM crystals) with realistic roughness levels, moreover the plasma treatments were performed at temperatures suitable for thermolabile materials processing.

Good sampling frequency of our in situ QCM technique was exploited to study the details of the etching rate kinetics. Results show that, for thin film contaminations, etching rates are not constant but can be described as a self-limiting process. Descriptive parameters were introduced to account for the kinetics of the removal process and mass loss curves were explained in terms of the modification induced by the plasma–protein interaction. Accumulation of non-reactive compounds and substrate exposure at the interaction interface were identified as the main causes. In particular the time constant of the etching process was found to depend stepwise both on the morphology and the chemical composition thus defining a transition between two regimes of the removal process. In an early regime the kinetic of the mass removal is dominated by non reactive species accumulation while during late stages of the treatment an endpoint regime dominated by reduction of the effective interaction area and substrate exposure was observed. Of importance for the development of a plasma-based decontamination technique, it was found that, in the second etching regime, the basic building blocks of the protein structure (the backbone polypeptide chains) have been destroyed by the plasma interaction and the residual structures are composed mainly by amorphous carbon.

Acknowledgements: This work is based upon work supported by the Nanobiosciences project at the JRC, Institute for Health and Consumer Protection. We thank Dott. Giacomo Ceccone for helpful discussions.

Received: May 20, 2011; Revised: September 5, 2011; Accepted: September 6, 2011; DOI: 10.1002/ppap.201100098

Keywords: decontamination; plasma etching; proteins; quartz crystal microbalance; self-limiting etching kinetic; surface

[1] I. Lipscomb, A. Sihota, C. Keevil, *J. Clin. Microbiol.* **2006**, *44*, 3728.
[2] H. Murdoch, D. Taylor, J. Dickinson, J. Walker, D. Perrett, N. Raven, J. Sutton, *J. Hosp. Infec.* **2006**, *63*, 432.
[3] D. Taylor, *J. Hosp. Infec.* **1999**, *43*, S69.
[4] S. Lerouge, C. Guignot, M. Tabrizian, D. Ferrier, N. Yagoubi, L. Yahia, *J. Biomed. Mater. Res.* **2000**, *52*, 774.
[5] P. Nair, *J. Biomater. Appl.* **1995**, *10*, 121.
[6] A. Mazzu, C. Smith, *J. Biomed. Mater.* **1984**, *18*, 961.
[7] K. Ryan, C. Ray, *Sherris Medical Microbiology*. McGraw Hill, New York, USA **2004**.
[8] S. Prusiner, *Proc. Natl. Acad. Sci.* **1998**, *95*, 13363.
[9] R. Hervé, T. Secker, C. Keevil, *J. Hosp. Infec.* **2010**, *75*, 309.
[10] M. Moisan, J. Barbeau, S. Moreau, J. Pelletier, M. Tabrizian, L' H. Yahia, *Int. J. Pharma.* **2001**, *226*, 1.
[11] S. Lerouge, A. C. Fozza, M. R. Wertheimer, R. Marchand, L'. H. Yahia, *Plasma Polym* **2001**, *5*, 31.
[12] F. Rossi, O. Kylián, M. Hasiwa, *Plasma Process. Polym.* **2006**, *3*, 431.
[13] F. Rossi, O. Kylián, H. Rauscher, M. Hasiwa, D. Gilliland, *New J. Phys.* **2009**, *11*, 115017.
[14] A. von Keudell, P. Awakowicz, J. Benedikt, V. Raballand, A. Yanguas-Gil, J. Opretzka, C. Flötgen, R. Reuter, L. Byelykh, H. Halfmann, K. Stapelmann, B. Denis, J. Wunderlich, P. Muranyi, F. Rossi, O. Kylian, N. Hasiwa, A. Ruiz, H. Rauscher, L. Sirghi, E. Comoy, C. Dehen, L. Challier, J. P. Deslys, *Plasma Process. Polym.* **2010**, *7*, 327.
[15] O. Kylián, H. Rauscher, D. Gilliland, F. Brétagnol, F. Rossi, *J. Phys. D: Appl. Phys.* **2008**, *41*, 095201.
[16] O. Kylián, H. Rauscher, B. Denis, L. Ceriotti, F. Rossi, *Plasma Process. Polym.* **2009**, *6*, 848.
[17] S. Prusiner, *Science* **1991**, *252*, 1515.
[18] I. Lipscomb, R. Hervé, K. Harris, H. Pinchin, R. Collin, C. W. Keevil, *J. Gen. Virol.* **2007**, *88*, 2619.
[19] I. Lipscomb, *J. Hosp. Infec.* **2010**, *62*, 141.
[20] M. Buck, *Q. Rev. Biophys.* **1998**, *31*, 297
[21] X. Shen, C. Ho, T. Wong, *J. Phys. Chem. B* **2010**, *114*, 5269.
[22] S. Heil, P. Kudlacek, E. Langereis, R. Engeln, M. van de Sanden, W. Kessels, *Appl. Phys. Lett.* **2006**, *89*, 131505.
[23] F. Rossi, O. Kylian, H. Rauscher, D. Gilliland, L. Sirghi, *Pure Appl. Chem.* **2008**, *80*, 1939.
[24] G. Friedli, *Phd Dissertation*. University of Surrey, Guildford, England **1996**.
[25] G. Baeamson, D. Briggs, *High Resolution XPS of Organic Polymers: The Scientia 3000 database*, Wiley, Chichester, Sussex, UK **1992**.
[26] C. Wagner, *Handbook of Photoelectron Spectroscopy*, Perkin Elmer, Eden Praire, Minnesota, USA **1979**.
[27] J. Dewez, V. Berger, Y. Schneider, P. Rouxhet, *J. Coll. Int. Sci.* **1997**, *191*, 1.
[28] J. Benedikt, C. Flötgen, G. Kussel, V. Raballand, A. von Keudell, *J. Phys. D: Conf. Ser.* **2008**, *133*, 012012.
[29] O. Kylián, J. Benedikt, L. Sirghi, R. Reuter, H. Rauscher, A. von Keudell, F. Rossi, *Plasma Process. Polym.* **2009**, *6*, 255.

Plasma Process. Polym. **2012**, *9*, 188–196

DOI: 10.1002/ppap.201100098

IOP Publishing Journal of Physics D: Applied Physics
J. Phys. D: Appl. Phys. **42** (2009) 085207 (7pp) doi:10.1088/0022-3727/42/8/085207

Sterilization and decontamination of medical instruments by low-pressure plasma discharges: application of $Ar/O_2/N_2$ ternary mixture

O Kylián[1] **and F Rossi**[2]

[1] Charles University, Faculty of Mathematics and Physics, V Holešovičkách 2, Prague 8, 180 00, Czech Republic
[2] European Commission, Joint Research Centre, Institute for Health and Consumer Protection, Via E Fermi 2749, 21027 Ispra (VA), Italy

E-mail: francois.rossi@jrc.it

Received 16 January 2009, in final form 26 February 2009
Published 2 April 2009
Online at stacks.iop.org/JPhysD/42/085207

Abstract
A low-pressure inductively coupled plasma discharge sustained in an argon–oxygen–nitrogen ternary mixture is studied in order to evaluate its properties in terms of sterilization and decontamination of surfaces of medical instruments. It is demonstrated by direct comparison with discharges operated in oxygen–nitrogen and oxygen–argon mixtures that application of an $Ar/O_2/N_2$ mixture offers the possibility to combine advantageous properties of the binary mixtures, namely, the capability of an O_2/N_2 plasma to emit intense UV radiation needed for effective inactivation of bacterial spores together with high removal rates of biological substances from Ar/O_2 discharge. Moreover, optimal conditions for both effects are obtained at a similar ternary discharge mixture composition, which is of much interest for real applications, since it offers a highly effective process desired for the safety of medical instruments.

1. Introduction

Cleaning, sterilization and decontamination of medical equipment are fundamental steps in health care facilities in order to assure safety of patients. However, there are numerous indications that currently used techniques are in many cases insufficient to guarantee complete inactivation or elimination of various pathogens (e.g. [1–5]); this consequently represents a serious problem mainly with respect to the possible transmission of lethal neurodegenerative diseases or the onset of immunological events of severe consequences caused by insufficiently cleaned instruments. Therefore, there is a clear demand from hospitals' sterile services for the development of alternative methods allowing complete elimination of highly resistant biological residues possibly present on the surfaces of medical tools. One of the options that gained increased attention in the last decade is the application of low-pressure, non-equilibrium plasma discharges that are capable of not only inactivating bacteria or bacterial spores (e.g. review papers [6–9]) but also eliminating bacterial endotoxins [9–11] or removing protein residuals (e.g. [9, 12–19]), i.e. substances that are difficult or impossible to remove by other techniques. Therefore, the possibility to assure sterility and complete elimination of biological pathogens from the surfaces of medical instruments makes the plasma based sterilization/decontamination technique one of the most promising approaches to fulfil requirements on a universal sterilization/decontamination method. However, as will be discussed in the following section, the conditions leading to inactivation of bacteria or physico-chemical removal of biological residues are different: while a maximum of UV emission is desirable in the first case, a maximum concentration of active species necessary for etching the residues is needed in the second case. The main intention of this paper is to demonstrate that both of these features can be achieved by the application of low-pressure inductively coupled plasma

(ICP) discharges sustained in a $Ar/O_2/N_2$ ternary gas mixture. To do so, the paper is organized as follows. First, the recent results regarding the possible approaches used for the inactivation of bacterial spores on the one hand and physical removal of biomolecules from surfaces on other hand are briefly summarized in section 2. The experimental set-up and methods used in the frame of this study are introduced in section 3. Finally, the results of this study are presented and discussed in section 4 and concluded in section 5.

2. Overview of approaches used for sterilization and decontamination of surfaces

Concerning recent results, two distinct strategies applicable for the sterilization and decontamination of surfaces by means of low-pressure plasma discharges can be followed.

The first one relates to the possibility to remove physically all kinds of pathogens by etching or sputtering. This is traditionally achieved by placing objects to be treated in the active zone of the discharges providing sufficient fluxes of etching agents or energetic ions that can either sputter treated samples or enhance their elimination via the process of chemical sputtering involving both charged particles and plasma radicals [20–22]. Although it has been demonstrated that bacterial spores or biomolecules can be removed from surfaces, or at least significantly eroded, using a wide range of gases, a majority of the research groups use different oxygen containing plasma discharges (e.g. pure oxygen [23–26], O_2/H_2 [9, 11, 18], O_2/N_2 [27], He/O_2 [15, 16] or Ar/O_2 [13, 17, 19]), which offer high removal rates, as demonstrated, for instance, by SEM images of treated bacteria [25–28] or proteins [29], but do not represent environmental risks as for example fluorine mixtures known to be also highly effective in etching of polymers (e.g. [30]). Nevertheless, it has to be noted that the approach based solely on the physico-chemical removal of pathogens, which at first glance seems to be an optimal and universal sterilization/decontamination method, has also certain limitations especially with respect to the inactivation of bacterial spores. It has been demonstrated that spores etching is much slower as compared with various biomolecules treated at otherwise identical operational conditions (e.g. [23]) and it is rather challenging to etch spores completely [30]. This is due to the high amount of inorganic compounds (e.g. calcium, sodium, etc) presented in the spores' walls. Such compounds are difficult to volatilize and therefore their fraction increases with treatment time, which leads to the formation of highly resistant inorganic layer and consequently to the slowing down of the removal rate. As a result of this, prolonged treatments are necessary, which can lead to extensive heating and degradation of treated objects.

The second approach used is based on the induction of chemical or structural modifications of treated pathogens leading to the suppression of their biological activity. Although it has been demonstrated that certain biomolecules can be inactivated in this way (concretely bacterial endotoxins [31]), this approach refers mainly to the sterilization of bacterial spores. According to the conclusions stated in recent papers, the most effective sporicidial agent in low-pressure plasma discharges is intense UV radiation (typically in the spectral range 200–300 nm [32, 33]) capable of penetrating the spores' outer walls and of inducing irreversible modifications of their DNA. The most commonly used discharge mixture to generate UV radiation is oxygen–nitrogen mixture, where the main source of photons in the desired spectral range constitute excited NO molecules. Moreover, excited NO molecules can be effectively produced also in the plasma discharge afterglows, which is mainly due to three body reaction involving atomic oxygen, nitrogen and N_2 molecules [34]:

$$N + O + N_2 \rightarrow NO(A) + N_2. \quad (1)$$

This allows objects to be sterilized to be placed downstream of the active plasma discharge zone while still maintaining a sufficient flux of UV photons and lowering the risk of possible damage of treated articles induced either by extensive heating or by the impact of chemically aggressive radicals.

However, optimizing only UV radiation or placing samples in the afterglow also has serious drawbacks, since it does not typically provide fast removal of biological agents from surfaces due to the low fluxes of chemically active species as well as due to the absence of charged particles that contribute significantly to the process of volatilization of biological systems [20–22]. Not only is this a limitation in terms of removal of pathogenic biomolecules such as infectious proteins or endotoxins but it also influences the overall efficiency of bacterial spores sterilization. Often the spores are stacked or covered with other biological substances, which represents a protective shield towards UV radiation and naturally slows down the sterilization effect of UV radiation. This can be, for instance, demonstrated on the survival curves of bacterial spores obtained in low-pressure discharge plasmas showing typically two phases—the first and the faster phase corresponds to the fast inactivation of spores that are in a direct view of UV radiation; the second phase, and a markedly slower one, is then connected to the killing of covered spores that needs a much longer time to accumulate lethal UV dose [35] and/or with gradual, and rather slow, removal of the shielding material through photo-desorption [6], etching or chemical sputtering.

Therefore, it is clear that an optimal sterilization/decontamination process should combine both the above-mentioned pathways, i.e. providing conditions offering *both* high intensity of UV radiation favourable for fast inactivation of spores *and* high removal rates of possible pathogens or materials shielding spores from direct action of UV radiation. This is commonly fulfilled using an O_2/N_2 mixture and placing objects to be treated in the active zone of the discharge (e.g. [27, 33]). However, it has been recently suggested that the desired effect can also be reached by the application of an Ar/NO discharge mixture [36] or utilizing a ternary mixture consisting of argon, oxygen and nitrogen [37]. In this paper the second option is followed. In order to show the advantageous properties of ternary mixtures, their capability to remove model biomolecules and to emit intense UV radiation in the range 235–270 nm will be compared directly with discharges sustained in O_2/N_2 and Ar/O_2 mixtures, i.e. mixtures identified to be optimal for UV radiation and elimination of biomolecules, respectively.

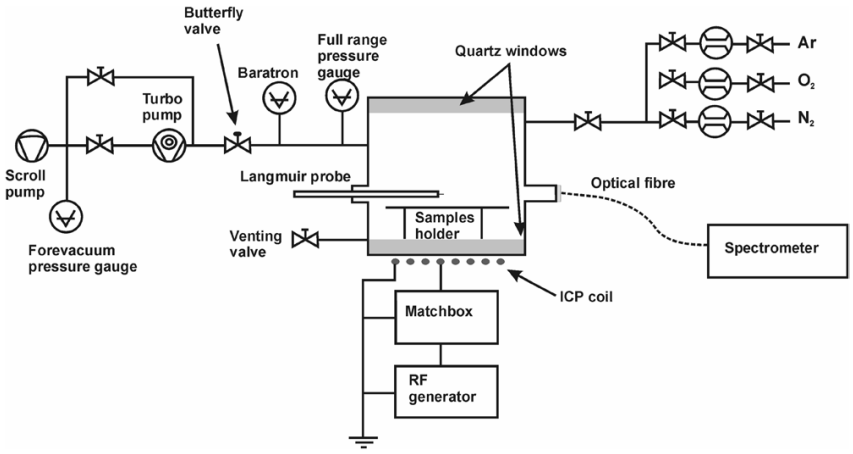

Figure 1. Experimental set-up.

3. Experimental

3.1. Discharge chamber

An ICP source schematically depicted in figure 1 was used in this study. The plasma discharges sustained in O_2, N_2, Ar and their binary and ternary mixtures (pressure 10 Pa, total gas flow 20 sccm and, if not stated otherwise in the text, applied RF power 350 W) were characterized by optical emission spectroscopy using an Avantes AVS-PC2000 monochromator equipped with a 2048-element linear CCD array and by means of a Langmuir probe (SmartProbe™; Scientific Systems Ltd) placed in the sample position.

Moreover, in order to limit the heating of the treated samples, which can significantly influence the kinetics of their etching [38], all the experiments were performed with a treatment duration of 15 s, i.e. the duration after which the substrate temperature measured by IR pyrometry stayed well below 80 °C.

3.2. Samples preparation and characterization

The efficiency of the studied plasma discharges to eliminate biological contamination from surfaces was evaluated on bovine serum albumin (BSA). It has to be noted that although this protein itself is harmless, it serves as a good model of biological contamination of surfaces of medical instruments. The BSA samples were prepared by spotting 0.1% aqueous solution of BSA (Sigma Aldrich) on the polished and cleaned Si wafers. After the deposition, the samples were dried overnight in a common flow hood and subsequently plasma treated. The treated and untreated samples were examined by means of stylus profilometry, which allows direct evaluation of the removal rates of proteins. For the measurements, an Alpha-step® profilometer (KLA-Tencor) was used with a scan speed of 20 μm min^{-1} and a sampling rate of 50 Hz. Equivalent force exerted from the stylus tip on the surface corresponded to 27.4 mg. Details regarding samples preparation and evaluation of etching rates can be found in the literature [19].

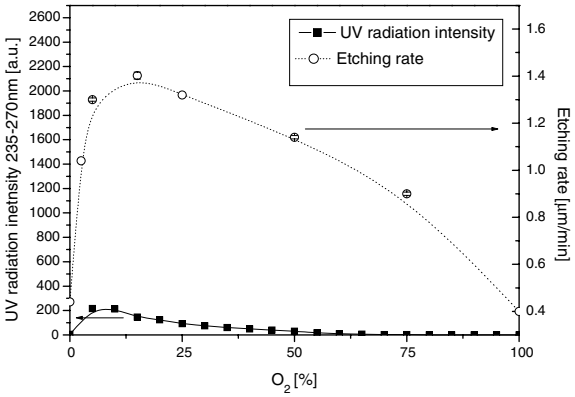

Figure 2. UV radiation intensity integrated in the spectral range 235–270 nm and BSA removal rate as a function of initial argon–oxygen mixture composition (10 Pa, 350 W, total gas flow 20 sccm).

4. Results

4.1. Oxygen containing binary mixtures

In a first step, we evaluated the most suitable discharge mixture in terms of sterilization and decontamination of surfaces by testing the capabilities of plasma discharges sustained in O_2–N_2 and Ar–O_2 mixtures in order to identify their advantages as well as limitations.

4.1.1. Argon–oxygen mixture. As can be seen in figure 2, the ICP discharge sustained in the Ar/O_2 mixture can effectively eliminate the BSA protein. From this perspective the optimal discharge mixture is the one having an argon/oxygen ratio of about 17/3, i.e. the mixture having approximately 15% of oxygen; this mixture produces a removal rate of 1.4 μm min^{-1} for an applied power of 350 W and a pressure of 10 Pa. Increasing either the argon or oxygen portion in the initial discharge mixture leads to a significant decrease in the BSA removal rate. As was demonstrated in previous studies

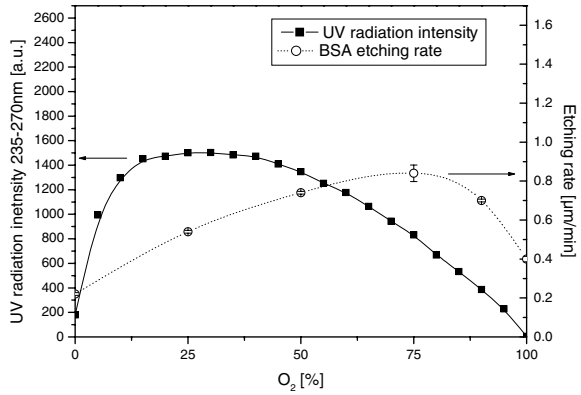

Figure 3. UV radiation intensity integrated in the spectral range 235–270 nm and BSA removal rate as a function of initial oxygen–nitrogen mixture composition (10 Pa, 350 W, total gas flow 20 sccm).

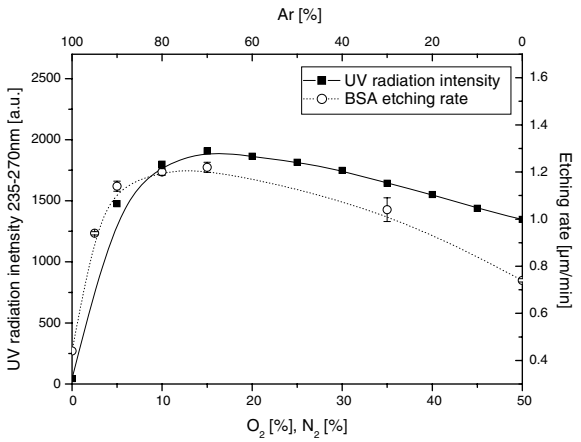

Figure 4. UV radiation intensity integrated in the spectral range 235–270 nm and BSA removal rate as a function of initial argon–oxygen–nitrogen X : 1 : 1 mixture composition (10 Pa, 350 W, total gas flow 20 sccm).

performed under similar experimental conditions [37, 39], the existence of a well-defined maximum of proteins removal rate cannot be interpreted solely by pure chemical etching induced by O atoms, since O atoms density increases monotonically with increasing fraction of O_2 in the mixture as shown both by optical emission actinometry [37] and mass spectroscopy [39]. Instead, the dominant role of chemical sputtering has been suggested in order to explain the observed results. In this reaction scheme the overall rate of BSA elimination is given by the simultaneous action of O atoms and energetic ions produced in the discharge plasma. The variations of the BSA removal rate can consequently be attributed either to the lowering of the flux of atomic oxygen needed for proteins volatilization (in the case of increasing Ar amount) or to a fast decrease in ion density (when the oxygen portion is increased) leading to the reduced rate of chemical sputtering.

Moreover, it can also be seen in figure 2 that Ar/O_2 is a bad source of UV radiation. The low emission observed in the 235–270 nm spectral range originates only from a small amount of nitrogen impurities present in the discharge chamber.

4.1.2. Oxygen–nitrogen mixture. As expected, much better results concerning UV radiation are observed using the O_2/N_2 discharge mixture. As can be seen in figure 3, the O_2/N_2 mixture offers almost one order of magnitude higher UV radiation intensity as compared with Ar/O_2. However, the removal rate of BSA using the O_2/N_2 mixture is considerably smaller than the values reached using the Ar/O_2 discharge (maximal removal rate observed in the O_2/N_2 plasma discharge is 0.84 μm min^{-1}, which is 40% lower as compared with the one observed using Ar/O_2). It is worth mentioning that unlikely to the argon–oxygen mixture, the variations of the BSA etching rate can be attributed solely to the changes in fluxes of active oxygen, since no significant variations of ion density were observed with changing the oxygen/nitrogen ratio in the initial discharge mixture, as will be demonstrated later. Moreover, it can be seen that the maximal values of the removal rate of BSA and the intensity of UV radiation are obtained at markedly different mixture compositions: the highest rate of protein removal was observed for mixture having around 80% of O_2, whereas the maximal UV intensity in the spectral range 235–270 nm can be achieved for fraction 20–30% of O_2 in the Ar/O_2 plasma. In other words, changing the O_2/N_2 ratio leads either to enhancement of UV light emission and decrease in capability of oxygen–nitrogen plasma discharge to eliminate biomolecules or vice versa.

4.2. $Ar/N_2/O_2$ ternary mixture

As was demonstrated above, discharges sustained in binary mixtures can be operated at conditions *either* favourable for the elimination of biomolecules *or* suitable for the emission of intense UV radiation. Moreover, the direct comparison of Ar/O_2 and N_2/O_2 discharges revealed that the first one offers a markedly higher rate of biomolecules removal, whereas the second one can be used as an effective source of UV radiation. In order to explore the possibility to combine these two properties, further experiments were performed in $Ar/N_2/O_2$ ternary mixture with fixed O_2 over N_2 ratio 1 : 1 and varying Ar portion in the discharge mixture, while keeping the total gas flow constant. As can be seen in figure 4, substitution of oxygen and nitrogen by argon up to 80% of Ar leads to the increase in *both* UV radiation intensity *and* BSA removal rate. Further increase in the Ar fraction in the discharge mixture subsequently causes a decrease in these two quantities. However, it is evident that these results are rather advantageous as compared to Ar/O_2 and N_2/O_2 binary discharge mixtures:

- First, the application of $Ar/N_2/O_2$ ternary mixture maintains a high removal rate of BSA (maximal value observed is approximately 1.2 μm min^{-1}) still comparable to the one obtained in the Ar/O_2 discharge and leads to the emission of UV radiation having an intensity even higher than the maximal one reachable at identical operational conditions (i.e. pressure, RF power and total gas flow) in the case of the nitrogen–oxygen plasma.

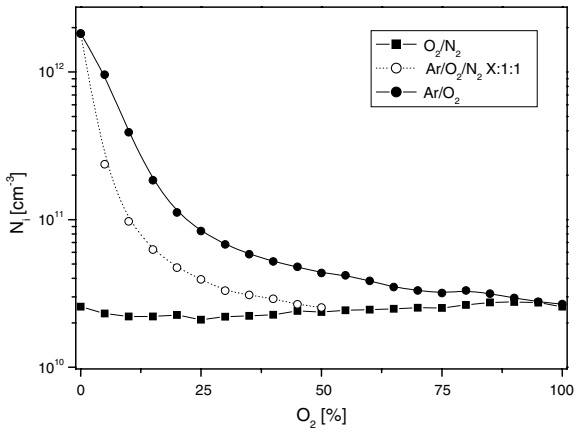

Figure 5. Positive ion density in studied discharge mixtures (10 Pa, 350 W, total gas flow 20 sccm).

- Second, the maximal values of both the protein removal rate and UV radiation intensity are obtained for similar discharge mixture compositions. This is a result of considerable importance, since it allows overcoming the principal drawback of discharges sustained in oxygen–nitrogen binary discharge mixture demonstrated in the previous section, i.e. the possibility to maximize either the UV intensity or the removal rate of biological systems.

The results obtained are most likely connected not only with the behaviour of the density of neutral species produced in the plasma but also with the variation of the plasma density. As can be seen in figure 5, argon addition into oxygen–nitrogen discharge mixture leads to an increase in plasma density similarly to the increase observed with increasing fraction of Ar in Ar/O_2 plasma. This effect is due to higher electron energy losses in interactions with molecular gases than with argon atoms (e.g. [40]). In other words, the energy supplied to the discharge is consumed in the case of molecular gases not only for their ionization but also for their vibrational and rotational excitations. Lowering the amount of molecular gases in the initial discharge mixture therefore reduces these energy losses and subsequently more energy is available for ionization, which results in a higher plasma density, which has important practical consequences:

First, the higher flux density of ions on the treated surfaces promotes the process of its chemical sputtering by enhanced rate of breaking of molecular bonds in the protein deposit by impinging ions, thus creating more surface active sites that are subsequently attacked by plasma produced radicals. This can explain the observed increase in the BSA removal rate when argon is added into the oxygen–nitrogen mixture in analogy to the case of Ar/O_2 plasma discharge as described for the cases of bacterial spores and hydrocarbon films [39].

Second, higher production of charged particles increases the production of electronically excited species. This can be demonstrated, for instance, on the behaviour of the intensities of the first and second positive systems of molecular nitrogen measured in O_2/N_2 and $Ar/O_2/N_2$ plasma discharges. As can be seen in figure 6, the intensity of these two spectral

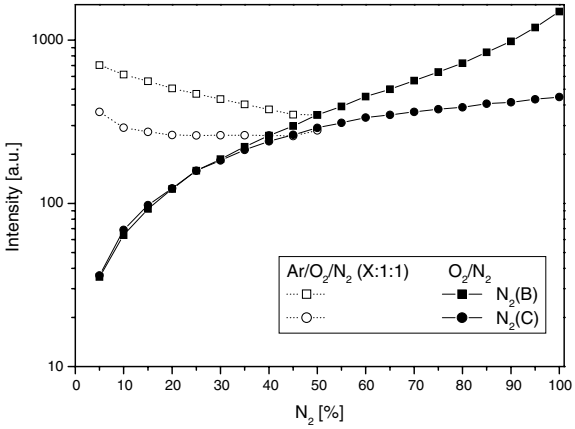

Figure 6. Intensity of the first positive system $N_2(B)$ and the second positive system $N_2(C)$ of molecular nitrogen as a function of nitrogen fraction in the initial discharge mixture (10 Pa, 350 W, total gas flow 20 sccm).

bands decreases monotonically with increasing oxygen over nitrogen ratio in the O_2/N_2 mixture, which is, taking into account almost constant plasma density, mainly due to the decrease in the N_2 portion in the plasma discharge. This trend is significantly altered when argon is added into the discharge mixture—intensities of both nitrogen spectral bands increase with decreasing N_2 amount, reflecting an increase in the density of nitrogen molecules in their higher electronically states. Although both $N_2(B)$ or $N_2(C)$ states do not contribute to the production of excited NO molecules responsible for the emission of UV radiation, one can expect similar tendencies also for $N_2(A)$ states that are strongly linked to the densities of the $N_2(B)$ molecules [41] and that were identified to play a dominant role for the production of $NO(A)$ molecules in the active zone of the discharge through reaction (e.g. [42, 43])

$$NO + N_2(A) \rightarrow NO(A) + N_2 \qquad (2)$$

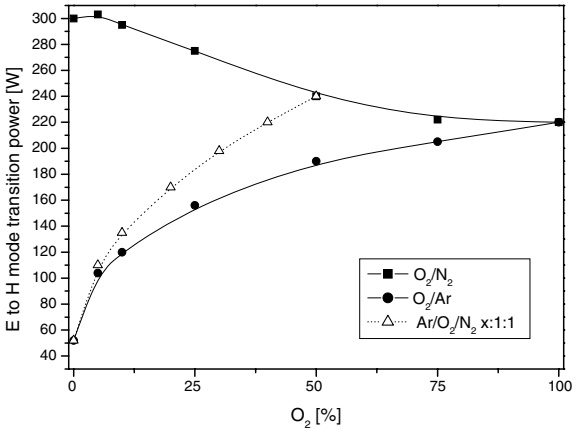

Figure 7. E to H mode transition power in studied discharge mixtures (10 Pa, total gas flow 20 sccm).

as well as to contribute to the process of creation of ground state NO molecules [41]:

$$N_2(A) + O \rightarrow NO + N(^2D). \quad (3)$$

The higher production of $N_2(A)$ resulting from the higher electron density can therefore explain the more effective excitation of NO molecules and consequently the higher intensity of NOγ spectral bands in the spectral range 235–270 nm in $Ar/O_2/N_2$ plasma discharges than in the oxygen–nitrogen one.

Moreover, higher plasma density in argon containing mixtures as compared with O_2/N_2 plasma discharge also has practical consequences for process optimization: it lowers the power transition point between E and H modes of ICP discharges, i.e. modes characterized by prevailing capacitive (E-mode) or inductive (H-mode) coupling [44], as depicted in figure 7. This allows decreasing the applied RF power maintaining high treatment efficiency connected with the H-mode [23] on the one hand and lowering the thermal load on the other hand. Especially the latter is of high interest from the point of view of the real applications, where thermo-labile materials have to be processed.

5. Conclusions

In summary, two different aspects of plasma discharges, namely, their capability to emit UV radiation in the spectral range suitable for fast inactivation of bacterial spores and efficiency of removal of model biological substance, were studied in order to explore the possibility to use $Ar/O_2/N_2$ discharge mixture for sterilization and decontamination of surfaces. The results presented clearly show that under otherwise identical operational conditions (RF power, pressure and total gas flow), discharges sustained in the ternary mixture of argon, oxygen and nitrogen combine advantageous properties of plasma discharges operated in O_2/N_2 and Ar/O_2 mixtures. This allows reducing the applied RF power fed to the discharge or to significantly shorten the treatment time necessary for the assurance of the safety of processed medical tools, which in turn limits undesirable damage induced by plasma action on treated articles. The observed results were furthermore related to the behaviour of plasma density that has been suggested to be the major agent governing both the production of UV radiation and the removal of BSA protein deposits, selected as a model of biological contamination of the surface.

Acknowledgments

This work has been supported by the FP6 2005 NEST project 'Biodecon' and the JRC Action 15008: NanoBiotechnology for Health.

References

[1] Miller D M, Youkhana I, Karunaratne W U and Pearce A 2001 *Anaesthesia* **56** 1069
[2] Dinakaran S and Kayarkar W 2002 *Eye* **16** 281
[3] Lipscomb I P, Sihota A K and Keevil C W 2006 *J. Clin. Microbiol.* **44** 3728
[4] Murdoch H, Taylor D, Dickinson J, Walker J T, Perrett D, Raven N D H and Sutton J M 2006 *J. Hosp. Infect.* **63** 432
[5] Baxter R L, Baxter H C, Campbell G A, Grant K, Jones A, Richardson P and Whittaker G 2006 *J. Hosp. Infect.* **63** 439
[6] Moisan M, Barbeau J, Moreau S, Pelletier J, Tabrizian M and Yahia L'H 2001 *Int. J. Pharm.* **226** 1
[7] Lerouge S, Fozza A C, Wertheimer M R, Marchand R and Yahia L'H 2000 *Plasma polym.* **5** 31
[8] Laroussi M 2005 *Plasma Process. Polym.* **2** 391
[9] Rossi F, Kylián O and Hasiwa M 2006 *Plasma Process. Polym.* **3** 431
[10] Kylián O, Hasiwa M and Rossi F 2006 *IEEE Trans. Plasma Sci.* **34** 2606
[11] Hasiwa M, Kylián O, Hartung T and Rossi F 2008 *Innate Immun.* **14** 89
[12] Mogul R, Bol'shakov A A, Chan S L, Stevens R M, Khare B N, Meyyappan M and Trent J D 2003 *Biotechnol. Prog.* **19** 776
[13] Baxter H C, Campbell G A, Richardson P R, Jones A C, Whittle I R, Casey M, Whittaker A G and Baxter R L 2006 *IEEE Trans. Plasma Sci.* **34** 1337
[14] Bernard C, Leduc A, Bardeau J, Saoudi B, Yahia L'Y and De Crescenzo G 2006 *J. Phys. D: Appl. Phys.* **39** 3470
[15] Deng X T, Shi J J, Chen H L and Kong M G 2007 *Appl. Phys. Lett.* **90** 013903
[16] Deng X T, Shi J J and Kong M G 2007 *J. Appl. Phys.* **101** 074701
[17] Baxter H C, Campbell G A, Whittaker A G, Jones A C, Aitken A, Simpson A H, Casey M, Bountiff L, Gibbard L and Baxter R L 2005 *J. Gen. Virol.* **86** 2393
[18] Ceccone G, Gilliland D, Kylián O and Rossi F 2006 *Czech. J. Phys.* **56** B672
[19] Kylián O, Rauscher H, Gilliland D, Brétagnol F and Rossi F 2008 *J. Phys. D: Appl. Phys.* **41** 095201
[20] Opretzka J, Benedikt J, Awakowicz P, Wunderlich J and von Keudell A 2007 *J. Phys. D: Appl. Phys.* **40** 2826
[21] Raballand V, Benedikt J, Wunderlich J and von Keudell A 2008 *J. Phys. D: Appl. Phys.* **41** 115207
[22] Kylián O, Benedikt J, Sirghi L, Reuter R, Rauscher H, von Keudell A and Rossi F 2009 *Plasma Process. Polym.* **6** doi:10.1002/ppap200800199

[23] Rossi F, Kylián O, Rauscher H, Gilliland D and Sirghi L 2008 *Pure Appl. Chem.* **80** 1939
[24] Vicoveanu D, Popesco S, Ohtsu Y and Fujita H 2008 *Plasma Process. Polym.* **5** 350
[25] Nagatsu M , Terashita F, Nonaka H, Xu L, Nagata T and Koide Y 2005 *Appl. Phys. Lett.* **86** 211502
[26] Vujošević D, Mozetič M, Cvelbar U, Krstulović N and Milošević S 2007 *J. Appl. Phys.* **101** 103305
[27] Kylián O, Sasaki T and Rossi F 2006 *Eur. Phys. J. Appl. Phys.* **34** 139
[28] Vratnica Z, Vujoševic D, Cvelbar U and Mozetic M 2008 *IEEE Trans. Plasma Sci.* **36** 1300
[29] Whittaker A G, Graham E M, Baxter R L, Jones A C, Richardson P R, Meek G, Campbell G A, Aitken A and Baxter H C 2004 *J. Hosp. Infect.* **56** 37
[30] Lerouge S, Wertheimer M R, Marchand R, Tabrizian M and Yahia L'H 2000 *J. Biomed. Mater. Res.* **51** 128
[31] Kylián O, Hasiwa M, Gilliland D and Rossi F 2008 *Plasma Process. Polym.* **5** 26
[32] Halfmann H, Denis B, Bibinov N, Wunderlich J and Awakowicz P 2007 *J. Phys. D: Appl. Phys.* **40** 5907
[33] Xu L, Nonaka H, Zhou H Y, Ogino A, Nagata T, Koide Y, Nanko S, Kurawaki I and Nagatsu M 2007 *J. Phys. D: Appl. Phys.* **40** 803
[34] Kutasi K, Saoudi B, Pintassilgo C D, Loureiro J and Moisan M 2008 *Plasma Process. Polym.* **5** 840
[35] Philip N, Saoudi B, Crevier M C, Moisan M, Barbeau J and Pelletier J 2002 *IEEE Trans. Plasma Sci.* **30** 1429
[36] Hueso J L, Rico V J, Frías J E, Cotrino J and Gonzáles-Rlipe A R 2008 *J. Phys. D: Appl. Phys.* **41** 092002
[37] Stapelmann K, Kylián O, Denis B and Rossi F 2008 *J. Phys. D: Appl. Phys.* **41** 192005
[38] Cvelbar U, Vujoševic D, Vratnica Z and Mozetic M 2006 *J. Phys.D: Appl. Phys.* **39** 3487
[39] Benedikt J, Flötgen C, Kussel G, Raballand V and von Keudell A 2008 *J. Phys.: Conf. Ser.* **133** 012012
[40] Gudmundsson J T, Kimura T and Lieberman M A 1999 *Plasma Sources Sci. Technol.* **8** 22
[41] Guerra V, Sá P A and Loureiro J 2001 *J. Phys. D: Appl. Phys.* **34** 1745
[42] Guerra V and Loureiro J 1997 *Plasma Sources Sci. Technol.* **6** 373
[43] Pintassilgo C D, Kutasi K and Loureiro J 2007 *Plasma Sources Sci. Technol.* **16** S115
[44] Turner M M and Lieberman M A 1999 *Plasma Sources Sci. Technol.* **8** 313

Effect of Low-Pressure Microwave Discharges on Pyrogen Bioactivity

Ondřej Kylián, Marina Hasiwa, and François Rossi

Abstract—**The effect of microwave discharge on pyrogen bioactivity has been studied in different oxygen- and hydrogen-containing mixtures with the aim of identifying the crucial depyrogenation agent. According to the obtained biological results and their comparison with properties of the plasma determined by means of optical emission spectroscopy and Langmuir probe measurements, it has been found that under experimental conditions tested, depyrogenation is not greatly affected by UV radiation or charged particles but is considerably accelerated by the presence of atomic hydrogen.**

Index Terms—**Depyrogenation, lipopolysaccharides (LPS), microwave discharge.**

I. Introduction

THE INTERACTION of specific microorganisms (bacterial spores, viruses, moulds, or yeast) or biomolecules (e.g., pyrogens, proteins, and prions) with the human body can lead to the onset of various diseases having frequently severe consequences. Such potentially harmful organisms and biomolecules must therefore be eliminated, inactivated, or removed from any surface that can come in direct contact with the human body, e.g., via surfaces of surgical tools, or indirectly through the injection of drugs taken from contaminated vials. Hence, it is not surprising that much effort has been devoted in the last years to develop and validate techniques of sterilization and decontamination, if possible operating at low temperature and therefore enabling treatment of heat-sensitive materials. It has been emphasized by many authors (e.g., [1]–[3]) that the application of low-pressure discharges has many advantages over conventionally used sterilization and decontamination methods as moist and dry heat sterilization, ionizing irradiation (X-rays, gamma rays, and electron beams), or chemical treatment (e.g., ethylene oxide (EtO) treatment). The strength of this approach is mainly related to the fact that nonequilibrium discharges offer the possibility of sufficiently fast sterilization and decontamination under relatively low temperatures using nontoxic gases and therefore enabling operator- and environment-friendly operation. Generally speaking, nonequilibrium discharges act as potent sources of a wide variety of both neutral and ionized chemically active species that effectively sputter, destroy, or alter the properties of biological contamination. Moreover, nonequilibrium plasmas can be used as sources of energetic UV/VUV photons that can also inactivate or destroy biomolecules.

However, it should be noted that while applicability of employing plasma for the sterilization of bacterial spores has been demonstrated by many groups (e.g., [1]–[7]) and is generally accepted, current knowledge concerning deactivation or destruction of other possible sources of infections or inflammations using gas discharges is still relatively poor. This is in particular true in the case of different kinds of pyrogens.

Pyrogens are fever-causing substances. Typical examples of them are lipopolysaccharides (LPS), which are a major part of the outer membranes of Gram-negative bacteria, and which have been identified to act as extremely strong stimulators of innate or natural mammalian immune system (e.g., [8]). The physiological effects of pyrogens in humans are various and dose dependent. Their presence in the blood stream leads to the release of several inflammatory mediators (e.g., IL-1 β, TNF-α), helping the body recognize sites of infection followed by the elimination of invading microorganisms. However, higher doses can lead to serious clinical events, like multiple organ failure, septic shock, and ultimately to patient death (e.g., [9] and [10]). Depyrogenation of all medical devices and pharmaceutical containers before their use is therefore essential. The problem is particularly important for pharmaceutical industry where the vials containing liquids to be injected must be totally free from pyrogenic contamination.

Nevertheless, pyrogens, once present, are hard to remove. This is mainly because they are extremely thermostable, and therefore, high temperatures for their destruction are required. At present, depyrogenation of vials is made by thermal treatment at 250 °C for 30 min or 200 °C for 60 min [11], which imposes the use of glass and is costly in terms of energy and floor space. Therefore, a depyrogenation method based on a mechanism different from heat is highly desired, and application of low-temperature plasmas is one of the promising candidates as suggested by several authors (e.g., [12] and [13]) and demonstrated in our previous publications ([14] and [15]). According to the obtained results, the following conclusions have been stated.

1) Two orders of magnitude decrease of LPS amount have been observed using low-pressure microwave discharge within several minutes of treatment.
2) The efficiency of LPS destruction depends on used gas mixtures.
3) The observed decrease of LPS bioactivity is predominantly caused by plasma–pyrogen interaction. In other words, it has been shown that in the condition tested, LPS bioactivity is not greatly affected by other possible

Manuscript received April 10, 2006; revised July 31, 2006. This work was supported in part by the EU Growth project Steriplas under Grant GRD1-1999-10584 and in part by the FP6 2005 NEST Project "Biodecon."

The authors are with the European Commission, Joint Research Centre, Institute for Health and Consumer Protection, 21020 Ispra, Italy (e-mail: ondrej.kylian@jrc.it; marina.hasiwa@jrc.it; francois.rossi@jrc.it).

Digital Object Identifier 10.1109/TPS.2006.885093

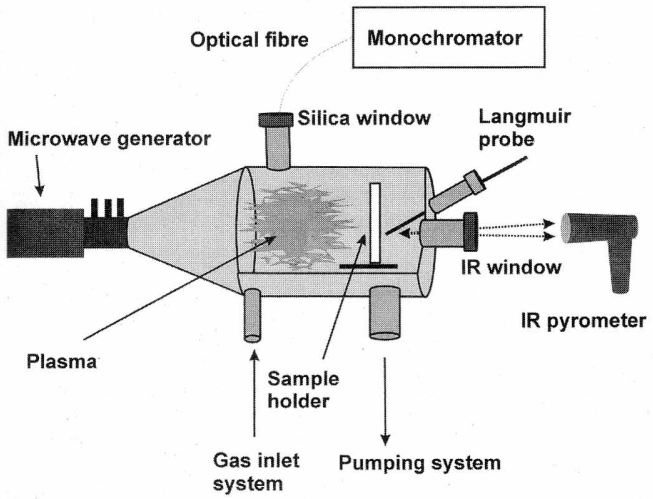

Fig. 1. Experimental setup.

mechanisms such as increased temperature, microwave radiation, or low-pressure conditions, at least within treatment time.

4) According to the crystal microbalance study and its comparison with biological results, it has been concluded that the loss of biological activity of Lipid A, which is the pyrogenic part of LPS, can be due to both its etching and the modifications of different chemical structures of Lipid A [15].

In order to obtain better insight into the mechanism of LPS deactivation during plasma treatment, new sets of experiments have been performed and focused on the estimation of the particular contribution of UV radiation, charged particles, and active species produced by the discharge for depyrogenation. In order to meet this objective, treatments of LPS samples have been performed in discharges sustained in different gas mixtures, and results of depyrogenation efficiency have been compared with discharge properties determined by plasma diagnostics methods. The aim of this paper is to summarize the results of this investigation.

II. Experimental

A. Depyrogenation Chamber

The experimental setup used for the depyrogenation tests is depicted in Fig. 1. It consists of a stainless steel cylindrical vacuum chamber (200 mm in diameter and 380 mm in length) equipped with several diagnostics windows and one port for the samples introduction. The processing chamber is connected to the gas inlet system composed of mass flow controllers attached to the gas lines (H_2, O_2, N_2, and Ar) and is evacuated by a primary pump and a roots blower allowing a base vacuum of 0.3 Pa.

The plasma is excited at a pressure of 13.3 Pa and a total gas flow of 100 sccm (standard cubic centimeter per minute) by a microwave power supply working at 2.45 GHz. The microwave circuit includes a microwave supply (maximal power 2 kW), a circulator, a three-stub impedance matching system, and a rectangular–circular waveguide transition. Microwaves are introduced to the plasma chamber through a silica window placed at the extremity of a circular 100-mm waveguide.

The discharge properties have been estimated by means of several diagnostic methods. The composition of discharge and the intensity of UV radiation in the spectral range of 200–300 nm have been determined by optical emission spectroscopy using an Avantes AVS-PC2000 monochromator equipped with a 2048-element linear charge-coupled device array. Charged particle densities have been measured by means of a Langmuir probe (Smart probe; Scientific Systems Ltd.; Ireland) at the sample position. The gas temperature has been monitored using the calibrated infrared pyrometer (Raynger MX4; Raytek; USA).

B. Determination of Pyrogen Bioactivity

The samples to be treated were plastic 24-well polystyrene tissue culture plates (Becton Dickinson Labware) covered with 100 μl of LPS extracted from *Escherichia coli* 0111 : B4 (Sigma Aldrich) diluted in pyrogen-free water (1 ng of LPS in 1 ml of water). After drying in the common flow-hood overnight, the well plates were introduced to the plasma chamber at the distance of 300 mm from the silica window and exposed to the plasma for 60 s.

The bioactivity of LPS after plasma treatment has been measured by human whole blood test (WBT) [16]. This test uses immune defense mechanisms based on cytokine release (e.g., IL-1 β, TNF-α) in the presence of an immune-stimulating substance in the human organism. Adding LPS to human whole blood and measuring the cytokines released (in current study IL-1 β) by a sandwich ELISA (enzyme-linked immunosorbent assay) enables us to simulate the human response to an immuno-stimulating event *in vitro*. The advantages of WBT over traditionally used tests (the Rabbit or Limulus Amebocyte Assay tests) are the possibility of performing measurements directly on surfaces and lower detection limit. The measurements of LPS bioactivity described in this paper are done in a physiological environment, donor independent, and at least three replicates have been used. More detailed description of the WBT can be found, e.g., in [16].

III. Results

The depyrogenation results obtained in different oxygen-containing mixtures (O_2:Ar, O_2:N_2, and O_2:H_2) are summarized in Fig. 2, which represents the biological response normalized to its value obtained after treatment in discharge in pure oxygen. It can be seen that the addition of Ar and N_2 into the oxygen discharge does not lead to significant changes of depyrogenation efficiency compared to the results obtained in discharge in pure oxygen in contrast to the case of H_2 addition that results in fast increase of LPS deactivation (more than one order of magnitude for 80% of hydrogen).

The obtained results allow us to estimate the importance of possible depyrogenation agents for LPS destruction. First, comparing the observed behavior of depyrogenation efficiency in different mixtures with UV radiation emitted by the discharges,

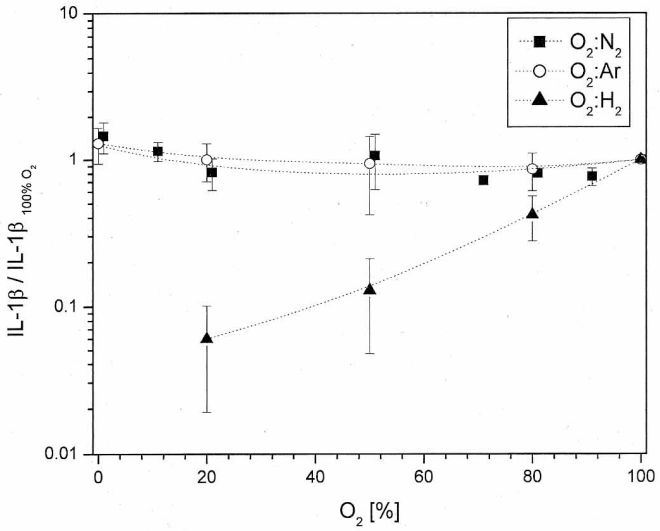

Fig. 2. Bioactivity after plasma treatment normalized to the bioactivity in discharge in pure oxygen (applied microwave power 1000 W, pressure 13.3 Pa, total gas flow 100 sccm, treatment time 60 s, LPS dilution 1 ng/ml).

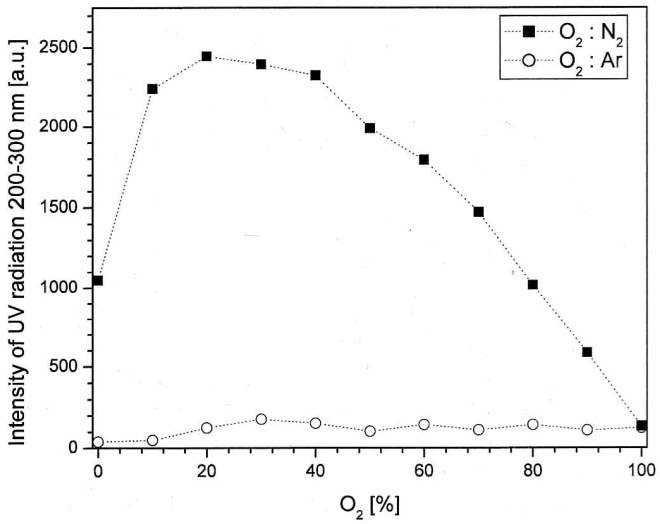

Fig. 3. Comparison of UV radiation intensities in $O_2:N_2$ and $O_2:Ar$ mixtures (applied microwave power 1000 W, pressure 13.3 Pa, total gas flow 100 sccm).

it is possible to conclude that there is no straight connection between depyrogenation and UV light intensity, and therefore, UV radiation is not under our experimental conditions the principle depyrogenation agent. This fact can be demonstrated by the comparison of depyrogenation results and intensity of UV radiation measured as the integral between 200 and 300 nm in $O_2:N_2$ and $O_2:Ar$ mixtures. For these two mixtures, almost the same treatment efficiency has been observed despite significant distinctions of the UV radiation intensities (Fig. 3).

The second possible mechanism that could markedly influence the bioactivity of LPS is the sputtering of the deposit by the charged particles. In order to estimate the importance of this mechanism, electron densities as well as their temperature have been determined by means of the Langmuir probe technique. However, it has been found that neither the charged particles are responsible for LPS deactivation. This can be demonstrated for example on the case of the $O_2:H_2$ mixture. As can be seen in

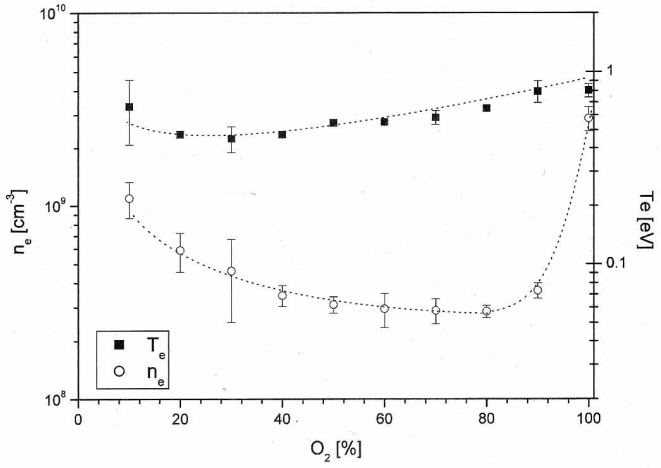

Fig. 4. Electron density and electron temperature in $O_2:H_2$ mixture (applied microwave power 1000 W, pressure 13.3 Pa, total gas flow 100 sccm).

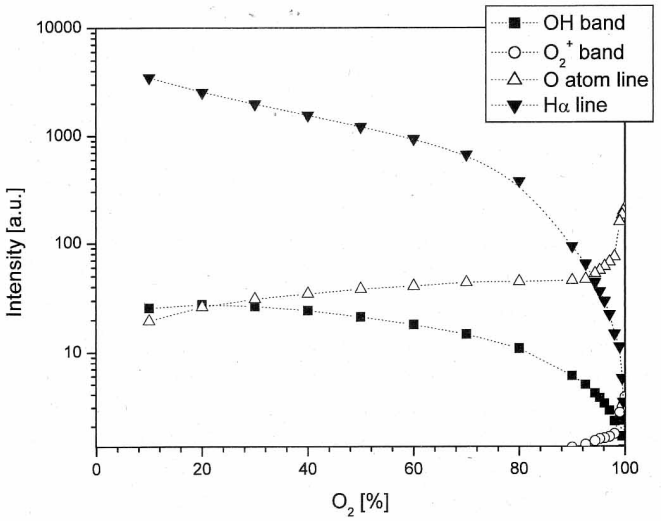

Fig. 5. Behavior of spectral lines and bands in $O_2:H_2$ mixture (applied microwave power 1000 W, pressure 13.3 Pa, total gas flow 100 sccm).

Fig. 4, the addition of hydrogen into oxygen discharge causes a dramatic decrease of electron density that is completely in opposite to the biological results obtained, which indicate an increase of the treatment efficiency after H_2 addition.

The acceleration of LPS deactivation observed with the increasing amount of H_2 in the $O_2:H_2$ mixture cannot be attributed to the increased energy release due to the oxygen–hydrogen combustion since it has been found that the temperature measured by means of the IR pyrometry stays, under the experimental conditions tested, almost constant for the addition of H_2 up to 50% (approximately 40 °C) in contrary to the depyrogenation results showing substantial alternations of the biological activity of LPS.

Finally, the LPS can be inactivated by interactions with active particles produced in the discharge. Since only the addition of hydrogen to oxygen discharge leads to the significant increase of depyrogenation efficiency, optical emission spectroscopy has been employed in order to estimate the behavior of active particles produced in the $O_2:H_2$ discharge. According to the obtained results (Fig. 5), it can be concluded that only the

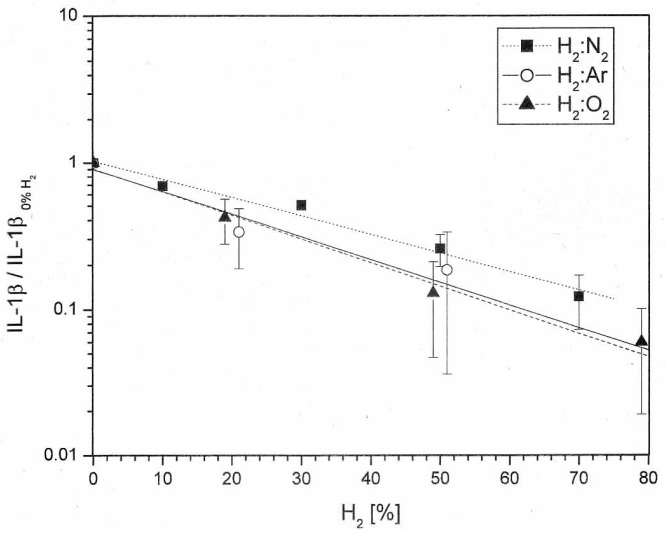

Fig. 6. LPS bioactivity after plasma treatment normalized to bioactivity of hydrogen free discharges (applied microwave power 1000 W, pressure 13.3 Pa, total gas flow 100 sccm, treatment time 60 s, LPS dilution 1 ng/ml).

spectral lines following the behavior of efficiency of LPS deactivation, i.e., lines whose intensities increase with the addition of hydrogen into oxygen discharge, are spectral lines belonging to neutral hydrogen atoms and OH molecules. The occurrence of both of these particles can therefore explain the rapid increase of depyrogenation efficiency when hydrogen molecules are added into an oxygen discharge. In order to estimate which of them is responsible for the increased efficiency of plasma treatment, additional experiments have been performed in other hydrogen-containing mixtures, namely in $Ar:H_2$ and $N_2:H_2$, i.e., mixtures that do not contain OH radicals.

As can be seen in Fig. 6, in all the studied hydrogen-containing mixtures, qualitatively the same behavior has been observed, i.e., the increase of depyrogenation efficiency with increasing amount of hydrogen in the discharge mixture. For all the three tested mixtures, the only common particles are hydrogen atoms and molecules. Since it has already been demonstrated elsewhere [14] that H_2 itself has no effect on the bioactivity of LPS, it can be concluded that an increase of depyrogenation efficiency under our experimental conditions is connected principally with H atoms.

IV. Conclusion

The main objective of this paper was to estimate the importance of several possible depyrogenation agents that can cause decrease of LPS bioactivity during its exposure to low-pressure microwave discharge. Comparison of the measured bioactivity after plasma treatment in different discharge mixtures, which consisted of oxygen, nitrogen, argon, and hydrogen, with the properties of these mixtures revealed that the depyrogenation efficiency is under our experimental conditions almost independent on the intensity of UV radiation in the 200- to 300-nm spectral range as well as on densities of charged particles. In contrast, it has been found that the efficiency of treatment can be significantly accelerated (in some cases, even more than by one order of magnitude) by atomic hydrogen. This result is of a great importance particularly for the optimization of plasma treatment in order to achieve 3 log reduction of pyrogen amount desired by legislative regulations within sufficiently short treatment time.

Though, reported results are promising there are still several open questions. This is in particular true concerning the mechanism of diminishing the LPS bioactivity. This topic is a subject of ongoing systematic investigation.

Acknowledgment

The authors would like to thank T. Hartung for useful discussions regarding the WBT.

References

[1] M. Moisan, J. Barbeau, S. Moreau, J. Pelletier, M. Tabrizian, and L'. H. Yahia, "Low-temperature sterilization using gas plasmas: A review of the experiments and an analysis of the inactivation mechanisms," *Int. J. Pharm.*, vol. 226, no. 1, pp. 1–21, Sep. 2001.

[2] S. Lerouge, A. C. Fozza, M. R. Wertheimer, R. Marchand, and L'. H. Yahia, "Sterilization by low-pressure plasma: The role of vacuum-ultraviolet radiation," *Plasmas Polym.*, vol. 5, no. 1, pp. 31–46, Mar. 2000.

[3] M. Laroussi, "Low temperature plasma-based sterilization: Overview and state-of-the-art," *Plasma Process. Polym.*, vol. 2, no. 5, pp. 391–400, 2005.

[4] I. A. Soloshenko, V. V. Tsiolko, V. A. Khomich, A. I. Schedrin, A. V. Ryabtsev, V. Y. Bazhenov, and I. L. Mikhno, "Sterilization of medical products in low-pressure glow discharge," *Plasma Phys. Rep.*, vol. 26, no. 9, pp. 792–800, Sep. 2000.

[5] J. Feichtinger, A. Schulz, M. Walker, and U. Schumacher, "Sterilization with low-pressure microwave plasmas," in *Proc. 8th Int. Conf. Plasma Surf. Eng.*, vol. 174/175, pp. 564–569, Sep./Oct. 2003.

[6] O. Kylián, T. Sasaki, and F. Rossi, "Plasma sterilization of *Geobacillus stearothermophilus* by O_2 : N_2 RF inductively coupled plasma," *Eur. Phys. J., Appl. Phys.*, vol. 34, no. 2, pp. 139–142, May 2006.

[7] M. Nagatsu, F. Terashita, H. Nonaka, L. Xu, T. Nagata, and Y. Koide, "Effects of oxygen radicals in low-pressure surface-wave plasma on sterilization,"*Appl. Phys. Lett.*, vol. 86, no. 21, pp. 128–130, May 2005. art. 211502 (3 pages)

[8] B. Beutler and E. T. Rietschel, "Innate immune sensing and its roots: The story of endotoxin," *Nat. Rev. Immunol.*, vol. 3, no. 2, pp. 169–176, Feb. 2003.

[9] C. A. Dinarello, "Proinflammatory cytokines," *Chest*, vol. 118, no. 2, pp. 503–508, Aug. 2000.

[10] M. T. Abreu and M. Arditi, "Innate immunity and toll-like receptors: Clinical implications of basic science research," *J. Pediatr.*, vol. 144, no. 4, pp. 421–429, Apr. 2004.

[11] W. Hecker, D. Witthauer, and A. Staerk, "Validation of dry heat inactivation of bacterial endotoxins," *PDA J. Pharm. Sci. Technol.*, vol. 48, no. 4, pp. 197–204, Jul./Aug. 1994.

[12] R. E. Peeples and N. R. Anderson, "Microwave coupled plasma sterilization and depyrogenation II. Mechanisms of action," *J. Parenter. Sci. Technol.*, vol. 39, no. 1, pp. 9–15, Jan./Feb. 1985.

[13] S. Lerouge, M. R. Wertheimer, and L'. H. Yahia, "Plasma sterilization: A review of parameters, mechanisms, and limitations," *Plasmas Polym.*, vol. 6, no. 3, pp. 175–188, Sep. 2001.

[14] O. Kylián, M. Hasiwa, and F. Rossi, "Plasma-based de-pyrogenization," *Plasma Process. Polym.*, vol. 3, no. 3, pp. 272–275, Apr. 2006.

[15] F. Rossi, O. Kylián, and M. Hasiwa, "Decontamination of surfaces by low pressure plasma discharges," *Plasma Process. Polym.*, vol. 3, no. 6/7, pp. 431–442, Aug. 2006.

[16] S. Hoffmann, A. Peterbauer, S. Schindler, S. Fennrich, S. Poole, Y. Mistry, T. Montag-Lessing, I. Spreitzer, B. Löschner, M. van Aalderen, R. Bos, M. Gommer, R. Nibbeling, G. Werner-Felmayer, P. Loitzl, T. Jungi, M. Brcic, P. Brügger, E. Frey, G. Bowe, J. Casado, S. Coecke, J. de Lange, B. Mogster, L. M. Næss, I. S. Aaberge, A. Wendel, and T. Hartung, "International validation of novel pyrogens tests based on human monocytoid cells," *J. Immunol. Methods*, vol. 298, no. 1/2, pp. 161–173, 2005.

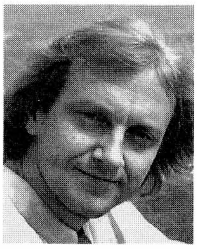

Ondřej Kylián was born in Prague, Czech Republic, in 1975. He received the M.S. and Ph.D. degrees in the physics of plasma and ionized media from Charles University, Prague, in 1998 and 2003, respectively.

He was a Research Fellow with the Institute of Atmospheric Physics, Academy of Sciences of the Czech Republic, Prague, and with Charles University. Since 2004, he has been a Contractual Agent with the European Commission, Joint Research Centre, Institute for Health and Consumer Protection, Ispra, Italy.

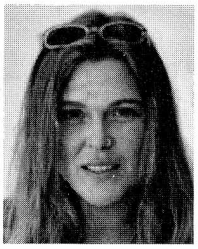

Marina Hasiwa was born in Wiesensteig, Gernany, in 1971. She received the Diploma in biology from the University of Konstanz, Konstanz, Germany, in 2002. She is currently working toward the Ph.D. degree in surface testing strategies by biological methods, especially in the field of immune stimulatory components on surfaces.

She is currently with the European Commission, Joint Research Centre, Institute for Health and Consumer Protection, Ispra, Italy.

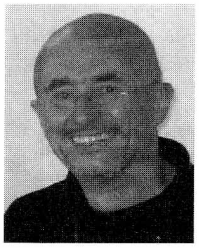

François Rossi was born in St. Etienne, France, in 1954. He received the Engineering degree from the Institut National Polytechnique, Grenoble, France, in 1977 and the Ph.D. degree in materials science from the Université Claude Bernard, Lyon, France, in 1989.

From 1981 to 1990, he was a Group Leader in materials science and surface engineering with the Commissariat a l'Energie Atomique. From 1991 to 1996, he was a Group Leader in plasma technologies with the Institute for Advanced Materials, European Commission, Joint Research Centre, Petten, The Netherlands. In 1996, he moved to the European Commission, Joint Research Centre, Institute for Health and Consumer Protection, Ispra, Italy, where he is now the Head of the NanoBiotechnology Laboratory.

IOP PUBLISHING
IOP FTC
JOURNAL OF PHYSICS D: APPLIED PHYSICS
J. Phys. D: Appl. Phys. **42** (2009) 142001 (4pp)
doi:10.1088/0022-3727/42/14/142001

FAST TRACK COMMUNICATION

Deposition of amino-rich thin films by RF magnetron sputtering of nylon

O Kylián, J Hanuš, A Choukourov, J Kousal, D Slavínská and H Biederman

Charles University, Faculty of Mathematics and Physics, V Holešovičkách 2, Prague 8, 180 00, Czech Republic

E-mail: ondrej.kylian@gmail.com

Received 11 May 2009, in final form 3 June 2009
Published 24 June 2009
Online at stacks.iop.org/JPhysD/42/142001

Abstract
RF magnetron sputtering of a nylon target in different gas mixtures was studied in order to evaluate the capability of this process to deposit amino-rich coatings needed in a wide range of biomedical applications. It has been demonstrated that both the deposition rate of the coatings and the surface density of primary amino groups are strongly linked with working gas mixture composition. From this point of view, a sufficiently high deposition rate as well as the highest amine efficiency reaching a NH_2/C value of 18% was observed in the N_2/H_2 discharge, which leads to the surface exhibiting a high rate of protein adsorption.

1. Introduction

Application of non-equilibrium plasma discharges for the fabrication of thin polymeric films has recently received increased attention. This is given by the possibility to deposit such coatings on a wide variety of substrate materials and also by the possibility to tailor the properties of the resulting deposits by selecting operational parameters such as working gas mixture composition, pressure, discharge power or by the application of discharge pulses having different ratios of on and off phases. Especially, the possibility to adjust the chemical and physical properties of deposited thin films is an aspect of paramount importance for the production of coatings needed for various biomedical applications. In this context, one of the most challenging objectives is to produce films having a high surface density of primary amines that were identified to play an important role in surface interactions with biological systems due to their ability to covalently immobilize biomolecules (e.g. proteins or DNA [1]) or to promote or facilitate cell colonization (e.g. [2]). Naturally, such advantageous properties of amino-rich surfaces triggered an investigation of possible ways for their fabrication by means of non-equilibrium plasma discharges (e.g. review papers [1, 3]). These studies resulted in the suggestion of two principal strategies suitable for the preparation of NH_2-functional surfaces by means of plasma discharges.

The first option is based on adding desired functionalities on the surfaces of polymers by their plasma treatment in ammonia or N_2/H_2 discharges (e.g. [3–5]). Although this approach offers a fast process and high amine selectivity, i.e. high ratio of NH_2 over N that can reach almost 100%, the surface densities of primary amines, also denoted in the literature as amine efficiency, expressed by the NH_2/C ratio, typically do not exceed several per cent. Moreover, since the plasma treatment in this case modifies only the topmost layer of a treated polymer it is not suitable for the applications requiring deposition of a polymeric thin film.

Due to these limitations of methods based solely on the surface modification, further investigation has been focused on the second possibility based on the process of plasma polymerization or co-polymerization (e.g. [6–13]). Concerning these strategies, the most promising results were achieved using NH_3 plasma or discharge mixtures composed of nitrogen and hydrogen combinedwith a suitable monomer. As demonstrated in previous works, this approach leads to the deposition rates of the coatings having values of several nanometres per minute and amine efficiency NH_2/C reaching 20% (e.g. [11]). Nevertheless, in all the suggested processes the starting material of the polymerization is provided in a

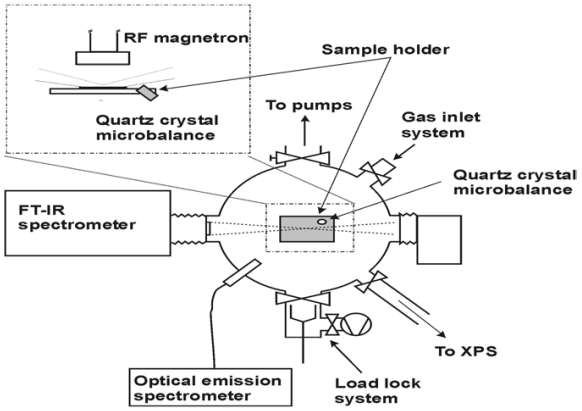

Figure 1. Experimental set-up.

gas phase, which requires safety precautions regarding the gas handling. Moreover, since the discharge is maintained in the volume, the scaling-up of the process requires an increase in the delivered power proportional to the increase in the volume of the active discharge, which is inconvenient in terms of the energetic balance of the process. It has been recently suggested that these intrinsic drawbacks can be overcome by utilizing RF magnetron sputtering of polymeric targets. This process is more practical in terms of possible technological applications, since the scaling in this case follows not the volume of the active discharge but rather the surface area of the sputtered target, and the material to be polymerized is provided in a solid state. Nevertheless, although the possibility to apply RF magnetron sputtering for the fabrication of amino-rich thin films has been proposed recently [14], no attempt has been devoted so far to the demonstration of the suitability of this process to produce surfaces having high density of NH_2 groups. The main intention of this paper is therefore to fill this experimental gap. Specifically, the aims of this study are (i) to determine the deposition rates of thin plasma polymeric films in different discharge mixtures, (ii) to estimate the chemical composition of the films and (iii) to evaluate the ability of the surfaces so prepared to adsorb proteins.

2. Experimental

2.1. Deposition of thin films

The thin films were deposited by sputtering a Nylon 6,6 (Goodfellow) target (80 mm diameter, 2 mm thickness) in different argon, nitrogen and hydrogen working gas mixtures using a cylindrical plasma reactor depicted in figure 1. The plasma was generated by means of a water-cooled RF planar magnetron operated at a frequency of 13.56 MHz, at an applied power of 40 W and at a pressure of 2 Pa. The substrates used for the thin films deposition were placed at a distance of 50 mm from the magnetron.

In order to monitor the process of thin films growth, the processing chamber was equipped with quartz crystal microbalance (QCM) used for the determination of the deposition rates. Moreover, to convert measured shifts of the crystal frequency caused by the growth of the polymeric thin film into the thickness of the deposited material, the heights of the thin films prepared in different working gas mixtures were measured *ex situ* by a Woollam M-2000DI spectroscopic ellipsometer in the spectral range 300–1200 nm. Such determined thicknesses together with the measured frequency shifts of the quartz crystal were subsequently used for the calibration of QCM data that were then expressed in terms of the layer thickness thus allowing to evaluate directly the deposition rate of the polymeric films.

2.2. Samples characterization

The chemical composition of the deposited thin films was first determined by a FT-IR spectrometer (Equinox 55, Bruker) allowing *in situ* monitoring of the chemical composition of the films. Furthermore, the deposition chamber was connected with XPS using an Al Kα x-ray source (1486.6 eV, Specs) and hemispherical energy analyzer (Phoibos 100, Specs), which enabled us to analyse the deposited samples within 5 min after their deposition without breaking vacuum. The fraction of primary amines on the samples prepared in different working gas mixtures was subsequently quantified by the derivatization technique based on the application of pentafluorobenzaldehyde.

Additionally to the characterization of deposited thin polymeric films from the point of view of their chemical composition, the capability of produced films to adsorb proteins was evaluated by means of QCM. In these experiments 80 nm thick films were deposited on gold coated quartz crystals that were subsequently immersed into a protein solution (50 μg ml^{-1} of albumin in PBS). Adsorption kinetics of proteins was then determined by measuring the temporal evolution of the frequency shift of the crystals.

3. Results

3.1. Deposition rates of thin films

The deposition rate was the first parameter studied. It was found that the fastest film growth can be achieved in Ar/N_2 (50 : 50) discharge, followed by the discharge sustained in a N_2/H_2 (50 : 50) mixture, Ar plasma and, finally, Ar/H_2 (50 : 50) plasmas as demonstrated in figure 2. In other words, the presence of hydrogen in the discharge mixture results in a decrease in the deposition rate, whereas nitrogen causes its increase. These results are consistent with previously published data and refer either to a significant contribution of etching of the growing film induced by highly reactive hydrogen atoms in the case of H_2 containing mixtures [3] or to the enhancement of the amount of sputtered molecular fragments connected with nitrogen in the second case. The latter effect, observed for instance during polypropylene sputtering [15], is most likely connected with the ability of N atoms to effectively passivate dangling bonds created close to the target surface by energetic ions bombarding the surface. This in turn results in a lower cross-linking of the target surface exposed to plasma, which consequently facilitates the release of shorter molecular fragments by subsequent impact of ions.

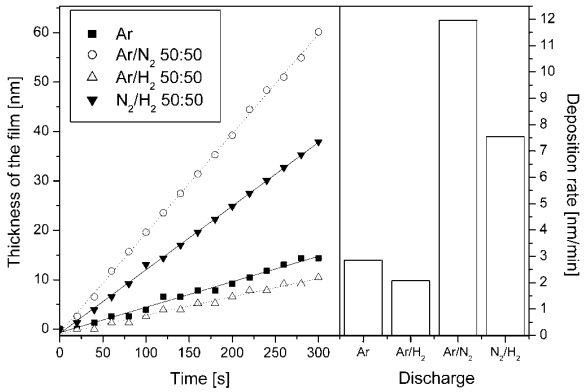

Figure 2. Time development of thin film thickness (left panel) and corresponding deposition rates (right panel) in discharges sustained in different gas mixtures (40 W, 2 Pa).

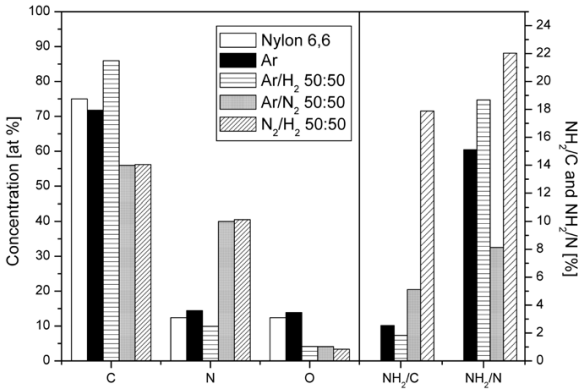

Figure 3. Elemental composition without hydrogen (left) and amine efficiency and amine selectivity of the thin plasma polymeric films deposited by RF sputtering of Nylon 6,6 (right) (40 W, 2 Pa).

Higher fluxes of sputtered fragments on the substrate surface then leads to an increase in the deposition rate.

3.2. Chemical composition of deposited samples and their bioadhesive properties

As expected, both FT-IR and XPS measurements revealed a strong dependence of the chemical composition of the deposits on the discharge mixture used, as can be seen in figures 3 and 4. The results can be summarized as follows.

Ar plasma results in the production of a film having elemental composition almost identical to the bare nylon 6,6.

Ar/H_2 plasma results in the rise of carbon content in the films at the expense of oxygen and nitrogen; the deposits have a structure similar to the classical plasma hydrocarbon films, which can be demonstrated by the dominance of FT-IR peaks corresponding to the stretching and bending vibrations of $–CH_2$and $–CH_3$ groups (3000–2800, 1460 and 1380 cm^{-1}) characteristic for such materials. Moreover, it is worth mentioning that although this discharge provides a relatively high degree of the amino selectivity in terms of the NH_2/N ratio, the surface density of NH_2 groups is even lower than in the case of discharge in Ar alone, which is caused by the reduced nitrogen content in the film.

In contrast to the Ar/H_2 plasma, discharge operated in an Ar/N_2 mixture was found to lead to substantial enhancement of the nitrogen fraction in the films as observed by XPS, and give rise to the absorption peaks corresponding to –NH stretching vibrations (3700–2700 cm^{-1}), nitriles and iso-nitriles (2500–2300 cm^{-1}) and bands in the range 1800–1500 cm^{-1} that can be assigned either to C=N, C=C or C=O stretching vibrations. Nevertheless, derivatization of the samples showed poor amine selectivity NH_2/N and consequently a relatively low amine efficiency NH_2/C that reaches a mere 5%. In other words, only a limited portion of N atoms incorporated in the film is in the form of primary amines.

Finally, N_2/H_2 plasma was found to combine the advantages of Ar/H_2 and Ar/N_2 discharges: its application leads to both nitrogen rich coatings comparable to those

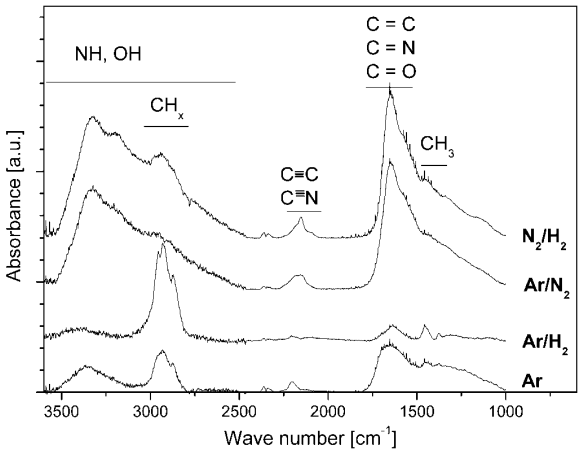

Figure 4. FT-IR spectra of deposited thin films in different discharge mixtures (40 W, 2 Pa).

prepared in Ar/N_2 plasma and high amine selectivity observed in discharge sustained in an Ar/H_2 mixture, which offers the possibility to reach amine efficiency close to 20%. This result is highly competitive with the results obtained by other methods, especially if one also considers the relatively high deposition rate achieved during RF sputtering in this discharge mixture.

The final step of the recent study was to evaluate the capability of prepared samples to adsorb proteins, i.e. a feature linking directly the surface properties with their response towards the biological environment. This has been performed in an additional set of experiments using QCM. As can be seen in figure 5 summarizing the results of these measurements, the rate of albumin adsorption corresponds to the NH_2 density determined by XPS, i.e. the fastest process was observed for samples prepared in N_2/H_2 mixture, followed by Ar/N_2, Ar and Ar/H_2 discharges. These findings represent a straight experimental confirmation of advantageous properties of thin films prepared by RF sputtering of nylon in nitrogen–hydrogen working gas mixture.

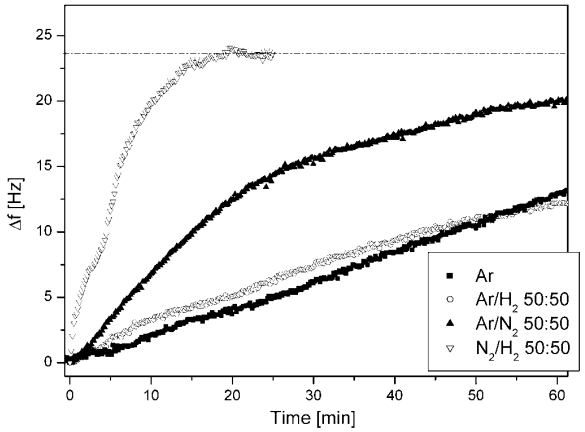

Figure 5. BSA adsorption kinetics.

4. Conclusions

In summary, the following conclusions can be drawn. First, it has been demonstrated that RF magnetron sputtering of the nylon target offers the possibility to prepare thin plasma polymer films having a high surface density of primary amines at relatively high deposition rates, a finding which is of high importance for possible application in technological production of such surfaces. Second, on comparing discharges sustained in selected gas mixtures it has been found that the highest NH_2/C ratio can be achieved in nitrogen–hydrogen discharge mixture. Finally, it has been confirmed that thin films deposited in N_2/H_2 mixture are indeed capable of adsorbing proteins at rates exceeding the values reached for films prepared in other mixtures tested.

Although the main intention of this paper was predominantly to explore the possibility to produce amino-rich coatings by the process based on the RF sputtering of a polymeric target, it has been found that this approach represents a real alternative to other techniques. Further investigations focused on the characterization of the deposition process and its optimization are the subject of ongoing experiments

Acknowledgments

This work was supported by the research plan MSM021620834 financed by the Ministry of Education of Czech Republic.

References

[1] Siow K S, Britcher L, Kumar S and Griesser H J 2006 *Plasma Proc. Polym.* **3** 392
[2] Nebe B, Finke B, Lüthen F, Bergemann C, Schröder K, Rychly J, Liefeith K and Ohl A 2007 *Biomol. Eng.* **24** 447
[3] Meyer-Plath A A, Schröder K, Finke B and Ohl A 2003 *Vacuum* **71** 391
[4] Meyer-Plath A A, Schröder K, Finke B and Ohl A 2003 *Surf. Coat. Sci. Technol.* **174–175** 877
[5] Král' M, Ogino A and Nagatsu M 2008 *J. Phys. D: Appl. Phys.* **41** 105213
[6] Harsch A, Calderon J, Timmons R B and Gross G W 2000 *J. Neurosci. Methods* **98** 135
[7] Choukourov A, Biederman H, Kholodkov I, Slavinska D, Trchova M and Hollander A 2004 *J. Appl. Polymer Sci.* **92** 979
[8] Swaraj S, Oran U, Lippitz A, Friedrich J F and Unger W E S 2005 *Surf. Coat. Technol.* **200** 494
[9] Brétagnol F, Ceriotti L, Lejeune M, Papadopoulou-Bouraoui A, Hasiwa M, Gilliland D, Ceccone G, Colpo P and Rossi F 2006 *Plasma Proc. Polym.* **3** 30
[10] Lejeune M, Brétagnol F, Ceccone G, Colpo P and Rossi F 2006 *Surf. Coat. Technol.* **200** 5902
[11] Truica-Marasescu F and Wertheimer M R 2008 *Plasma Proc. Polym.* **5** 44
[12] Denis L, Cossement D, Godfroid T, Renaux F, Bittencourt C, Snyders E and Hecq M 2009 *Plasma Proc. Polym.* **6** 199
[13] Finke B, Schröder K and Ohl A 2009 *Plasma Proc. Polym.* **6** at press doi:10.1002/ppap.200930305
[14] Kousal J, Hanuš J, Choukourov A, Polonskyi O, Biederman H and Slavínská D 2009 *Plasma Proc. Polym.* **6** at press doi:10.1002/ppap.200932001
[15] Hanuš J, Kousal J, Choukourov A, Biederman H and Slavinska D 2007 *Plasma Proc. Polym.* **4** S806

Surface & Coatings Technology 205 (2011) S558–S561

Contents lists available at ScienceDirect

Surface & Coatings Technology

journal homepage: www.elsevier.com/locate/surfcoat

Deposition of amino-rich coatings by RF magnetron sputtering of Nylon: In-situ characterization of the deposition process

O. Kylián *, J. Kousal, A. Artemenko, A. Choukourov, M. Petr, O. Polonskyi, D. Slavinska, H. Biederman

Charles University in Prague, Faculty of Mathematics and Physics, Department of Macromolecular Physics, V Holešovičkách 2, 180 00 Prague, Czech Republic

ARTICLE INFO

Available online 21 January 2011

Keywords:
Plasma polymers
Mass spectrometry
Optical emission spectroscopy
XPS
Amino-rich coatings

ABSTRACT

This study concerns the detailed characterization of RF magnetron sputtering of Nylon in Ar, Ar/N_2 and N_2/H_2 working gas mixtures; the main attention is paid to the evaluation of influence of operational parameters on the deposition rate, plasma composition as well as on the chemical composition of the deposited thin films without their exposure to open air. Operational conditions were found to have strong impact on the composition of gaseous species flux on the substrate, namely on the presence of CN containing molecules, and in the case of ions also on their energy. This subsequently influences both the deposition rate and the chemical composition of the films. Regarding the deposition rate, the presence of nitrogen in the working gas mixture was found to cause higher production of longer chain fragments that enhances the deposition rate of the plasma polymeric films. The films deposited in Ar/N_2 and N_2/H_2 mixtures possess also high and comparable amount of nitrogen. Nevertheless, the way in which nitrogen is bonded in the films is different in these two mixtures: according to the XPS analysis in films deposited in N_2/H_2 mixture higher portion of nitrogen is present in the form of amines while films deposited in Ar/N_2 mixture exhibit a higher fraction of nitriles and imines.

1. Introduction

RF sputtering of polymeric targets has been used to deposit various plasma polymers having interesting properties with respect to their possible application (e.g. [1,2]). This is also the case of RF sputtering of Nylon 6,6 that was recently reported by our group [3]. It was shown that in this case the resulting plasma polymer films have surface density of primary amino groups exceeding, or at least comparable to the films prepared by other plasma based techniques (e.g. [4–9]). Such coatings are highly advantageous in a wide range of biomedical and biotechnological applications. This is mainly due to the capability of amino-rich surfaces to covalently bind diverse biomolecules and to promote or facilitate cell colonization, which was already proved by many authors (e.g. [10,11]).

However, for the effective use of RF magnetron sputtering of Nylon for the fabrication of the above mentioned coatings suitable for biomedical applications it is of highest importance to find out the relationship between deposition parameters and the properties of resulting coatings. Therefore, it was decided to characterize in detail the film deposition process that uses argon, Ar/N_2 and N_2/H_2 1:1 as working gas mixtures. The characterization includes a combination of optical emission spectroscopy and mass spectrometry for plasma characterization, quartz crystal microbalance for the determination of deposition rates and, finally, X-Ray photoelectron spectroscopy (XPS) for the characterization of the chemical structure of fabricated films immediately after their deposition, i.e. without their exposure to open air. Results of this *in-situ* characterization of the deposition process are reported below.

2. Experimental

Experiments reported in this contribution were performed in a plasma reactor introduced in the previous studies [3,12]. It consists of a cylindrical processing chamber (volume of 50 l) equipped with several ports for plasma diagnostics as well as for *in-situ* characterization of growth of thin films of plasma polymers. The working gases were introduced into the reactor through the gas inlet system composed of needle valves connected to argon and nitrogen gas containers and hydrogen generator (HG 2200, Claind). The processing chamber was pumped by means of a rotary and a diffusion pumps to the base pressure of 2×10^{-3} Pa.

The plasma was sustained using water cooled planar RF magnetron, operated at a frequency of 13.56 MHz, equipped with Nylon 6,6 (Goodfellow) target with thickness 2 mm and diameter 80 mm. Plasma was operated in pure argon, Ar/N_2 1:1 and N_2/H_2 1:1 gas mixtures, in the pressure range 0.5-6 Pa and applied RF powers up to 80 W.

The deposition rate (in terms of deposited mass) was monitored *in-situ* by means of quartz crystal microbalance by measuring the frequency shift Δf of the oscillating quartz crystal (AT cut coated by

* Corresponding author. Tel.: +420 22191 2258; fax: +420 22191 2350.
E-mail address: ondrej.kylian@gmail.com (O. Kylián).

0257-8972/$ – see front matter © 2011 Elsevier B.V. All rights reserved.
doi:10.1016/j.surfcoat.2011.01.036

Au/Cr) placed at a distance of 60 mm from the sputtered target. In our conditions the frequency shift of 1 Hz per minute corresponds to the deposition rate of 45 ng/cm^{2}min.

The plasma was characterized by optical emission spectroscopy and mass spectrometry. The emission spectra were acquired through a quartz window by thermo-electrically cooled AvaSpec spectrometer (Avantes) in the spectral range 230-750 nm. The mass spectra of positive ions and neutrals presented in the plasma phase were recorded by Hiden EQP 300 spectrometer. The mass spectrometer was differentially pumped by a turbomolecular pump and the pressure in the spectrometer during the acquisition of mass spectra was lower than 3×10^{-4} Pa. The sampling orifice of the spectrometer was placed at the distance of 70 mm from the sputtered magnetron target.

The chemical composition of the deposited films was determined by XPS using an Al Kα x-ray source (1486.6 eV, Specs) and hemispherical energy analyzer (Phoibos 100, Specs). XPS measurements were performed in a separate vacuum chamber connected by a vacuum system with the deposition chamber allowing acquisition of XPS spectra of samples within 5 minutes after the deposition without their exposure to open air. The charging was corrected by referencing all peaks with respect to the carbon C1s peak at binding energy 285.0 eV. The deconvolution of C1s peaks was carried out using a 30:70 Gaussian-to-Lorentz curve fitting with FWHM of 1.9 ± 0.2 eV taken equal for all the components. In these measurements one-side polished Si wafers were used as substrates.

3. Results

3.1. Deposition rate

The first parameter studied was the deposition rate in dependence on the operational conditions. It was observed that increasing applied RF power leads to an increase of the deposition rate. However, it was found that for powers higher than 40 W the temporal evolution of the deposited mass starts to deviate from the linear trend as it is demonstrated in Fig. 1 on the example of measurements performed in Ar/N_2 mixture. This suggests insufficient cooling of the target at such powers and its gradual evaporation which contributes to the deposition process. Therefore, in order to avoid this rather uncontrollable phenomenon, further experiments were performed at 40 W power.

Two different trends were observed regarding the pressure dependence of the deposition rate. Whereas in the case of plasma sustained in pure Ar the deposition rate monotonously increases with pressure from 36 ng/cm^{2}min at 0.5 Pa up to approximately 80 ng/cm^{2}min for a pressure of 6 Pa, the deposition rate exhibits a maximum value for about 2 Pa in discharges operated in both Ar/N_2 (around 420 ng/cm^{2}min) and N_2/H_2 (around 270 ng/cm^{2}min) mixtures. Therefore, the pressure of 2 Pa was used in the following experiments.

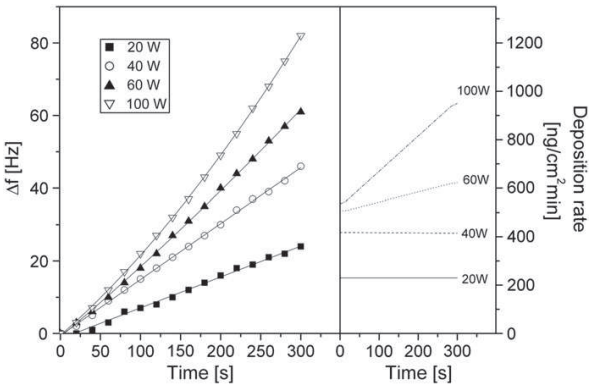

Fig. 1. Temporal evolutions of the frequency shift of quartz crystal observed during the deposition of thin films of plasma polymer in Ar/N_2 1:1 mixture at 2 Pa and different applied RF powers (left) and corresponding time evolution of the deposition rate (right).

3.2. Mass spectrometry

Mass spectra of both positively charged ions and neutral species revealed that besides the mass peaks corresponding to the working gases and peaks characteristic for the presence of water molecules, which are present in the processing chamber most likely as an impurity, also various carbon, nitrogen, hydrogen and oxygen containing species are produced in the plasma. This is shown in Fig.2 that gives energy resolved mass spectra of positive ions that were recorded in discharges sustained in all three employed working gas mixtures. Furthermore, it can be seen that the densities of detected ions as well as their energies are affected by the used working gas. Two main observations can be summarized as follows.

First, it is obvious that there is considerably higher production of heavier ions in the case of Ar/N_2 and N_2/H_2 mixtures as compared to the plasma operated in pure argon. This behavior, i.e. enhanced production of heavier species, which was observed also in the case of neutral species (data not shown), is most likely connected with the

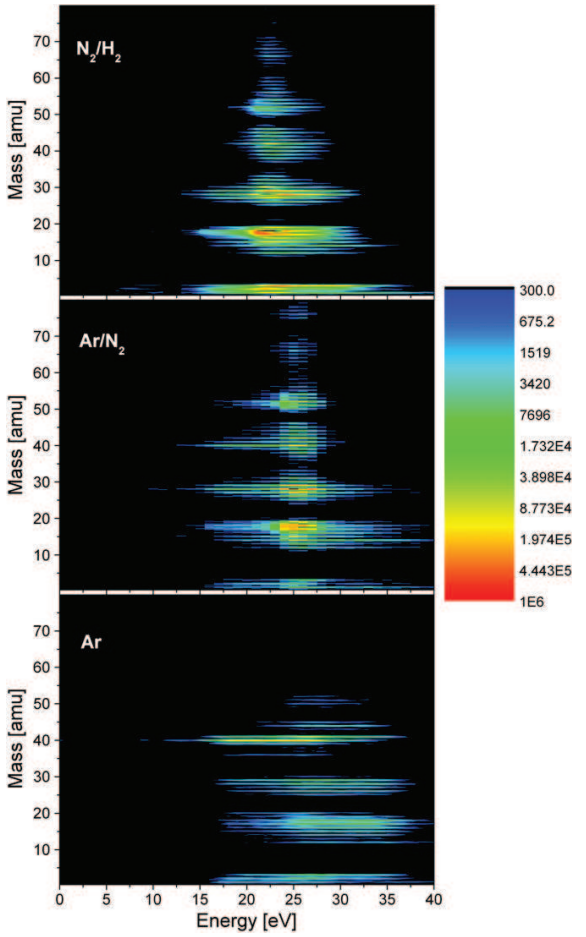

Fig. 2. Energy resolved mass spectra of positive ions recorded in discharges sustained in N_2/H_2 1:1, Ar/N_2 1:1 and pure argon (2 Pa, 40 W).

transition from the pure physical sputtering in the case of Ar plasma to the ion assisted etching of the target when Ar/N_2 and N_2/H_2 mixtures are used. In the later process the chemically active species produced in the plasma interact with broken bonds created on the target surface by the impact of energetic ions. This lowers the level of cross-linking and facilitates release of molecular fragments from the target by subsequent ion bombardment. Moreover, the highest production of longer molecular fragments in Ar/N_2 mixture that is followed by N_2/H_2 mixture and plasma operated in pure argon correlates well with the deposition rates measured by quartz crystal microbalance. This is plausible since these longer fragments reaching the substrate surface can contribute to the film growth and enhance its deposition rate.

Second, it can be seen in Fig. 2 that the energy of ions reaching the mass spectrometer is highest in the case of argon plasma. The presence of nitrogen and, in particular, hydrogen in the working gas mixture causes a slight decrease of mean ion energies and narrows the ions energy distribution.

Appearance mass spectroscopy was used to distinguish mass peaks of hydrocarbons and nitrogen containing species present in the mass spectra at the same m/z values. This technique is based on recording the signal at a selected m/z value in dependence on the energy of ionizing electrons in the mass spectrometer. In this study we present results reached for mass peak at $m/z=26$ that can be attributed either to $C_2H_2^+$ or CN^+. Two different kinds of electron energy scans were found: whereas the electron energy scan acquired in the discharges operated in both nitrogen containing mixtures shows two well separated phases having appearance energies at approximately 12 and 20 eV, only a single phase electron energy scan is observed in the discharge operated in pure argon, with appearance energy of 12 eV (see Fig. 3).

The presence of the second phase in nitrogen containing plasmas and its appearance potential suggests that this phase of electron energy scan is connected with the presence of nitrogen containing molecules (e.g. 19.4 eV for HCN, 20 eV for C_3HN, 19.5 eV for C_4H_5N or 20.4 eV for C_2N_2 [13]), whose dissociative ionization in the mass spectrometer gives rise to CN^+ ions. This finding is again in the agreement with the mechanism of the ion assisted etching suggested to play an important role in the plasmas operated in nitrogen containing mixtures, since nitrogen atoms can interact with the target material, which in turn should result in more enhanced release of nitrogen containing molecular fragments.

3.3. Optical emission spectroscopy

In addition to mass spectroscopy, optical emission spectra of studied plasma were recorded. As depicted in Fig. 4, in the emission spectra of discharges sustained in Ar/N_2 and N_2/H_2 mixtures it was possible to detect intense CN spectral band that was absent in the spectra recorded in Ar plasma. This confirms the presence of CN containing molecules suggested by mass spectrometry. Furthermore, traces of spectral band of NH at 336 nm were found in the emission spectra of plasma operated in N_2/H_2. This peak was not observed in discharges operated in Ar and Ar/N_2 mixture.

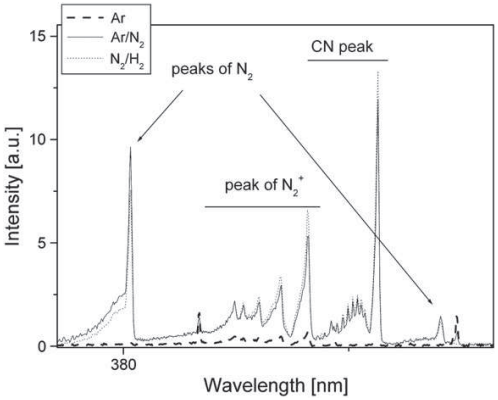

Fig. 4. Parts of optical emission spectra recorded in discharges sustained in N_2/H_2 1:1, Ar/N_2 1:1 and pure argon (2 Pa, 40 W).

3.4. Chemical composition of the deposited films

The deposited films of plasma polymers differ markedly in their chemical composition as witnessed by XPS. It has been found that the

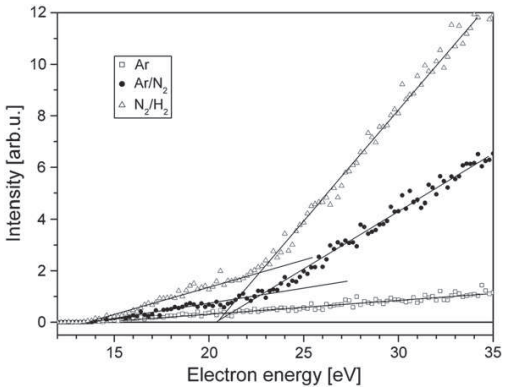

Fig. 3. Electron energy scans of mass peak at $m/z=26$ recorded in discharges sustained in N_2/H_2 1:1, Ar/N_2 1:1 and pure argon (2 Pa, 40 W).

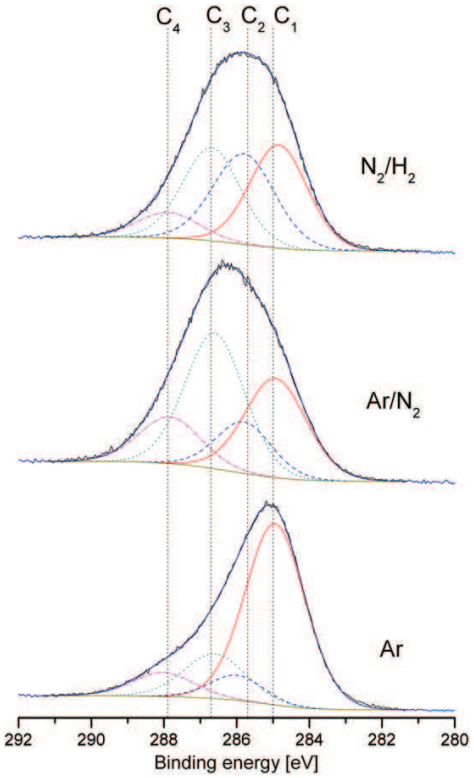

Fig. 5. High resolution XPS scans of C1s peak of samples deposited in N_2/H_2 1:1, Ar/N_2 1:1 and pure argon (2 Pa, 40 W).

elemental composition of the deposited films without hydrogen is almost the same when Ar/N_2 and N_2/H_2 discharge mixtures were used (C/N ratio is 1.4 or 1.39, respectively, and O atom concentration is in both cases lower than 4%), in contrast to films resulting from Nylon 6,6 sputtering in pure argon that were found to have chemical composition similar to the one of Nylon 6,6 (C/N ratio close to 5 and O atom concentration 13.8%). The relatively high and comparable amount of nitrogen incorporated into the films deposited in both nitrogen-containing mixtures is in good agreement with the results of mass spectrometry and optical emission spectroscopy that indicated the presence of CN and CN-containing molecules in the discharge.

Nevertheless, in spite of similar elemental composition of coatings deposited in both nitrogen containing working gas mixtures, the high resolution XPS scans revealed distinct differences in the chemical structure of these films. This can be seen in Fig. 5, which shows high resolution C1s peaks deconvoluted in accordance with [8]. When argon is used as the working gas, the most dominant peak in the C1s spectrum is the one at 285.0 eV (denoted C_1 in Fig. 5), which corresponds to C-C and C-H bonds. The importance of the C_1 peak is reduced when Ar/N_2 and N_2/H_2 mixtures are used, which leads either to enhancement of the peak at 285.7 eV belonging to various amine C-N groups (denoted C_2 in Fig. 5) in the case of N_2/H_2 mixture, or the peak corresponding to C=N, C≡N, hydroxyl or ether groups at 286.7 eV in the case of Ar/N_2 mixture (denoted C_3 in Fig. 5). Moreover, due to relatively low density of oxygen in the films that is below 4%, the contribution from hydroxyls and ethers can be neglected and the C_3 component could be assigned predominantly to nitriles and imines. The minor component C_4 at 287.9 eV is attributed to the C=O and N-C=O species and is present in equal amounts in all the spectra. XPS is not capable of distinguishing between the primary, secondary and tertiary amines, however the above observations, i.e. highest contribution of the overall amine C-N component to the C1s peak for films deposited in N_2/H_2 mixture, are in a good agreement with previously published results on the high density of primary amino groups in such coatings determined by the derivatization technique [3].

4. Conclusions

This study provides detailed characterization of the processing plasma during RF magnetron sputtering of Nylon 6,6 target as well as *in-situ* determination of chemical composition of deposited films of plasma polymers. The deposition rates were found to be considerably enhanced when Ar/N_2 and N_2/H_2 mixtures are used as compared to sputtering performed in pure argon. This effect is ascribed to higher production of longer molecules and molecular fragments in these two mixtures, as observed by mass spectrometry. Moreover, application of appearance mass spectrometry and optical emission spectroscopy showed that in both Ar/N_2 and N_2/H_2 mixtures CN containing molecules are effectively produced in the processing plasma. This in turn leads to the deposition of coatings having relatively high nitrogen content (C/N ratio close to 1.4) as witnessed by XPS. Nevertheless, substitution of argon in the Ar/N_2 mixture by hydrogen causes significant change in the way in which the nitrogen is bonded in the films: whereas in the case of Ar/N_2 working gas mixture a large fraction of nitrogen is present in the form of nitriles and imines, application of N_2/H_2 mixture leads to higher production of amines. Based on these results, which showed that a mixture of nitrogen and hydrogen results in deposition rate comparable to the one measured in Ar/N_2 mixture and high density of amines in the deposited films, it seems that this working gas mixture is highly promising for the fabrication of amino-rich films. Nevertheless, due to the nature of biomedical applications there exist additional requirements on the coatings: their stability in air, resistance towards liquids and possibility to sterilize such coatings. These issues are the subjects of on-going studies.

Acknowledgements

This work was supported by the research plan MSM0021620834 financed by the Ministry of Education of the Czech Republic and by the Grant Agency of Charles University in Prague under the contract GAUK 110-10/251265.

References

[1] H. Biederman, Vacuum 59 (2000) 594.
[2] M. Drábik, O. Polonskyi, O. Kylián, J. Čechvala, A. Artemenko, I. Gordeev, A. Choukourov, D. Slavínská, I. Matolínová, H. Biederman, Plasma Process Polym. 7 (2010) 544.
[3] O. Kylián, J. Hanuš, A. Choukourov, J. Kousal, D. Slavinska, H. Biederman, J. Phys. D Appl. Phys. 42 (2009) 142001.
[4] A.A. Meyer-Plath, K. Schröder, B. Finke, A. Ohl, Vacuum 71 (2003) 391.
[5] M. Král, A. Ogino, M. Nagatsu, J. Phys. D Appl. Phys. 41 (2008) 105213.
[6] A. Choukourov, H. Biederman, I. Kholodkov, D. Slavinska, M. Trchova, A. Holländer, J. Appl. Polymer. Sci. 92 (2004) 979.
[7] L. Denis, P. Marsal, Y. Olivier, T. Gogfroid, R. Lazzaroni, M. Hecq, J. Cornil, R. Snyders, Plasma Process Polym. 7 (2010) 172.
[8] F. Truica-Marasescu, M.R. Wertheimer, Plasma Process. Polym. 5 (2008) 44.
[9] P.-L. Girard-Lauriault, F. Mwale, M. Iordanova, C. Demers, P. Desjardins, M.R. Wertheimer, Plasma Process. Polym. 2 (2005) 263.
[10] K.S. Siow, L. Britcher, S. Kumar, H.J. Griesser, Plasma Process. Polym. 3 (2006) 392.
[11] B. Nebe, B. Finke, F. Lüthen, C. Bergemann, K. Schröder, J. Rychly, K. Liefeith, A. Ohl, Biomol. Eng. 24 (2007) 447.
[12] J. Kousal, J. Hanuš, A. Choukourov, O. Polonskyi, H. Biederman, D. Slavinska, Plasma Process Polym. 6 (2009) S803.
[13] P.J. Linstrom, W.G. Mallard, Eds., NIST Chemistry WebBook, NIST Standard Reference Database Number 69, National Institute of Standards and Technology, Gaithersburg MD, 20899, http://webbook.nist.gov.

Surface & Coatings Technology 205 (2011) S529–S533

Contents lists available at ScienceDirect

Surface & Coatings Technology

journal homepage: www.elsevier.com/locate/surfcoat

Deposition of amino-rich coatings by RF magnetron sputtering of Nylon: Investigation of their properties related to biomedical applications

A. Artemenko, O. Kylián *, J. Kousal, A. Choukourov, O. Polonskyi, D. Slavinska, H. Biederman

Charles University in Prague, Faculty of Mathematics and Physics, Department of Macromolecular Physics, V Holešovičkách 2, 180 00 Prague, Czech Republic

ARTICLE INFO

Available online 13 April 2011

Keywords:
Plasma polymers
Amino-rich coatings
Stability
Solubility

ABSTRACT

Amino-rich polymeric coatings are widely used in biomedical applications, since they promote adsorption of diverse biomolecules or facilitate cell growth. As a consequence, there is a growing interest in fabrication of such coatings that is focused predominantly on the optimization of the deposition process in terms of high density of primary amino groups. In addition, the nature of biomedical applications requires also sufficient stability of the films in aqueous environments. This aspect is investigated in this contribution. In particular, the effect of water and phosphate buffer saline on the coatings prepared by RF magnetron sputtering of Nylon 6,6 in Ar/N_2 and N_2/H_2 gas mixtures is evaluated. The samples exposed to liquids are characterized by various diagnostic methods and their properties are compared with samples stored on open air. It is found that the solubility of the coatings is strongly dependent on the working gas mixture: while the films prepared in Ar/N_2 mixtures are relatively stable in an aqueous environment, much faster dissolving and roughening of the films deposited using N_2/H_2 gas mixtures was observed, which limits their applicability in the biomedical field. Moreover, it was found that chemical changes of the coatings are not significantly different for samples immersed into water or stored on open air.

1. Introduction

Deposition of plasma polymers is a well established technique for the fabrication of coatings used in diverse biotechnological applications. This is mostly due to the fact that plasma based methods allow to prepare homogeneous films on virtually any substrate material as well as thanks to the possibility of tailoring physical and chemical properties of deposited films. This is also the case of nitrogen-rich and in particular of amino-rich coatings that are being used for controlling adherence, growth and differentiation of cells (e.g. [1,2]) or covalent binding of diverse biomolecules (e.g. [3]).

Amino-rich coatings were already prepared by a wide range of plasma based methods employing either the plasma polymerization or co-polymerization from gaseous precursors performed both at low and atmospheric pressures (e.g. [4–7]), or by means of RF magnetron sputtering of Nylon targets in Ar/N_2 and N_2/H_2 atmospheres [8,9]. Nevertheless, the surface density of $-NH_2$ functional groups is not the only parameter important for the use of such coatings in biotechnological applications, where two additional requirements exist: the coatings should be temporally stable to provide their sufficient shelf-life and they should exhibit high resistance towards an aqueous environment. Regarding the first aspect, i.e. temporal stability of the coatings, it has been reported by many authors that the coatings gradually lose their amino rich character, which is ascribed mainly to the oxidation of primary amino groups and formation of more stable amides (e.g. [10]). Nevertheless, the recent studies indicated that loosening of primary amino groups does not in some cases necessarily compromise the ability of such coatings to promote cells adhesion and proliferation (e.g. [11]). Therefore, we focus in this paper on the second aspect, which is of a paramount importance for the good performance of amino-rich coatings, since the coated surfaces are coming into a direct contact with liquids (e.g. body fluids or culture media), which can lead to significant alterations of their properties.

For instance Zhang et al. [12] showed that the exposure of plasma polymerized amino-rich coatings to liquids can lead depending on the applied power and used precursor to variations of their thickness as measured by surface plasmon resonance spectroscopy. Effect of power on stability of amino-rich films was studied also by Abas et al. [13]. These authors showed that plasma polymerized allylamine either dissolves in water in the case of films deposited at low applied powers or swell when prepared at higher powers. Vasilev et al. [14] reported that amine plasma polymer coatings prepared using n-heptylamine dissolve in water, which is in certain cases accompanied by the formation of porous microstructures observed by atomic force microscopy. The loss of the thickness of the coatings was clearly demonstrated also by Ruiz et al. [10] for the samples deposited from nitrogen or ammonia mixed with ethylene either at low-pressure or at atmospheric pressure or by VUV photo-polymerization. The solubility of the coatings was, moreover, found to be dependent on the used deposition method (the relative decrease of the thickness after 24 or 20 h of immersion of the samples into water or PBS varied from few percent up to almost 100%) and is accompanied by alteration of the chemical structure of the coatings,

* Corresponding author.
E-mail address: ondrej.kylian@gmail.com (O. Kylián).

0257-8972/$ – see front matter © 2011 Elsevier B.V. All rights reserved.
doi:10.1016/j.surfcoat.2011.03.139

Table 1
Elemental composition (excluding hydrogen) of samples determined by XPS together with [O]/[C] and [N]/[C] ratios.

		Ar/N_2					N_2/H_2				
		O [%]	C [%]	N [%]	[O]/[C]	[N]/[C]	O [%]	C [%]	N [%]	[O]/[C]	[N]/[C]
In-situ		3.8	56.7	39.5	0.07	0.69	3.3	56.6	40.1	0.06	0.71
1 h on open air		14.9	54.2	30.9	0.27	0.57	10.8	54.9	34.3	0.19	0.63
1 Day	Air	17.0	53.7	29.3	0.31	0.55	12.7	55.5	31.7	0.23	0.57
	Water	18.5	55.0	26.6	0.34	0.48	14.5	58.9	26.5	0.25	0.45

concretely by their oxidation and reduction of nitrogen content. However, these authors observed, on the contrary to work of Vasilev et al. [14], no significant changes of the morphology of the samples after their immersion into liquids. Based on the above reported results it can be concluded that whereas the loss of the thickness is a common feature of most of the amino-rich plasma polymers exposed to liquids, its rate as well as morphological changes are strongly linked with the employed deposition method. Therefore, we have decided to investigate the influence of water and phosphate buffer saline (PBS) on the films fabricated by RF magnetron sputtering of Nylon in Ar/N_2 and N_2/H_2 1:1 working gas mixtures. These mixtures were selected since they have similar elemental composition without hydrogen as revealed by *in-situ* XPS ([N]/[C] ratio is in both cases close to 0.5) [15], but markedly different density of primary amino groups ($[NH_2]/[C]$ ratio is approximately 3 times higher in the case of coatings deposited using N_2/H_2 mixture as compared to Ar/N_2 mixture) [9].

2. Experimental

2.1. Samples preparation

The deposition of amino-rich coatings was performed in a plasma reactor introduced in more detail in previous papers [8,9,15]. It consists of a cylindrical processing chamber connected to a gas inlet system and pumped by means of a rotary and a diffusion pumps (base pressure of 2×10^{-3} Pa). The plasma was sustained using water-cooled, RF planar magnetron operated at frequency of 13.56 MHz and equipped with Nylon 6,6 (Goodfellow) target having thickness of 2 mm and diameter of 80 mm. Plasma discharges were operated in Ar/N_2 and N_2/H_2 mixtures at pressure of 2 Pa, total gas flow of 5 sccm and applied RF power of 40 W. The substrates (one side polished Si wafers, gold coated quartz crystals or glass) were introduced into the deposition chamber by a load–lock system and were placed 50 mm from the sputtered target.

2.2. Determination of the influence of liquids on the thickness of coatings

The thickness of coatings submersed into liquids reflects two effects: swelling and loss of material that is dissolved in liquids. In order to estimate influence of these two effects, the procedure introduced by Abbas et al. [13] was employed. First, the initial thickness of the samples T_0 was measured immediately after the deposition by means of spectral ellipsometry (SE) using a variable angle spectroscopic ellipsometer (Woolam M-2000DI) in the wavelength range of $\lambda = 192–1690$ nm at an angle of incidence AOI = 45–75° in air at room temperature. In order to obtain the thickness of the coatings, recorded SE spectra were fitted with multilayer model (Si/SiO_2/plasma polymer) using the CompleteEASE analysis software. Afterwards, the samples were soaked for 24 h in de-ionized water and dried by a flush of air. Immediately after the drying step the thickness T_1 of the samples was measured. Subsequently, the samples were placed into an oven heated to 100 °C for 30 min to evaporate water absorbed in the plasma polymer network and the thickness T_2 of the films was measured.[1] The thickness of the swelling T_{swell} of the coatings can be then determined as $T_{swell} = T_1 - T_2$, whereas the loss of the thickness T_{loss} is given by relation $T_{loss} = T_0 - T_2$.

The evolution of the dissolving of deposited films in PBS was performed also by measuring a QCM (Maxtek, Inc.) resonance frequency shift, which is directly related to the mass on the crystal surface. In these experiments, the crystals pre-deposited with a plasma polymer were submerged into a beaker with 100 ml of a PBS solution and the temporal evolution of QCM frequency was measured.

2.3. Determination of the influence of liquids on the morphology of coatings

Morphology of the samples was evaluated by atomic force microscopy (AFM). AFM measurements were performed in the semi-contact mode using NSC-16 silicon cantilevers (Schaefer Technologie, GmbH) by means of Quesant Q-scope atomic force microscope. Each reported value of surface root mean square (RMS) roughness represents an average over three 7.5×7.5 μm scans (scan rate 2 s and resolution 512×512 points). The standard deviation of measured values of RMS roughness was in all cases less than 0.2 nm. Moreover, the samples exposed to PBS were prior to the AFM measurements gently rinsed by de-ionized water to remove salt residuals formed after the liquid evaporation.

2.4. Determination of the influence of liquids on the chemical structure of coatings

Characterization of chemical composition was performed on polished silicon substrates by XPS using Al Kα X-ray source (1486.6 eV, Specs) equipped with a hemispherical energy analyzer (Phoibos 100, Specs). The XPS scans were acquired at constant take-off angle of 90°. Wide scans used for the evaluation of elemental composition of the films (0–1300 eV) were recorded using pass energy 40 eV (step 0.5 eV and dwell time 0.1 s). The accuracy of the determination of the atomic fractions is 10%. The high resolution scans were recorded at pass energy 10 eV (step 0.05 eV, dwell time 0.1 s and 10 repetitions). All the binding energies were referenced to the C1s carbon peak at 285.0 eV, to compensate for the effect of surface charging.

In addition to XPS also FT-IR spectroscopy was employed. The FT-IR measurements were performed by FT-IR spectrometer (Equinox 55, Bruker) allowing *in-situ* and *ex-situ* determination of the chemical composition of the deposited coatings. For the FT-IR measurements were used gold coated glass slides as substrate material.

3. Results

3.1. Chemical composition

Concerning the variations of the chemical composition of the coatings it was observed that the films deposited in both discharge mixtures readily oxidize on air, which can be seen in Table 1 on the increasing of relative density of [O] atoms as well as on the increasing ratio of [O]/[C]. This increase in oxygen fraction in the coatings occurs almost solely at the expense of nitrogen, whose fraction was found to rapidly decrease after the exposure of the samples to open air ([N]/[C] ratio decreases by more than 30%). In other words incorporation of one

[1] It is important to mention that no considerable change of the thickness of reference samples that were not soaked into water was observed after 2 h in an oven.

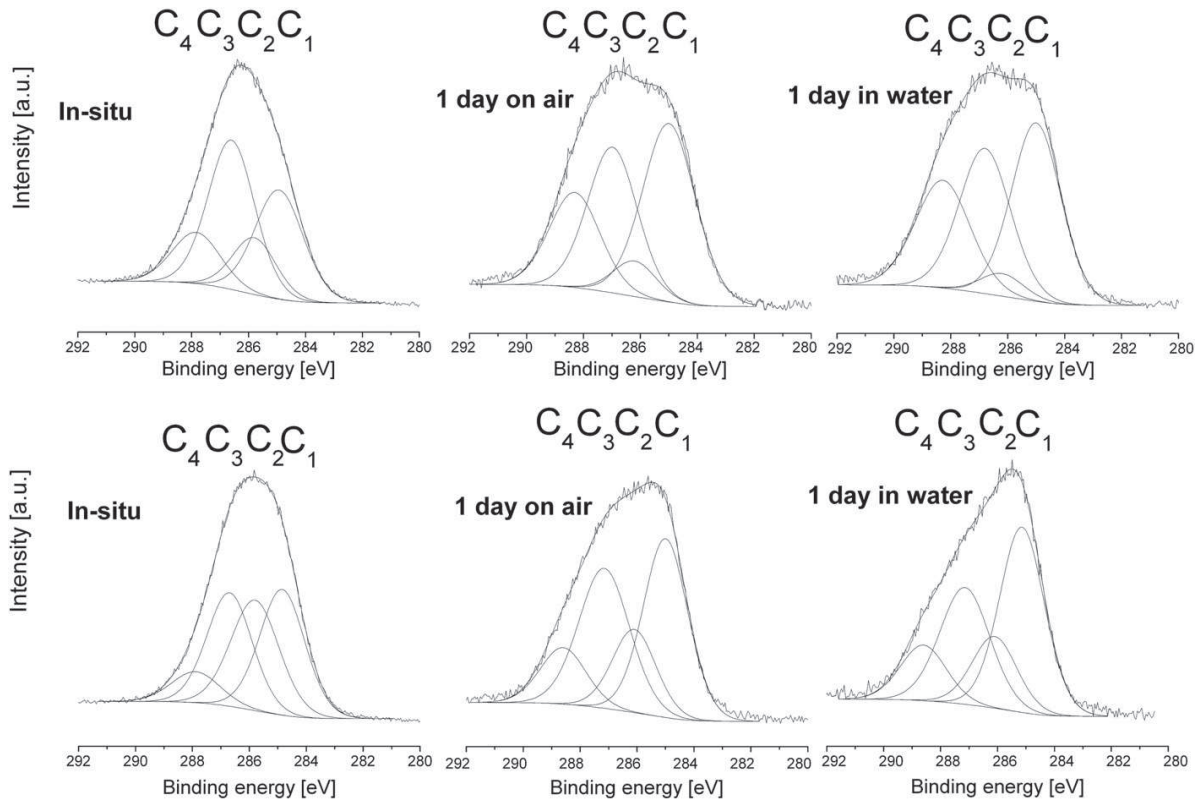

Fig. 1. High resolution XPS scans of C1s peak of samples prepared in Ar/N_2 1:1 mixture (up) and in N_2/H_2 1:1 mixture (down) measured *in-situ* (left), after 1 day on air (center) and after 1 day in water (right). Assignment of components of C1s peak is C1) C—C and C—H C2) C—N C3) C=N and C—O and C4) C=O and N—C=O (e.g. [10]).

oxygen atom is accompanied by the loss of one nitrogen atom. Such behavior indicates that the hydrolysis by atmospheric humidity, i.e. processes suggested by Foerch et al. [16], plays an important role in our case. This distinguishes our results from the ones reported previously by Truica-Marasescu and Wertheimer for low pressure plasma polymerized ethylene [5].

Also the chemical structure of samples exposed to air is altered as witnessed by high resolution XPS scans of C1s peak (Fig. 1). Although

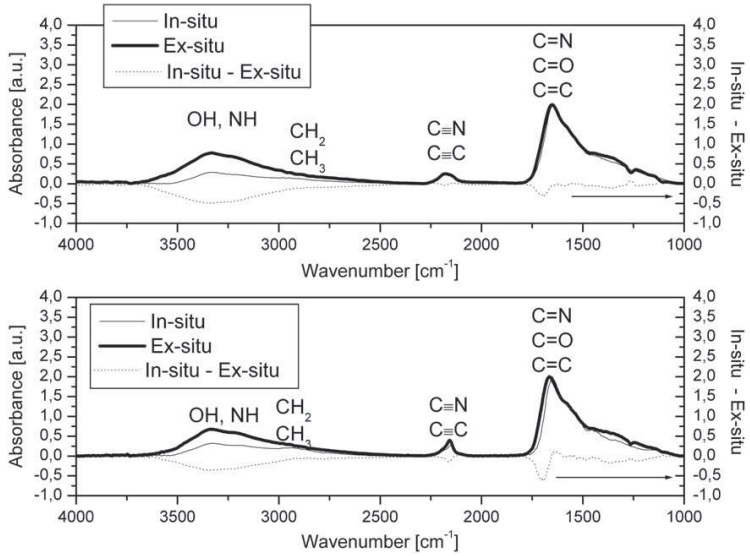

Fig. 2. FT-IR spectra of samples deposited in Ar/N_2 1:1 (upper panel) and N_2/H_2 1:1 (lower panel) working gas mixtures measured *in-situ* immediately after the deposition and after their exposure to open air for 1 h. The differences of the FT-IR spectra acquired *in-situ* and *ex-situ* are also depicted.

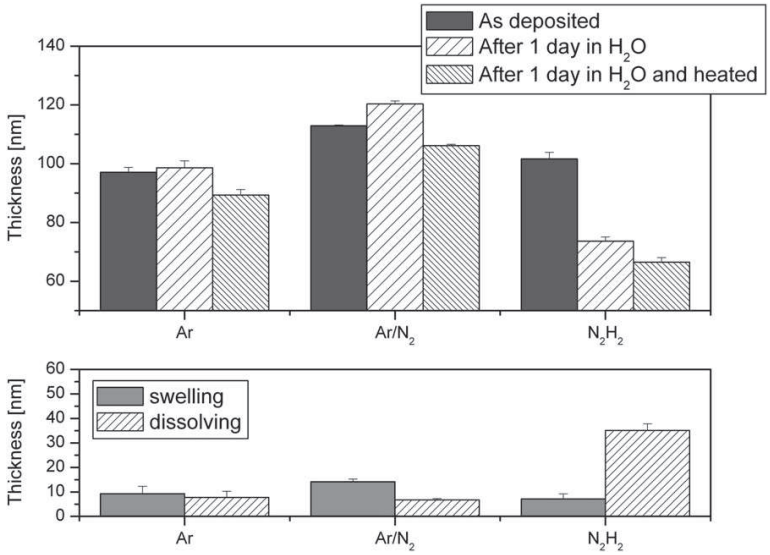

Fig. 3. Thicknesses of films prepared in pure argon, Ar/N_2 1:1 and N_2/H_2 1:1 mixtures after the deposition, after immersion into water for 24 h and after additional heating (upper panel) together with estimated thickness changes caused by swelling and dissolving (lower panel).

the deconvolution of the C1s peak always poses certain uncertainty, following conclusions can be drawn.

First, it can be seen that the exposure of samples deposited in both Ar/N_2 and N_2/H_2 working gas mixture to open air causes an increase of N—C═O and C═O bonds (in both cases was observed the increase of corresponding C4 component of C1s peak by more than 40%). This is confirmed by FT-IR measurements that showed significant increase of C═O stretching vibrations in the FT-IR spectra after the exposure of coatings to open air (see Fig. 2). Such changes are consistent with hydrolysis of imines that give rise to the C═O functionalities as well as with formation of amides by the oxidation of primary amines (e.g. [10]).

Second, the XPS results revealed differences in ageing of the samples prepared in both employed working gas mixtures: whereas the decrease of both C2 and C3 components of C1s peak (see Fig. 1), which can be attributed in our case mainly to amines and imines, respectively [15], was observed for samples prepared in Ar/N_2 mixture, the C3 component is relatively stable in the case of N_2/H_2 mixture.

It can be seen in Table 1 and Fig. 1 that the above described changes in the chemical composition of deposited coatings are only slightly accelerated by soaking the samples into water. Concretely, immersion into water causes faster decrease of nitrogen content in the coatings and leads to higher increase of N—C═O and C═O bonds as compared to samples stored on open air. However, the differences in the XPS spectra of samples immersed into water and stored on open air are relatively small. This suggests that the changes in the chemical composition of deposited films are linked mostly with the time after the deposition and do not change significantly if the samples are exposed directly to water or kept in humid open air.

3.2. Thickness evolution of samples immersed into liquids

The thickness of the coatings in dependence on their residence time in de-ionized water was determined by means of spectral ellipsometry as described above. As can be seen in Fig. 3, the decrease of the thickness of films as well as their swelling was observed for all tested samples immersed in water. Regarding the swelling, values of T_{swell} were found to be around 10% of the initial thickness of the films deposited using all three discharge mixtures. On the contrary, it has been found that the rate at which the coatings dissolve in water differs markedly with the working gas mixture employed for the thin films deposition: whereas the coatings prepared in N_2/H_2 mixture dissolve readily already after being 1 day in water (reduction of the thickness was 35%), much slower decrease of the thickness of the samples fabricated using Ar or Ar/N_2 was observed (reduction of the thickness was less than 9%).

The same trends were observed for samples immersed into PBS. However, in this case the results are compromised by the presence of salt residuals that have to be rinsed first. Therefore, in addition to ellipsometry, QCM was applied to measure the evolution of mass of coatings presented on the surface directly in PBS. As can be seen in Fig. 4, also these experiments showed stability of the films prepared using Ar and Ar/N_2 in contrast to the films deposited in N_2/H_2 mixtures that readily dissolved in PBS.

The higher solubility of the coatings prepared in N_2/H_2 mixture is consistent with their higher amino content as compared to the films deposited in Ar/N_2 mixture [9]. As already reported in the previous studies (e.g. [10]) the higher portion of polar $-NH_2$ groups in plasma polymers is connected with presence of higher amount of low

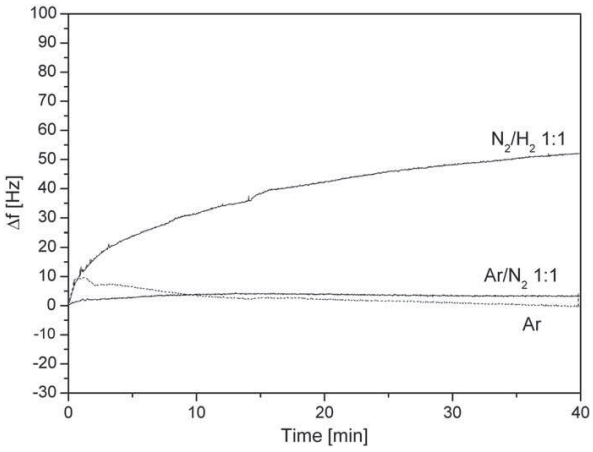

Fig. 4. Temporal evolution of QCM frequency shift of films immersed into PBS.

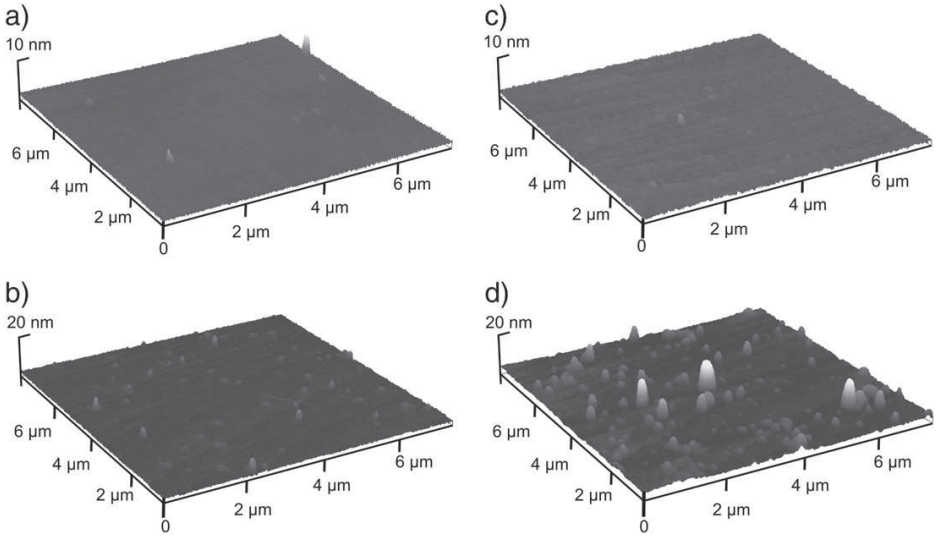

Fig. 5. AFM 7.5×7.5 μm scans of a) sample prepared in Ar/N_2 1:1 mixture b) sample prepared in Ar/N_2 1:1 mixture and immersed for 1 day in water c) sample prepared in N_2/H_2 mixture d) sample prepared in N_2/H_2 mixture and immersed for 1 day in water.

molecular weight fractions (so called oligomers) in the coatings that are highly soluble in water.

3.3. Morphology of samples

The deposited films were found to be very smooth independently on the working gas mixture used for their fabrication (RMS roughness 0.2–0.3 nm) as can be seen in Fig. 5. After the exposure of samples to both liquids, different trends in the evolution of the morphology of films were observed. Whereas water and PBS caused only negligible changes of RMS roughness of the samples prepared in Ar/N_2 mixture (from 0.2 nm to 0.4 nm), considerably higher alterations of the morphology were observed on samples deposited in N_2/H_2 mixture, for which randomly distributed 'mounds' on the surface were observed (see Fig. 5). These 'mounds' can be soluble part of the films that remained on the surface after drying. Nevertheless, even in the later case the surfaces remained rather smooth with the values of RMS roughness around 1 nm. Moreover, no formation of porous microstructures reported previously by Vasilev et al. [14] was observed.

4. Conclusions

In this study we have investigated stability of amino-rich coatings prepared by RF magnetron sputtering from Nylon target in liquids, i.e. aspect that can significantly influence the performance of such coatings in biomedical filed. It is shown that the coatings prepared using N_2/H_2 1:1 working gas mixture dissolve in water or PBS, whereas much better stability was observed for films deposited in Ar/N_2 mixture that is comparable with the films prepared in pure Ar. The same tendency, i.e. higher impact of both liquids on samples fabricated in N_2/H_2, was observed also for morphology of the coatings. Moreover, it has been found that samples immersed into water exhibit the same changes of their chemical structure as compared with samples stored on open air.

Acknowledgement

This work is a part of the research plan MSM0021620834 financed by the Ministry of Education of Czech Republic and was partly supported by the grant of the Grant Agency of Charles University in Prague GAUK 110-10/251265.

References

[1] K. Wende, K. Schröder, U. Lindequist, A. Ohl, Plasma Process. Polym. 3 (2006) 524.
[2] B. Nebe, B. Finke, F. Lüthen, C. Bergemann, K. Schröder, J. Rychly, K. Liefeith, A. Ohl, Biomol. Eng. 24 (2007) 447.
[3] K.S. Siow, L. Britcher, S. Kumar, H.J. Griesser, Plasma Process. Polym. 3 (2006) 392.
[4] A. Choukourov, H. Biederman, I. Kholodkov, D. Slavinska, M. Trchova, A. Holländer, J. Appl. Polym. Sci. 92 (2004) 979.
[5] F. Truica-Marasescu, M.R. Wertheimer, Plasma Process. Polym. 5 (2008) 44.
[6] L. Denis, P. Marsal, Y. Olivier, T. Gogfroid, R. Lazzaroni, M. Hecq, J. Cornil, R. Snyders, Plasma Process. Polym. 7 (2010) 172.
[7] P.-L. Girard-Lauriault, F. Mwale, M. Iordanova, C. Demers, P. Desjardins, M.R. Wertheimer, Plasma Process. Polym. 2 (2005) 263.
[8] J. Kousal, J. Hanuš, A. Choukourov, O. Polonskyi, H. Biederman, D. Slavinska, Plasma Process. Polym. 6 (2009) S803.
[9] O. Kylián, J. Hanuš, A. Choukourov, J. Kousal, D. Slavinska, H. Biederman, J. Phys. D Appl. Phys. 42 (2009) 142001.
[10] J.-C. Ruiz, A. St-Georges-Robillard, C. Thérésy, S. Lerouge, M.R. Wertheimer, Plasma Process. Polym. 7 (2010) 737.
[11] B. Finke, F. Hempel, H. Testrich, J. Meichsner, A. Artemenko, O. Kylián, H. Biederman, H. Rebl, B. Nebe, K.-D. Weltmann, K. Schröder, Surf. Coat. doi:10.1016/j.surfcoat.2010.12.044.
[12] Z. Zhang, Q. Chen, W. Knoll, R. Förch, Surf. Coat. Technol. 174–175 (2003) 588.
[13] A. Abbas, C. Vivien, B. Bocquet, D. Guillochon, P. Supiot, Plasma Process. Polym. 6 (2009) 593.
[14] K. Vasilev, L. Britcher, A. Casanal, H.J. Griesser, J. Phys. Chem. B 112 (2008) 10915.
[15] O. Kylián, J. Kousal, A. Artemenko, A. Choukourov, M. Petr, O. Polonskyi, D. Slavinska, H. Biederman, Surf. Coat. Technol. doi:10.1016/j.surfcoat.2011.01.036.
[16] R. Foerch, N.S. McIntyre, R.N.S. Sodhi, D.H. Hunter, J. Appl. Polym. Sci. 30 (1990) 40.

Thin Solid Films 520 (2012) 7115–7124

Contents lists available at SciVerse ScienceDirect

Thin Solid Films

journal homepage: www.elsevier.com/locate/tsf

Effect of sterilization procedures on properties of plasma polymers relevant to biomedical applications

A. Artemenko [a], O. Kylián [a,*], A. Choukourov [a], I. Gordeev [a], M. Petr [a], M. Vandrovcová [b], O. Polonskyi [a], L. Bačáková [b], D. Slavinska [a], H. Biederman [a]

[a] Charles University in Prague, Faculty of Mathematics and Physics, Department of Macromolecular Physics, V Holešovičkách 2, 180 00 Prague, Czech Republic
[b] Institute of Physiology, Academy of Sciences of the Czech Republic, Department of Growth and Differentiation of Cell Populations, Videnska 1083, 142 20, Prague 4, Czech Republic

ARTICLE INFO

Article history:
Received 4 April 2012
Received in revised form 30 July 2012
Accepted 30 July 2012
Available online 3 August 2012

Keywords:
Plasma polymers
Cell adhesion
Effect of sterilization

ABSTRACT

This study is focused on the evaluation of resistance of plasma polymers toward common sterilization techniques, i.e. property important for possible use of such materials in biomedical applications. Three kinds of plasma polymers having different bioadhesive natures were studied: plasma polymerized poly(ethylene oxide), fluorocarbon plasma polymers, and nitrogen-rich plasma polymers. These plasma polymers were subjected to dry heat, autoclave and UV radiation treatment. Their physical, chemical and bioresponsive properties were determined by means of different techniques (ellipsometry, atomic force microscopy, wettability measurements, X-ray photoelectron spectroscopy and biological tests with osteoblast-like cells MG63). The results clearly show that properties of thin films of plasma polymers may be significantly altered by a sterilization process. Moreover, observed changes induced by selected sterilization methods were found to depend strongly on the sterilized plasma polymer.

1. Introduction

Plasma polymers are nowadays used in a wide range of biomedical applications, where they act as interfacial layers modifying biological response of coated objects (e.g. [1–4]). It has been demonstrated by many groups that by proper selection of deposition condition plasma polymers may either significantly promote or suppress protein adsorption or cell attachment on surfaces. Typical example of material facilitating cell colonization of surfaces desired for instance for smooth integration of implants is amino-rich coatings (e.g. [5–7]). On the contrary, material that has weak cell-surface interaction characterized by scarce adhesion, low spreading and low coverage is plasma polymerized polytetrafluoroethylene, at least if deposited as a smooth film [8]. Finally, non-bioadhesive properties needed to prevent adhesion of biomolecules presented in body fluids were reported for instance for plasma polymerized poly(ethylene oxide) (pPEO) (e.g. [9–14]). The deposition of plasma polymers is, however, advantageous not only because of a high versatility of their possible chemical composition, but also by the fact that they can be produced in the form of ultrathin homogeneous films virtually on any substrate material. This makes plasma polymers highly suitable also for integration to biosensing devices or as a platform for further functionalization of surfaces (e.g. [15,16]). Moreover, the deposition is a relatively fast process (common deposition rates are in tens of nm per minute), often without a need of toxic substances and suitable for in-line production. As a consequence of these benefits various methods of fabrication of thin films of plasma polymers were suggested including for instance plasma enhanced chemical vapor deposition using gaseous precursors (e.g. [17–22]), RF magnetron sputtering of polymeric targets (e.g. [23–27]) or plasma assisted thermal vapor deposition (e.g. [14,28–31]). Naturally, the main objective of investigations related to biomedical use of plasma polymers was identification of the conditions leading to the production of plasma polymers having desired bioresponsive properties, high temporal stability as well as stability in aqueous environments (e.g. [32–36]). Nevertheless, due to the nature of biomedical applications, the coatings should also withstand a sterilization process. The resistance of plasma polymers toward common sterilization processes was, however, overlooked in the literature, and there exists only limited number of studies devoted to this topic, which are focused on one selected plasma polymer only (e.g. plasma polymerized acrylic acid [37], PEO [38]). This paper is therefore focused on this phenomenon, which may be in some cases determinant for the use of plasma polymers as biomaterials.

As stated above, plasma polymers may be prepared by various techniques and their properties (e.g. density of functional groups or degree of cross-linking) can be largely varied in dependence on used deposition parameters. In this study we have selected three examples of surfaces with different biological responses: hydrophobic fluorocarbon plasma polymers, bioadhesive nitrogen-rich plasma polymers and biologically non-fouling PEO-like plasma polymers. These samples were subjected to the three sterilization procedures commonly employed in

* Corresponding author. Tel.: +420 22191 2258; fax: +420 22191 2350.
E-mail address: ondrej.kylian@gmail.com (O. Kylián).

0040-6090/$ – see front matter © 2012 Elsevier B.V. All rights reserved.
http://dx.doi.org/10.1016/j.tsf.2012.07.123

biomedical praxis (dry heat, autoclave and UV radiation treatment) and their physical, chemical and bioresponsive properties were determined by means of different techniques.

2. Experimental details

2.1. Deposition of plasma polymers

RF magnetron sputtering of polymeric targets was shown to be very effective in fabrication of thin plasma polymer films. Here, polytetrafluoroethylene (PTFE) and nylon 6, 6 were chosen as targets for RF magnetron sputtering. A previous study showed that sputtering of PEO did not prove to be suitable for deposition of PEO-like plasma polymers [29]. Plasma-assisted vacuum evaporation of PEO was chosen instead of RF magnetron sputtering to produce plasma polymers with chemical composition close to original PEO.

2.1.1. Deposition of RF sputtered PTFE

The deposition of PTFE-like films (pPTFE) was performed in a deposition chamber schematically depicted in Fig. 1A and described in more details in the previous studies [39,40]. It consists of a cylindrical parallel plate processing chamber (volume of 50 l) pumped by means of a rotary and a diffusion pump (base pressure 2×10^{-3} Pa) and connected to an Ar line. The plasma was sustained using a water-cooled, RF planar magnetron operated at applied power of 100 W and frequency of 13.56 MHz. The magnetron was equipped with a PTFE (Goodfellow) target with the thickness of 3 mm and diameter of 80 mm. The substrates (1.25×1.25 cm one side polished Si wafers or glass slides) were introduced into the deposition chamber by a load-lock system and were placed 170 mm from the sputtered target. RF discharge was operated in Ar at pressure of 5 Pa and a total gas flow of 12 sccm. Deposition time was 5 min.

2.1.2. Deposition of RF sputtered nylon

RF magnetron sputtering of nylon was performed in a plasma reactor similar to the one used for the deposition of the pPTFE films presented in Fig. 1A and introduced in more detail in previous papers (e.g. [41,42]). The magnetron was equipped with nylon 6,6 (Goodfellow) target that was 80 mm in diameter and 2 mm thick. RF discharge was operated at an RF applied power of 40 W in a mixture of 1:1 of argon and nitrogen at a pressure of 2 Pa and a total gas flow of 5 sccm. The sputtered nylon films (pSN) were deposited on the substrates positioned in a distance of 50 mm from the sputtered target. These deposition conditions were selected on the basis of the previous experiments that showed that resulting films pose sufficient surface density of $-NH_2$ groups [40] and good stability in liquids [35]. Deposition time was 10 min.

2.1.3. Deposition of films of plasma polymerized PEO

The deposition of pPEO plasma polymers was performed by plasma assisted vapor deposition in an experimental set-up presented in Fig. 1B and described in previous articles [14,29]. It consists of a vacuum chamber pumped with rotary and diffusion pumps to a base pressure of 10^{-3} Pa. A copper crucible designed for the evaporation of PEO (Sigma-Aldrich, M = 2500) was electrically heated up to a temperature of 280–340 °C. The crucible was located coaxially with and above an RF magnetron equipped with graphite target (Goodfellow) fed by an RF generator (13.56 MHz, Dressler Ceasar) at power of 5 W. The substrates (1.25×1.25 cm one side polished Si wafers or glass slides) were placed 10 cm above the crucible. Argon at pressure of 1 Pa and flow rate of 5 sccm was used as a working gas. These deposition conditions assure the fabrication of the films with high retention of the PEO character and with good stability in aqueous environment [31]. Deposition time was 10 min.

2.2. Sterilization of plasma polymers

The deposited samples were sterilized by three commonly used techniques—UV radiation, dry heat and autoclave. The treatment by UV radiation was performed using a UV–C lamp (SANKYO DENKI G20T10) for the irradiation time of 2 h. Dry heat sterilization was done at a temperature of 160 °C by a hot air sterilizer (HS202A) for 2 h. The autoclaving was performed at temperature of 120 °C in de-ionized water for 1 h by means of a commercial autoclave (Tuttnauer 2540 ELC).

In order to limit possible aging effects connected for instance with relaxation of residual radicals in the films of plasma polymers, the samples were left for 2 days on the open air prior to sterilization, i.e. for the time long enough to cause substantial decrease of the amount of free radicals trapped in common plasma polymers (e.g. [43–45]).

2.3. Characterization of plasma polymers

The thickness of the coatings before and after sterilization was determined by means of spectral ellipsometry using a variable angle spectroscopic ellipsometer (Woolam M-2000DI) in the wavelength range of $\lambda = 192–1690$ nm at an angle of incidence AOI = 55–75° in air and at room temperature. The samples were modeled as Si/SiO_2/plasma polymer system and the final thickness value given is calculated as the mean from three measurements on each sample (the maximal standard error of mean is 2 nm).

Morphology of the samples was evaluated by atomic force microscopy (AFM). The AFM measurements were performed in a semi-contact mode using NSC-16 silicon cantilevers (Schaefer Technologie, GmbH) by means

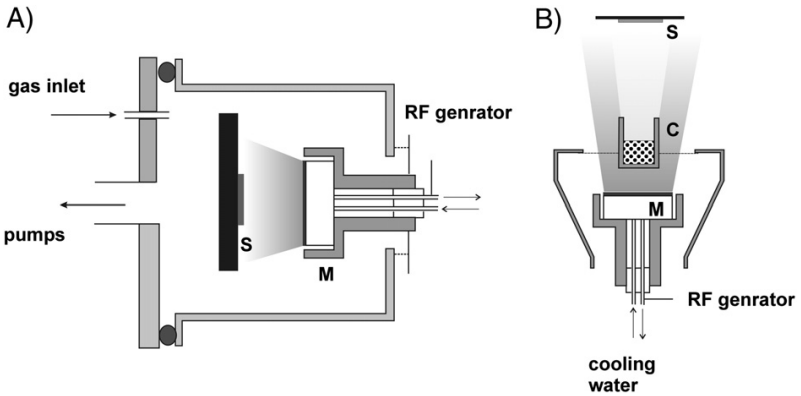

Fig. 1. The scheme of the experimental setup for deposition of A) plasma sputtered PTFE and B) pPEO films. (S—substrate, C—crucible, M—magnetron).

of a Quesant Q-scope 350 atomic force microscope. In all the cases, the scans of 5×5 μm^2 with resolution 512×512 points were taken.

The chemical composition of the samples before and after their sterilization was analyzed by X-Ray Photoelectron Spectroscopy (XPS, Phoibos 100, Specs) using an Al Kα X-ray source (1486.6 eV, Specs). The X-Ray Photoelectron spectra were acquired at a constant take-off angle of 90° with pass energy of 40 eV (wide spectra) and 10 eV (high-resolution spectra). Peak fitting of the high-resolution spectra was performed by the Casa software and depended on the type of the sample. For the pPTFE films, the XPS spectra were referenced to the peak at 292 eV, which corresponded to the CF_2 functional groups. Other components for fitting of the C 1s peak were positioned at 287.4 eV (C–CF), at 290.0 eV (C–F) and at 294.1 eV (CF_3). The additional component at 285.0 eV (C–C) was added where relevant. In the case of RF sputtered nylon, all the binding energies were referenced to the C 1s carbon peak at 285.0 eV. The C 1s was fitted by three components at 285.0 eV (C–C/C–H bonds), 286.5 eV (collective contribution from the C–N, the C═N and the C≡N groups) and 288.1 eV (C═O, N–C═O). The PEO-like plasma polymers prepared by plasma-assisted vacuum evaporation of PEO have been recently shown to consist predominantly of the C–O–C groups [14,30,31] and therefore the XPS spectra were charge referenced for ethers at 286.5 eV. The C 1s peak was fitted by three peaks at 285.0 eV (C–C/C–H), at 286.5 eV (C–O–C) and at 287.8 eV (C═O). The fourth component at 289.0 eV (O–C═O) was introduced where relevant.

The wettability of the samples was determined by means of a sessile drop method using a goniometer.

2.4. Biological tests

The samples were seeded with human osteoblast-like MG 63 cells (European Collection of Cell Cultures, Salisbury, UK), suspended in Dulbecco's modified Eagle's Minimum Essential Medium (Sigma, U.S.A., Cat. No. D5648) with 10% fetal bovine serum (Sebak GmbH, Aidenbach, Germany) and gentamicin (40 μg/ml, LEK, Ljubljana, Slovenia). Each well contained 20,000 cells (i.e., approximately 5,500 cells/cm^2) and 3 ml of the medium. The cells were cultured for 1 day at 37 °C in a humidified air atmosphere containing 5% CO_2. For each experimental group, three samples were used.

1 day after the seeding the samples were rinsed with phosphate-buffered saline (PBS; Sigma, USA), fixed with 70% frozen ethanol (room temperature, 20 min) and stained with a combination of two fluorescence dyes, i.e. cell membrane dye Texas Red C2-maleimide (excitation maximum 595 nm, emission maximum 615 nm; Molecular Probes, Invitrogen, USA, Cat. No. T6008; 20 ng/ml of PBS) and nuclear dye Hoechst #33342 (excitation max. 346 nm, emission max. 460 nm; Sigma, USA; 5 μg/ml of PBS) for 2 h at room temperature. The number of cells on the surface was evaluated on microphotographs taken under an IX-50 microscope, equipped with a DP 70 digital camera (both from Olympus, Japan, obj. 20×).

The quantitative data are presented as mean ± standard error of mean. The statistical analyses were performed using Origin software. The multiple comparison procedures were carried out by the analysis of variance method. The value $p<0.05$ was considered significant.

3. Results and discussion

3.1. Influence of sterilization methods on thickness and morphology of the plasma polymers

The first studied parameter was variation of the thickness of the plasma polymers depending on the sterilization method used. Regarding the films of pPTFE, no significant variations of their thickness were observed after sterilization by UV radiation, dry heat or autoclave as can be seen in Fig. 2A.

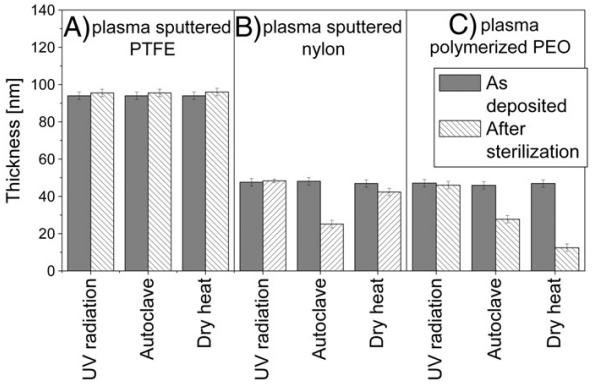

Fig. 2. Comparison of thicknesses of plasma polymers before and after their sterilization. A) plasma sputtered PTFE, B) plasma sputtered nylon and C) plasma polymerized PEO.

In the case of the pSN plasma polymers, only combination of moist environment with elevated temperature caused a significant decrease of the film thickness. It can be seen in Fig. 2B that almost one half of the deposited coating was removed by autoclaving. Dry heat was less detrimental to the thickness of the pSN films.

Comparison of the pPEO films before and after their sterilization shows that only UV radiation did not change the thickness of the films (Fig. 2C). Both autoclave and, even to more extent, dry heat caused reduction of the film thickness, which suggests thermal instability of the pPEO films.

Obviously, different plasma polymers possess different resistance toward main sterilization techniques in terms of their thickness. This is of high importance especially for ultrathin coatings (i.e. coatings having thickness of several nanometers) needed for instance for various biosensors including those based on surface plasmon resonance. In this case, the thickness reduction may cause exposure of underlying substrate, which can subsequently interact with biological samples and give false signal.

In contrast to the thickness, AFM scans revealed that none of the used sterilization techniques modified markedly the roughness of the deposited coatings. In all the cases, the films remain very smooth (root mean square roughness is below 1 nm), with only few "spikes" on a surface induced by the sterilization process.

3.2. Influence of sterilization methods on chemical composition of plasma polymers

The XPS showed that the pPTFE films were composed mainly of F and C atoms. Insignificant incorporation of oxygen was also detected (Table 1). After the sterilization, the F/C ratio remained the same for the UV-treated and dry heated samples but a decrease was observed for the autoclaved samples for which the F/C value dropped to 0.81. These changes in F/C are further evidenced by the high-resolution spectra and by the water contact angle (WCA) measurements. The C 1s spectra of the as-deposited, UV-treated and dry heated samples are identical (Fig. 3, Table 1) and their WCA are very close. The C 1s of the autoclaved sample differs from the others by enhanced contribution from the C–C

Table 1
The XPS analysis of the non-sterilized and sterilized pPTFE films.

	F [%]	C[%]	O[%]	F/C	C–C, %	C–CF, %	CF, %	CF_2,%	CF_3,%
As deposited	49.3	49.7	1.0	0.99	1	26	27	27	19
UV radiation	48.8	50.0	1.2	0.98	2	25	28	26	19
Autoclave	42.4	52.6	5.0	0.81	25	22[a]	20	22	11
Dry heat	48.9	49.6	1.5	0.99	1	26	28	27	18

[a] In case of autoclaved sample this peak overlaps with C–O peak.

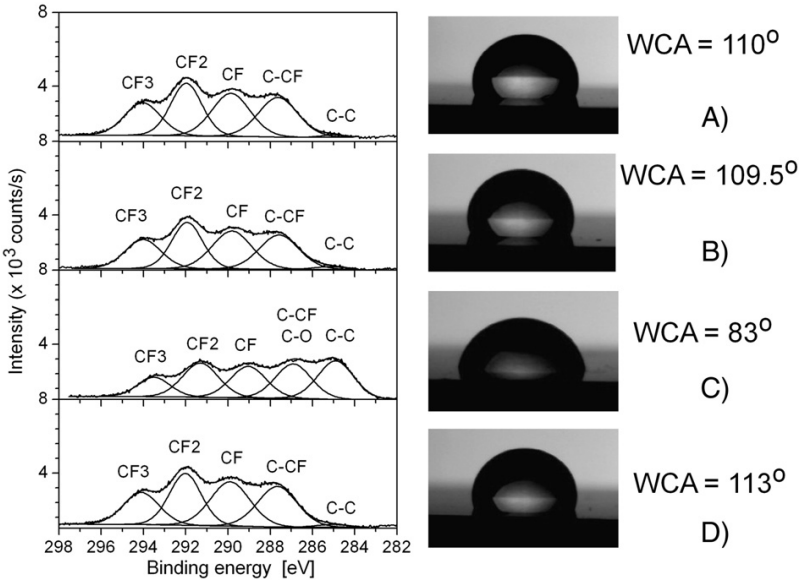

Fig. 3. High resolution XPS scans of C1 s peak of pPTFE films (left) and water droplets on pPTFE films. A) non-sterilized sample, B) sample sterilized by UV radiation, C) autoclaved sample and D) sample treated by dry heat.

bonds which occurs at the expense of the F-containing bonds (C – CF, C – F, CF_2 and CF_3). Correspondingly, WCA decreased from about 110° observed for the non-sterilized, UV and dry heated films down to 83° for the autoclaved samples. Such decrease is consistent with the typical WCA values reported for fluorocarbon polymers (109°, PTFE) and hydrocarbon polymers (80–90°, PE).

Conventional PTFE is very stable thermally and chemically. Its thermal degradation starts at temperatures exceeding 750 K [46]. Other fluorocarbon polymers, especially those containing tertiary carbon atoms in their structure, are less stable and degrade at temperatures below 570 K [47]. The pPTFE plasma polymers are much more branched and contain considerable amounts of tertiary carbon atoms (represented in the high-resolution XPS by the CF groups). It can be therefore suggested that the pPTFE films have worse thermal stability than conventional PTFE. Nevertheless, the temperature of 160 °C (433 K) used here for the dry heat treatment is neither sufficient to induce noticeable changes in chemical composition of the plasma polymers nor to result in their weight loss.

In contrast to other sterilization techniques, autoclaving causes chemical changes that are not negligible. Both the decrease of the F/C ratio and the enhancement of the C – C bonds evidence that the pPTFE films become deficient with fluorine. The fact that the thickness of the films does not change leads to a conclusion that the release of fluorine-bearing species is compensated from outside, oxygen being responsible for such contribution. The concentration of oxygen increases from about 1% for the as-deposited films to 5% after autoclaving. The mechanism of such substitution as well as the type of the fluorine-bearing species released is not clear as the data on thermal degradation of fluorocarbon polymers under purely water vapor atmosphere are scarce in the literature, yet. At present only certain speculations can be drawn.

The main product of thermal degradation of conventional fluorocarbon polymers under anaerobic environment (vacuum, dry nitrogen) is tetrafluoroethylene, TFE, while oxidative pyrolysis gives COF_2 as the principal evolved gas with smaller amounts of TFE, CO, CO_2, and other species [47,48]. Baker and Kasprzak studied thermal degradation of commercial fluoropolymers in 50% humid air and found a significant formation of HF [48]. The controversial release of HF by perfluorinated (and therefore dehydrogenated) polymers was explained by oxygen reacting with polymer radical with the emission of COF_2 which further hydrolyzed by reaction:

$$COF_2 + H_2O \rightarrow CO_2 + 2HF. \quad (1)$$

Our experiments were performed at much lower temperature, at lack of oxygen and at excess of water vapors. Hence, it was the action of water molecules themselves that lead to the pPTFE films partially losing fluorine and acquiring oxygen. Apparently, in this process the fluorine-bearing species should be sufficiently small to be volatile. The release of low molar mass fluorocarbons including TFE is unlikely as it would lead to the weight loss of the material which was not the case. The lack of oxygen should also render the release of COF_2 impossible. Therefore, hydrogen fluoride, HF, seems to be an appropriate candidate to serve as an escaping species. In this case, however, HF is formed rather as a result of a direct attack of H_2O on the fluorocarbon chain and not as a product of hydrolysis of COF_2. Since the CF bond weakens with less fluorine atoms attached to carbon [49], tertiary carbon atoms are most likely to take part in hydrolysis as they are weakest and therefore most vulnerable to such attack. The assumption of cleavage of the fluorine atoms from the tertiary carbon atoms is supported by the decrease of the CF and C–CF bonding environments in the C 1s XPS (Fig. 3, Table 1).

The pSN films were found to be composed of O, N and C (see Table 2). UV sterilization did not result in the change of the elemental content and produced the minimal changes in the chemical bonding. The concentration of the C – C/C – H bonds increased and the concentration of various CN bonds decreased slightly, which can be seen in Fig. 4.

Table 2
The XPS analysis of the non-sterilized and sterilized pSN films.

	O [%]	C[%]	N[%]	O/N	N/C	C – C, C – H %	CN, [a]%	C═O, N – C═O,%
As deposited	14.0	54.3	31.7	0.44	0.58	34	41	25
UV radiation	14.0	54.2	31.8	0.44	0.59	38	37	25
Autoclave	16.4	57.3	26.3	0.62	0.46	45	31	24
Dry heat	13.1	56.6	30.3	0.43	0.54	44	39	16

[a] CN stands for various C – N, C═N and C≡N species which cannot be resolved by XPS and which are represented by a single C 1s component at 286.5 eV.

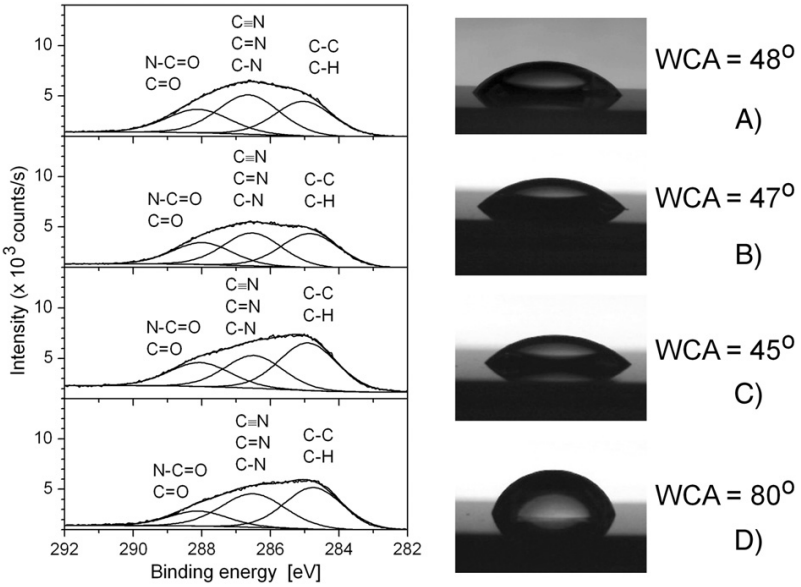

Fig. 4. High resolution XPS scans of C 1s peak of pSN films (left) and water droplets on PSN films. A) non-sterilized sample, B) sample sterilized by UV radiation, C) autoclaved sample and D) sample treated by dry heat.

Dry heat induced more significant changes. The films became more carbonized with the C – C/C – H groups reaching 44% as compared to 34% in the as-deposited samples. The total concentration of various CN groups remained almost at the initial level (39% against 41% in the as-deposited samples) but the concentration of the carbonyl- and amide-based species decreased significantly from 25% to 16%. Although nylon sputtered films have little in common with nylon itself, certain correlation in their thermal behavior can be noticed. Conventional nylons including nylon 6, 6 do not decompose thermally below 615 K [46]. At temperatures above 615 K cleavage of the weakest C – N and CO – CH_2 bonds occurs and volatile species are emitted. The main gaseous products of thermal degradation of nylon are CO_2 and H_2O. At even higher temperatures the release of HCN is possible [46]. Here, significantly lower temperature of 160 °C (433 K) was applied to the pSN films. Nevertheless, slight loss of mass (Fig. 2) implies that small amounts of volatile products were released as a result of thermal degradation. Furthermore, the reduction of the C═O/N – C═O XPS peak indicates that, as in the case of conventional nylons, carbon dioxide may be considered as the main escaping species. Apparently, oxidation of the pSN films by oxygen from air does not play a significant role here as it should

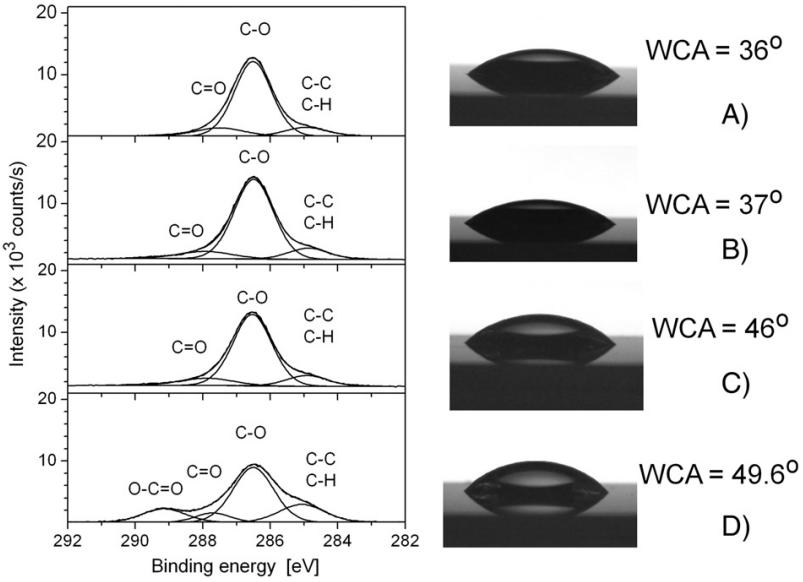

Fig. 5. High resolution XPS scans of C 1s peak of pPEO films (left) and water droplets on pPEO films. A) non-sterilized sample, B) sample sterilized by UV radiation, C) autoclaved sample and D) sample treated by dry heat.

Table 3
The XPS analysis of the non-sterilized and sterilized pPEO films.

	O [%]	C [%]	O/C	C–C, C–H %	C–O–C, %	C═O, %	O–C═O, %
As deposited	37.6	62.4	0.60	11	77	12	–
UV radiation	37.8	62.2	0.61	12	77	11	–
Autoclave	38.2	61.8	0.62	14	72	14	–
Dry heat	42.2	42.2	0.73	21	55	9	15

proceed to formation of the carbonyl-based species (via peroxy- and hydroperoxy radicals) [47] and thus lead to increase of oxygen content. None of this was detected by XPS.

Although performed at lower temperature than dry heat treatment, autoclave produced the most pronounced changes in the chemical composition of the pSN films. The increase of oxygen and simultaneous decrease of nitrogen content were detected. This resulted in an increase of O/N ratio approximately by 40% as compared to the O/N ratios observed for the not sterilized, UV and dry heat samples. Oxidation can also be ruled out here as autoclaving is performed in water vapors without presence of air. Therefore, reactions of certain functional groups with water, i.e. hydrolysis, should be considered. Significant loss of mass detected for the pSN films indicates that hydrolysis should be accompanied by the release of volatile species. The analysis of the C 1s XPS shows that the hydrocarbon content increases similar to the dry heat treatment, the concentration of the CN species decreases from initial 41% to 31% and the concentration of the C═O/N–C═O species remains constant. The CN component of the C 1s peak is contributed by the C–N (primary, secondary and tertiary amines), the C═N (imines) and the C≡N (nitriles) groups. Of all these species, imines are most prone to hydrolysis by reaction:

$$-C{=}N- + H_2O \rightarrow -C=O + NH_3\uparrow. \quad (2)$$

In fact, this reaction was proposed as a possible route of aging of amine-containing plasma polymers in air [50]. Those plasma polymers were found to degrade slowly with the loss of nitrogen over extended periods of time. In our case, the mechanism of the imine hydrolysis is accelerated due to elevated temperature and higher concentration of water. Amines and nitriles can hardly take part in hydrolysis with elimination of ammonia [51]. Amines get partially protonated upon reaction with water and this is the final step of their hydrolysis which cannot explain the observed transformation of the XPS spectrum. Nitriles undergo hydrolysis with formation of amides and with further elimination of ammonium ions or ammonia. However, the rate of the reaction is extremely low and normally acidic or basic catalysts should be used which is not the case here. Thus, it is likely hydrolysis of imines that is predominantly responsible for the loss of nitrogen content and decrease of the CN species in the pSN films during autoclaving.

It is worth noting that hydrolysis of imines results also in formation of the carbonyl-based species and therefore it should lead to the increase of the C═O/N–C═O component of the C 1s XPS peak. Nevertheless, it remains at the same level as in the as-deposited films. We suppose here that the mechanism of thermal degradation described above for the dry heat treatment is also active at some extent in the case of autoclaving and the supply of carbonyls as a result of hydrolysis of imines is counterbalanced by the loss of carbonyls due to release of CO_2.

The WCA data also reveal interesting correlation with the XPS spectra, with intensity of the C═O/N–C═O component in particular. For the as-deposited, UV and autoclaved samples the WCA of approximately 47° was measured whereas for the dry heat sample it reached the value of 80° (see Fig. 5). This strongly correlates with lower amount of the C═O/N–C═O groups after dry heat treatment as compared to other samples. Therefore its seems that carbonyl-based

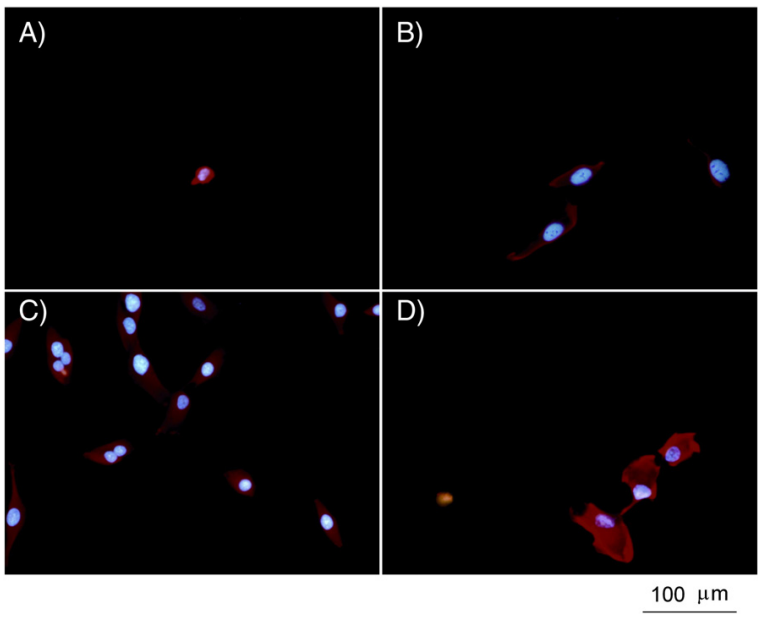

Fig. 6. Human osteoblast-like MG63 cells in 1-day-old cultures on pPTFE A) without sterilization or subjected to B) UV radiation treatment, C) autoclave treatment or D) dry heat treatment.

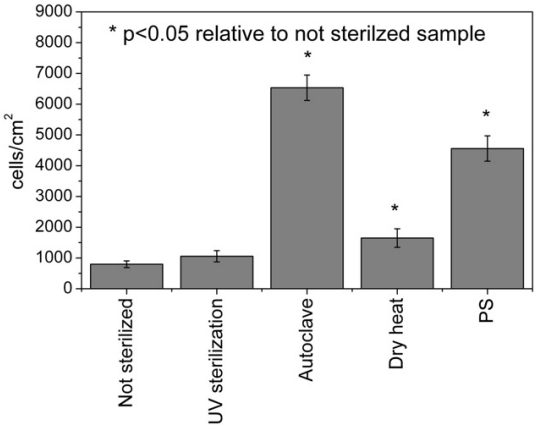

Fig. 7. Number of adhering MG63 cells 1 day after seeding on pPTFE films sterilized by different methods. For comparison the number of cells adhering on polystyrene dish (PS) is also given.

species, even though being in minority, govern polarity of the surface and have strong influence on the wettability of the pSN films.

The as-deposited pPEO films were composed of carbon and oxygen with O/C ratio of 0.6 (Table 3). The high resolution C 1s XPS revealed that the most dominant peak corresponded to the C–O–C bonds (77%), followed by the C═O bonds (12%) and the C–C/C–H bonds (11%) (Fig. 5). The contribution of these three peaks to the C 1s envelope remained almost unaffected when the samples were exposed to UV radiation. Similarity between the as-deposited and the UV irradiated samples was also confirmed by the WCA measurements giving 36° and 37° for both.

Minimal chemical changes can be also expected after autoclaving as ethers do not hydrolyze. Indeed, good retention of the PEO-like character was observed for the autoclaved samples. Slight decrease of the concentration of the C–O–C bonds to 72% was detected, which was accompanied by the enhancement of the C–C/C–H bonds (14%). Higher fraction of hydrophobic C–C/C–H bonds caused the small increase of WCA to the value of 46°.

Despite the small changes of chemical composition, the loss of mass after autoclaving for the pPEO films was significant. Since hydrolysis can be excluded from consideration, another mechanism should account for the observed loss of the material. It has been previously shown that pPEO films prepared by plasma-assisted evaporation are heterogeneous systems in which a cross-linked network co-exists with a mixture of oligomers with very broad molar mass distribution [14,31]. The oligomers are not linked chemically to the network but held within by physical entanglements. Upon contact with water, such macromolecules leave plasma polymer by diffusion and can be detected in the liquid phase by GPC and NMR. In particular, the pPEO film prepared at identical conditions as those used here lost about 12% of its thickness simply by out-diffusion of the unbonded species away from the film. Here, the film was autoclaved, i.e. brought in contact with water vapors. Nevertheless, the elevated temperature is responsible for intensification of the macromolecular dynamics and unbonded oligomers, especially of lower molar mass, get higher probability to disentangle and to escape from the plasma polymer.

This effect is even more pronounced in the case of dry heat treatment at which the higher temperature was used. The film lost about 70% of its thickness after such treatment (Fig. 2). Note also the changes in chemical composition. The C–O–C content drops down to 55%, which is accompanied by an increase of the C–C/C–H bonds (21%) and formation of the O–C═O bonds (15%). Significant change in the O/C ratio was also observed with oxygen content increased at the expense of carbon and the O/C raised to the value of 0.73. Formation of the O–C═O bonds is also consistent with the findings of Han with co-workers who elucidated esterification of PEO by the random chain

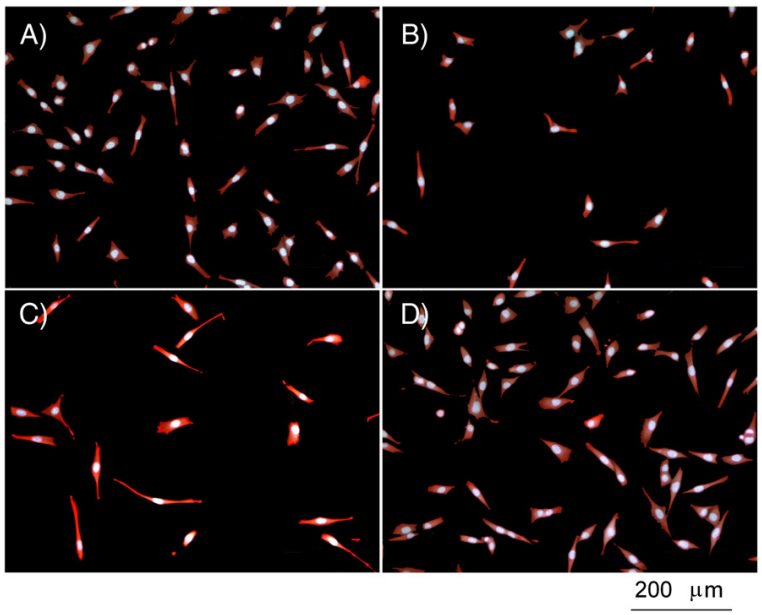

Fig. 8. Human osteoblast-like MG63 cells in 1-day-old cultures on pSN A) without sterilization or subjected to B) UV radiation treatment, C) autoclave treatment or D) dry heat treatment.

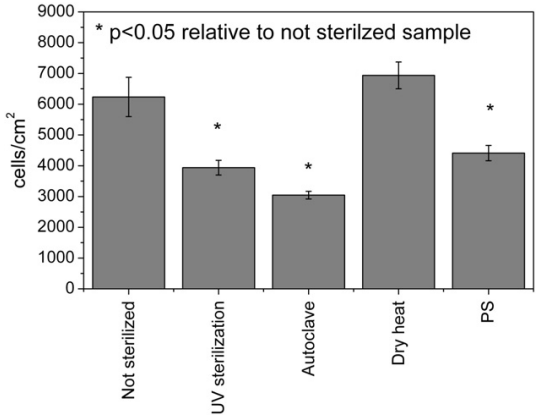

Fig. 9. Number of adhering MG63 cells 1 day after seeding on pSN films sterilized by different methods. For comparison also the number of cells adhering on polystyrene dish (PS) is given.

scission mechanism during thermal degradation in air [52]. In agreement with the chemical changes, an increase of WCA to the value close to 50° was observed.

3.3. Influence of sterilization methods on MG63 growth on the plasma polymers

The final step of this study was evaluation of bioadhesive properties of plasma polymers without and with application of different sterilization processes.

Regarding the MG63 cells behavior on the pPTFE surfaces, it has been found that the poor cell adhesive character of the non-sterilized samples was retained for the UV irradiated samples and for the samples sterilized by dry heat (see Figs. 6 and 7). This is consistent with the minimal changes of chemical composition of the pPTFE surfaces sterilized by these two sterilization methods. However, for the autoclaved samples significant increase of the number of adhering cells was observed, which was even higher as compared to the polystyrene dish used as a control. This behavior may be explained by the dramatic changes of the chemical composition of the autoclaved samples described in the previous section, in particular by the decrease of the F/C ratio that resulted in lowering of hydrophobic character of the surface. It is well known that materials with higher surface hydrophilia have more beneficial effects on cell colonization and cell phenotypic maturation [53]. The explanation of this phenomenon is that the surface hydrophilia leads to the adsorption of cell adhesion-mediating ECM molecules in advantageous spatial conformations, i.e. with specific amino acid sequences, serving as ligands for cell adhesion receptors, exposed to these receptors [54,55].

For plasma sputtered nylon, the number of adhering cells did not correlate with the WCA values. The as-deposited, UV-treated and autoclaved samples were of similar wettability but attached different numbers of cells (see Figs. 8 and 9). Nevertheless, the correlation can be found with the total amount of the C–N, C═N and C≡N species. The as-deposited and dry heated samples have close (and highest) concentration of the CN groups and both accumulate the largest amount of cells. Note also significantly different wettability of the two surfaces (46° against 80°) which almost does not manifest in the number of cells attached. For the UV-radiated sample the concentration of the CN is lower and so is the number of cells. The autoclaved samples, albeit with wettability comparable to the as-deposited ones, contain the lowest amount of the CN groups and are least favorable for the cell adhesion.

For the pPEO samples, the sterilization methods also had a diverse impact on the cell behavior as can be seen in Figs. 10 and 11. The MG63 cells do not adhere to the non-sterilized films, which supports our previous reports on the non-fouling properties of such plasma polymers [14,31]. The UV treatment does not influence the ability of the films to withstand the accumulation of cells either. However, the autoclaved and the dry heated samples lost the non-fouling character and the number of cells adhering to them approached the value observed for the polystyrene dish. These results are in agreement with alterations of the chemical composition of the films: the loss of the ether bonds results in enhancement of the cell adhesion. The previous studies established a critical concentration of 65–70% of the

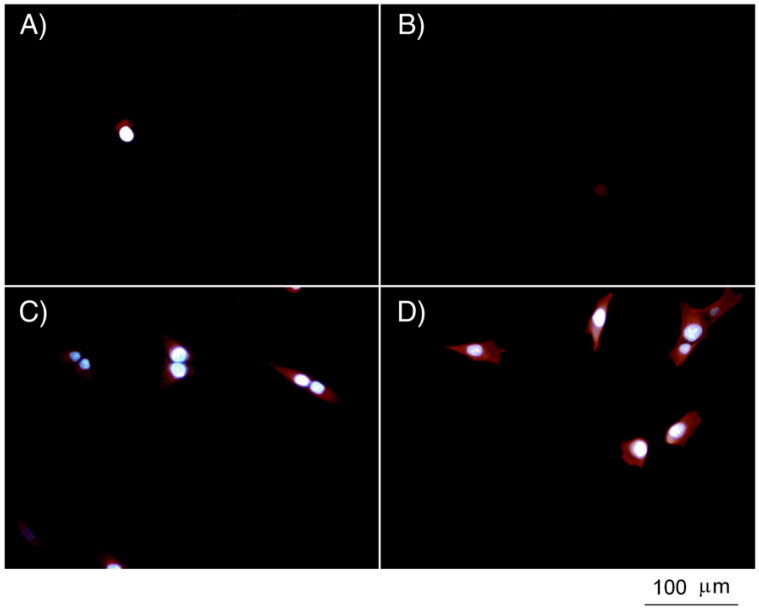

Fig. 10. Human osteoblast-like MG63 cells in 1-day-old cultures on pPEO A) without sterilization or subjected to B) UV radiation treatment, C) autoclave treatment or D) dry heat treatment.

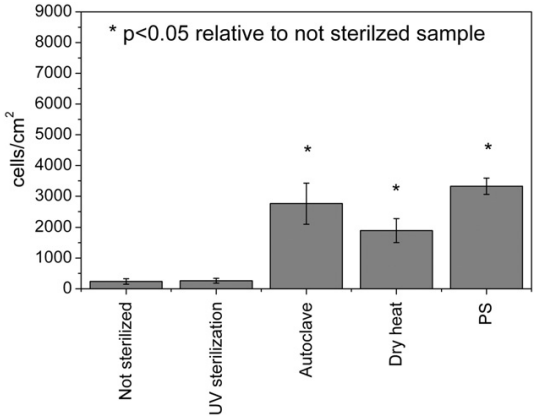

Fig. 11. Number of adhering MG63 cells 1 day after seeding on pPEO films sterilized by different methods. For comparison also the number of cells adhering on polystyrene dish (PS) is given.

C – O – C bonds at which the non-fouling properties of pPEO films disappear [14,31,56]. Here, the autoclaved sample with 72% of the C – O – C groups shows significant accumulation of cells. Surprisingly, lower amount of cells was observed on the dry heated samples which had the lowest concentration (55%) of ethers. This effect cannot be explained by the chemical changes detected and is probably related with other properties of the films (elasticity, flexibility of the chain segments etc.).

4. Conclusions

The results presented here clearly show that the properties of selected plasma polymers may be significantly altered by a sterilization process. Moreover, the comparative study of the effects of dry heat, autoclaving and UV based sterilization on three distinctly different kinds of plasma polymers shows that the selection of the sterilization process for a particular plasma polymer is of high importance with respect to their possible use in biomedical applications.

First of all, it was demonstrated that sterilization methods may have strong impact on the thickness of plasma polymers. The thickness of pPEO was reduced mostly by dry heat sterilization, the highest reduction of the thickness of pSN was caused by autoclaving and, finally, thickness of pPTFE films was not changed by any of the tested sterilization methods. The same can be said in connection with chemical composition of the plasma polymers or their bioadhesive properties: the changes induced by the selected sterilization method depend strongly on a sterilized plasma polymer. The pPTFE and pSN films were most sensitive chemically to autoclaving due to hydrolysis whereas the pPEO films exhibited the strongest chemical changes after the dry heat treatment due to thermal degradation/oxidation. In other words, there exists no universal sterilization method that assures preservation of the properties of all kinds of plasma polymers and thus resistance of each plasma polymer toward sterilization methods has to be tested separately. This is an important finding with respect to the design of plasma polymers intended for use in the biomedical field: for the application of a plasma polymer, a suitable sterilization method must be also identified. Finally, it has to be stressed that properties of plasma polymers may be varied in large extent by alteration of deposition conditions (applied power, pressure, working gas composition, use of continuous or pulsed plasma etc.), which may in turn influence also their resistance to sterilization process. Therefore the results presented here are not meant as description of general trends valid for all PEO-like films and for films of plasma sputtered nylon or PTFE, but should be considered more as a demonstration of the necessity to perform sterilization tests for each particular plasma polymer separately.

Acknowledgments

This work was supported by the grant SVV-2012-265305 and by the GAUK 110-10/251265 grant of the Grant Agency of Charles University in Prague.

References

[1] H. Yasuda, M. Gazicki, Biomaterials 3 (1982) 68.
[2] R. Förch, A.N. Chifen, A. Bousquet, H. Khor, M. Jungblut, L.Q. Chu, Z. Zhang, I. Osey-Mensah, E.K. Sinner, W. Knoll, Chem. Vap. Deposition 13 (2007) 280.
[3] D.G. Castner, B.D. Ratner, Surf. Sci. 500 (2002) 28.
[4] C. Oehr, Nucl. Instrum. Methods Phys. Res., Sect. B 208 (2003) 40.
[5] K.S. Siow, L. Britcher, S. Kumar, H.J. Griesser, Plasma Processes Polym. 3 (2006) 392.
[6] P.-L. Girard-Lauriault, F. Truica-Marasescu, A. Petit, H.T. Wang, P. Desjardins, J. Antoniou, F. Mwale, M.R. Wertheimer, Macromol. Biosci. 9 (2009) 911.
[7] B. Finke, F. Hempel, H. Testrich, A. Artemenko, H. Rebl, O. Kylián, J. Meichsner, H. Biederman, B. Nebe, K.-D. Weltmann, K. Schröder, Surf. Coat.Technol. 205 (2011) S520.
[8] R. Di Mundo, R. Gristina, E. Sardella, F. Intranuovo, M. Nardulli, A. Milella, F. Palumbo, R. D'Agostino, P. Favia, Plasma Processes Polym. 7 (2010) 212.
[9] Y. Wu, R. Timmons, J. Jen, F. Molock, Colloids Surf. B Biointerfaces 18 (2000) 235.
[10] E.E. Johnston, J.D. Bryers, B.D. Ratner, Langmuir 21 (2005) 870.
[11] F. Brétagnol, M. Lejeune, A. Papadopoulou-Bouraoui, M. Hasiwa, H. Rauscher, G. Ceccone, P. Colpo, F. Rossi, Acta Biomater. 2 (2006) 165.
[12] F. Brétagnol, O. Kylián, M. Hasiwa, L. Ceriotti, H. Rauscher, G. Ceccone, D. Gilliland, P. Colpo, F. Rossi, Sens. Actuators B 123 (2007) 283.
[13] E. Sardella, R. Gristina, G.S. Senesi, R. D'Agostino, P. Favia, Plasma Processes Polym. 1 (2004) 63.
[14] A. Choukourov, I. Gordeev, O. Polonskyi, A. Artemenko, L. Hanyková, I. Krakovský, O. Kylián, D. Slavínská, H. Biederman, Plasma Processes Polym. 7 (2010) 445.
[15] C. Rodriguez-Emmenegger, O. Kylián, M. Houska, E. Brynda, A. Artemenko, J. Kousal, A.B. Alles, H. Biederman, Biomacromolecules 12 (2011) 1058.
[16] B. Yameen, H.U. Khan, W. Knoll, R. Förch, U. Jonas, Macromol. Rapid Commun. 32 (2011) 1735.
[17] H. Kobayashi, A.T. Bell, M. Shen, Macromolecules 7 (1974) 277.
[18] P. Favia, R. D'Agostino, Surf. Coat.Technol. 98 (1998) 1102.
[19] B. Nebe, B. Finke, F. Lüthen, C. Bergemann, K. Schröder, J. Rychly, K. Liefeith, A. Ohl, Biomol. Eng. 24 (2007) 447.
[20] A. Choukourov, H. Biederman, D. Slavinska, L. Hanley, A. Grinevich, H. Boldyryeva, A. Mackova, J. Phys. Chem. B 109 (2005) 23086.
[21] F. Truica-Marasescu, P.-L. Girard-Lauriault, A. Lippitz, W.E.S. Unger, M.R. Wertheimer, Thin Solid Films 516 (2008) 7406.
[22] D. Hegemann, M.M. Hossain, E. Körner, D.J. Balazs, Plasma Processes Polym. 4 (2007) 229.
[23] D. Morrison, T. Robertson, Thin Solid Films 15 (1973) 87.
[24] H. Biederman, P. Bílková, J. Ježek, P. Hlídek, D. Slavínská, J. Non-Cryst. Solids 218 (1997) 44.
[25] H. Biederman, Vacuum 59 (2000) 594.
[26] I. Kholodkov, H. Biederman, D. Slavinska, A. Choukourov, M. Trchova, Vacuum 70 (2003) 505.
[27] S. Iwamori, K. Noda, Mater. Lett. 66 (2012) 349.
[28] A. Choukourov, J. Hanuš, J. Kousal, A. Grinevich, Y. Pihosh, D. Slavínská, H. Biederman, Vacuum 80 (2006) 923.
[29] A. Choukourov, O. Polonskyi, J. Hanus, J. Kousal, A. Grinevich, D. Slavinska, H. Biederman, Plasma Processes Polym. 6 (2009) S21.
[30] A. Choukourov, A. Grinevich, O. Polonskyi, J. Hanus, J. Kousal, D. Slavinska, H. Biederman, J. Phys. Chem. B 113 (2009) 2984.
[31] A. Choukourov, I. Gordeev, D. Arzhakov, A. Artemenko, O. Kylián, J. Kousal, O. Polonskyi, J. Pešička, D. Slavínská, H. Biederman, Surf. Coat.Technol. 205 (2011) 2830.
[32] Z. Zhang, Q. Chen, W. Knoll, Surf. Coat.Technol. 175 (2003) 588.
[33] A. Tarasova, P. Hamilton-Brown, T. Gengenbach, H.J. Griesser, L. Meagher, Plasma Processes Polym. 5 (2008) 175.
[34] K. Vasilev, L. Britcher, A. Casanal, H.J. Griesser, J. Phys. Chem. B 112 (2008) 10915.
[35] J.-C. Ruiz, A. St-Georges-Robillard, C. Thérésy, S. Lerouge, M.R. Wertheimer, Plasma Processes Polym. 7 (2010) 737.
[36] A. Artemenko, O. Kylián, J. Kousal, A. Choukourov, O. Polonskyi, D. Slavinska, H. Biederman, Surf. Coat.Technol. 205 (2011) S529.
[37] L. Detomaso, R. Gristina, G.S. Senesi, R. D'Agostino, P. Favia, Biomaterials 26 (2005) 3831.
[38] F. Brétagnol, H. Rauscher, M. Hasiwa, O. Kylián, G. Ceccone, L. Hazell, A.J. Paul, O. Lefranc, F. Rossi, Acta Biomater. 4 (2008) 1745.
[39] M. Drábik, O. Polonskyi, O. Kylián, J. Čechvala, A. Artemenko, I. Gordeev, A. Choukourov, D. Slavínská, I. Matolínová, H. Biederman, Plasma Processes Polym. 7 (2010) 544.
[40] O. Kylián, M. Drábik, O. Polonskyi, J. Čechvala, A. Artemenko, I. Gordeev, A. Choukourov, I. Matolínová, D. Slavínská, H. Biederman, Thin Solid Films 519 (2011) 6426.

[41] O. Kylián, J. Hanuš, A. Choukourov, J. Kousal, D. Slavínská, H. Biederman, J. Phys. D: Appl. Phys. 42 (2009) 142001.
[42] O. Kylián, J. Kousal, A. Artemenko, A. Choukourov, M. Petr, O. Polonskyi, D. Slavinska, H. Biederman, Surf. Coat.Technol. 205 (2011) S558.
[43] T.R. Gengenbach, R.C. Cbatelier, H.J. Griesser, Surf. Interface Anal. 24 (1996) 271.
[44] T.R. Gengenbach, H.J. Griesser, Surf. Interface Anal. 26 (1998) 498.
[45] V. Stundžia, P. Bilková, H. Biederman, D. Slavinská, P. Hlidek, Vacuum 50 (1998) 23.
[46] C. Beyler, M. Hirschler, in: Ph.J. DiNenno (Ed.), SFPE Handbook of Fire Protection Engineering, National Fire Protection AssociationQuincy, Massachusetts, 2002.
[47] A. Hollaender, J. Thome, in: H. Biederman (Ed.), Plasma Polymer Films, Imperial College Press, London, 2004.
[48] B. Baker, D. Kasprzak, Polym. Degrad. Stab. 42 (1993) 181.
[49] E. Giannetti, J. Fluorine Chem. 126 (2005) 625.
[50] T.R. Gengenbach, H.J. Griesser, J. Polym. Sci. A 37 (1999) 2191.
[51] J. Clayden, N. Greeves, S. Warren, P. Wothers, Organic Chemistry, OUP, Oxford, 2001.
[52] S. Han, C. Kim, D. Kwon, Polymer 38 (1997) 317.
[53] J. He, W. Zhou, X. Zhou, X. Zhong, X. Zhang, P. Wan, B. Zhu, W. Chen, J. Mater. Sci. Mater. Med. 19 (2008) 3465.
[54] L. Bačáková, E. Filová, F. Rypáček, V. Švorčík, V. Starý, Physiol. Res. 53 (2004) S35.
[55] L. Bacakova, V. Svorcik, in: D. Kimura (Ed.), Cell Growth Processes: New Research, Nova Sci. Publ., New York, 2008, p. 5.
[56] E. Sardella, P. Favia, R. Gristina, M. Nardulli, Plasma Processes Polym. 3 (2006) 456.

BIOMACROMOLECULES

ARTICLE

pubs.acs.org/Biomac

Substrate-Independent Approach for the Generation of Functional Protein Resistant Surfaces

Cesar Rodriguez-Emmenegger,*[,†,‡] Ondřej Kylián,[§] Milan Houska,[†] Eduard Brynda,[†] Anna Artemenko,[§] Jaroslav Kousal,[§] Aldo Bologna Alles,[‡] and Hynek Biederman[§]

[†]Institute of Macromolecular Chemistry, Academy of Sciences of the Czech Republic, v.v.i., Czech Republic

[‡]College of Engineering, Universidad de la Republica, Uruguay

[§]Faculty of Mathematics and Physics, Charles University in Prague, Czech Republic

Supporting Information

ABSTRACT: A new route for coating various substrates with antifouling polymer layers was developed. It consisted in deposition of an amino-rich adhesion layer by means of RF magnetron sputtering of Nylon 6,6 followed by the well-controlled, surface-initiated atom transfer radical polymerization of antifouling polymer brushes initiated by bromoisobutyrate covalently attached to amino groups present in the adhesion layer. Polymer brushes of hydroxy- and methoxy-capped oligoethyleneglycol methacrylate and carboxybetaine acrylamide were grafted from bromoisobutyrate initiator attached to a 15 nm thick amino-rich adhesion layer deposited on gold, silicon, polypropylene, and titanium−aluminum−vanadium alloy surfaces. Well-controlled polymerization kinetics made it possible to control the thickness of the brushes at a nanometer scale. Zero fouling from single protein solutions and a reduction of more than 90% in the fouling from blood plasma observed on the uncoated surfaces was achieved. The feasibility of functionalization with bioactive compounds was tested by covalent attachment of streptavidin onto poly(oligoethylene glycol methacrylate) brush and subsequent immobilization of model antibodies and oligonucleotides. The procedure is nondestructive and does not require any chemical preactivation or the presence of reactive groups on the substrate surface. Contrary to current antifouling modifications, the developed coating can be built on various classes of substrates and preserves its antifouling properties even in undiluted blood plasma. The new technique might be used for fabrication of biotechnological and biomedical devices with tailor-made functions that will not be impaired by fouling from ambient biological media.

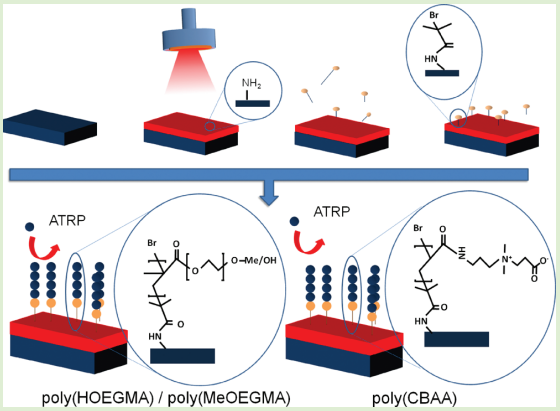

INTRODUCTION

Protein fouling in complex biological fluids, particularly, blood, plasma, and serum, is an adverse event that can impair the properties or functions of various biotechnological and biomedical devices.[1−3] Some examples include stopping flow through separation columns and porous membranes,[4] nonspecific response of affinity biosensors,[2,3,5] reduced circulation time of nanocarriers in bloodstream due to colloidal instability or opsonization,[6−10] bacteria attachment on contact lenses[11] and synthetic grafts,[12] or disabling of cardiovascular devices by thrombus formation.[12,13] Thus, the development of a technology by which antifouling interfaces between biological media and various types of materials can be prepared is an important challenge for contemporary research.

Current surface modifications with antifouling self-assembled monolayers (SAMs),[14] grafted polymer layers, and polymer brushes reduce considerably or suppress the adsorption from single protein solutions. The authors have often claimed that they have obtained perfectly antifouling,[15] superlow fouling,[16] ultralow fouling,[17] and even nonfouling[18] surfaces because they had not observed any adsorption from solutions of the main plasma proteins, human serum albumin (HSA), and fibrinogen (Fbg). However, a reduction or even total prevention of the adsorption of the main blood plasma proteins (HSA and Fbg), immunoglobulin G (IgG) or lysozyme (Lys), is not evidence that the surface is resistant to blood plasma.[3,19,20] Only much fewer works showed a reduction of the fouling from blood plasma.[1−3] Grafted carboxymethyldextrane or polyethyleneglycol have been used, but just a minor decrease in blood plasma fouling was reached. Theoretical treatment predicted enhanced antifouling properties

Received: November 24, 2010
Revised: March 2, 2011
Published: March 07, 2011

with increasing grafting density and chain length of the polymers, that is, the polymer chains in the brush regime.[21] The development of new surface-initiated controlled radical polymerization allowed to coat surfaces with well-defined, highly densed polymers brushes with tunable chain length.[22] Polymer brushes of poly(vinyl pyrrolidone), poly(phosphorylcholine methacrylate) (polyPCMA), or poly(N-isopropyl acrylamide) were shown to reduce the fouling from single protein solutions.[3,23] Zwitterionic polysulfobetaine brushes were also studied due to their high wettability and neutral electric charge. Although these brushes totally suppressed the fouling from single protein solution,[16] they were highly fouling in blood plasma.[3] More recent attempts include the use of polyampholytes composed of positively and negatively charged monomers, which resisted the fouling from single proteins solution and reduced the fouling from diluted blood plasma.[24,25] Oligosaccharides and brushes of N-substituted acrylamide containing different carbohydrates were also used to reduced protein fouling.[17,26,27] Kizhakkedathu et al. have done extensive studies on polymer brushes based on acrylamide backbone,[17,28,29] that is, poly(oligoethyleneglycol acrylamide) and poly(*N*,*N*-dimethylacrylamide) brushes grafted from gold or polystyrene particles reduced their interaction with proteins and diluted blood plasma.[28,29] It must be stressed, however, that so far only polymer brushes of oligoethylene glycol methacrylate and poly(carboxybetaine acrylamide) (poly(CBAA)) have provided sufficient resistance to fouling when incubated with undiluted blood plasma[1,19,30,31] being attractive candidates for the development of ultrathin antifouling layers for the preparation of protein arrays,[32] polymeric nanocapsules stable in blood plasma,[19] or cell-resistant surfaces.[30]

Polymer brushes with controlled thickness and well-defined composition and architecture can only be grafted from surfaces containing immobilized initiators for surface-initiated atom transfer radical polymerization (ATRP) or chain transfer agents (CTAs) for reversible addition−fragmentation transfer (RAFT).[22,33] Such initiators or CTAs can be attached via different chemical reactions to the surface of the substrate, for example, chemisorption of thiols on gold and silver, silane chemistry on glass or silicon, complexation to metal oxides, via hydroxyls or carboxylic groups available in some of polymers, and so on. The modification of more inert substrates such as polymers without functional groups poses a more difficult challenge to the attachment of initiators that often require specific pretreatment or activation steps, for example, plasma and oxidative surface treatments. An extensive overview of techniques that allow functionalization of various substrates with the initiating or mediating agents can be found in review by Klok's group.[22] Different substrates often requires very different strategies for surface modification and not all the attached agents provide stable anchoring to polymer brush layers.[34] Entropic force imposed by the stretching of the polymer chains can compromise the stability of polymer brushes attached to surfaces.[35,36] Klok reported the detachment of layers of polymer brushes anchored via the ill-defined silane chemistry onto silicon and glass, and other authors have shown that the force exerted by the brushes could cleave covalent bonds.[34−37] The development of a versatile strategy for a stable functionalization of multiple classes of materials is challenging as only one generalized method for accomplishing this task has been previously reported. Messersmith's group used self-polymerization of dopamine to create a primary coating adherent to a broad variety of substrates, inorganic, organic, metals, and so on, and secondary reactions to prepare ad-layers with different properties and functionalities.[38] However, it has been shown that dopamine undergoes oxidation during the polymerization, which reduces its adhesion to Ti.[39] As an alternative way, dopamine molecules were immobilized on titanium, iron oxides, silicon oxide, and gold surfaces via their chelating catechol groups and their amino groups to anchor antifouling polymer chains[40,41] or ATRP initiator. Nevertheless, the use of dopamine as an anchoring group lacks the versatility of poly(dopamine), being applicable only for metallic surfaces.[42] Additional problems with stability arose and more than one catechol unit per chain was required, resulting in complicated synthetic procedures. Therefore, more versatile and easily applicable techniques are desirable.

The main goal of this work was to develop a versatile, nondestructive, and robust approach for making antifouling and bioactive interfaces between various classes of materials and biological media, particularly, blood plasma, that could be prepared. The essential step of such modification was the coating of a substrate with a stable antifouling layer. Polymer brushes of methoxy- and hydroxy-capped oligoethylene glycol methacrylate (poly(MeOEGMA) and poly(HOEGMA)) or poly(carboxybetaine acrylamide) (poly(CBAA)) prepared by surface-initiated ATRP were selected for the coating because only these surfaces could prevent efficiently fouling from blood plasma. An amino-rich film (hereafter, plasma sputtered nylon (PSN) films) was initially deposited on gold, silicon, glass, polypropylene and Ti surface by radio frequency (RF) magnetron sputtering of nylon in mixtures of argon and nitrogen using the technique developed by us earlier.[43,44] ATRP initiators were covalently attached to amino groups present in the film and brushes were grown from the surface. The procedure was nondestructive and did not require any chemical preactivation or the presence of reactive groups on the substrate surface. Thus, it can be applied for modification of various materials including the inert ones. The tunable thickness and density of amino groups in the plasma deposited film makes it possible to prepare brushes with equivalent properties independently of the substrate material. This is particularly important for minimizing fouling in blood plasma, which is sensitive to an optimal brush architecture. Biorecognition elements were covalently attached to poly(HOEGMA) brushes via their hydroxyl groups as a model example. The plasma deposition of amino-rich films followed by the growth polymer brushes from its surface resulted in a new type of antifouling coatings. Contrary to other antifouling modifications, the coating can be built on various classes of substrates and preserves its antifouling properties even in undiluted blood plasma. This work offers a promising technology for the facile fabrication of different surface-based biotechnological and biomedical devices able to perform tailor-made functions while resisting to the fouling from the complex biological media where they operate.

EXPERIMENTAL SECTION

Materials. *Reagents.* All chemical reagents were used without further purification. CuCl, CuBr, $CuBr_2$, 2,2′-dipyridyl (BiPy), 1,4,8,11-tetramethyl-1,4,8,11-tetraazacyclotetradecane (Me_4Cyclam), α-bromoisobutyl bromide, 11-mercapto-1-undecanol, *N*,*N*′-disuccinimidyl carbonate (DSC), triethylamine, and 4-(dimethylamino) pyridine were purchased from Sigma-Aldrich. *N*-[3-(Dimethylamino)propyl] acrylamide (DMAPA, 98%) and β-propiolactone (90%) were from TCI Europe and Serva Electrophoresis GmbH, respectively. Nylon 6,6

targets were from Goodfellow. Initiator ω-mercaptoundecylbromoisubutyrate was synthesized by reacting α-bromoisobutyl bromide with 11-mercapto-1-undecanol according to the method published earlier.[45] Macromonomers, oligo(ethylene glycol) methyl ether methacrylate M_n 300 (MeOEGMA) and oligo(ethylene glycol) methacrylate M_n 526, inhibited with 900 ppm of hydrochinone monomethyl ether were from Aldrich. The inhibitor was removed by passing through a basic alumina column immediately before the polymerization experiment.

Biochemicals. Human serum albumin (HSA, 99% by electrophoresis), fibrinogen from human blood plasma (Fbg), lysozyme human (Lys), fetal bovine serum (FBS), and pooled human blood plasma (BP) and serum (BS) were from Sigma. Human immunoglobulin G (IgG) was from Seva Imuno, Prague, Czech Republic. Streptavidin (SA) Rabbit IgG (Rb IgG) conjugated with biotin (b-Rb IgG), mouse antiboby against rabbit IgG (anti- Rb IgG), were purchased from Thermo Scientific. Oligonucleotide **1** [5′-CTACTGAAATACACAGAA-3] (ONC **1**) conjugated with biotin (b-ONC **1**) and oligonucleotide **2** (complementary to ONC1) conjugated with bovine serum albumin (BSA-ONC **2**) were kind gifts from Vidia, Prague.

Solvents. Ethanol (96%), tetrahydrofuran (THF, 99.5%), and methanol (99.6%) were purchased from Lachner. *N*,*N*-Dimethylformamide (DMF, 99.5%), phosphate buffered saline, pH 7.4 (PBS), and TRIS buffer, 50 mM, pH 7.2, were from Sigma-Aldrich.

Synthesis of Carboxybetaine Acrylamide. (3-Acryloylaminopropyl)-(2-carboxy-ethyl)-dimethyl-ammonium (CBAA) was synthesized by the modified procedure published earlier.[46] DMAPA (7.8 g, 55 mmol) was dissolved in 100 mL of anhydrous THF and cooled to 0 °C. Subsequently, β-propiolactone (5.0 g, 69 mmol) was dissolved in 40 mL of THF and added dropwise under nitrogen. The reaction was allowed to proceed for 24 h at 4 °C. The white precipitate was washed with dry THF and ether. Yield: 80%. ^{1}H NMR (Bruker 250 MHz in D_2O: 6.32 (t, 1H, CHH═C*H*), 6.2 (t, 1H, C*H*H═CH), 5.87 (t, 1H, C*H*H═CH), 3.66 (t, 2H, N-CH_2-CH_2-COO), 3.48 (m, 4H, NH-CH_2-CH_2-CH_2), 3.17 (s, 6H, N-$(CH_3)_2$), 2.75 (t, 2H, CH_2-COO).

Substrates. Silicon wafers, gold-coated silicon wafers, gold-coated BK7 glass plates (SPR chips), and TiAlV alloy discs were rinsed with ethanol and water twice and cleaned in a UV-ozone cleaner (Jeligth) for 20 min. Polypropylene sheets were rinsed with acetone, ethanol, and water, mechanically wiped with cotton buds, and rinsed again.

Deposition of Plasma Sputtered Nylon Films. The deposition of the primary anchoring layer was performed in the plasma reactor schematically depicted in the Supporting Information and described in details in previous publications.[44] A cylindrical processing chamber (50 L) equipped with a water-cooled planar RF magnetron operated at a driving frequency of 13.56 MHz fed by a RF generator (Cesar 136 RF generator, Dressler) and manually operated matching unit (MFJ-962D, MFJ Enterprises) was pumped by a rotary and a diffusion pump. A Nylon 6,6 disk (diameter of 80 mm and thickness of 2 mm) was used as a target. Prior to each deposition the deposition chamber was pumped down to the base pressure of 2×10^{-3} Pa. The freshly cleaned substrates were introduced to the deposition chamber by means of a load-lock system and were placed at a distance of 40 mm from the sputtered target. For a typical deposition, RF power of 40 W was applied and the reflected power was kept below 2 W. The plasma was sustained at a pressure of 2 Pa in a mixture of argon and nitrogen (1:1) and total gas flow of 5 sccm. A smooth plasma polymer films with a N/C ratio of about 0.5 and NH_2/C of about 0.05, as determined by XPS and chemical derivatization, respectively, were deposited at a rate of 10.7 nm min^{-1}.[44] Thickness of the deposited PSN films used for additional modifications and following experiments was 15 nm.

Immobilization of Initiator. *On Plasma Sputtered Nylon Films.* The initiator, α-bromoisobutyrate bromide, was covalently attached to the surface of the PSN by acylation with surface amino groups.[44] Freshly coated substrates were immersed in 15 mL solution of triethylamine 0.24 M at 0 °C. A solution of α-bromoisobutyrate bromide (0.24 M in 7.5 mL THF, 0 °C) was added dropwise to the samples placed in a shaker. After 3 min at room temperature, the substrates were removed, rinsed successively with THF, ethanol, and water, and dried with nitrogen.[47]

On Gold-Coated Substrates. The substrates were immersed in a 1 mM solution of ω-mercaptoundecylbromoisobutyrate for 24 h to allow the formation of a self-assembled monolayer of the initiator.[3]

Preparation of Polymer Brushes by Surface-Initiated Atom Transfer Radical Polymerization (SI ATRP). *Poly-(MeOEGMA) and Poly(HOEGMA).* A solution of $CuBr_2$ (24.3 mg, 109.2 μmol), 2,2′-dipyridyl (435 mg, 2.79 mmol), and MeOEGMA (17.1 g, 57 mmol) or HOEGMA (30 g, 57 mmol) in 30 mL of water was degassed using Ar bubbling for 1 h. CuCl (111 mg, 1.13 mmol) was added under an Ar atmosphere and the Ar bubbling was carried out for the next 30 min. The polymerization mixture was subsequently transferred under an Ar atmosphere to six reactors (carousel-12, Radley U.K.). Each reactor contained two substrates, one coated with plasma sputtered nylon film and initiator and a gold-coated silicon substrate with a SAM of ω-mercaptoundecylbromoisobutyrate initiator. The polymerization was carried out at 30 °C. Samples were taken out of the reactors at different polymerization times, washed successively with ethanol and water, and stored in water.

Poly(CBAA). The solvent, ethanol (10 mL), was degassed using three freeze−pump−thaw cycles. Afterward it was transferred under an Ar atmosphere to a Schlenk tube containing CuBr (19.1 mg, 133 μmol), $CuBr_2$ (5.9 mg, 26.5 μmol), and Me_4Cyclam (40.9 mg, 160 μmol). The blue solution of the catalyst was added to another Schlenk tube containing the monomer, CBAA (1500 mg, 6.7 mmol). Finally, the polymerization solution was transferred to the reactors containing the substrates as for the polymerization of OEGMAs. The reaction was allowed to proceed for 2 h at 30 °C. The samples were washed with ethanol and water and stored in water.

Characterization of Polymer Films. *Spectroscopic Ellipsometry (SE).* The measurements of polymer films prepared on silicon wafers were performed using Variable Angle Spectroscopic Ellipsometer (Woolam M-2000DI) in a wavelength range of λ = 192−1690 nm and an angle of incidence range of AOI = 55−75° in air at room temperature. The obtained SE spectra were fitted with multilayer models using the CompleteEASE analysis software. The thickness and refractive index of polymer layers were obtained from simultaneous fitting the obtained ellipsometric data using the Tauc-Lorentz oscillator model.

Contact Angle. The wettability of surfaces was examined by dynamic sessile water drop method using DataPhysics OCA 20 contact angle system. A 5 μL drop was placed on the surface, and advancing and receding contact angles were determined while the volume of the drop was increased up to 15 μL and decreased at a flow rate of 0.5 μL·min^{-1}. Data were evaluated using circular fitting algorithm.

X-ray Photoelectron Spectroscopy(XPS). Samples coated with an amino-rich plasma polymer were transferred from the plasma reactor without breaking the vacuum into an XPS apparatus (X-ray source Specs XR50, Al Kα line, hemispherical electron analyzer Phoibos 100 Specs) and the surface elemental composition (except hydrogen) was determined from the wide scans using appropriate relative sensitivity factors for XPS peaks.

Atomic Force Microscopy. Morphology of the films was characterized by AFM (Quesant Q-scope) operated in semi-contact mode in dry state using NSC-16 silicon cantilevers (Schaefer Technologie, GmbH). Each reported value of surface root-mean-square (RMS) roughness represents an average over three 10 × 10 μm scans.

Fourier Transform Infrared Grazing Angle Specular Reflectance (FTIR GASR). FTIR GASR spectra of the dry polymer brushes grown from initiator attached to plasma sputtered nylon film, with a thickness of 15 nm, deposited on gold-coated glass plates or from SAM of the initiator formed on gold-coated glass plates were measured using FTIR

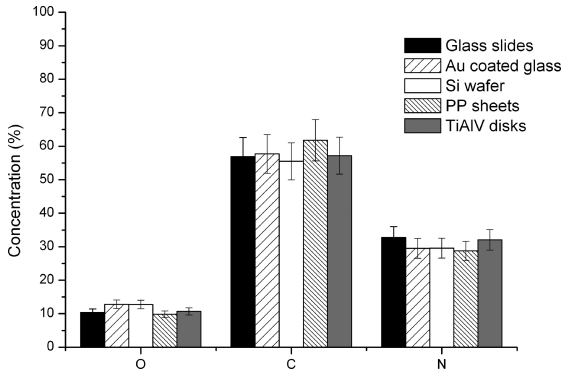

Figure 1. Elemental composition (without hydrogen) of plasma sputtered nylon films deposited on different substrates.

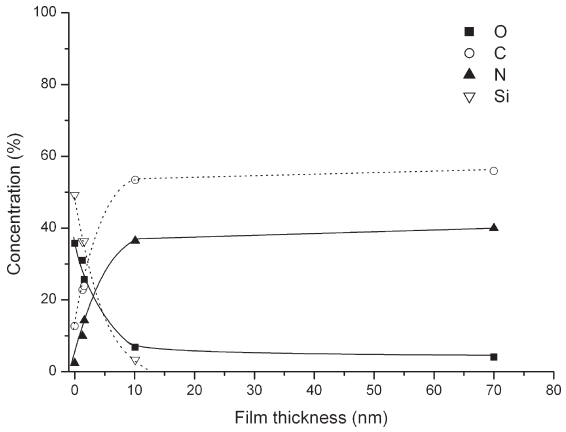

Figure 2. Evolution of the chemical composition of amino-rich plasma sputtered nylon films on silicon wafer with increasing film thickness.

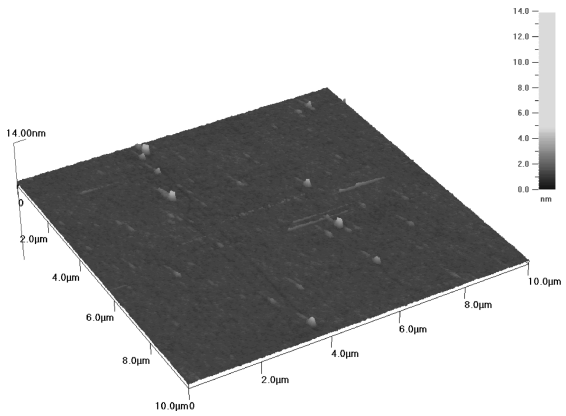

Figure 3. AFM image of a 15 nm thick plasma sputtered nylon film deposited on silicon.

Bruker IFS 55 spectrometer equipped with Pike Technologies 80Spec GASR attachment and polarizer (grazing angle 80°, p-polarization, MCT detector, resolution 2 cm^{-1}, 128 scans). The spectrometer was purged continuously with dried air.

Fourier Transform Infrared Attenuated Total Reflection (FTIR-ATR). The IR spectra of the polymer brushes grown from initiator attached to a 15 nm thick plasma sputtered nylon film, deposited on a polypropylene sheet and the spectra of proteins adsorbed on these surfaces were measured using the same spectrometer equipped with Wilks Sci ATR attachment Model 9. The sheets with dried samples were pressed onto Ge 45° reflection prism.

Measurement of Nonspecific Protein Adsorption. *On Gold-Coated BK7 Glass SPR Chips.* Surface plasmon resonance (SPR) was measured with an instrument based on the Kretschmann geometry and spectral interrogation of the SPR conditions custom-built in the Institute of Photonics and Electronics, Academy of Sciences of the Czech Republic, Prague.[46] Tested single protein solutions of Fbg (1 $mg \cdot mL^{-1}$), HSA (5 $mg \cdot mL^{-1}$), IgG (8 $mg \cdot mL^{-1}$), or Lys (1 $mg \cdot mL^{-1}$) in PBS, undiluted fetal bovine serum (FBS), human blood plasma (BP), and human blood serum (BS) were driven by a peristaltic pump through four channels of a flow cell in which the protein deposition on modified SPR chip surface was observed in situ as a shift in the surface plasmon resonant wavelength, $\Delta\lambda_{res}$. The increase in λ_{res} was proportional to an increase in mass deposited at the surface.[3,5]

On Polypropylene. Fouling on polypropylene modified sheets was assessed by FTIR-ATR. Bare polypropylene, coated with plasma sputtered nylon and coated with plasma sputtered nylon and poly(MeOEGMA) were immersed into phosphate buffered saline (PBS), which was then replaced by HSA solution (5 $mg \cdot mL^{-1}$) or undiluted blood plasma so that any sample−air interface was avoided.[30] After 15 min contact time at 25 °C, HSA or blood plasma were gradually replaced by flowing through copious amounts of PBS, and samples in PBS were gently shaken for 5 min. Then the samples were shortly rinsed with water and left to dry before FTIR ATR measurements.

Functionalization of Poly(HOEGMA) Films. Poly(HOEGMA) brushes grafted from plasma sputtered nylon-coated SPR chips were activated by incubation overnight in a solution of DSC (0.1 M) and DMAP (0.1 M) in anhydrous DMF.[48] After washing with DMF and water, the chip was fixed in the SPR flow cell and the covalent attachment of streptavidin to the activated surface from a 20 $\mu g \cdot mL^{-1}$ solution of PBS was observed in situ by SPR. Biotinylated Rb IgG solution, 20 $\mu g \cdot mL^{-1}$ in PBS, or a biotinylated oligonucleotide **1**, 1 μM in PBS were flowed for 30 min to attach them to the immobilized streptavidin. SPR responses to anti-Rb IgG, 20 $\mu g \cdot mL^{-1}$ in PBS, or the complementary oligonucleotide **2** conjugated with BSA (5 $\mu g \cdot mL^{-1}$ in TRIS) were observed to prove the binding activities of the immobilized Rb IgG or oligonucleotide **1**, respectively.

RESULTS AND DISCUSSION

Amino-Rich Films Deposited by RF Magnetron Sputtering of Nylon. Thin films deposited by RF magnetron sputtering of nylon were prepared on bare and gold-coated silicon, gold-coated glass, polypropylene, and TiAlV using gas mixture of Ar/N_2 (1:1). The elemental composition of 15 nm thick plasma sputtered nylon films on glass, gold-coated glass, silicon, polypropylene, and TiAlV was determined by XPS (Figure 1). Only minor differences in the chemical composition of the sputtered film on different substrates were observed, practically within the standard deviation of the method. A high N/C ratio of about 0.5 was achieved in accordance with our previous results.[44] XPS was used to optimize the thickness of the coatings for further experiments. Ultrathin RF coatings might be attractive for various applications in which a sufficient adhesion to a flexible substrate under dynamic conditions or copying a submicrometer

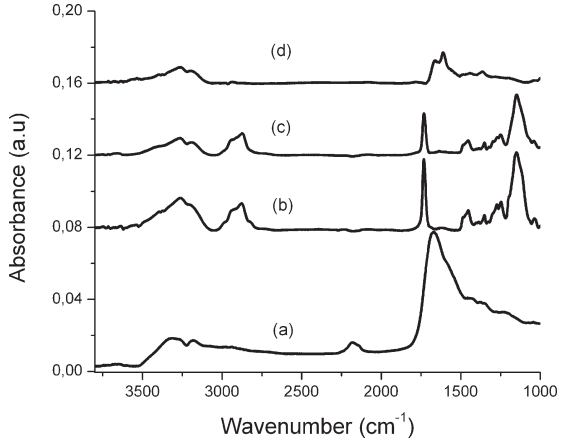

Figure 4. FTIR GASR spectra of amino-rich plasma sputtered nylon film (15 nm) deposited on gold (a), and polymer brushes of poly-(HOEGMA) (30 nm) (b), poly(MeOEGMA) (30 nm) (c), and poly-(CBAA) (12 nm) (d) grafted from the amino-rich plasma sputtered nylon film.

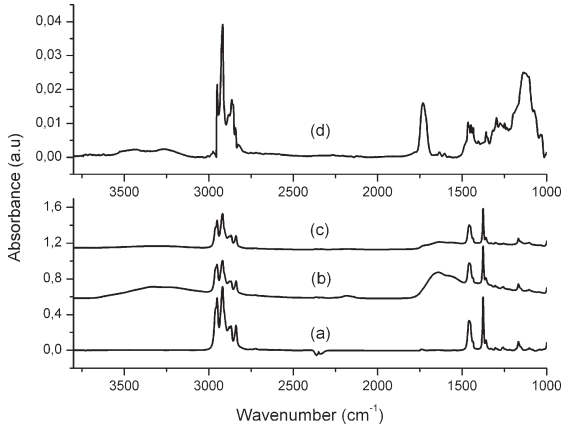

Figure 5. FTIR-ATR of polypropylene (a), amino-rich plasma sputtered nylon film deposited on polypropylene (15 nm) (b), poly-(MeOEGMA) brush (30 nm) grafted from the amino-rich plasma sputtered nylon film (c), and spectrum of the poly(MeOEGMA) brush after subtracting the substrate background (d).

surface relief is required. A thickness below about 40 nm is necessary, particularly, for optical biosensors based on evanescent electromagnetic field, such as, SPR, interferometer, resonance mirror, and so on.

Therefore, in this work, the optimum thickness of amino-rich film was selected as minimum thickness at which no pin-holes were present assuring complete and homogeneous coverage of the substrates. Films of different thicknesses were sputtered from Nylon on silicon and XPS spectra were measured. A thickness greater than 13−15 nm was necessary to obtain XPS spectra without the silicon peak (Figure 2), indicating a complete coating of the silicon surface. The homogeneous, smooth (RMS roughness: 0.14 nm), and pinhole-free surface of the deposited plasma sputtered nylon film was observed by AFM (Figure 3).

Table 1. Water/Air Contact Angles Measured on Polymer Brushes Grafted from Amino-Rich Plasma Sputtered Nylon Film Deposited on Gold Surface

	water contact angle	
surface	advancing	receding
Au	76	63
Au-Nylon-CBAA	20	8
Au-Nylon-HOEGMA	48	23
Au-Nylon-MeOEGMA	48	20

FTIR GASR spectrum of a plasma sputtered nylon film deposited on a gold-coated glass SPR chip (Figure 4a) shows a highly complex chemical structure of the film, which has been thoroughly studied by FTIR reflection absorption spectroscopy (FTIR-RAS) in our previous papers.[44,49] Briefly, the dominant envelope of absorption bands centered around maximum at 1670 cm^{-1} corresponds to various nitrogen compounds, including primary amines and C═N and N═N structures. The shoulder band at about 1550 cm^{-1} indicates the presence of amides, and the absorption at about 2180 cm^{-1} indicates the presence of nitriles and isocyanates. The amino content cannot be derived from infrared spectra, but the ratio of amino nitrogen to the total nitrogen, NH_2/N, was estimated by chemical derivatization as about 8%.[44] Similar IR spectrum of the plasma sputtered nylon film deposited on a polypropylene sheet was observed using FTIR ATR (Figure 5b).

Polymer Brushes. FTIR GASR spectra of poly(HOEGMA), poly(MeOEGMA), and poly(CBAA) grafted from plasma sputtered nylon films deposited on gold-coated glass are shown in Figure 4b, c, and d, respectively. The peak of ester carbonyl at 1733 cm^{-1} and a group of bands between 1300 and 900 cm^{-1} in spectra (b) and (c) are characteristic of methacrylate polymers. The spectrum (d) of poly(CBAA) shows amide I band at 1664 cm^{-1}, dominant peak of ionized carboxyl at 1609 cm^{-1} (COO^- asymmetric stretching) overlapping the amide II band at about 1550 cm^{-1} and its symmetric stretching at 1370 cm^{-1}. Brushes grafted from the plasma sputtered nylon film deposited on polypropylene with nonreflective surface, were studied by FTIR ATR. Figure 5 shows spectra of bare polypropylene (a), polypropylene with plasma sputtered nylon film (b), and poly-(MeOEGMA) brushes (c) grafted from plasma sputtered nylon on polypropylene. The spectrum (d) shows poly(MeOEGMA) after subtraction of plasma sputtered nylon film and polypropylene bands.

The coating with polymer brushes grown from an adhesive amino-rich plasma sputtered nylon film made gold substrate more hydrophilic (Table 1). The hysteresis between advancing and receding contact angles might be due to the reorganization of the brushes when being wetted and surface roughness. AFM images (data not shown) indicated that the coatings copied accurately the substrate surface relief.

Poly(MeOEGMA) Brushes. A fast initiation and ability to keep most of the growing chains in a dormant state play key role in well controlled SI ATRP. A bromine-based initiator was chosen to ensure fast initiation since bromide-carbon bond requires less energy to cleave.[50,51] Bromoisobutyrate-based initiators are the most commonly used for ATRP of nonstyrenic monomers. Cu(II) was added to minimize the losses of initiator to achieve equilibrium between dormant and active species.[52,53] As

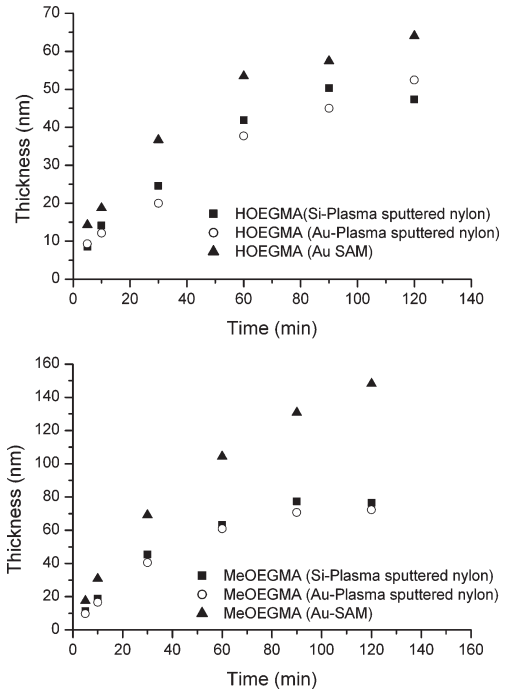

Figure 6. Kinetics of HOEGMA and MeOEGMA polymerization initiated by α-bromoisobutyrate covalently attached to the amino-rich plasma sputtered nylon film deposited on silicon (circles Si-nylon) and gold (squares, Au-nylon) or initiated by SAM of ω-mercaptoundecyl-bromoisobutyrate attached to gold (triangles, Au-SAM). Film thickness was measured using ellipsometry and silicon wafer substrates.

described by Matyjaszewski, the use of mixed halide (bromide and chloride) systems represents a valuable tool for shifting the equilibrium to dormant species.[50] Chlorine with higher bond energy replaces bromine in the dormant species. Higher energies are required to remove chlorine and therefore the equilibrium is further shifted toward the dormant chains. Temperatures above 30 °C were not necessary for the polymerization to proceed. No initial jump in the polymerization kinetic was observed. Kinetics of HOEGMA polymerization from the initiators attached to amino-rich plasma sputtered nylon films deposited on gold or silicon surface were reasonably controlled for about 90 min and then started to level off (see Figure 6), probably due to termination. Worse control was observed for MeOEGMA brushes. However, in the region of our targeted thickness, below 40 nm, a linear increase in the brush thickness with time was observed indicatinged well-controlled polymerization kinetics. Kinetics of MeOEGMA and HOEGMA polymerization initiated from SAM of ω-mercaptoundecylbromoisobutyrate immobilized on gold were faster and resulted in thicker films.

Poly(CBAA). SI ATRP of CBAA was not controlled. However, the thickness could be tuned reproducibly between 7 and 100 nm by changing the polymerization system, for example, by changing solvent, amount of catalyst, or ratio Cu(I) to Cu(II). The selected conditions resulted in a 12 nm film (grown from plasma sputtered nylon film) and 18 nm when grown from SAM on gold. The lack of control for CBAA may be attributed to nucleophilic displacement or inactivation of catalyst by complexation.[54−56]

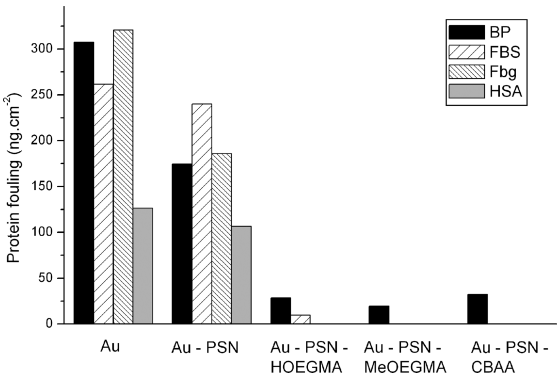

Figure 7. Irreversible fouling on polymer brushes grefted from amino-rich plasma sputtered nylon film after 15 min of incubation with BP (black), FBS (blue), and PBS solutions of Fbg (green) and HSA (red). The deposits were determined from SPR measured in PBS before and after the incubation.

Changing the bromine in the catalytic system for chlorine nor the addition of external halide (LiCl) did not significantly improve the polymerization.

Antifouling Properties. Fouling was studied on bare gold, a plasma sputtered nylon film deposited on gold, and poly-(MeOEGMA), poly(HOEGMA), and poly(CBAA) brushes grafted from the plasma sputtered nylon film (Figure 7). Fouling properties of brushes polymerized from SAM of initiator on gold in identical conditions to the brushes grafted from PSN film were tested as a comparative study (Supporting Information, Table 1). The selection of the optimal thickness was taken as the minimum thickness for achieving the minimal plasma fouling, 30 nm for poly(HOEGMA) and poly(MeOEGMA) brushes and 12 nm for CBAA brushes. The fouling from FBS, BS, and BP and single protein solutions of HSA, Fbg, IgG, or Lys on the surfaces was observed by SPR (Figure 7). A huge fouling was observed on gold and the plasma sputtered nylon film. The fouling from the single protein solutions was totally suppressed by all the polymer brushes. FBS, which is commonly used for tissue culture, did not adsorb on poly(CBAA) and poly(MeOEGMA), but deposits of 9.7 ng·cm^{-2} and 4.5 ng·cm^{-2} were observed on poly-(HOEGMA) grafted from PSN film and gold, respectively. The adsorbed deposit from FBS on poly(HOEGMA) grafted from PSN film was less than 4% of that on gold. The fouling from BP was 28.3, 32.4, and 19.5 ng.cm^{-2} on poly(HOEGMA), poly(CBAA), and poly(MeOEGMA) brushes grafted from PSN, respectively. A fouling from BP of 19.5 ng·cm^{-2} on poly(MeOEGMA) grafted from PSN was about 5.3 and 11% of those observed on bare gold (307 ng·cm^{-2}) and the plasma sputtered nylon film (177 ng·cm^{-2}), respectively, or less than 9 and 20% of the fouling observed earlier on widely used antifouling SAMs of oligoethyleneglycol-terminated alkanethiols and the PEG grafted to the gold surface, respectively.[3] The fouling from blood plasma observed on brushes of grafted from SAM on gold was 15.0, 16.3, and 18.9 ng·cm^{-2} for poly(CBAA), poly-(HOEGMA), and poly(MeOEGMA), respectively. Although the fouling from blood plasma on brushes grafted from SAM on gold was generally lower than that on brushes grafted from PSN film, the differences were negligible, only between 0.2 to 5% of the fouling observed on gold.

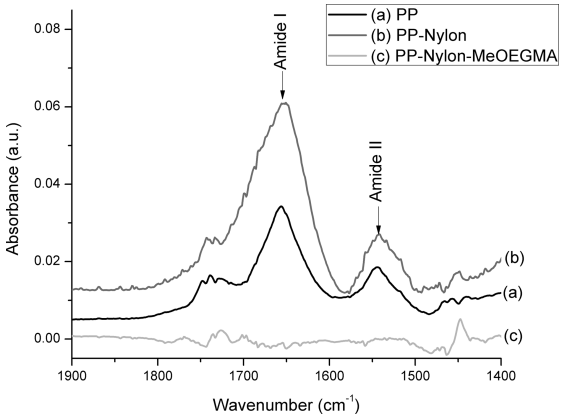

Figure 8. FTIR ATR spectra of deposits from blood plasma on (a) polypropylene (PP), (b) polypropylene coated with amino-rich plasma sputtered nylon film (PP-nylon), and (c) polypropylene coated with plasma sputtered nylon film and poly(methoxyoligoethyleneglycol methacrylate) (PP-nylon-MeOEGMA). Spectral bands of PP, plasma sputtered nylon film, and poly(MeOEGMA) were subtracted.

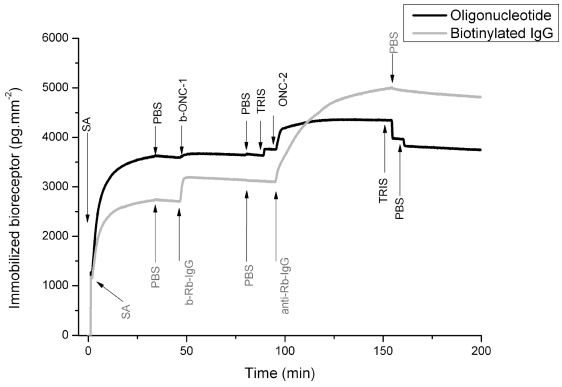

Figure 9. Functionalization of poly(HOEGMA) grafted from plasma sputtered nylon film by covalent attachment of streptavidin (SA) and subsequent immobilization of biotinylated oligonucleotide 1 (b-ONC**1**), curve 1, or biotinylated Rb IgG (b-Rb IgG), curve 2, observed by SPR. Activities of the immobilized oligonucleotide 1 and Rb IgG were tested by hybridization with oligonucleotide **2** (complementary to ONC1) conjugated with BSA, curve 1, and binding anti-Rb IgG, curve 2, respectively.

Fouling on polypropylene and polypropylene coated with plasma sputtered nylon film and with poly(MeOEGMA) grafted from plasma sputtered nylon film was studied using FTIR ATR. Figure 8 shows amide region of differential spectra of the deposits, if any, after contact with blood plasma with polypropylene, polypropylene coated with plasma sputtered nylon film and polypropylene coated with plasma sputtered nylon and poly(MeOEGMA). The exposition to HSA showed similar results (data not shown). The spectral bands of amidic group typical for adsorbed proteins at 1648 cm^{-1} and 1545 cm^{-1} confirm proteinaceous nature of the deposit from blood plasma on polypropylene and polypropylene coated with plasma sputtered nylon film. On the other hand, the adsorption from blood plasma on polypropylene with the plasma sputtered nylon film overcoated with poly(MeOEGMA) is below the detection limit of FTIR ATR (15 ng·cm^{-2}). The spectra clearly demonstrate the antifouling effect of poly(MeOEGMA) brushes.

Stability of Poly(MeOEGMA) Brushes. Although the long-term stability of polymer brushes is very important in many applications, this topic has received only limited attention. The degradation and cleavage of brushes may result in impaired fouling properties with time or even lead to a total loss of the polymer layer as observed by Klok.[34] Long polymer chains stretching out from the surface cause a huge entropic pressure imposed over the anchoring sites that has been shown to be able to cleave covalent bonds.[35,37] Detachment of poly(MeOEGMA) brushes polymerized from glass or silicon substrates modified with a trimethoxysilane-based ATRP initiator resulted in an increase in nonspecific protein adsorption.[34]

Long-term stability of poly(MeOEGMA) brush grafted from plasma sputtered nylon films deposited on gold surface on SPR chips was achieved in our work. No significant differences in the fouling from BP, FBS, Fbg, and HSA on the freshly coated SPR chip and an identical chip stored for 5 months in PBS in dark were observed. The unchanged properties of our system indicated a satisfactory adhesion of plasma sputtered nylon film to the substrate and a good stability of the attached polymer brush layer. Similar results have been shown for poly(MeOEGMA) brushes grown from SAM of ω-mercaptoundecylbromoisbutyrate.[30] On the other hand, a poor stability of long poly(MeOEGMA) chains was observed when they were grown from the ill-defined initiator layer of trialkoxysilanes on silicon[34] the stability of our system was superior.

Functionalization of Poly(HOEGMA) Brushes. Most of the potential applications of nonfouling surfaces require covalent attachment of bioactive molecules[5,20] to perform specific functions. Affinity surfaces were prepared by immobilization of biorecognition elements on poly(HOEGMA) brushes grafted from a plasma sputtered nylon film deposited on an SPR bosensor chip (Figure 8). Hydroxyl groups present in poly(HOEGMA) brush were activated by DSC[48] and subsequently coupled with streptavidin via its primary amine (Figure 9, first parts of the curves 1 and 2). The same technique can be applied to attach covalently proteins and other molecules containing primary amines. By the attachment of streptavidin we obtained a versatile surface capable of immobilizing commonly prepared conjugates of biotin with various bioactive molecules. As model examples, biotinylated rabbit-IgG (Figure 8, curve 1) and biotinilated oligonucleotide (Figure 8, curve 2) were immobilized. No immobilization of the biotinilated oligonucleotide or antibody was observed on reference surfaces on which streptavidin was not attached. The highly specific binding of polyclonal mouse antirabbit-IgG or complementary oligonucleotide strands conjugated with bovine serum albumin were observed on surfaces with immobilized rabbit-IgG or the oligonucleotides, respectively.

■ CONCLUSIONS

A new route for antifouling modifications of various substrates was developed. The technique consists of the initial deposition of an amino-rich film by radio RF magnetron sputtering of nylon followed by grafting antifouling polymer brushes from initiators covalently bound to the sputter deposited primer film. Polymer brushes of CBAA, HOEGMA, and MeOEGMA grown from the primer film by surface-initiated ATRP suppressed completely the

fouling from single protein solutions of the main blood plasma proteins (HSA, IgG, Fbg) and fetal bovine serum and even reduced fouling from undiluted human blood plasma by more than 90%. Gold, silicon, glass, TiAlV, and poly(propylene) were coated with the primer film but since virtually any substrate can be coated with such a film, it represents a general method by which any substrate could be made resistant to fouling without any chemical preactivation. The thickness of the polymer brushes were tuned reproducibly by controlled ATRP for HOEGMA and MeOEGMA or by changing the polymerization system for CBAA. It can be supposed, that such coatings could be potentially prepared independently of the substrate surface with thickness of the antifouling brushes optimized to suppress fouling from complex biological media at specific biomedical applications. The feasibility of functionalization of the coating with bioactive compounds was shown by covalent attachment of streptavidin and subsequent immobilization of model antibody and oligonucleotide on the top poly(HOEGMA) brush layer. Thus, the technique might become a base for the facile preparation of different surface-based biotechnological and biomedical devices capable of performing tailor-made functions without the interference from fouling in biological media where they operate.

■ ASSOCIATED CONTENT

Supporting Information. A scheme of the plasma reactor for RF magnetron sputtering nylon films, XPS spectra of plasma sputtered nylon coating on Si wafer, a study of fouling from human blood plasma, human blood serum, fetal bovine serum, and single protein solutions of human IgG, human fibrinogen, human serum albumin, and human lysozime on polymer brushes grown from sputtered nylon surface or grown from a monolayer of initiator self-assembled on gold surface is shown. This material is available free of charge via the Internet at http://pubs.acs.org.

■ AUTHOR INFORMATION

Corresponding Author
*E-mail: rodriguez@imc.cas.cz.

■ ACKNOWLEDGMENT

This research was supported by the Academy of Sciences of the Czech Republic under Contract No KAN200670701, by Grant SVV-2011-263 305, and partly by the GAUK 110-10/251265 Grant of the Grant Agency of Charles University in Prague.

■ REFERENCES

(1) Hucknall, A.; Rangarajan, S.; Chilkoti, A. *Adv. Mater.* **2009**, *21* (23), 2441–2446.
(2) Jiang, S.; Cao, Z. *Adv. Mater.* **2010**, *22* (9), 920–932.
(3) Rodriguez Emmenegger, C.; Brynda, E.; Riedel, T.; Sedlakova, Z.; Houska, M.; Alles, A. B. *Langmuir* **2009**, *25* (11), 6328–6333.
(4) Rana, D.; Matsuura, T. *Chem. Rev.* **2010**, *110* (4), 2448–2471.
(5) Homola, J. *Chem. Rev.* **2008**, *108* (2), 462–493.
(6) Verma, A.; Stellacci, F. *Small* **2010**, *6* (1), 12–21.
(7) Lynch, I.; Cedervall, T.; Lundqvist, M.; Cabaleiro-Lago, C.; Linse, S.; Dawson, K. A. *Adv. Colloid Interface Sci.* **2007**, *134*−*135*, 167–174.
(8) Lundqvist, M.; Stigler, J.; Elia, G.; Lynch, I.; Cedervall, T.; Dawson, K. A. *Proc. Natl. Acad. Sci. U.S.A.* **2008**, *105* (38), 14265–14270.
(9) Lynch, I.; Dawson, K. A. *Nano Today* **2008**, *3* (1−2), 40–47.
(10) Knop, K.; Hoogenboom, R.; Fischer, D.; Schubert, U. S. *Angew. Chem., Int. Ed.* **2010**, *49*, 6288–6308.
(11) Thissen, H.; Gengenbach, T.; du Toit, R.; Sweeney, D. F.; Kingshott, P.; Griesser, H. J.; Meagher, L. *Biomaterials* **2010**, *31* (21), 5510–5519.
(12) Ratner, B. D. *Biomaterials* **2007**, *28* (34), 5144–5147.
(13) Ratner, B. D. *J. Biomed. Mater. Res.* **1993**, *27* (3), 283–287.
(14) Li, L. Y.; Chen, S. F.; Jiang, S. Y. *J. Biomater. Sci., Polym. Ed.* **2007**, *18* (11), 1415–1427.
(15) Luk, Y.-Y.; Kato, M.; Mrksich, M. *Langmuir* **2000**, *16* (24), 9604–9608.
(16) Zhang, Z.; Chen, S.; Chang, Y.; Jiang, S. *J. Phys. Chem. B* **2006**, *110* (22), 10799–10804.
(17) Yu, K.; Kizhakkedathu, J. N. *Biomacromolecules* **2010**, *11* (11), 3073–3085.
(18) Ma, H.; He, J. a.; Liu, X.; Gan, J.; Jin, G.; Zhou, J. *ACS Appl. Mater. Interfaces* **2010**, *2* (11), 3223–3230.
(19) Rodriguez-Emmenegger, C.; Jäger, A.; Jäger, E.; Stepanek, P.; Alles, A. B.; Guterres, S. S.; Pohlmann, A. R.; Brynda, E. *Colloids Surf., B* **2011**, *83* (2), 376–381.
(20) Yang, W.; Zhang, L.; Wang, S.; White, A. D.; Jiang, S. *Biomaterials* **2009**, *30* (29), 5617–5621.
(21) Li, L.; Chen, S.; Zheng, J.; Ratner, B. D.; Jiang, S. *J. Phys. Chem. B* **2005**, *109* (7), 2934–2941.
(22) Barbey, R. l.; Lavanant, L.; Paripovic, D.; Schüwer, N.; Sugnaux, C.; Tugulu, S.; Klok, H.-A. *Chem. Rev.* **2009**, *109* (11), 5437–5527.
(23) Kinnane, C. R.; Such, G. K.; Antequera-García, G.; Yan, Y.; Dodds, S. J.; Liz-Marzan, L. M.; Caruso, F. *Biomacromolecules* **2009**, *10* (10), 2839–2846.
(24) Li, G.; Xue, H.; Gao, C.; Zhang, F.; Jiang, S. *Macromolecules* **2009**, *43* (1), 14–16.
(25) Chang, Y.; Shu, S.-H.; Shih, Y.-J.; Chu, C.-W.; Ruaan, R.-C.; Chen, W.-Y. *Langmuir* **2009**, *26* (5), 3522–3530.
(26) Morra, M.; Cassineli, C. *J. Biomater. Sci., Polym. Ed.* **1999**, *10* (10), 1107–1124.
(27) Raynor, J. E.; Petrie, T. A.; Fears, K. P.; Latour, R. A.; García, A. J.; Collard, D. M. *Biomacromolecules* **2009**, *10* (4), 748–755.
(28) Lai, B. F. L.; Creagh, A. L.; Janzen, J.; Haynes, C. A.; Brooks, D. E.; Kizhakkedathu, J. N. *Biomaterials* **2010**, *31* (26), 6710–6718.
(29) Kizhakkedathu, J. N.; Janzen, J.; Le, Y.; Kainthan, R. K.; Brooks, D. E. *Langmuir* **2009**, *25* (6), 3794–3801.
(30) Gautrot, J. E.; Trappmann, B.; Oceguera-Yanez, F.; Connelly, J.; He, X.; Watt, F. M.; Huck, W. T. S. *Biomaterials* **2010**, *31* (18), 5030–5041.
(31) Vaisocherova, H.; Zhang, Z.; Yang, W.; Cao, Z. Q.; Cheng, G.; Taylor, A. D.; Piliarik, M.; Homola, J.; Jiang, S. Y. *Biosens. Bioelectron.* **2009**, *24* (7), 1924–1930.
(32) Hucknall, A.; Kim, D.-H.; Rangarajan, S.; Hill, R. T.; Reichert, W. M.; Chilkoti, A. *Adv. Mater.* **2009**, *21* (19), 1968–1971.
(33) Advincula, R. C.; Brittain, W. J.; Caster, K. C.; Jürgen, R. *Polymer Brushes: Synthesis, Characterization, Applications*; Wiley Interscience: New York, 2004.
(34) Tugulu, S.; Klok, H.-A. *Biomacromolecules* **2008**, *9* (3), 906–912.
(35) Deng, Y.; Zhu, X. Y. *J. Am. Chem. Soc.* **2007**, *129* (24), 7557–7561.
(36) Rubinstein, M.; Colby, R. H. *Polymer Physics*; OUP: Oxford: 2003.
(37) Sheiko, S. S.; Sun, F. C.; Randall, A.; Shirvanyants, D.; Rubinstein, M.; Lee, H.-i.; Matyjaszewski, K. *Nature* **2006**, *440* (7081), 191–194.
(38) Lee, H.; Dellatore, S. M.; Miller, W. M.; Messersmith, P. B. *Science* **2007**, *318* (5849), 426–430.
(39) Lee, H.; Scherer, N. F.; Messersmith, P. B. *Proc. Natl. Acad. Sci. U.S.A.* **2006**, *103* (35), 12999–13003.
(40) Fan, X.; Lin, L.; Dalsin, J. L.; Messersmith, P. B. *J. Am. Chem. Soc.* **2005**, *127* (45), 15843–15847.
(41) Zhang, L.; Xue, H.; Gao, C.; Carr, L.; Wang, J.; Chu, B.; Jiang, S. *Biomaterials* **2010**, *31* (25), 6582–6588.

(42) Waite, J. H.; Andersen, N. H.; Jewhurst, S.; Sun, C. *J. Adhes.* **2005**, *81* (3), 297–317.
(43) Biederman, H.; Stelmashuk, V.; Kholodkov, I.; Choukourov, A.; Slavínská, D. *Surf. Coat. Technol.* **2003**, *174*−*175*, 27–32.
(44) Kylian, O.; Hanus, J.; Choukourov, A.; Kousal, J.; Slavinska, D.; Biederman, H. *J. Phys. D: Appl. Phys.* **2009**, *42* (14), 142001.
(45) Jones, D. M.; Brown, A. A.; Huck, W. T. S. *Langmuir* **2002**, *18* (4), 1265–1269.
(46) Vaisocherová, H.; Yang, W.; Zhang, Z.; Cao, Z.; Cheng, G.; Piliarik, M.; Homola, J.; Jiang, S. *Anal. Chem.* **2008**, *80* (20), 7894–7901.
(47) Bao, Z.; Bruening, M. L.; Baker, G. L. *Macromolecules* **2006**, *39* (16), 5251–5258.
(48) Diamanti, S.; Arifuzzaman, S.; Elsen, A.; Genzer, J.; Vaia, R. A. *Polymer* **2008**, *49* (17), 3770–3779.
(49) Kousal, J.; Hanus, J.; Choukourov, A.; Polonskyi, O.; Biederman, H.; Slavínská, D. *Plasma Processes Polym.* **2009**, *6* (S1), S803–S807.
(50) Matyjaszewski, K.; Shipp, D. A.; Wang, J.-L.; Grimaud, T.; Patten, T. E. *Macromolecules* **1998**, *31* (20), 6836–6840.
(51) Kerr, J. A. *Chem. Rev.* **1966**, *66* (5), 465–500.
(52) Matyjaszewski, K.; Nanda, A. K.; Tang, W. *Macromolecules* **2005**, *38* (5), 2015–2018.
(53) Brown, A. A.; Khan, N. S.; Steinbock, L.; Huck, W. T. S. *Eur. Polym. J.* **2005**, *41* (8), 1757–1765.
(54) Jewrajka, S. K.; Mandal, B. M. *Macromolecules* **2002**, *36* (2), 311–317.
(55) Rademacher, J. T.; Baum, M.; Pallack, M. E.; Brittain, W. J.; Simonsick, W. J. *Macromolecules* **1999**, *33* (2), 284–288.
(56) Teodorescu, M.; Matyjaszewski, K. *Macromolecules* **1999**, *32* (15), 4826–4831.

IOP Publishing Journal of Physics D: Applied Physics
J. Phys. D: Appl. Phys. **45** (2012) 495301 (8pp) doi:10.1088/0022-3727/45/49/495301

Nylon-sputtered nanoparticles: fabrication and basic properties

O Polonskyi, O Kylián, P Solař, A Artemenko, J Kousal, D Slavínská, A Choukourov and H Biederman

Charles University in Prague, Faculty of Mathematics and Physics, V Holesovickach 2, 180 00 Prague 8, Czech Republic

E-mail: polonskyi.oleksandr@gmail.com

Received 14 June 2012, in final form 25 September 2012
Published 9 November 2012
Online at stacks.iop.org/JPhysD/45/495301

Abstract
Nylon-sputtered nanoparticles were prepared using a simple gas aggregation cluster source based on a planar magnetron (Haberland type) and equipped with a nylon target. Plasma polymer particles originated in an aggregation chamber and travelled to a main (deposition) chamber with a gas flow through an orifice. The deposited nanoparticles were observed to have a cauliflower-like structure. The nanoparticles were found to be nitrogen-rich with N/C ratio close to 0.5. An increase in rf power from 60 to 100 W resulted in a decrease in mean particle size from 210 to 168 nm whereas an increase in their residence time in the cluster source from 0.7 to 4.6 s resulted in an increase in the size from 73 to 231 nm.

(Some figures may appear in colour only in the online journal)

1. Introduction

Formation of micrometre- and sub-micrometre-sized particles of plasma polymers was first reported in the 70s of the last century by Kobayashi *et al* [1, 2]. Since then, such particles have become a subject of numerous studies and have given rise to a new discipline called physics of dusty or complex plasmas (see, e.g., the review papers [3, 4]). In this field, particular interest was devoted to the investigation of the mechanisms of particle formation as well as to the evaluation of changes in plasma properties induced by the presence of such 'dust' in plasma volume. Nevertheless, only little interest was paid to the possibility of technological use of plasma-polymerized particles. This situation is changing nowadays, since controlled deposition of particles seems to have a large potential for use in various technological applications, such as for instance fabrication of super-hydrophobic coatings based on films of plasma-polymerized fluorocarbon nanoparticles (e.g. [5, 6]) or biomedical applications, where plasma-polymerized nanoparticles are used for tuning the nanoroughness of surfaces for enhancement of their bioadhesive properties [7].

Various plasma-based methods have been developed that enabled deposition of plasma-polymerized nanoparticles of various sizes using rf plasmas (e.g. [5, 6, 8–11]) or pulsed dc magnetron plasma sources [12, 13]. In this study, a gas aggregation source (GAS) was employed that involves a low-temperature plasma in the process of production of nanoparticles. This concept, originally introduced by Haberland *et al* [14] was previously used for the production of various metal nanoparticles (see, e.g., [15]). Until recently, magnetron sputtering of polymers was employed only to deposit thin films of plasma polymers [16–20]. Over the last few years, it has been found that magnetron sputtering of poly(tetrafluoroethylene) may also be used for the production of nanoparticles of fluorocarbon plasma polymers [11]. The aim of this work is to investigate the applicability of the GAS technique for production of nitrogen-containing plasma polymer nanoparticles and to characterize them especially from the point of view of their size and chemical structure.

2. Experimental

The experimental arrangement used in this work is depicted in figure 1. Nylon-sputtered nanoparticles were fabricated using the gas aggregation cluster source based on a planar magnetron 81 mm in diameter and equipped with a Nylon 6,6 target. This type of GAS was developed in our laboratory and was described in detail in previous studies [21–23]. Different power values were applied to the magnetron (60, 80 and

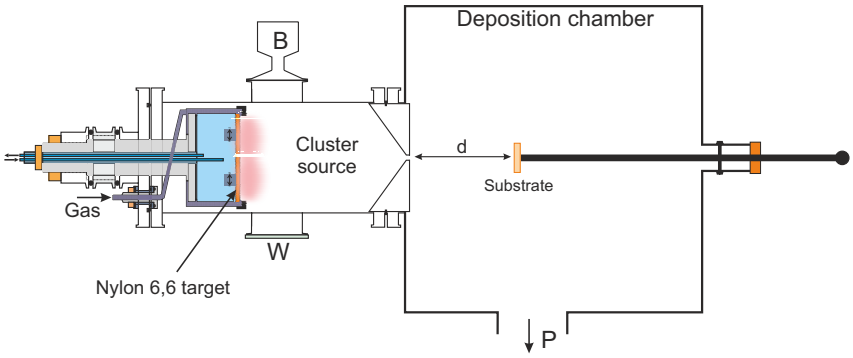

Figure 1. Experimental arrangement for deposition of nylon-sputtered nanoparticles: B—baratron; W—window; d—distance from the orifice to the substrate; P—to rotary and diffusion pumps.

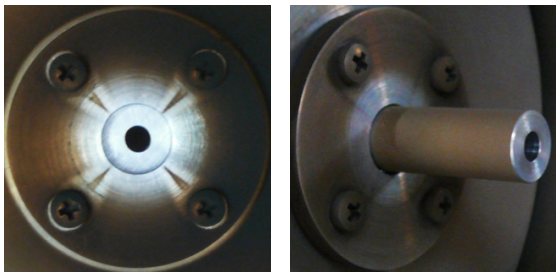

Figure 2. Photos of 4 mm orifices used: (*a*) 3 mm long; (*b*) 35 mm long.

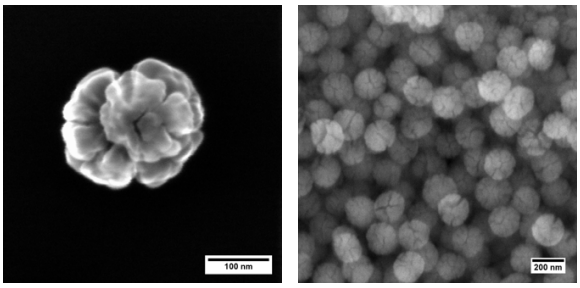

Figure 3. The SEM images of the cauliflower-shaped nylon-sputtered nanoparticles at different coverage of the substrate. Deposition parameters: (*a*) 80 W, residence time 2.5 s; (*b*) 80 W, residence time 4.6 s.

100 W) by an rf generator (ENI AGC-6B, 13.56 MHz) through a matching box. The sputtering process was performed in an argon/nitrogen (3/1) gas mixture. The gases were introduced to the GAS by needle valves. A constant pressure of 75 Pa in the GAS and 4 Pa in the deposition chamber were used in all the experiments. Aggregation chambers with different lengths (10, 16 and 26 cm) were used. Nylon-sputtered nanoparticles formed in the GAS were dragged by the gas flow through an orifice to the deposition chamber. Two exchangeable orifices were used with lengths of 3 and 35 mm and both with the same diameter of 4 mm (figure 2). Different resistances of the two orifices to the gas flow allowed reaching 75 Pa in the GAS at the gas flow rates of 47 sccm and 18.5 sccm, respectively. The particles were deposited onto the earthed silicon substrates positioned 20 cm away from the orifice in the deposition chamber (figure 1). The deposition chamber was pumped down by diffusion and rotary pumps.

A scanning electron microscope (SEM, Tescan Mira II) working at an acceleration voltage of 15 kV and equipped with a SE detector was used to observe the morphology of the deposits and to determine the size distribution of nylon-sputtered nanoparticles. The chemical composition of the deposits was characterized by means of Fourier transform infrared reflection absorption spectroscopy (FTIR-RAS, Bruker Equinox 55) and x-ray photoelectron spectroscopy (XPS, Phobios 100, Specs). The FTIR spectra were acquired in reflectance–absorbance mode with gold-coated glass used as substrates. For sample measurement, 400 scans were acquired with a resolution of 4 cm^{-1}. The x-ray photoelectron spectra were obtained with pass energies of 40 eV (wide spectra) and 10 eV (high-resolution spectra).

3. Results and discussion

An example of nanoparticles produced in this work is presented in figure 3, where the SEM images of individual particles as well as of the film composed thereof are shown. It can be seen that the particles have a cauliflower-like shape, commonly observed for particles produced in dusty plasmas (e.g. [3]).

An important aspect of production of nanoparticles involves the possibility to control their size by a proper choice of operational conditions. The first parameter studied in this work was rf power applied to the magnetron. The SEM images of the particles deposited at different rf powers are shown in figure 4 together with the corresponding size histograms. An increase in discharge power from 60 to 100 W results in the decrease in the particle mean size from 210 to 168 nm. In all the cases, the particles have a quite narrow size distribution, the mean deviation in diameter being below 15%.

The slowing down of the particle growth can be attributed to the increased particle temperature. It has been previously shown that the temperature of the nanoparticles produced in

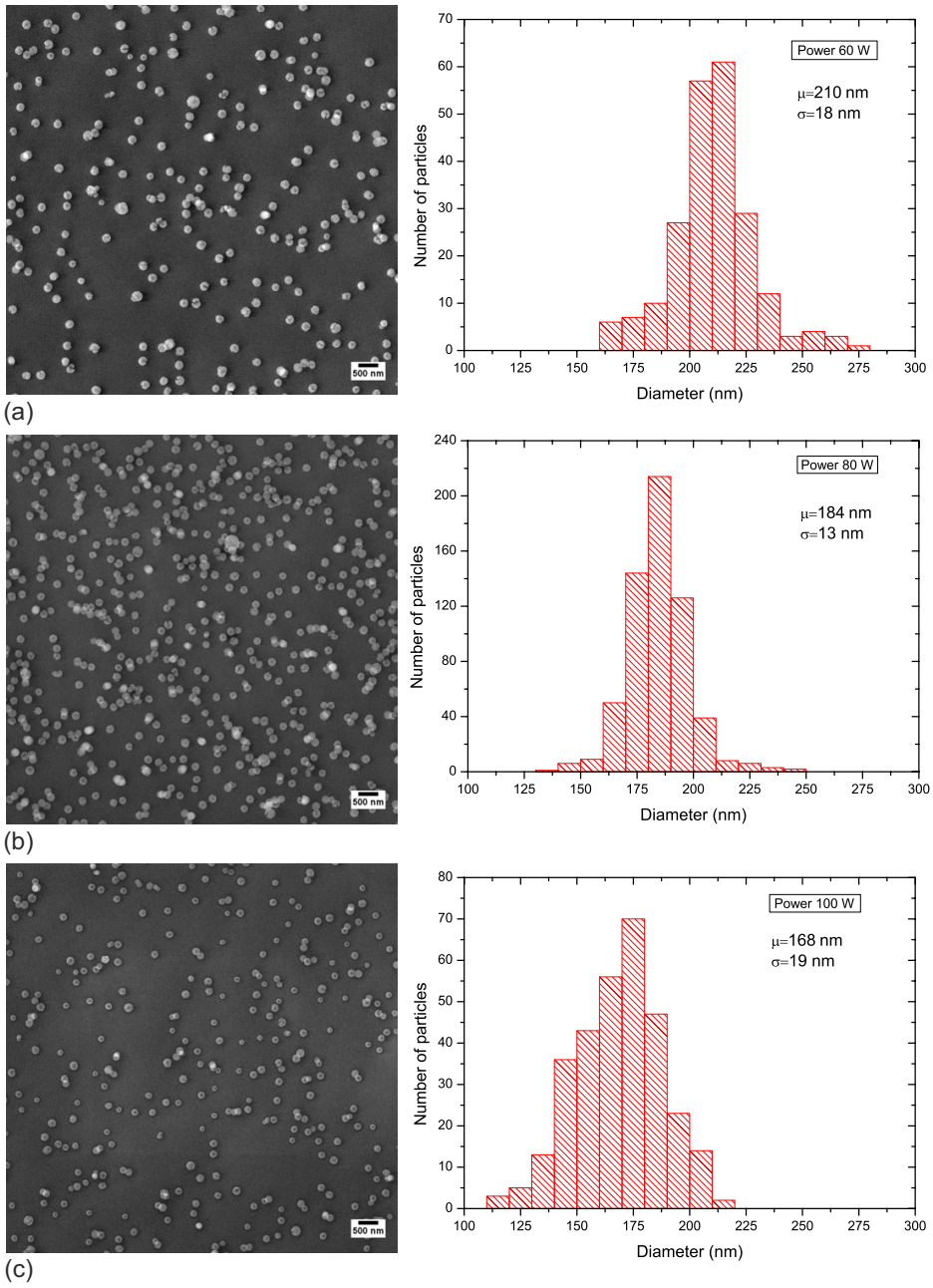

Figure 4. SEM images and the corresponding size distribution histograms for nylon-sputtered particles prepared at different discharge power: (*a*) 60 W, deposition time 1 min; (*b*) 80 W, deposition time 2 min; (*c*) 100 W, deposition time 1 min. The flow rate is 18.5 sccm (μ—mean particle diameter, σ—standard deviation). Note the different deposition times of the nylon-sputtered particles.

low-temperature plasmas may reach high values and exceed the gas temperature of the plasma by several hundred kelvins [24]. As a result, thermal cleavage of bonds with release of small fragments from the surface of the polymeric particles may occur (some authors reported that higher temperatures delay the appearance of particles in the plasma volume [25]). The growth of the particles is therefore strongly influenced by an integral energy influx density in which electron/ion recombinations at the particle surface play the dominant role [24]. The electron density increases with discharge power and this leads to intensification of the recombination processes on the particle surface. Hence, a larger recombination energy released to the particles hinders their growth at a higher discharge power.

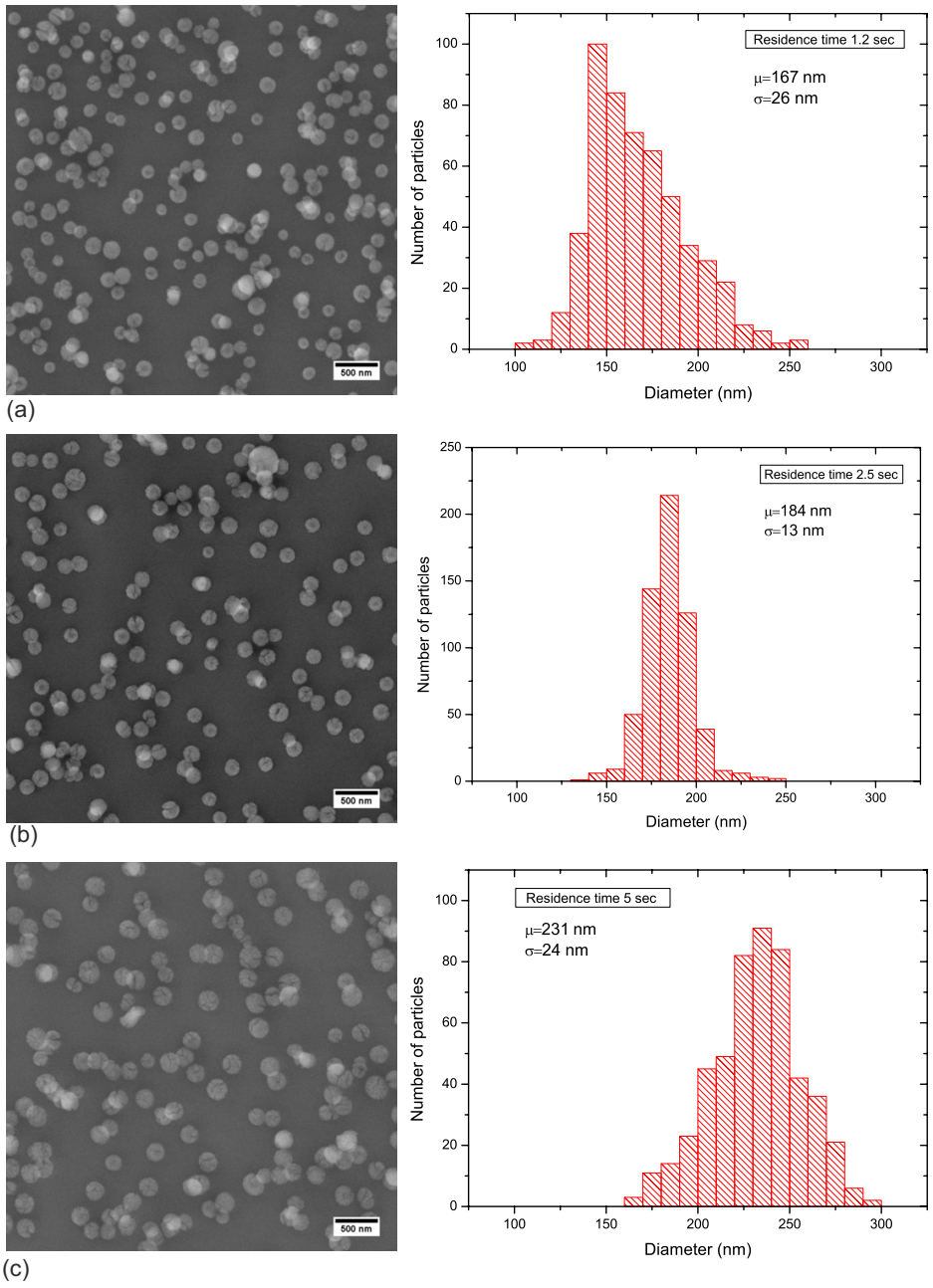

Figure 5. SEM images and the corresponding size distribution histograms for the nylon-sputtered particles prepared by the GAS with different aggregation lengths: (*a*) 10 cm (residence time 1.4 s), (*b*) 16 cm (residence time 2.5 s) and (*c*) 26 cm (residence time 4.6 s); gas flow rate 18.5 sccm, discharge power 80 W, orifice length 35 mm (μ—mean particle diameter, σ—standard deviation).

The second parameter that may influence the size of the nanoparticles produced in the GAS is the time they spend in the aggregation chamber on the way to the orifice (residence time). In order to evaluate this dependence, two different approaches were used: (1) variation of the aggregation length of the GAS and (2) variation of the gas flow rate through the GAS, other process parameters being kept constant.

The influence of the aggregation length on the size of the nylon-sputtered particles is shown in figure 5. The mean particle diameter increased from 167 to 231 nm with the increase in the aggregation chamber length from 10 to 26 cm.

The observed changes are consistent with increasing residence time of growing nanoparticles in the aggregation volume, which has already been reported in the literature in

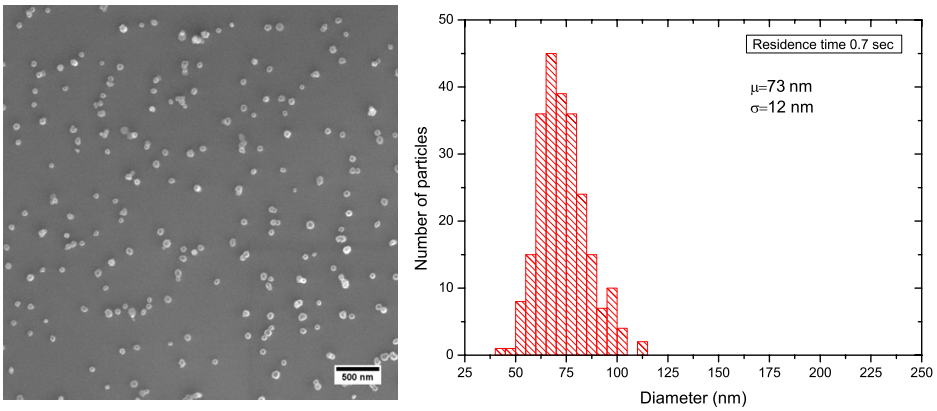

Figure 6. SEM image and the corresponding size distribution histogram for nylon-sputtered particles deposited with high gas flow rate 47 sccm (residence time 0.7 s). Other deposition parameters, e.g. pressure 75 Pa, power 80 W and aggregation length 16 cm, are the same as in figure 5(*b*); μ—mean particle diameter, σ—standard deviation.

the case of dusty particles [3] as well as for metal clusters [21]. On the assumption that the drift velocity of the nanoparticles is equal to the velocity of the carrier gas flow, the residence time can be easily calculated from the parameters of the GAS: pressure (75 Pa), gas flow rate (18.5 sccm) and volume (about 600, 1000 and 1900 cm^3 for the employed lengths of the aggregation chambers) using

$$t = pV/Q, \tag{1}$$

where p is the pressure in the aggregation chamber of volume V and Q denotes the gas flow rate. Thus, the corresponding residence times were 1.4 s, 2.5 s and 4.6 s, respectively.

In order to confirm the effect of the residence time of nanoparticles in the GAS on their final size, an additional experiment was performed in which an orifice of the shorter length (3 mm) was used. Shortening the length of the orifice resulted in a dramatic increase in the gas flow rate (from 18.5 up to 47 sccm) needed to reach the same pressure in the aggregation chamber (75 Pa). This causes a decrease in the residence time of nanoparticles from 2.5 s to the value of 0.7 s for the 16 cm long aggregation chamber. As can be seen from a comparison of figures 6 and 5(*b*), such a change in the residence time led to a decrease in the mean particle diameter from 184 down to 73 nm.

The dependence of the particle volume on residence time was plotted as a conclusion from figures 5 and 6 (figure 7). The volume of particles was simply calculated from the mean diameter obtained from the SEM images. The graph shows a monotonic and almost linear increase in mean volume of deposited nanoparticles from 73 to 231 nm with increasing residence time 'covering' the range from 0.7 to 4.6 s. Such behaviour is similar to the growth of nanoparticles in PEVCD systems, and may be explained in the frame of a three-step process (e.g. [3]). First, stable nanosized particles are created as the result of complex plasmochemical reactions. Such particles, if created in sufficient number, readily coagulate and form particles with diameters in the range of tens of nanometres. This is, however, accompanied by a steep decrease in the number of nanoparticles, which also lowers

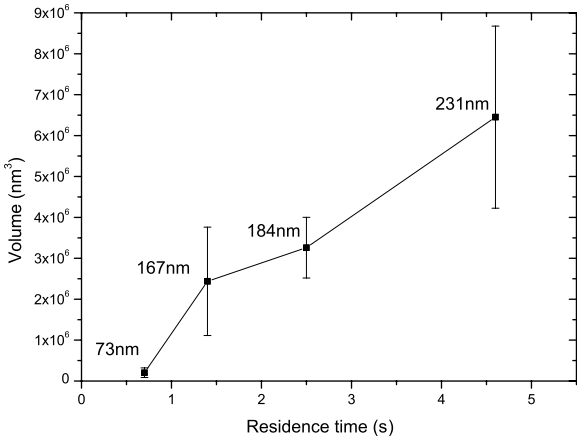

Figure 7. Particle volume and mean particle diameter as a function of residence time in the aggregation chamber. The particles were prepared at the same pressure (75 Pa) and discharge power (80 W).

the probability of their collisions and thus their further growth is on a longer time scale driven mainly by sticking of gas-phase particles (radicals) to big nanoparticles. In our case, the particles created in the aggregation chamber are dragged by a carrier gas towards the exit orifice of the aggregation chamber and thus the above-mentioned time evolution may be translated to the position in the aggregation chamber. Assuming that the first two phases occur in the vicinity of the sputtered target, or at least at a distance shorter than the length of the aggregation chamber, the main process that determines the final size of the particles is the sticking of gas-phase species to nanoclusters travelling through the aggregation chamber. Under this assumption, the time the nanoparticles spend in the aggregation zone will be directly proportional to their size, which corresponds to the experimental results.

The chemical composition of the nylon-sputtered particles was investigated by FTIR and XPS. As can be seen in figure 8, where the FTIR spectra of unaltered Nylon 6,6 and spectra of deposited nylon-sputtered particles are presented,

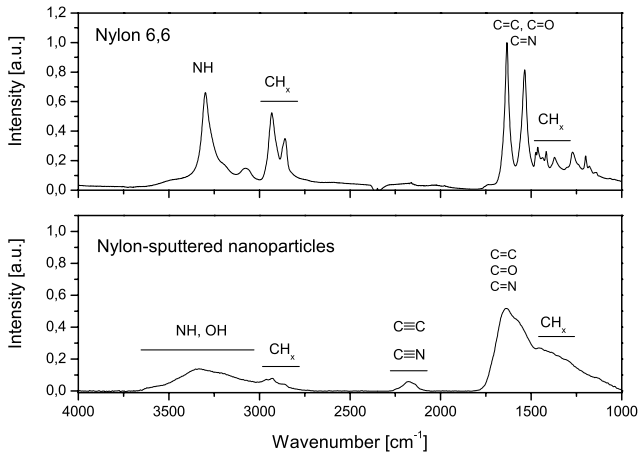

Figure 8. FTIR spectra: Nylon 6,6 (top) and nylon-sputtered nanoparticles deposited at aggregation pressure 75 Pa, magnetron power 80 W (bottom).

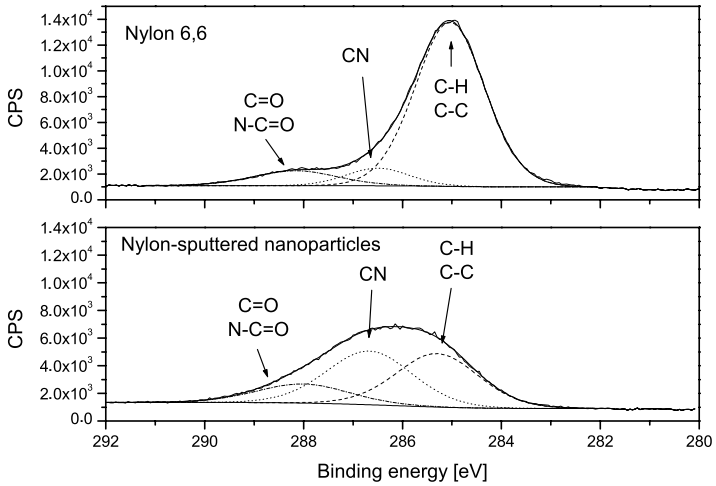

Figure 9. C 1s XPS: Nylon 6,6 (top) and nylon-sputtered nanoparticles deposited at aggregation pressure 75 Pa, magnetron power 80 W (bottom).

the nanoparticles have a composition markedly different from that of conventional Nylon 6,6: in contrast to FTIR spectra of Nylon 6,6 that is characterized by narrow peaks, the individual peaks broaden into wide bands in the case of nylon-sputtered particles. This suggests a more irregular and cross-linked structure of nanoparticles that is similar to the structure usual for plasma polymers (e.g. [20, 26]). In addition to this general trend, a peak at about 2200 cm^{-1} also appears in the spectra of the nylon-sputtered particles that can be assigned to nitriles or to the C≡C bonds, which was not observed in the case of Nylon 6,6.

The XPS analysis revealed that the elemental composition of the nanoparticles was 60% C, 28% N and 12% O and this was not markedly affected by the deposition conditions. These values are close to those of thin films of magnetron-sputtered nylon [26, 27], but distinctly different from the elemental composition of unaltered Nylon 6,6 (75% C, 12.5% N and 12.5% O). The main difference is in considerably higher N/C ratio (close to 0.5) in the case of sputtered nylon particles as compared with Nylon 6,6. The higher fraction of N in the deposited particles is due to the incorporation of nitrogen, which was used in the working gas mixture. The differences between conventional Nylon and sputtered nylon particles may also be clearly seen on the high-resolution XPS spectra of C 1s peak (figure 9). In both cases the C1 s peak may be fitted by three main groups of binding environments that correspond to the C–C/C–H bonds (binding energy 285.0 eV), the C–N, the C=N and C≡N groups (average binding energy 286.5 eV, indicated as CN in figure 9) and the C=O, N–C=O groups (average binding energy 288.1 eV). However, whereas in the case of Nylon 6,6 the most abundant chemical bonds are C–C and C–H (83%), in the case of nylon-sputtered particles the fraction of CN and C–C/C–H bonds becomes comparable (41% and 43%).

4. Conclusions

Plasma polymer nanoparticles were produced by magnetron sputtering of nylon in a GAS of the Haberland type. The particles have complex shape with cauliflower-like features. As was shown by both FTIR and XPS, the chemical composition of the deposited particles differs markedly from the structure of unaltered Nylon 6,6. Unlike Nylon 6,6, the fabricated particles resemble the chemical structure of thin films of plasma polymers prepared by magnetron sputtering of Nylon, concretely their higher cross-linking and higher N/C ratio.

The increase in rf power from 60 to 100 W resulted in a slight decrease in the particle mean diameter from 210 to 168 nm. It has also been shown that an increase in the residence time of the particles in the aggregation chamber from 0.7 to 4.6 s resulted in a dramatic increase in their diameter from about 73–231 nm.

Unlike other plasma-based systems, the formation of nanoparticles and their deposition occur in two separate parts: the nanoparticles are created in the high-pressure aggregation chamber and are dragged by a working gas through a small orifice to the low-pressure deposition chamber where they are deposited on the substrates. The separation of the high-pressure GAS from the low-pressure deposition chamber represents a technological advantage mainly with respect to possible simultaneous deposition of nanoparticles of different materials from independent GASs or for fabrication of nanocomposite materials based on the incorporation of nanoparticles into simultaneously deposited matrix. Nanostructured films deposited from these nanoparticles can also be used in multilayer structures that combine nanoparticles and plain films. In this way, the films with arbitrary roughness (in a broad range) and independently controlled surface chemistry may be prepared.

Acknowledgments

This research has been supported by grant SVV-2012-265305 and grant GAUK 134510 from the Grant Agency of Charles University in Prague and the project COST FA0904 and COST CZ LD11032 grant. The authors are indebted to I Khalakhan for SEM images.

References

[1] Kobayashi H, Bell A T and Shen M 1973 Formation of an amorphous powder during the polymerization of ethylene in a radio frequency discharge *J. Appl. Polym. Sci.* **17** 885–92

[2] Kobayashi H, Shen M and Bell A T 1974 Effects of reaction conditions on the plasma polymerization of ethylene *J. Macromol. Sci. A: Chem.* **8** 373–91

[3] Berndt J, Kovačević E, Stefanović I, Stepanović O, Hong S H, Boufendi L and Winter J 2009 Some aspects of reactive complex plasmas *Contrib. Plasma Phys.* **49** 107–33

[4] Watanabe Y 2006 Formation and behaviour of nano/micro-particles in low pressure plasmas *J. Phys. D: Appl. Phys.* **39** R329–61

[5] Feng J C, Huang W, Fu G D, Kang E-T and Neoh K-G 2005 Deposition of well-defined fluoropolymer nanospheres on PET substrate by plasma polymerization of heptadecafluorodecyl acrylate and their potential application as a protective *Plasma Process. Polym.* **2** 127–35

[6] Yang S H, Liu C-H, Hsu W-T and Chen H 2009 Preparation of super-hydrophobic films using pulsed hexafluorobenzene plasma *Surf. Coat. Technol.* **203** 1379–83

[7] Solař P, Kylián O, Polonskyi O, Artemenko A, Arzhakov D, Drábik M, Slavínská D, Vandrovcová M, Bačáková L and Biederman H 2012 Nanocomposite coatings of Ti/C : H plasma polymer particles providing a surface with variable nanoroughness *Surf. Coat. Technol.* **206** 4335–42

[8] Buss R and Hareland W 1994 Gas phase particulate formation in radiofrequency fluorocarbon plasmas *Plasma Sources Sci. Technol.* **3** 268–72

[9] Teare D O H, Spanos C G, Ridley P, Kinmond E J, Roucoules V, Badyal J P S, Brewer S A, Coulson S and Willis C 2002 Pulsed plasma deposition of super-hydrophobic nanospheres *Chem. Mater.* **14** 4566–71

[10] Denysenko I, Berndt J, Kovacevic E, Stefanovic I, Selenin V and Winter J 2006 The response of a capacitively coupled discharge to the formation of dust particles: Experiments and modeling *Phys. Plasmas* **13** 073507

[11] Drábik M, Serov A, Kylián O, Choukourov A, Artemenko A, Kousal J, Polonskyi O and Biederman H 2012 Deposition of Fluorocarbon Nanoclusters by Gas Aggregation Cluster Source *Plasma Process. Polym.* **9** 390–7

[12] Vriendt V D, Maseri F, Nonet A and Lucas S 2009 Study of nanoparticles formation in a pulsed magnetron discharge in acetylene *Plasma Process. Polym.* **6** S6–S10

[13] Vriendt V D, Felten A, Blondeau J J-P, Maseri F, Pireaux J J-J and Lucas S 2011 Deposition of superhydrophobic structures by magnetron discharge *Surf. Coat. Technol.* **205** S582–5

[14] Haberland H, Karrais M, Mall M and Thurner Y 1992 Thin films from energetic cluster impact: a feasibility study *J. Vac. Sci. Technol.* A **10** 3266–71

[15] Biederman H, Kylian O, Drabik M, Choukourov A, Polonskyi O and Solar P 2011 Nanocomposite and nanostructured films with plasma polymer matrix *Surf. Coat. Technol.* doi:10.1016/j.surfcoat.2011.09.011

[16] Biederman H, Stelmashuk V, Kholodkov I, Choukourov A and Slavinska D 2003 RF sputtering of hydrocarbon polymers and their derivatives *Surf. Coat. Technol.* **174–175** 27–32

[17] Kholodkov I, Biederman H, Slavinska D, Choukourov A and Trchova M 2003 Plasma polymers prepared by RF sputtering of polyethylene *Vacuum* **70** 505–9

[18] Choukourov A, Hanus J, Kousal J, Grinevich A, Pihosh Y, Slavinska D and Biederman H 2006 Plasma polymer films from sputtered polyimide *Vacuum* **81** 517–26

[19] Drábik M *et al* 2010 Super-hydrophobic coatings prepared by RF magnetron sputtering of PTFE *Plasma Process. Polym.* **7** 544–51

[20] Kylian O, Hanus J, Choukourov A, Kousal J, Slavinska D and Biederman H 2009 Deposition of amino-rich thin films by RF magnetron sputtering of nylon *J. Phys. D: Appl. Phys.* **42** 142001

[21] Polonskyi O, Solař P, Kylián O, Drábik M, Artemenko A, Kousal J, Hanuš J and Pešička J 2012 Nanocomposite metal/plasma polymer films prepared by means of gas aggregation cluster source *Thin Solid Films* **520** 4155–62

[22] Solař P, Polonskyi O, Choukourov A, Artemenko A, Hanuš J, Biederman H and Slavínská D 2011 Nanostructured thin

films prepared from cluster beams *Surf. Coat. Technol.* **205** S42–S47

[23] Drabik M, Choukourov A, Artemenko A, Polonskyi O, Kylian O, Kousal J, Nichtova L, Cimrova V, Slavinska D and Biederman H 2011 Structure and composition of titanium nanocluster films prepared by gas aggregation cluster source *J. Phys. Chem.* C **115** 20937–44

[24] Maurer H R and Kersten H 2011 On the heating of nano-and microparticles in process plasmas *J. Phys. D: Appl. Phys.* **44** 174029

[25] Boufendi L and Bouchoule A 1994 Particle nucleation and growth in a low-pressure argon-silane discharge *Plasma Sources Sci. Technol.* **3** 262

[26] Kousal J, Hanuš J, Choukourov A, Polonskyi O, Biederman H and Slavínská D 2009 *In situ* diagnostics of RF magnetron sputtering of nylon *Plasma Process. Polym.* **6** S803–7

[27] Hanuš J, Ceccone G and Rossi F 2012 Amino-rich Plasma polymer films prepared by rf magnetron sputtering *Plasma Process. Polym.* **9** 371–9

Control of Wettability of Plasma Polymers by Application of Ti Nano-Clusters

Ondřej Kylián,* Oleksandr Polonskyi, Jiří Kratochvíl, Anna Artemenko, Andrei Choukourov, Martin Drábik, Pavel Solař, Danka Slavínská, Hynek Biederman

Two-step process that allows controlling independently roughness and chemical composition of plasma polymers, i.e., two parameters determining the wettability of such materials, is presented. In the first step a film composed of Ti nano-clusters is deposited on a smooth substrate. Nano-cluster films of different roughness can be obtained depending on deposition time. In the second step the nano-cluster films are overlaid by a thin layer of plasma polymer having the desired chemical structure. This approach allows the tuning of wettability of the deposited films to as much as 50% of the wettability of the films having the same chemical structure but deposited on a smooth substrate.

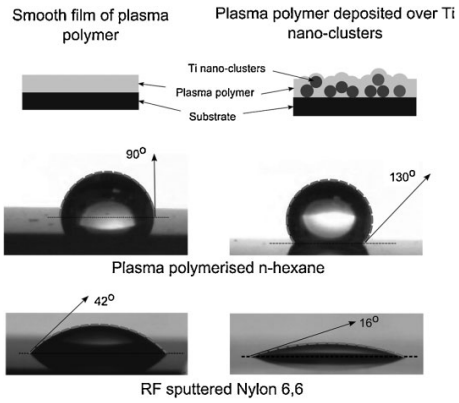

1. Introduction

Methods of fabrication of polymeric surfaces that allow the tuning of their hydrophilic/hydrophobic character are of a high interest from practical perspectives. The materials so prepared can be used in diverse applications including textile, lithography, food packaging, or biomedical applications, where such surfaces can be employed for instance as assays for selective protein or cell adhesion.

It is well known that the wettability of polymeric surfaces is given by a combination of their chemical composition and topography (e.g.,[1]).

The chemical composition of the surface determines its surface energy: whereas surfaces rich in non-polar groups (e.g., $-CH_x$ or $-CF_2$) have low surface energies and thus are hydrophobic, surfaces with high density of polar groups (e.g., $-OH$, $-COOH$, $-C=O$, or $-NH_x$) exhibit high surface energies and are hydrophilic. The differences in polarity of various functional groups were employed for the fabrication of coatings with desired wettability in a wide range of water contact angles,[2–4] or even for production of films with gradient wettability.[5,6] Nevertheless, approaches that control the wettability solely by tuning the chemical composition of surfaces suffer from certain disadvantages. First, the contact angles that can be reached by these methods do not overcome 120°.[7] Moreover, in some cases it is crucial to control wettability independently of the chemical composition of the surface in order to maintain its proper function.

The second parameter that determines the wettability of a surface is its topography: in general, an increase of the roughness of the surface for its given chemical composition causes either increase of the surface hydrophilicity (in the case of hydrophilic materials) or hydrophobicity (in the case of hydrophobic surfaces). This phenomenon can be explained by models assuming that the liquid is in contact

O. Kylián, O. Polonskyi, J. Kratochvíl, A. Artemenko, A. Choukourov, M. Drábik, P. Solař, D. Slavínská, H. Biederman
Charles University, Faculty of Mathematics and Physics,
V Holešovičkách 2, Prague 8, 180 00, Czech Republic
Fax: +420 2 2191 2350; E-mail: ondrej.kylian@gmail.com

DOI: 10.1002/ppap.201100113

with all the parts of the irregular surface (Wenzel's model),[8] or that the drop sits on the surface protrusions and thus does not wet the entire surface (Cassie–Baxter's model).[9] The most common methods employed for the control of surface roughness are based either on the direct growth of nanostructured films (e.g., in the case of plasma polymerized fluorocarbon coatings[10–12]), etching of polymeric materials,[13] or by two-step processes comprising fabrication of nanostructured surface for instance by etching, reactive ion etching, photolithography, or laser irradiation of substrates, which is followed by modification of chemical composition of such prepared surfaces or by their coating with films that have desired chemical composition.[14–23] In addition, alternative approaches appeared recently that use nano-particles embedded in a polymeric matrix, e.g., by spray casting of nano-particle/polymer suspensions,[24] embedding silica nano-particles into a polymeric matrix prepared by sol-gel technique,[25] or spin coating of polystyrene mixed with silica nano-particles.[26]

In this study, we present an alternative method that uses a combination of the deposition of Ti nano-clusters by a gas aggregation cluster source used for control of roughness and plasma polymerization that enables tuning the chemical composition of the surface. The main aim of this work is to show that this approach allows producing coatings with independently controllable roughness and chemical composition.

2. Experimental Section

2.1. Deposition of Films of Ti Nano-Clusters

The deposition of Ti nano-clusters was performed using the gas aggregation cluster source depicted in Figure 1 and characterized in detail in the previous work.[27] This cluster source was based on the Haberland's concept employing sputtering from a water cooled planar magnetron (50 mm in diameter) and equipped with Ti target (Goodfellow, purity 99.3%). The magnetron was powered by a DC power source (AE MDX 1.5K) operated in the constant current mode (0.2 A in this study). The magnetron was installed in a water cooled gas aggregation chamber terminating in an exit cone with an orifice 1.5 mm in diameter. The entire assembly of the cluster source was mounted on the main deposition chamber pumped by rotary and diffusion pumps. In this study argon (purity 99.8%) was used as a buffer gas. The pressure inside the gas aggregation chamber was 100 Pa and gas flow was 13.7 sccm, whereas pressure in the deposition chamber was lower than 1 Pa. Ti nano-clusters were deposited on 1×1 cm one-side polished Si wafers positioned in the main chamber 25 cm away from the exit orifice of the nano-cluster source.

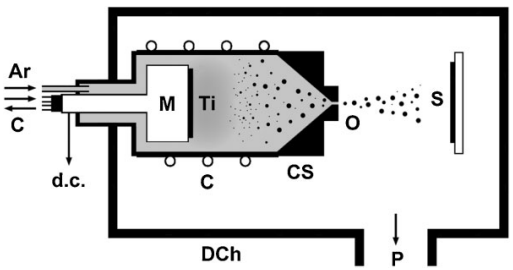

Figure 1. Schematic drawing of the vacuum deposition system. Ar, inlet of working gas (argon); C, water cooling of magnetron and cluster source chamber; CS, gas aggregation cluster source chamber; d.c., to d.c. power source; DCh, deposition chamber; M, magnetron; O, orifice; P, to rotary and diffusion pumps; S, substrate holder or QCM head; Ti, titanium target. Adapted from Drabik et al.[27]

2.2. Deposition of Plasma Polymerized *n*-Hexane

The deposition of plasma polymerized *n*-hexane took place in a stainless steel vacuum chamber by means of RF (13.56 MHz) unbalanced magnetron placed at a 100 mm distance from the substrates. This magnetron, which served as a source for plasma polymerization process, was operated at a constant power of 50 W and equipped by a graphite target 80 mm in diameter. The graphite target used in these experiments was selected because of its low sputter yield, which limits possible effects connected with the release of the material from the magnetron. The deposition of plasma polymerized *n*-hexane was performed at a pressure of 2 Pa in the Ar/*n*-hexane 1:1 working gas mixture at a total flow of 8 sccm. Under these conditions, the deposition of 40 nm thick films of plasma polymerized *n*-hexane took 3 min.

2.3. RF Magnetron Sputtering of Nylon

The RF magnetron sputtering of Nylon 6,6 target (80 mm in diameter, 2 mm thick) was performed in a deposition chamber described in detail in the previous works.[28,29] The magnetron was powered from the CESAR® 136 (Dressler) power supply (driving frequency of 13.56 MHz) and was positioned 50 mm above the substrate. Ar (purity 99.99%) was used as the working gas. The films of RF sputtered Nylon were deposited at a pressure of 2 Pa, gas flow of 5 sccm and applied power of 40 W. The deposition rate was $4\ \mathrm{nm \cdot min^{-1}}$.

2.4. Sample Characterization

SEM observation of the Ti nano-cluster films was performed by Mira/II scanning electron microscope (Tescan). Morphology of the samples was evaluated by atomic force microscopy (AFM, Quesant Q-scope 350) in the semi-contact mode using NSC-16 silicon cantilevers (Schaefer Technologie, GmbH). Chemical composition of the deposited films was determined by X-ray photoelectron spectroscopy (XPS, Specs Phobios 100). The XPS spectra were acquired at a constant take-off angle of 90°. Wide scans (0–1 300 eV) were recorded using 40 eV pass energy (step 0.5 eV, dwell time 0.1 s), whereas high resolution scans were recorded at 10 eV pass energy (step 0.05 eV, dwell time 0.1 s, 10 repetitions). All the binding energies were referenced to the C1 s carbon peak at 285.0 eV, to compensate for the effect of surface charging. The surface wetting properties were evaluated on a goniometer of own

construction. The static water contact angles were obtained by averaging the measurements on three water droplets randomly placed on the sample surface. Finally, the thickness of the coatings was determined by means of ellipsometry using a variable angle spectroscopic ellipsometer (Woolam M-2000DI) in the wavelength range of $\lambda = 192–1\,690$ nm at an angle of incidence AOI = 55–75°. All measurements were performed in air on the coatings deposited on smooth Si wafers. The samples were modeled as Si/SiO_2/plasma polymer system and the optical constants of the plasma polymer were fitted using oscillator model consisting of one Tauc–Lorentz oscillator and two pole oscillators.

3. Results and Discussion

3.1. Characterization of Ti Nano-Clusters

Ti nano-clusters ranging from 15 to 30 nm in diameter are produced under the deposition conditions used in this study. Figure 2 presents examples of typical $5 \times 5\ \mu m^2$ SEM micrographs of cluster films deposited in 10, 60, and 240 s. These three different deposition periods illustrate three different stages of growth of the nano-cluster films. It can be seen that the deposition lasting 10 s results in the formation of sub-monolayer of randomly distributed Ti nano-clusters. After the 60-s deposition, the Si substrate is still partially visible, but the clusters do not form a single layer — some clusters are attached to the neighbors lying below. Finally, 240-s deposition results in fully covered Si wafer with rather porous film of Ti nano-clusters. Moreover, although the surface roughness of Ti nano-cluster films was not evaluated directly in this study due to relatively low adhesion of Ti nano-clusters on Si wafers, which disabled AFM measurements, it can be seen in Figure 2 that the deposition time of nano-clusters has a strong influence on the topography of the surface of nano-cluster films: an increase of the deposition time of Ti nano-clusters leads to

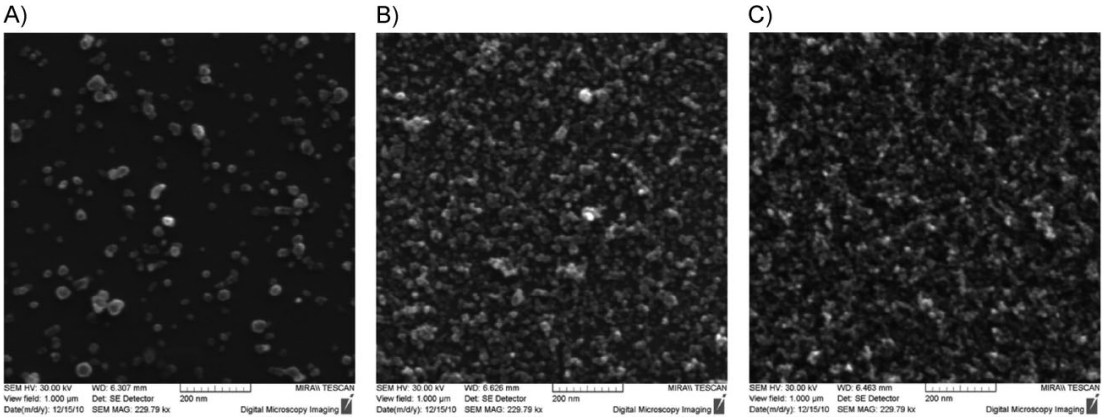

Figure 2. SEM micrographs of Ti nano-clusters deposited in (A) 10 s, (B) 60 s and (C) 240 s.

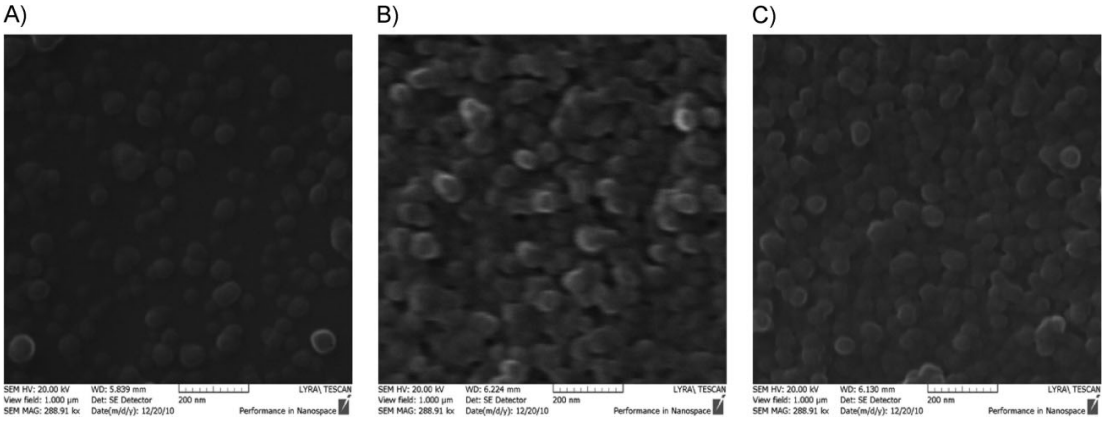

Figure 3. SEM micrographs of Ti nano-clusters deposited in (A) 10 s, (B) 60 s, (C) 240 s and coated by 40 nm thick film of plasma polymerized *n*-hexane.

DOI: 10.1002/ppap.201100113

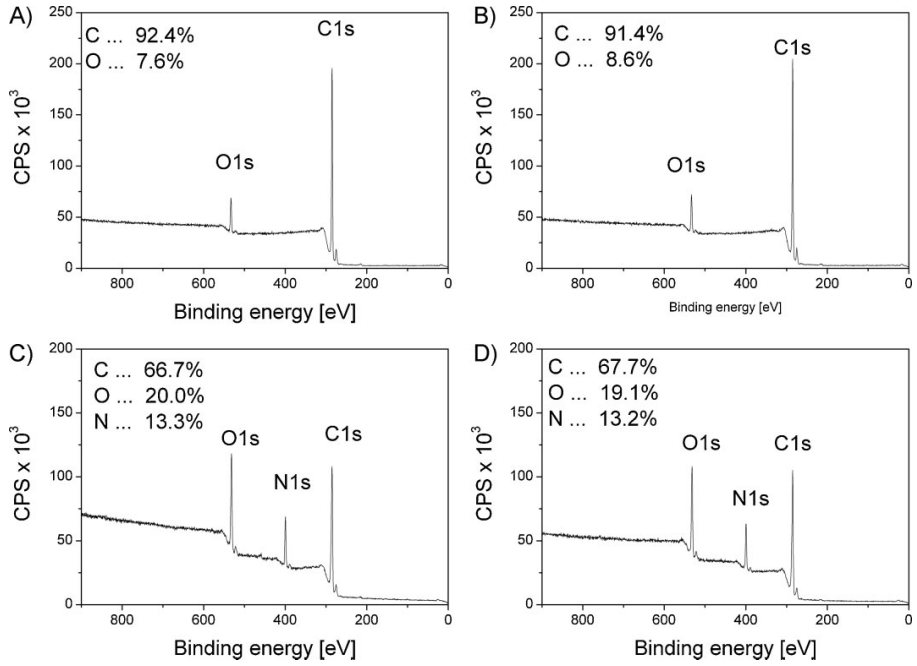

Figure 4. XPS spectra of (A) Ti nano-clusters deposited in 1 min and coated with plasma polymerized *n*-hexane, (B) plasma polymerized *n*-hexane deposited on a smooth Si wafer, (C) Ti nano-clusters deposited in 1 min and coated with RF sputtered Nylon and (D) sputtered Nylon film deposited on a smooth Si wafer. The thickness of films of plasma polymers is 40 nm.

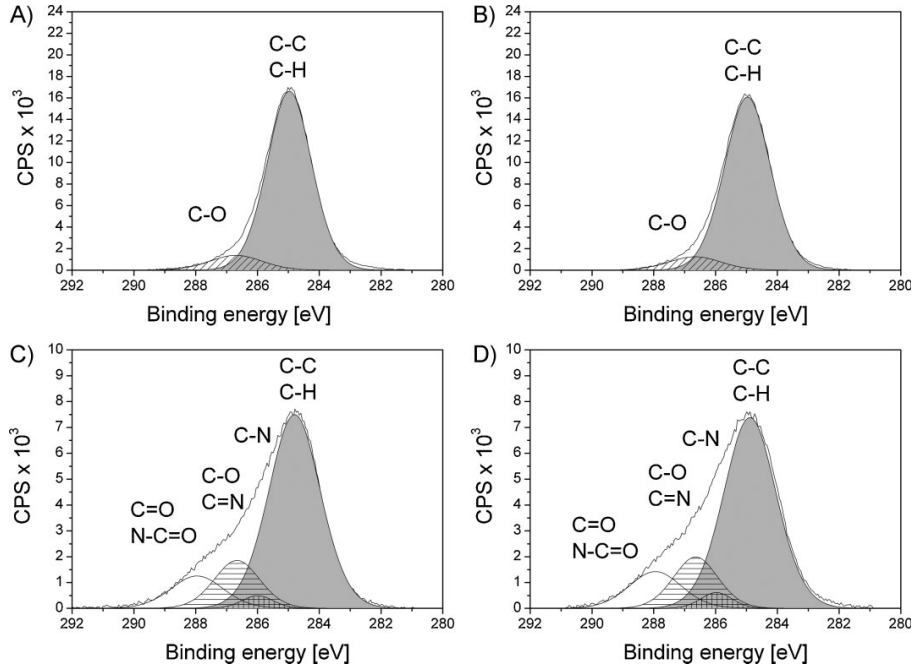

Figure 5. High resolution XPS spectra of C1 s peak of (A) Ti nano-clusters deposited in 1 min and coated with plasma polymerized *n*-hexane, (B) plasma polymerized *n*-hexane deposited on a smooth Si wafer, (C) Ti nano-clusters deposited in 1 min and coated with RF sputtered Nylon and (D) sputtered Nylon film deposited on a smooth Si wafer. The thickness of films of plasma polymers is 40 nm.

an increase of roughness of the resulting films. This will be discussed in more detail in the subsequent text.

3.2. Characterization of Ti Nano-Clusters Covered by Plasma Polymers

The Ti nano-cluster films were in the second step coated with plasma polymerized *n*-hexane or RF sputtered Nylon. These two plasma polymers were selected as examples of materials that have either hydrophilic character (in the case of sputtered Nylon) or slightly hydrophobic nature (in the case of plasma polymerized *n*-hexane) when deposited as smooth films. The deposition of 40 nm thick coating on the Ti nano-clusters changes the visual appearance of the samples: whereas SEM imaging showed the diameter of Ti nano-clusters in the range 15–30 nm, nano-clusters coated by plasma polymers appeared as considerably larger structures. Figure 3 shows examples of SEM micrographs of Ti nano-clusters coated with plasma polymerized *n*-hexane.

A 40 nm thickness of the overlayer film of plasma polymers was moreover found to be sufficient to cover entirely the Ti nano-clusters, since the XPS spectra acquired on such samples did not reveal any presence of titanium. This can be seen in Figure 4 showing the XPS spectra of Ti nano-clusters deposited in 1 min and coated thereafter with plasma polymerized *n*-hexane and RF sputtered Nylon. Moreover, it has been found that the presence of Ti nano-clusters has no effect on the chemical composition of the surface of the resulting films: the elemental composition of the samples without hydrogen determined from the XPS wide scans (Figure 4) as well as their chemical structure as determined from high resolution XPS scans of C1 s peak (Figure 5) remains, within an experimental error, the same as for the films deposited on cleaned Si wafers. In other words, Ti nano-clusters do not alter the mode of the films growth and can be, from this point of view, considered as a part of the substrate and not as an "active" component of the deposited layer. This is an important finding, since it allows discarding the effect of the surface chemistry on the wettability changes of such prepared samples, which should therefore be influenced solely by the surface topography.

The topography of the samples was evaluated in detail by means of AFM. As can be seen in Figure 6, where are presented $5 \times 5\,\mu m^2$ AFM scans of Ti nano-clusters overcoated with 40 nm thick films of plasma polymerized *n*-hexane or sputtered Nylon, the surface topography is not largely affected by the selection of the overcoat material. Moreover, the roughness of the samples was found to increase for given thickness of the overcoat with increasing time of Ti nano-cluster deposition. This is demonstrated in Figure 7, which shows typical $5 \times 5\,\mu m^2$ AFM scans of plasma polymerized *n*-hexane deposited either on smooth

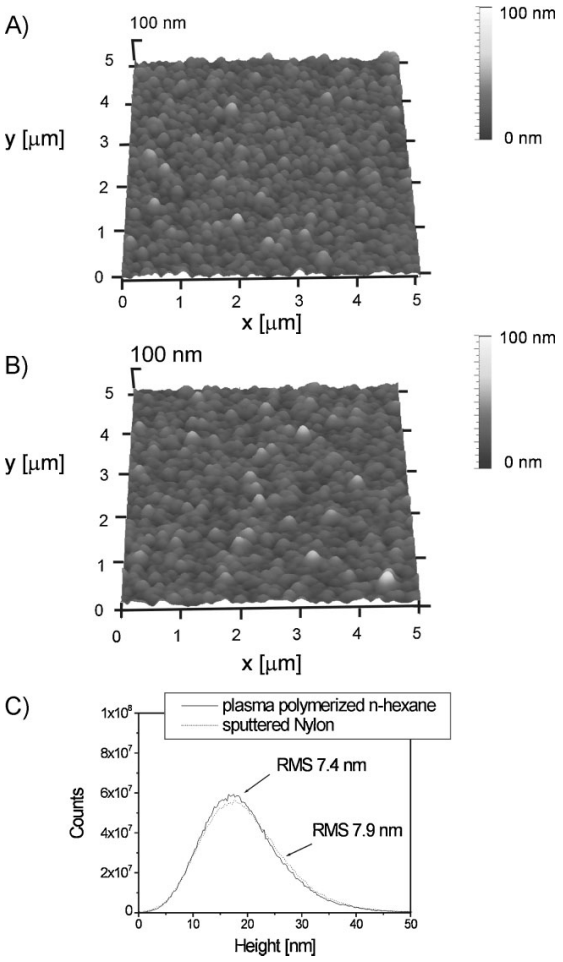

Figure 6. $5 \times 5\,\mu m^2$ AFM scans of Ti nano-clusters deposited in 60 s and overcoated with (A) plasma polymerized *n*-hexane and (B) RF sputtered Nylon together with (C) corresponding height histograms. The thickness of the films of plasma polymers was 40 nm.

Si wafers or on Ti nano-cluster films. In addition, Figure 8 gives the dependence of the root mean square (RMS) roughness of the samples on the deposition time of Ti nano-cluster films as measured both for Ti nano-clusters coated with plasma polymerized *n*-hexane and sputtered Nylon. Based on these results, it can be concluded that the most pronounced increase of surface roughness as compared to the films of plasma polymers deposited on polished Si wafers occurs for deposition times of Ti nano-clusters shorter than 120 s. Further increase of the deposition time has only a limited effect on the surface roughness of the samples. In other words, this represents a limit, in which the surface roughness can be tuned using the deposition time of Ti nano-clusters as the only process variable.

Plasma Process. Polym. **2012**, *9*, 180–187

DOI: 10.1002/ppap.201100113

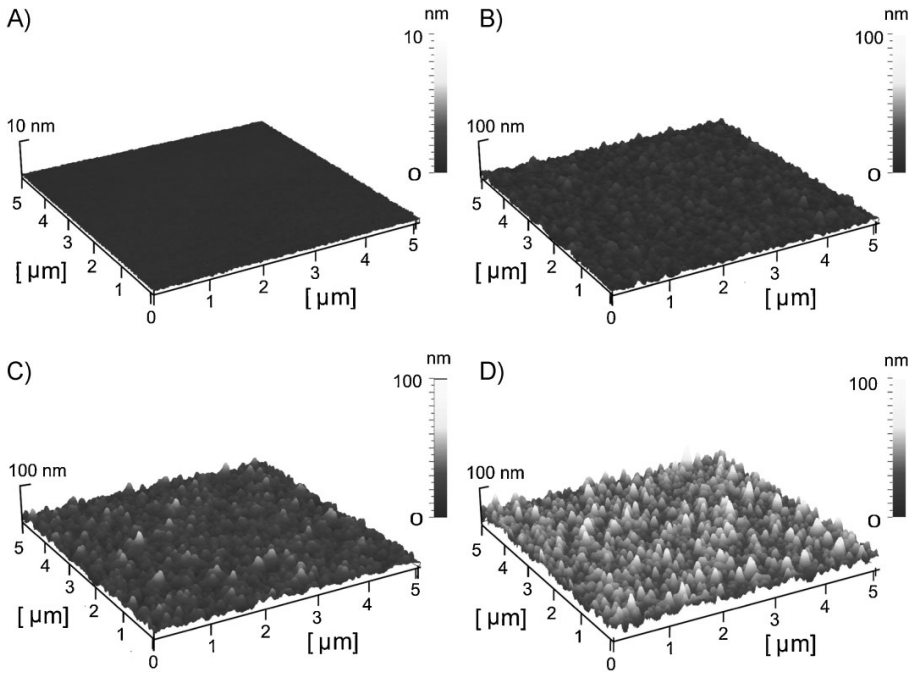

Figure 7. 5 × 5 µm² AFM scans of plasma polymerized *n*-hexane deposited on (A) cleaned Si wafer and on Ti nano-clusters deposited in (B) 10 s, (C) 60 s and (D) 240 s. The thickness of the films of the overcoat layer was 40 nm.

It is important to mention that the surface roughness may be varied also by the change of the thickness of the overcoat film. Nevertheless, in this case the change of the RMS roughness is considerably less pronounced as compared to the effect of the deposition time of Ti nano-clusters.

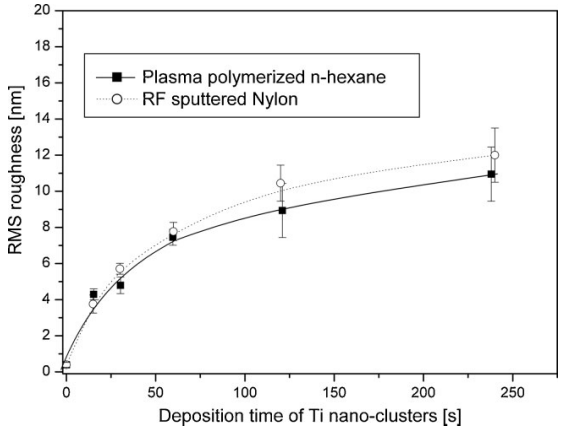

Figure 8. Variation of RMS roughness of samples with deposition time of Ti nano-cluster films. The thickness of the films of plasma polymers was 40 nm.

For instance an increase of the thickness of plasma polymerized *n*-hexane deposited over Ti nano-clusters from 40 to 100 nm resulted in the increase of RMS roughness from 7.4 to 8.8 nm only. From this reason, further experiments were done solely using deposition time of the nano-clusters as the only variable for the control of surface roughness.

3.3. Wettability of Ti Nano-Clusters Covered by Plasma Polymers

The wettability of the Ti nano-cluster films covered by a 40 nm thick layer of plasma polymerized *n*-hexane and RF sputtered Nylon is presented in Figure 9 for surfaces with different values of RMS roughness. Two different effects can be observed. In the case of RF sputtered Nylon, the increasing surface roughness leads to a monotonic decrease of static contact angle of water from 42° (observed on a smooth surface) down to approximately 16° (on a surface with RMS roughness of approximately 12 nm). In contrary, the static contact angle of water on plasma polymerized *n*-hexane increases with roughness from about 90° to slightly above 130°. Considering the same chemical composition of samples reported above, the observed variations of the water contact angles can be ascribed solely to the roughness of the surface.

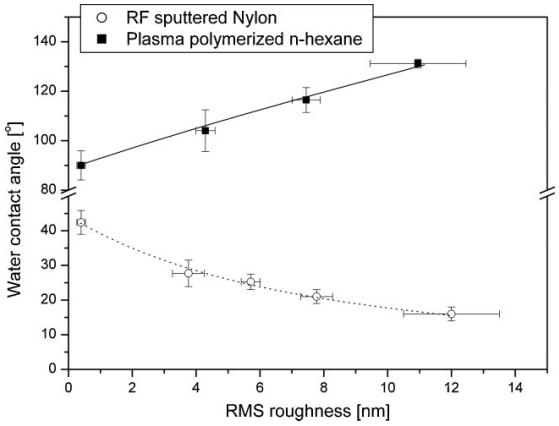

Figure 9. Static water contact angle of samples in dependence on their RMS roughness.

4. Conclusion

It has been shown that the two-step process combining the deposition of nano-cluster films by the gas aggregation cluster source with subsequent coating of such pre-prepared films by plasma polymers makes it possible to adjust independently the chemical composition of the resulting surfaces and their roughness. This in turn allows tuning of wettability of such samples by the mere variation of their roughness without changing their surface chemical composition.

We showed that the controlled roughness of the prepared surfaces can be achieved by variation of the deposition time of Ti nano-clusters. The chemical composition of the surface is then determined by the plasma polymer used (*n*-hexane or RF sputtered Nylon in this study). It was demonstrated that this approach makes it possible either to increase (in the case of the overlayer having hydrophobic character) or decrease (in the case of hydrophilic overlayer) static water contact angle by approximately 50% as compared to the samples without Ti nano-clusters. This limit in an achievable range of static water contact angles is given by the size of the employed Ti nano-clusters (15–30 nm used in this study) that does not allow reaching higher surface roughness even at longer deposition times.

In addition, it should be stressed that the method of surface design described herein utilizes only vacuum methods, which brings several advantages related to the process efficiency, scalability and costs, and overcomes environmental aspects connected with the use of wet chemistry, and it is virtually substrate independent. Furthermore, although in this study the depositions of Ti nano-clusters and films of plasma polymers were accomplished in separate deposition chambers, this deposition technique can be easily performed in one vacuum chamber, which makes it interesting for the industrial use since it enables in-line processing of materials and thus offers higher throughput.

Acknowledgements: This work was supported by the Grant Agency of the Academy of Sciences of the Czech Republic under contract KAN 101120701, by the research plan MSM021620834 financed by the Ministry of Education of the Czech Republic and partially by COST CZ grant LD11032. O. Polonskyi and A. Artemenko acknowledge also the support from the Grant Agency of Charles University in Prague within the frames of grants GAUK 134510 and GAUK 251265, respectively. The authors are indebted to S. Haviar for SEM images.

Received: June 6, 2011; Revised: August 27, 2011; Accepted: September 4, 2011; DOI: 10.1002/ppap.201100113

Keywords: gas aggregation cluster sources; nanostructures; plasma polymers; surface roughness; wettability

[1] W. A. Zisman, "Relation of the Equilibrium Contact Angle to Liquid and Solid Constitution", in *Contact Angle, Wettability, and Adhesion*, F. Fowkes, Ed., Advances in Chemistry, American Chemical Society, Washington, DC **1964**.
[2] D. Hegemann, H. Brunner, C. Oehr, *Nucl. Instr. Meth. Phys. Res. B* **2003**, *208*, 281.
[3] M. Drabik, J. Kousal, Y. Pihosh, A. Choukourov, H. Biederman, D. Slavinska, A. Mackova, A. Boldyreva, J. Pesicka, *Vacuum* **2007**, *81*, 920.
[4] Y. W. Park, N. Inagaki, *Polymer* **2003**, *44*, 1569.
[5] M. Zelzer, R. Majani, J. W. Bradley, F. R. A. J. Rose, M. C. Davies, M. R. Alexander, *Biomaterials* **2008**, *29*, 172.
[6] S. Y. Lee, J. Y. Youn, B. S. Kim, Y. H. Cho, M. S. Kim, G. Khang, H. B. Lee, *Colloids Surf. A: Physicochem. Eng. Aspects* **2008**, *313–314*, 136.
[7] T. Nishino, M. Meguro, K. Nakamae, M. Matsushita, Y. Ueda, *Langmuir* **1999**, *15*, 4321.
[8] R. N. Wenzel, *Ind. Eng. Chem.* **1936**, *28*, 988.
[9] A. B. D. Cassie, S. Baxter, *Trans. Faraday Soc.* **1944**, *40*, 546.
[10] F. Intranuovo, E. Sardella, P. Rossini, R. d'Agostino, P. Favia, *Chem. Vap. Deposition* **2009**, *15*, 95.
[11] A. Milella, F. Palumbo, P. Favia, G. Cicala, R. d'Agostino, *Pure Appl. Chem.* **2005**, *77*, 399.
[12] M. Drábik, O. Polonskyi, O. Kylián, J. Čechvala, A. Artemenko, I. Gordeev, A. Choukourov, D. Slavínská, I. Matolínová, H. Biederman, *Plasma Process. Polym.* **2010**, *7*, 544.
[13] K. Tsougeni, N. Vourdas, A. Tserepi, E. Gogolides, *Langmuir* **2009**, *25*, 11748.
[14] M. Lejeune, L. M. Lacroix, F. Bretagnol, A. Valsesia, P. Colpo, F. Rossi, *Langmuir* **2006**, *22*, 3057.
[15] K. Teshima, H. Sugimura, Y. Inoue, O. Takai, A. Takano, *Langmuir* **2003**, *19*, 10624.
[16] A. Ruiz, A. Valsesia, G. Ceccone, D. Gilliland, P. Colpo, F. Rossi, *Langmuir* **2007**, *23*, 12984.
[17] D. E. Weibel, A. F. Michels, A. F. Feil, L. Amaral, S. R. Teixeira, F. Horowitz, *J. Phys. Chem. C* **2010**, *114*, 13219.

DOI: 10.1002/ppap.201100113

[18] K.-Y. Yeh, L.-J. Chen, *Langmuir* **2008**, *24*, 245.
[19] T. Baldacchini, J. E. Carey, M. Zhou, E. Mazur, *Langmuir* **2006**, *22*, 4917.
[20] K. Tsougeni, A. Tserepi, G. Boulousis, V. Constantoudis, E. Gogolides, *Plasma Process. Polym.* **2007**, *4*, 398.
[21] F. Palumbo, R. Di Mundo, D. Cappelluti, R. d'Agostino, *Plasma Process. Polym.* **2011**, *8*, 118.
[22] A. W. Hassel, S. Milenkovic, U. Schűrmann, H. Greve, V. Zaporojtchenko, R. Adelung, F. Faupel, *Langmuir* **2007**, *23*, 2091.
[23] Y. B. Zhou, Y. Yang, W. M. Liu, Q. Ye, B. He, Y. S. Zou, P. F. Wang, X. J. Pan, W. J. Zhang, I. Bello, S. T. Lee, *Appl. Phys. Lett.* **2010**, *97*, 133110.
[24] A. Steele, I. Bayer, E. Loth, *Nano Lett.* **2009**, *9*, 501.
[25] M. Manca, A. Cannavale, L. De Marco, A. S. Aricò, R. Cingolani, G. Gigli, *Langmuir* **2009**, *25*, 6357.
[26] M. Y. Yűce, A. L. Demirel, F. Menzel, *Langmuir* **2005**, *21*, 5073.
[27] M. Drábik, A. Choukourov, A. Artemenko, J. Kousal, O. Polonskyi, P. Solař, O. Kylián, J. Matoušek, J. Pešička, I. Matolínová, D. Slavínská, H. Biederman, *Plasma Process. Polym.* **2011**, *8*, 640.
[28] O. Kylián, J. Hanuš, A. Choukourov, J. Kousal, D. Slavínská, H. Biederman, *J. Phys. D: Appl. Phys.* **2009**, *42*, 142001.
[29] C. Rodriguez-Emmenegger, O. Kylián, M. Houska, E. Brynda, A. Artemenko, J. Kousal, A. B. Alles, H. Biederman, *Biomacromolecules* **2011**, *12*, 1058.

Surface & Coatings Technology 206 (2012) 4335–4342

Contents lists available at SciVerse ScienceDirect

Surface & Coatings Technology

journal homepage: www.elsevier.com/locate/surfcoat

Nanocomposite coatings of Ti/C:H plasma polymer particles providing a surface with variable nanoroughness

P. Solař [a], O. Kylián [a], O. Polonskyi [a], A. Artemenko [a], D. Arzhakov [a], M. Drábik [a], D. Slavínská [a], M. Vandrovcová [b], L. Bačáková [b], H. Biederman [a,*]

[a] Charles University in Prague, Faculty of Mathematics and Physics, Department of Macromolecular Physics, V Holešovičkách 2, 180 00 Prague, Czech Republic
[b] Institute of Physiology, Academy of Sciences of the Czech Republic, Department of Growth and Differentiation of Cell Populations, Videnska 1083, 142 20 Prague 4, Czech Republic

ARTICLE INFO

Article history:
Received 26 September 2011
Accepted in revised form 3 February 2012
Available online 12 February 2012

Keywords:
Plasma polymer particles
Cluster source
Composite film
Surface roughness
Cell adhesion
Wettability

ABSTRACT

Nanocomposite metal plasma polymer films were prepared by deposition of C:H plasma polymer particles using a Haberland type cluster source and overcoating of these particles by titanium layer by means of planar magnetron. This study is focused mainly on characterization of surface roughness of such films and its influence on other properties, such as surface chemistry and wettability. Selected samples were also subjected to biotests, namely to evaluate adhesion of human osteoblast-like MG63 cells.

1. Introduction

A large variety of applications of nano-rough surfaces have already been proposed comprising for instance fabrication of surfaces with controllable wettability ranging from super-hydrophilic to super-hydrophobic ones (e.g. [1,2]), tailoring adsorption of proteins and adhesion of tissue cells on surfaces (e.g. [3–5], or production of surfaces having high specific surface area needed, e.g., for production of catalysts or for photovoltaic applications. Because of a wide range of possible applications, numerous methods that allow modifying the roughness of surfaces on a nanometer scale have been developed. The most common ones are based either on the direct growth of nanostructured films, e.g. in the case of plasma polymerized fluorocarbon coatings [5–7], deposition of columnar structures in a GLAD (GLancing Angle Deposition) arrangement [8] or sol–gel technique (e.g. [9]), etching or sputtering of surfaces [10,11], or on two-step processes comprising fabrication of nanostructured surface, for instance by etching, photolithography or laser irradiation of substrates, which is followed by coating of such prepared surfaces by films having desired chemical composition (e.g. [12–17]).

In this study, we follow an alternative vacuum process allowing fabricating of surfaces with well controlled surface roughness [18]. This approach uses a combination of the deposition of particles, in our case plasma polymerized C:H particles produced in a gas aggregation cluster source, and deposition of thin coating, in our case magnetron sputtered Ti, for overcoating the film of particles. This method makes it possible to control independently the roughness of the coatings that is determined by the properties of deposited film of C:H particles and of surface chemical composition of resulting coatings, which is given solely by the properties of overlayer film. The main emphasis of this investigation is to provide morphological and chemical characterization of such prepared coatings, as well as the evaluation of their wetting behavior and attractiveness for the adhesion of osteoblast-like cells.

2. Materials and methods

2.1. Sample deposition

The deposition was performed in the deposition chamber schematically depicted in Fig. 1. Plasma polymer particles were deposited using a cluster source developed in our laboratory [19]. It used a 2-inch planar RF magnetron mounted within a water cooled cylindrical aggregation chamber. The aggregation chamber (11 cm long and 6 cm in diameter) was capped with conical shaped lid ending in an orifice of 1.5 mm diameter. The whole cluster source was attached to a high vacuum chamber pumped by rotary and diffusion pumps. The polymeric particles were produced using a gas mixture of argon and hexane (hexane flow 0.8 sccm, argon flow 10.7 sccm). The pressure inside the aggregation chamber was 160 Pa and power input to the RF magnetron was 120 W. These conditions were selected on the basis of a

* Corresponding author. Tel.: +420 22191 2360; fax: +420 22191 2350.
E-mail address: bieder@kmf.troja.mff.cuni.cz (H. Biederman).

0257-8972/$ – see front matter © 2012 Elsevier B.V. All rights reserved.
doi:10.1016/j.surfcoat.2012.02.005

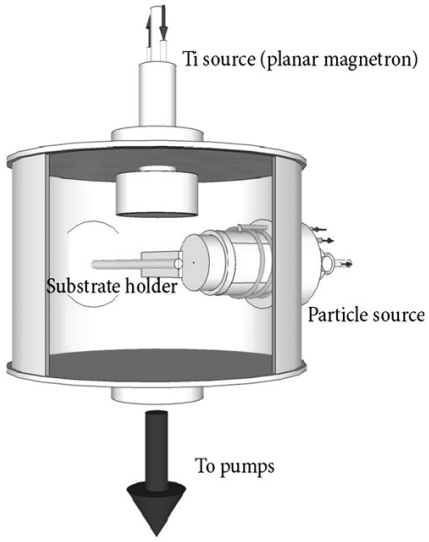

Fig. 1. Scheme of experimental setup for deposition of C:H plasma polymer particles overcoated by titanium. Substrate holder could be rotated around its axis to face both sources.

previous study [20], since they provide the highest rate of production of C:H particles.

The C:H particles were first deposited for a certain period of time, then without breaking vacuum (only by rotating the substrate holder by 90°) overcoated by a titanium layer using another magnetron mounted perpendicularly to the cluster source. Standard 3-inch planar, water cooled DC magnetron equipped with titanium target was used. The deposition conditions used in this step were: pressure 0.15 Pa of argon and magnetron current 0.45 A. The distance between target and substrate was 9 cm.

2.2. Sample characterization

Scanning Electron Microscope (SEM) observation of the C:H nanoparticle films as well as C:H nanoparticles overcoated by titanium films was performed by Mira/II scanning electron microscope (Tescan). Cross-sectional SEM micrographs were also used to determine film thickness. Thickness of the titanium overlayer was determined from a sample without C:H particles, which is possible, because magnetron sputtering has very stable deposition rate. Morphology of the samples was evaluated by Atomic Force Microscopy (AFM, NTEGRA Prima, NT-MDT) operated in the semi-contact mode using silicon cantilevers. Chemical composition of the deposited films was determined by X-ray Photoelectron

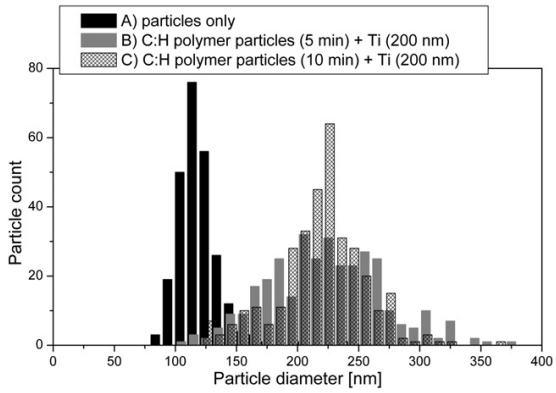

Fig. 2. Size distribution of A) standalone C:H particles, B) submonolayer of C:H particles (deposited for 5 min) overcoated with 200 nm of titanium, and C) approximately monolayer of C:H particles (deposited for 10 min) overcoated with 200 of titanium.

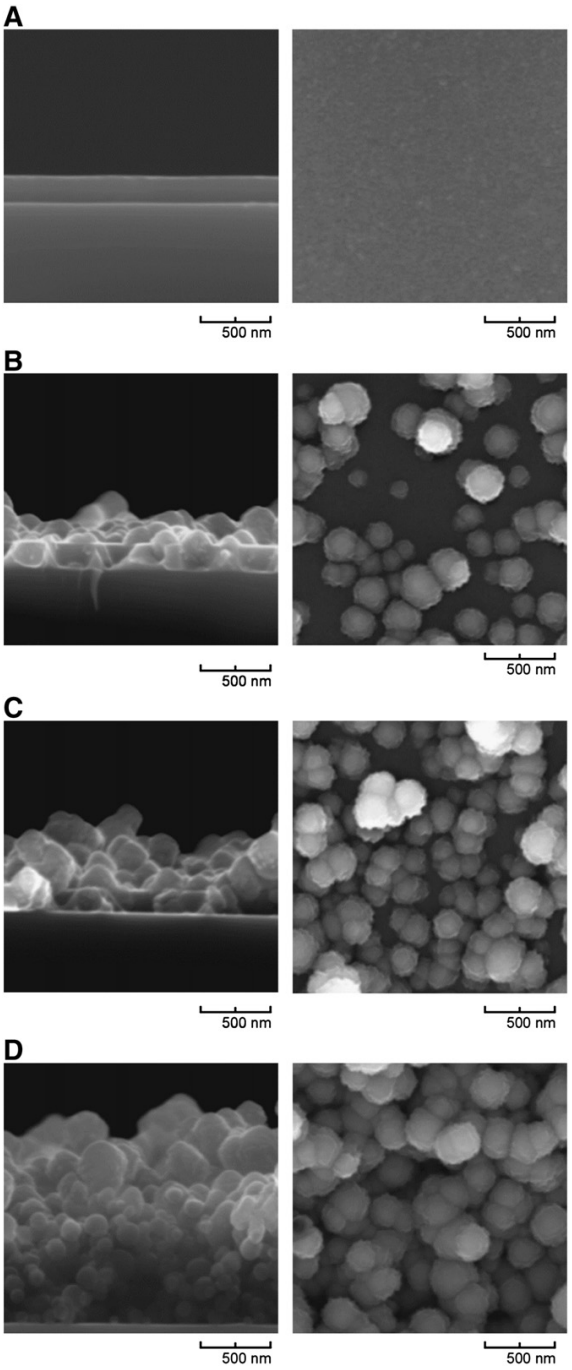

Fig. 3. SEM micrographs of C:H plasma polymer particles embedded in titanium matrix; particle deposition time: A) 0 min (no particles), B) 5 min, C) 10 min, and D) 20 min, matrix deposition time: 10 min. Left side cross-sectional view, right side top view.

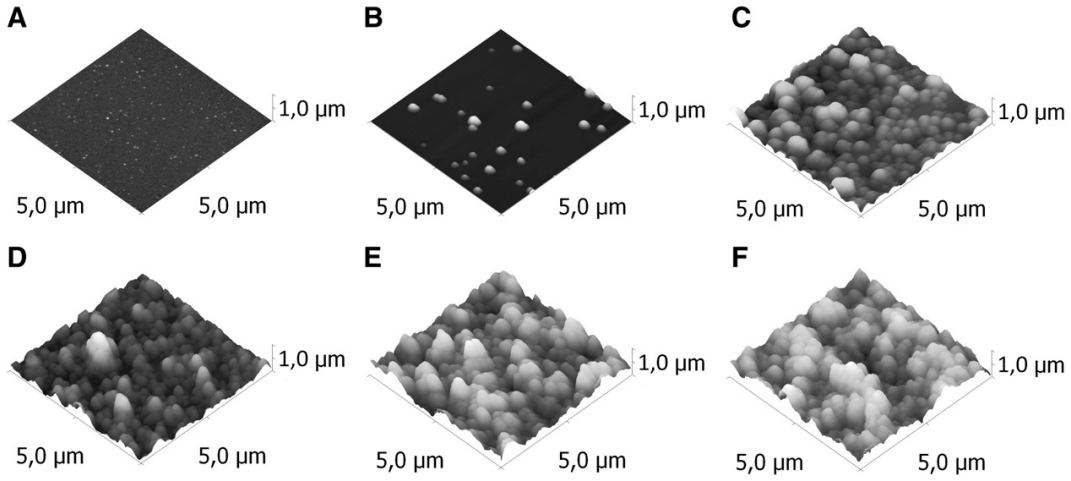

Fig. 4. AFM micrographs of C:H plasma polymer particles embedded in titanium matrix; particle deposition time: A) 0 min (no particles), B) 2 min, C) 5 min, D) 10 min, E) 20 min, and F) 30 min, matrix deposition time: 10 min.

Spectroscopy (XPS, Specs Phobios 100). The XPS spectra were acquired at a constant take-off angle of 90°. Wide scans (0–1300 eV) were recorded using 40 eV pass energy (step 0.5 eV, dwell time 0.1 s), whereas high resolution scans were recorded at 10 eV pass energy (step 0.05 eV, dwell time 0.1 s, 10 repetitions). In all cases the binding energies were referenced to the C1s carbon peak at 285.0 eV. Water contact angle of the samples was measured in static mode by a sessile drop method by means of a goniometer.

2.3. Biotests

TiAlV polished disks were used as substrates for cell culture experiments. Samples were inserted into 12-well polystyrene cell culture plates (TPP, Switzerland; internal well diameter 21.6 mm) and seeded with human osteoblast-like MG 63 cells (European Collection of Cell Cultures, Salisbury, UK), suspended in Dulbecco's modified Eagle's Minimum Essential Medium (DMEM; Sigma, USA, Cat. No. D5648) supplemented with 10% fetal bovine serum (FBS; Sebak GmbH, Aidenbach, Germany) and gentamicin (40 µg/ml, LEK, Ljubljana, Slovenia). Each well contained 30 000 cells (i.e. approximately 8 200 cells/cm^2) and 3 ml of the medium. The cells were cultured for 1, 3 and 7 days at 37 °C in a humidified air atmosphere containing 5% CO_2.

The number of cells on the material surface was evaluated on microphotographs taken under an IX-51 microscope, equipped with a DP-70 digital camera (both from Olympus, Japan, obj. 20×).

3. Results

3.1. Morphology of deposited coatings

The morphology of coatings composed of C:H particles overcoated by titanium film can be influenced both by the number of C:H particles and by the thickness of the overlayer. Both of these possible ways that allow controlling the roughness of resulting samples were therefore evaluated in this study.

Regarding the influence of the deposition time of C:H particles on the resulting coatings, the thickness of the titanium overlayer was kept constant at a value of 200 nm (10 min deposition, thickness measured from cross-sectional SEM image), i.e. thickness about two times higher than the mean size of C:H particles that is 110 nm; see Fig. 2 for particle size distribution. As can be seen in Figs. 3 and 4, which present SEM and AFM images of samples prepared at different deposition times of C:H particles, two distinct phases of the coating formation can be distinguished. In the first phase randomly distributed and well separated structures appear on the surface, but the area between them remains smooth. Moreover, it can be seen on the cross-sectional images that the titanium is moving even under the particles and bonds directly to the substrate. This situation, which reflects rather low coverage of substrate surface by C:H particles that form a sub-monolayer, changes as soon as the deposition time of C:H particles reaches approximately 10 min (Figs. 3C, 4D). In this case the substrate surface is already fully covered by C:H particles, which are then forming a multilayer structure (Figs. 3D, 4E, F) and rather rough surface is created. As can be seen in Fig. 2, the size distribution of resulting bumps on the surface becomes wider as compared to dimensions of uncoated C:H particles and shifts to higher values with maximum around 220 nm.

The above mentioned two phases of the film growth, corresponding to the situation before formation of the first monolayer of C:H particles and situation when the substrate is fully covered by C:H particles, respectively, have a dramatic impact on the evolution of roughness of the deposited coatings. In the first phase a rapid increase of the root-

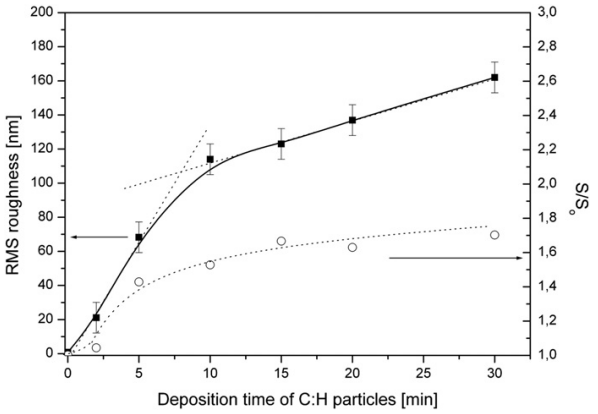

Fig. 5. RMS roughness of films of C:H plasma polymer particles embedded in titanium matrix as measured by AFM. Error bars were calculated as a mean deviation from several measurements.

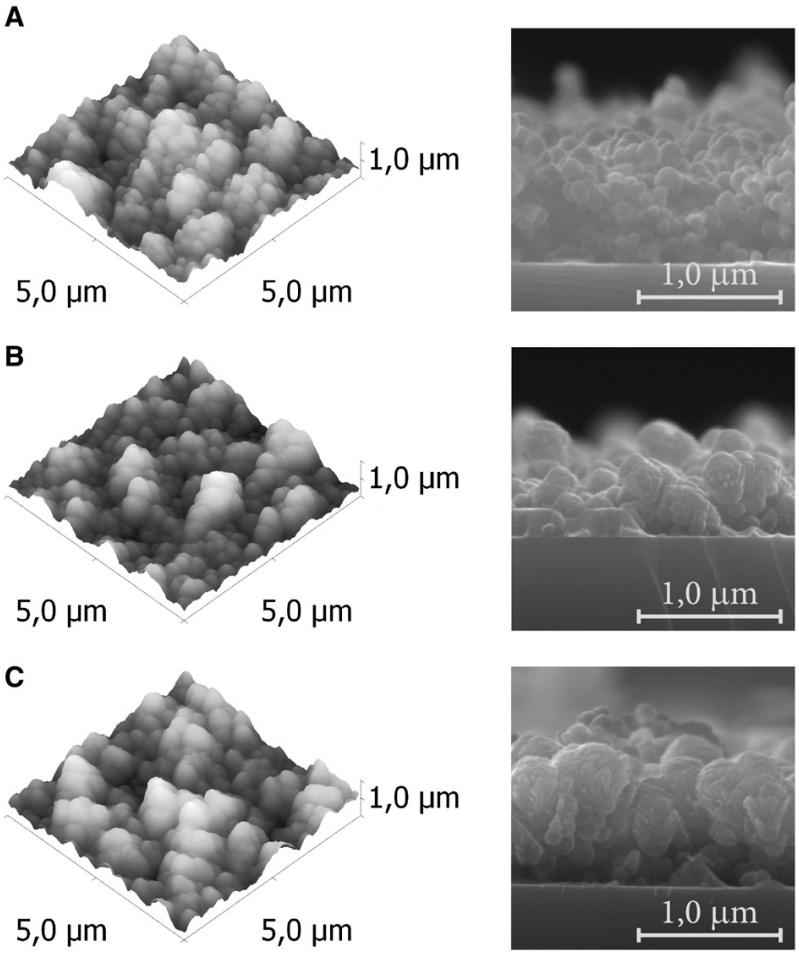

Fig. 6. AFM (left) and cross-sectional SEM images (right) of C:H plasma polymer particles embedded in titanium matrix; deposition time of titanium matrix: A) 5 min, B) 10 min, and C) 20 min, C:H particle deposition time: 10 min.

mean-square (RMS) roughness from about 1 nm to more than 110 nm was observed as the C:H deposition time increased from 0 (i.e. no C:H particles were deposited) to 10 min. Considerably slighter enhancement of RMS roughness was observed in the second phase — additional 10 min of C:H particle deposition enhanced the RMS roughness of the surface by less than 20%. This behavior, which is documented in Fig. 5, where dependences of both RMS roughness and ratios of actual surface area S and planar surface area S_0 on the deposition time of C:H particles are depicted, qualitatively agrees with the results of a previous study performed with Ti nanoclusters overcoated either by plasma polymerized hexane or nylon [18], and may be explained as follows. With the approximation that the substrate is completely flat, it can be concluded that until the first monolayer is formed only the areas with particles contribute to the roughness. Therefore each new particle that lands directly on the substrate contributes to the roughness with its full diameter. After the first monolayer is formed and there is no bare substrate accessible for incoming particles, contribution of a single particle to the roughness stops to be simple addition, because particles fall onto other particles and into pits formed by (spherical) particles. Therefore, the further increase of roughness starts to be slower. Error bars in Fig. 5 were calculated as mean deviations of several measurements. For lower substrate coverage by C:H particles the relative error is large, because even a few particles added or omitted can

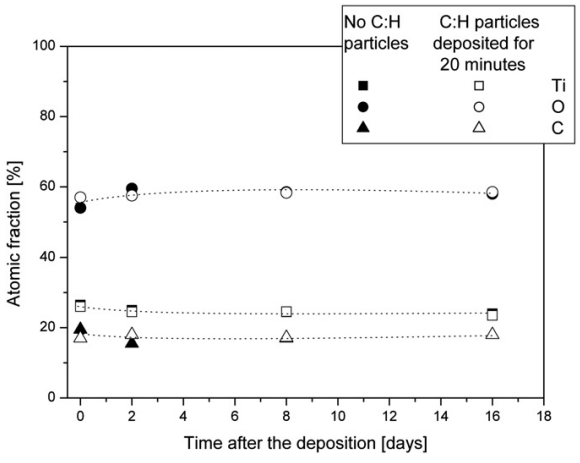

Fig. 7. Temporal evolution of elemental composition without hydrogen as determined by XPS on smooth Ti sample and C:H plasma polymer particles overcoated with titanium.

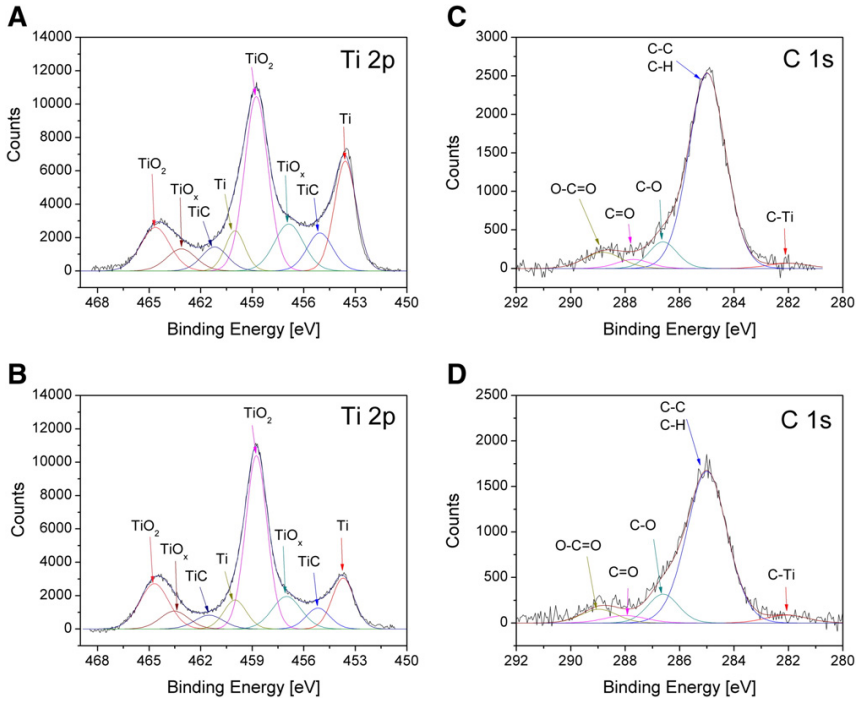

Fig. 8. High resolution spectra deconvolution evaluation of Ti2p peak for A) flat sample; B) rough sample (20 min of particle deposition) and C1s peak for C) flat sample and D) rough sample (20 min of particle deposition) measured immediately after the deposition.

cause significant change in calculated roughness. With more particles present, the relative error is decreasing even though absolute error is not changing much.

An example of the dependence of the surface morphology on the thickness of titanium overcoat at fixed deposition time of C:H particles is presented in Fig. 6. As can be seen in this figure, the deposition time of titanium film modifies the appearance of the surface: increasing time causes a fading of the finer height structure and bigger structures can be seen on the surface.

Cross-sectional SEM images show the reason for such behavior. Even in the case of the thinnest overlayer in Fig. 6A it can be concluded that particles on the top seem to be bigger than those on the bottom. That is actually because the titanium is capping the particles and, with increasing deposition time, Ti columnar-cauliflower growth proceeds. However, the increasing thickness of Ti layer leads to a lower number of bigger hills. These two opposing effects, i.e. formation of bigger bumps, but at lower quantity, cause that the surface roughness expressed by RMS value increases with the thickness of titanium markedly slowly as compared to the effect of deposition time of C:H particles discussed above. For instance, on keeping the deposition time of C:H particles fixed at 20 min and increasing the deposition time of titanium film from 5 min, which corresponds to the film thickness of 100 nm, to 20 min (400 nm thick titanium film), the RMS rises from 107 ± 10 nm to 145 ± 15 nm, i.e. by approximately 35%.

To conclude this part, it was observed that the deposition time of both C:H particles and titanium film influences the roughness of the deposited coatings. The strongest effect was observed when the C:H deposition time was varied, which allows to modify the RMS roughness by more than 2 orders of magnitude. The alteration of the thickness of the overlayer was found to have only a modest influence on the surface roughness. Therefore in further experiments only deposition time of C:H particles was varied and the thickness of the titanium films was kept constant at 200 nm.

3.2. Chemical composition of deposited coatings

Selected samples were subjected to XPS analysis. One flat and one rough sample (20 min of particles deposition, which corresponds to RMS roughness of 134 nm) were chosen to compare their surface chemistry to determine their differences and differences during the aging process. The results of these experiments are summarized in Fig. 7. As can be seen the elemental composition, as determined from XPS measurements, is quite similar in both cases of flat and rough surface. Besides Ti, also relatively high amount of oxygen and carbon in the films was observed, which is usual situation for sputtered titanium films exposed to atmosphere, as reported previously [8]. Due to the fact that portion of carbon (about 4%) is directly bonded to Ti (C–Ti bond at binding energy 281.9 eV) part of carbon contamination originates from the deposition process (e.g. hydrocarbon residuals in the deposition chamber). Nevertheless, as can be seen in Fig. 8, the major part of carbon is bonded in C–C/C–H backbone chains that can be attributed to the film contamination after its exposure to open air as observed recently in a study focused on the evaluation of aging of Ti nanoclusters [21]. Also the high resolution

Table 1
High resolution spectra deconvolution evaluation of Ti2p peak for A) flat sample; and B) rough sample (20 min of particle deposition).

Aging time (days)	A)				Aging time (days)	B)			
	Ti (%)	Ti–C (%)	TiO_x (%)	TiO_2 (%)		Ti (%)	Ti–C (%)	TiO_x (%)	TiO_2 (%)
0	26	13	17	44	0	19	10	16	55
2	17	11	15	57	2	19	6	14	61
8	16	11	15	58	8	19	8	14	60
16	16	11	15	58	16	17	7	14	62

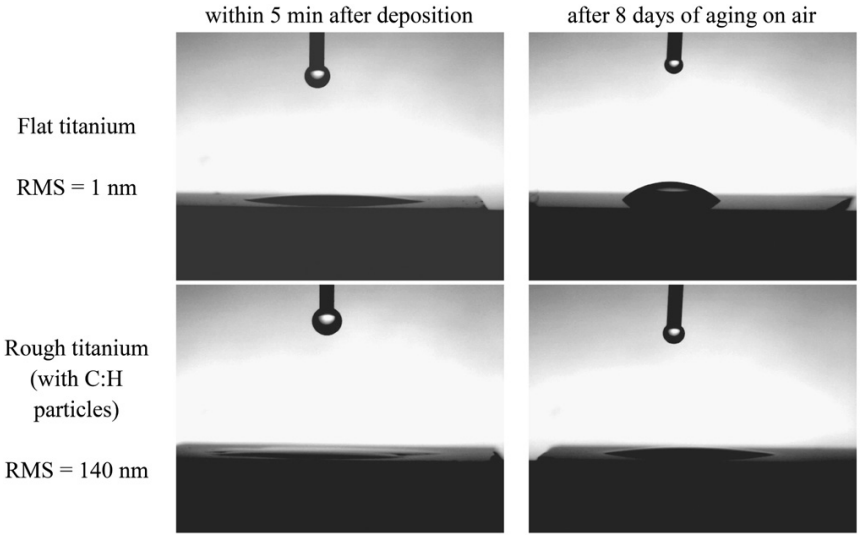

Fig. 9. Visual comparison of contact angles on flat and rough surface right after deposition and after aging in air.

spectra showed no significant difference except for a slightly higher percentage of TiO_2 at the expense of metallic Ti for the rough sample — see Fig. 8 and Table 1.

Moreover, it can be seen in Fig. 7 and in Table 1 that the surface composition varies slightly within the first two days after the deposition, indicating an increase of oxygen content in the coatings. After the first 2 days, the chemical composition remains constant.

3.3. Wettability of the deposited coatings

Water contact angles (WCA) were measured on the samples in order to determine wetting behavior of films with different values of roughness. Because the contact angle measurement and XPS are both highly surface sensitive methods, and we expect films to have approximately the same surface chemical composition, as confirmed by XPS, the changes in the wetting properties should be dependent only on the surface roughness (e.g. [22]). However, the water contact angles measured on the samples within 5 min after the deposition were for all the samples 6° or less (see Fig. 8A and B).

In spite of similar water contact angles measured on samples immediately after the deposition, distinct variations were found in dependence on their storage time. Whereas smooth samples, i.e. samples without C:H particles, lost their super-hydrophilic character during the first two days after being in open air (WCA reached the value of 33° after two days in open air), the increase of water contact angle was found to be much slower for roughened samples; for those having RMS roughness of 140 nm the water contact angle remained below 10° even after 16 days in open air, as can be seen in Fig. 9. This is a rather important finding since long term super-hydrophilicity is generally rather difficult to achieve.

3.4. Cell adhesion on deposited coatings

Samples without C:H particles and C:H particles deposited for 5 and 10 min were selected for testing the possible effect of nanoroughness on adhesion of osteoblast-like cells; this corresponds to RMS roughness of 1 nm, 70 nm and 115 nm, respectively. As can be seen in Figs. 10 and 11, on day 1 after seeding, the number of initially adhering cells was slightly higher on both roughened samples, but these differences were nonsignificant, i.e. all values were comparable. This situation, however, markedly changed 3 and 7 days after seeding, when the cell numbers started to be significantly higher on surfaces with RMS roughness of 70 nm. This could be explained by the size of the bumps on the material surface. Nanostructured surfaces, i.e. those containing bumps of less than 100 nm, are believed to mimic the nanoarchitecture of natural tissues, e.g. the size of some extracellular matrix (ECM) molecules or irregularities on these molecules, and also the size of the extracellular parts of cell adhesion receptors. On nanostructured surfaces, cell adhesion-mediating ECM molecules are adsorbed in advantageous, almost physiological geometrical conformations, and thus the specific bioactive sites in these molecules, such as amino acid sequences like Arginine–Glycine–Aspartic acid or osteoblast-binding sequence Lysine–Arginine–Serine–Arginine, are well accessible to cell adhesion receptors [23–25]. The RMS roughness of 1 nm was probably too small to have considerable effects on cell behavior. These surfaces rather resembled flat surfaces like cell culture polystyrene or microscopic glass coverslips (RMS roughness of the latter was 0.51 nm, [26]). On the other hand, the irregularities on the surfaces with RMS roughness 115 nm, i.e. submicron-scale nanostructures, could be sufficiently big to hamper, at least partly, the adhesion, spreading and subsequent proliferation of cells. In our earlier study performed on nanocrystalline diamond films, the number of bovine

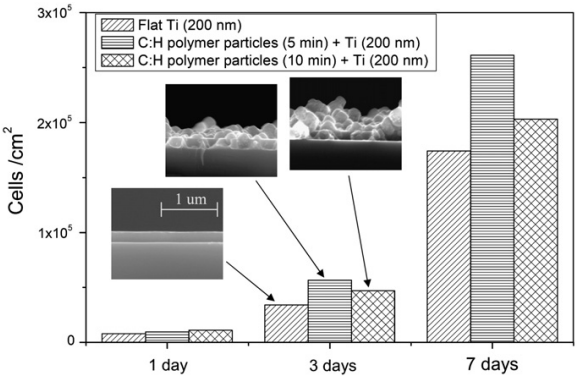

Fig. 10. Evolution of the osteoblast-like cell population on titanium films with different roughness values. Displayed populations are calculated as a median of measured values.

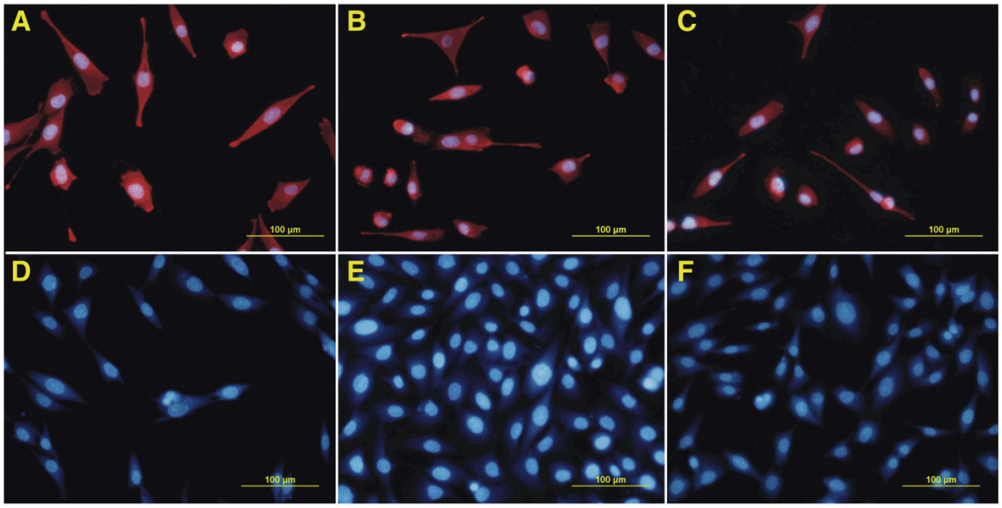

Fig. 11. Human osteoblast-like MG 63 cells in 1-day-old (A–C) and 3-day-old (D–F) cultures on samples without C:H particles (A, D) or with C:H particles deposited for 5 min (B, E) and 10 min (C, F). Cells were fixed with ethanol and stained with a combination of Hoechst 33342 (blue fluorescence) and Texas Red C_2-maleimide (red fluorescence, A–C) or Hoechst 33342 alone (D–F). Olympus IX 51 microscope, obj. 20×, DP 70 digital camera. Bar = 100 µm.

pulmonary artery endothelial cells of the CPAE line was significantly lower on the surfaces with submicron scale roughness (RMS roughness up to 301 nm) than on nanostructured surfaces (RMS roughness 8.2 nm; [27]). Similarly, the number of MG 63 cells on titanium disks with submicron surface roughness (R_a of 700 and 400 nm) reached lower values than on nanostructured surfaces (R_a = 60 nm), and had a less spread, elongated morphology [28].

4. Conclusion

Composite films of C:H plasma polymer particles with titanium matrix with controllable roughness were prepared by overcoating the particles with sputtered titanium. The surface roughness was found to be directly proportional to the coverage or deposition time of the C:H particles, its increase being very rapid until formation of first monolayer and somewhat slower afterwards. Moreover, it has been shown that the surface roughness can be influenced in a limited range also by the thickness of the overcoating titanium layer. Chemical analysis performed using XPS revealed no significant difference between flat and rough titanium surface. However, increased roughness had a large influence on the temporal stability of water contact angle and on the osteoblast-like cell adhesion on such surfaces. In relation to the former phenomenon it was found that roughened surface made wettability of surface much more stable than a flat surface. Although the super-hydrophilic state of roughened surfaces gradually vanished, it was maintained for several times longer time period than in the case of flat surface.

Regarding the adhesion of cells on roughened surfaces, this study revealed that there seems to be an optimum RMS surface roughness between 1 and 115 nm — probably in tens of nm. This finding is very interesting with respect to designing novel implant materials.

Acknowledgments

This work was supported by the Grant Agency of the Academy of Sciences of the Czech Republic under contract KAN 101120701 and by the grant SVV-2012-265305. P. Solar acknowledges also the support from the Grant Agency of Charles University in Prague within the frames of grant GAUK 437411. The authors are indebted to S. Haviar and I. Khalaghan for SEM images.

References

[1] T. Ishizaki, N. Saito, O. Takai, Langmuir 26 (11) (2010) 8147.
[2] Yan-Hong Lin, Su. Kai-Ling, Ping-Szu Tsai, Feng-Lin Chuang, Yu-Min Yang, Thin Solid Films 519 (2011) 5450.
[3] L. Richert, F. Vetrone, J.-H. Yi, S.F. Zalzal, J.D. Wuest, F. Rosei, A. Nanci, Adv. Mater. 20 (2008) 1488.
[4] A.J. Campillo-Fernández, R.E. Unger, K. Peters, S. Halstenberg, M. Santos, M.S. Sánchez, J.M.M. Dueñas, M.M. Pradas, J.L.G. Ribelles, C.J. Kirkpatrick, Tissue Eng. Part A 15 (6) (2009) 1331.
[5] R. Di Mundo, R. Gristina, E. Sardella, F. Intranuovo, M. Nardulli, A. Milella, F. Palumbo, R. d'Agostino, P. Favia, Plasma Processes Polym. 7 (2010) 212.
[6] M. Drabik, O. Polonskyi, O. Kylian, J. Cechvala, A. Artemenko, I. Gordeev, A. Choukourov, D. Slavinska, I. Matolinova, H. Biederman, Plasma Processes Polym. 7 (2010) 544.
[7] F. Intranuovo, E. Sardella, P. Rossini, R. d'Agostino, P. Favia, Chem. Vap. Deposition 15 (2009) 95.
[8] A. Choukourov, P. Solar, O. Polonskyi, J. Hanus, M. Drabik, O. Kylian, E. Pavlova, D. Slavinska, H. Biederman, Plasma Processes Polym. 7 (2010) 25.
[9] V. Zorba, X. Chen, S.S. Mao, Appl. Phys. Lett. 96 (2010) 093702.
[10] K. Tsougeni, N. Vourdas, A. Tserepi, E. Gogolides, Langmuir 25 (2009) 11748.
[11] E. Wohlfart, J.P. Fernández-Blázquez, E. Arzt, A. del Campo, Plasma Processes Polym. 8 (2011) 876.
[12] K. Teshima, H. Sugimura, Y. Inoue, O. Takai, A. Takano, Langmuir 19 (2003) 10624.
[13] M. Lejeune, L.M. Lacroix, F. Bretagnol, A. Valsesia, P. Colpo, F. Rossi, Langmuir 22 (2006) 3057.
[14] T. Baldacchini, J.E. Carey, M. Zhou, E. Mazur, Langmuir 22 (2006) 4917.
[15] K. Tsougeni, A. Tserepi, G. Boulousis, V. Constantoudis, E. Gogolides, Plasma Processes Polym. 4 (2007) 398.
[16] A. Ruiz, A. Valsesia, G. Ceccone, D. Gilliland, P. Colpo, F. Rossi, Langmuir 23 (2007) 12984.
[17] Y.B. Zhou, Y. Yang, W.M. Liu, Q. Ye, B. He, Y.S. Zou, P.F. Wang, X.J. Pan, W.J. Zhang, I. Bello, S.T. Lee, Appl. Phys. Lett. 97 (2010) 133110.
[18] O. Kylián, O. Polonskyi, J. Kratochvíl, A. Artemenko, A. Choukourov, M. Drábik, P. Solař, D. Slavinska, H. Biederman, Plasma Proc. Polym. 9 (2012) 180.
[19] O. Polonskyi, P. Solař, O. Kylián, M. Drábik, A. Artemenko, J. Kousal, J. Hanuš, J. Pešička, I. Matolínová, E. Kolíbalová, D. Slavínská, H. Biederman, Thin Solid Films (2011), doi:10.1016/j.tsf.2011.04.100.
[20] P. Solař, O. Polonskyi, A. Choukourov, A. Artemenko, J. Hanuš, H. Biederman, D. Slavínská, Surf. Coat.Technol. 205 (2011) S42.
[21] M. Drabik, A. Choukourov, A. Artemenko, O. Polonskyi, O. Kylian, J. Kousal, L. Nichtova, V. Cimrova, D. Slavinska, H. Biederman, J. Phys. Chem. C 115 (2011) 20937.
[22] M. Flemming, L. Coriand, A. Dupareé, in: A. Carré, K.L. Mittal (Eds.), Superhydrophobic Surfaces, Koninklijke Brill NV, Leiden, 2009, p. 19.
[23] T.J. Webster, C. Ergun, R.H. Doremus, R.W. Siegel, R. Bizios, J. Biomed. Mater. Res. A 51 (2000) 475.

[24] T.J. Webster, C. Ergun, R.H. Doremus, R.W. Siegel, R. Bizios, Biomaterials 21 (2000) 1803.
[25] R.L. Price, K. Ellison, K.M. Haberstroh, T.J. Webster, J. Biomed. Mater. Res. A 70 (2004) 129.
[26] M. Vandrovcová, J. Vacík, V. Švorčík, P. Slepička, N. Kasálková, V. Vorlíček, V. Lavrentiev, V. Voseček, L. Grausová, V. Lisá, L. Bačáková, Phys. Stat. Sol. (a) 205 (2008) 2252.
[27] L. Grausová, A. Kromka, L. Bačáková, S. Potocký, M. Vaněček, V. Lisá, Diamond Relat. Mater. 17 (2008) 1405.
[28] G. Zhao, O. Zinger, Z. Schwartz, M. Wieland, D. Landolt, B.D. Boyan, Clin. Oral Implants Res. 17 (3) (2006) 258.